Louvain School of Engineering
Institute of Condensed Matter and Nanoscience

Transferring biomolecules with gas cluster ion beams

Thèse soutenue en vue de l'obtention du grade de Docteur en Sciences de l'Ingénieur par

Vincent Delmez

Composition du Jury

Pr. Arnaud Delcorte (UCLouvain) – Promoteur
Pr. Christine Dupont-Gillain (UCLouvain) – Promotrice
Pr. Xavier Urbain (UCLouvain) – Président
Pr. Sophie Demoustier (UCLouvain)
Pr. Clément Lauzin (UCLouvain)
Pr. Laurent Houssiau (UNamur)
Pr. David Scurr (University of Nottingham)

Louvain-La-Neuve

Novembre 2022

Remerciements

Une thèse est certes un accomplissement personnel, et, de l'extérieur, elle peut paraître comme un projet mené à bien de façon individuelle. Néanmoins, en réalité, l'accomplissement de ces 4 années de travail a été rendu possible grâce à la contribution et au soutien de toute une série de personnes qui me sont chères : promoteurs, collègues, amis et famille.

En premier lieu, je voudrais remercier mes promoteurs, les professeurs Christine Dupont et Arnaud Delcorte. Merci déjà de m'avoir donné la possibilité d'entreprendre ma thèse au sein de votre laboratoire. Merci ensuite pour votre soutien sans faille au cours de ces 4 années. Ce travail n'aurait certainement pas été aussi abouti sans vous. Toujours disponibles et emballés à l'idée de discuter des résultats scientifiques, vous êtes également constamment à l'écoute et avez toujours fait preuve d'une extrême bienveillance. Votre laboratoire fut un cadre de travail exceptionnel, une bonne ambiance mélangée à une bonne dose de rigueur scientifique, et nul doute que vous y êtes pour beaucoup. Ces 4 années de thèse étaient également mes 4 premières années de travail, en tant que chercheur. Merci de m'avoir formé, de m'avoir appris à chercher (et parfois à trouver), de m'avoir guidé tout en me laissant une énorme part de liberté et d'autonomie. Pour tout cela, pour votre confiance, et pour bien d'autres choses encore, MERCI.

I would also like to acknowledge Prof. Sophie Demoustier, Prof. Clément Lauzin, Prof. Laurent Houssiau, Prof. David Scurr, and Prof. Xavier Urbain, the members of my Jury. Thank you for the time you devoted to reading my manuscript, for your comments and for the valuable discussions we had at the private defense. All your suggestions and inputs contributed to improving the quality of the manuscript.

Je souhaiterais remercier le Fonds National de la Recherche Scientifique (FNRS) de m'avoir financé durant ces 4 années, ainsi que de m'avoir permis de participer à des conférences à l'étranger.

Ces 4 années m'auront permis, d'une part, d'établir une série de collaborations scientifiques, et, d'autre part, de partager du temps avec mes collègues, devenus amis. En arrivant au laboratoire, je ne savais même pas de quoi ToF-SIMS était l'acronyme… Merci Claude de m'avoir formé sur

l'instrument, et d'avoir ensuite été d'un précieux support, tant pour l'interprétation de résultats que pour tes interventions d'urgence lorsque la machine avait décidé de nous pourrir une journée de manips. Merci également à Pierre pour la partie XPS. Merci aussi à celles et ceux qui rendent notre quotidien dans le labo plus agréable, en nous aidant pour une série de tâches administratives et techniques : Rose-Anne, Nathalie, Anne, Françoise, Yasmine. Mon sujet de recherche étant assez pluridisciplinaire, j'ai été amené à faire une série d'expériences hors de notre laboratoire. Je souhaiterais dès lors remercier la team Boltzmann, Cécile, Delphine et Naïma, pour m'avoir formé et permis de venir faire des mesures d'AFM et d'éllipsométrie au sein de votre labo. Merci aussi à la team Carnoy, Joseph et Hervé, de m'avoir régulièrement (et chaleureusement) accueilli dans votre laboratoire, de m'avoir appris à faire des gels d'électrophorèse et d'avoir réalisé une série de mesures ESI-MS.

Evidemment, le deuxième étage de l'aile C du bâtiment Lavoisier est l'endroit où j'ai passé le plus de temps ces 4 années. Merci donc à tous les énergumènes qui l'ont peuplé durant mon passage, et qui en font un haut lieu du travail dans un climat plutôt décontracté (et sportif). Dans le désordre, merci à mes collègues de bureau pour la bonne ambiance qui y a toujours régné. Misha, don't forget, « water is life », I hope water is as good up North. Cédrik, qui m'aura démontré qu'il est possible de faire la sieste dans à peu près n'importe quelle position sur un bureau ou par terre. Plus récemment Ian et Samuel. Merci à Aurélien, parti trop tôt… du labo (ou est-ce moi qui suis arrivé avec un peu de retard ?), pour m'avoir aidé à prendre mes marques à mon arrivée, et m'avoir obligé à venir tester l'escalade, finalement pas si mal comme sport. Dommage que notre cohabitation au labo ait été si courte. Merci à Thibaut (aka la Pince), d'avoir été mon binôme sportif et de craquage nutritif, mais pas que, entre autres séances de grimpe, de bad, sorties VTT, on est aussi devenu colocs le temps de quelques mois. Je n'aurais pas imaginé démarrer une si belle amitié sur mon lieu de travail. Dans le même bureau on trouvait également Arnaud et Cédric. Merci à vous trois de m'y avoir accueilli un nombre incalculable de fois, que ce soit pour m'entendre me plaindre, pour un fou rire de 5 min, ou une discussion de 30 pour refaire le monde et finalement se demander ce qu'on faisait encore là. Arnaud, on se voit aux Lofoten d'ici peu d'ailleurs. Merci aussi à Thomas et Benjamin, mes compères du projet iBeam. J'ai adoré bosser avec vous, et vous avez également été d'excellents partenaires sportifs, probablement les meilleurs pour ce qui est d'organiser la troisième mi-temps. Merci aussi aux

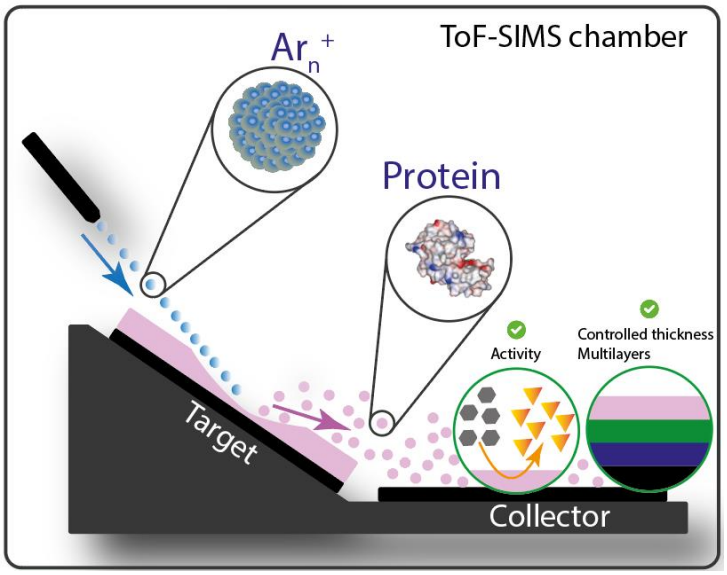
trois mémorants que j'ai eu la chance d'encadrer : Thomas, William et Charline. Ce fut un vrai plaisir de travailler avec vous, et vous avez chacun contribué de façon significative à cette thèse.

Merci également à toute la team du C3, avec qui on a partagé d'innombrables temps de midi, pauses « café » et afterworks. Merci pour votre présence bien nécessaire en des temps où le C2 semblait parfois quelque peu dépeuplé.

Je voudrais également remercier toutes les personnes extérieures à mon environnement direct de travail. La team chimiste : Merci Benoît, François, Simon et Déléguée (aka Carole) pour toutes les soirées « girafe », l'organisation de la STEL, et tous les autres moments partagés ensemble depuis de si nombreuses années. Une pensée particulière pour Benoît, qui, durant ces 4 années, m'aura aidé à relativiser quand les résultats ne suivaient pas, en me rappelant à sa façon que « tout cela n'était pas si important ». Merci à la team « EVG Augu » et à la team « Jeudrewhist », ils se reconnaîtront, pour toutes les soirées et autres moments que l'on partage régulièrement, ainsi que pour vos encouragements ces derniers mois.

Merci à ma famille, sur qui je peux toujours compter. Merci Papa et Maman, pour votre soutien indéfectible depuis tant d'années. Je ne serais certainement pas là où j'en suis aujourd'hui sans vous. Mon parcours académique n'a pas toujours été rectiligne, et, je le sais, vous a causé l'apparition de quelques cheveux blancs. Néanmoins, vous m'avez toujours laissé prendre mes décisions concernant mes études, les avez toujours soutenues, et avez su me remettre sur les rails quand il le fallait. Merci de m'avoir éduqué comme vous l'avez fait, et de m'avoir transmis vos valeurs. Merci à mes frères et sœurs, Nicolas et Françoise, savoir que je peux compter sur vous en toute circonstance est très réconfortant. Merci également à Vincent et Bérénice, de m'avoir accueilli au sein de votre famille si naturellement depuis le premier jour il y a 5 ans. Enfin, merci infiniment à Pauline. Merci de m'accepter comme je suis, de supporter ma présence (et mes absences, je ne te remercierai jamais assez de me laisser vivre à fond mon addiction au sport) au quotidien. Que ce soit dans la vie de tous les jours ou professionnelle, tu me pousses toujours pour le meilleur. En particulier, je voudrais te remercier pour ton soutien inconditionnel durant les mois de rédaction, pendant lesquels tu as tout fait que je puisse me consacrer entièrement à l'écriture de ma thèse. Je n'aurais certainement pas pu mener à bien cette thèse et cette rédaction de façon aussi sereine sans toi.

Abstract



Surface biofunctionalization with proteins is the key to many biomedical applications. In this work, a novel biomolecule immobilization method is proposed and developed. This solvent-free approach relies on the use of large argon gas cluster ion beams to transfer controlled amounts of protein from a solid reservoir to any chosen substrate. This method was explored with a series of peptides and proteins: angiotensin, bradykinin, neurotensin, insulin and lysozyme, which were all successfully transferred. Time-of-flight secondary ion mass spectrometry (ToF-SIMS) revealed the deposition pattern, allowed measuring the deposited film thickness and, combined with SDS-PAGE electrophoresis, confirmed the presence of non-fragmented protein molecules on the collectors. Lysozyme enzymatic activity could be detected on the collectors, suggesting the preservation or easy recovery in solution of the three-dimensional structure of at least a fraction of the transferred proteins. Furthermore, lowering the energy per atom in the cluster projectiles down to 1 eV allowed more than 60% of bradykinin molecules to be transferred intact. The possibility to achieve alternate multilayer buildup was demonstrated with the construction of a well-organized trilayer composed of bradykinin, neurotensin and Irganox antioxidant. These results pave the way to well-controlled protein deposition using ion beams and to the investigation of more complex multilayer architectures.

The author contributed to the following papers:

- Delcorte, A., Delmez, V., Dupont-Gillain, C., Lauzin, C., Jefford, H., Chundak, M., Poleunis, C., and Moshkunov, K. (2020). Large cluster ions: soft local probes and tools for organic and bio surfaces. **Physical Chemistry Chemical Physics**, 22(31), 17427-17447.
- Chundak, M., Poleunis, C., Delmez, V., Jefford, H., Bonnaud, L., Jonas, A. M., and Delcorte, A. (2020). Argon gas cluster fragmentation and scattering as a probe of the surface physics of thermoset polymers. **Applied Surface Science**, 533, 147473.
- Moshkunov, K., Tomasetti, B., Daphnis, T., Delmez, V., Vanvarenberg, K., Préat, V., Lorenz, M., Quanico, J., Baggerman, G., Lemiere, F., Dupont-Gillain, C., and Delcorte, A. (2021). Improvement of biomolecular analysis in thin films using in situ matrix enhanced secondary ion mass spectrometry. **Analyst**, 146(21), 6506-6519.
- Delmez, V., Degand, H., Poleunis, C., Moshkunov, K., Chundak, M., Dupont-Gillain, C., & Delcorte, A. (2021). Deposition of Intact and Active Proteins In Vacuo Using Large Argon Cluster Ion Beams. **The Journal of Physical Chemistry Letters**, 12(2), 952-957.
- Chundak, M., Poleunis, C., Delmez, V., Jonas, A. M., & Delcorte, A. (2022). Probing the Surface Curie Temperature of Ferroelectric P (VDF-ran-TrFE) Copolymers by Argon Gas Cluster Ion Scattering. **The Journal of Physical Chemistry C**, 126(2), 1125-1131.
- Delmez, V., Tomasetti, B., Daphnis, T., Poleunis, C., Lauzin, C., Dupont-Gillain, C., & Delcorte, A. (2022). Gas Cluster Ion Beams as a Versatile Soft-Landing Tool for the Controlled Construction of Thin (Bio) Films. **ACS Applied Bio Materials**, 5(7), 3180-3192.

The author participated to the following international scientific events:

- Oral presentation at **The 22nd International Conference on Secondary Ion Mass Spectrometry (2019)** – Kyoto (Japan)
- Oral presentation at **the Réunion des Utilisateurs Francophones ToF-SIMS (IONTOF) (2021)** – Paris (France), ONLINE
- Oral presentation at the **1st User Workshop on Secondary ion Mass spectrometry (2021)** – Houston (USA), ONLINE
- Oral presentation at the **16th European Vacuum Conference (2021)** – Marseille (France)

- Oral presentation at the **Réunion des Utilisateurs Francophones ToF-SIMS (IONTOF) (2022)** – Bordeaux (France)
- Oral presentation at **The 23rd International Conference on Secondary Ion Mass Spectrometry (2022)** – Minneapolis (USA)

The author has been honored with the following awards:

- ***SFV Michel Cantarel Student Grant*** for the best poster presentation at the 16th European Vacuum Conference (2021) – Marseille (France)
- ***Biointerphases Award*** for the best oral presentation related to biological or biomaterial SIMS research at The 23rd International Conference on Secondary Ion Mass Spectrometry (2022) – Minneapolis (USA)

List of abbreviations

4-MUB	4-methylumbelliferyl β-D-N,N',N''-triacetylchitotrioside
AFM	Atomic force microscopy
BCA	Bicinchoninic acid
CD	Circular dichroism
DESI	Desorption electrospray ionization
DMSO	Dimethyl sulfoxide
E/n	Energy per constituent atom in the clusters
EDI	Electrospray droplet impact
ESI	Electrospray ionization
EtOH	Ethanol
GCIB	Gas cluster ion beam
GOx	Glucose oxidase
HRP	Horseradish peroxidase
Ins	Insulin
LbL	Layer-by-layer
LMIG	Liquid metal ion gun
LMIS	Liquid metal ion source
Lys	Lysozyme
MALDI	Matrix-assisted laser desorption ionization
MCI	Massive cluster impact
MCP	Microchannel plate
ME-SIMS	Matrix-enhanced SIMS
MOSFET	Metal Oxide Semiconductor Field Effect Transistor
MW	Molecular weight
PAA	Poly(acrylic acid)
PAGE	Polyacrylamide gel electrophoresis
PAH	Poly(allylamine hydrochloride)
PC	Principal component
PCA	Principal component analysis
PDI	Polydispersity index
PDMS	polydimethylsiloxane
PE	Polyethylene
PEG	Polyethylene glycol
PET	Polyethylene terephthalate
PLA	Polylactic acid
pMS	Preparative mass spectrometry
PPCs	Protein-polyelectrolyte complexes
PSS	Polystyrene sulfonate
RFU	Relative fluorescence units

SAM	Self-assembled monolayer
SIMS	Secondary ion mass spectrometry
TFA	Trifluoroacetic acid
tfac	Trifluoroacetylacetonates
ToF	Time-of-flight
Try	Trypsin
UHV	Ultra-high vacuum
WP	Work packages
XPS	X-ray photoelectron spectroscopy
Δm	Mass shift

Table of contents

Chapter 1: Introduction 1
1.1. On the importance of surfaces 1
1.2. Biomaterials 1
1.3. Proteins at interfaces 3
1.3.1. On the nature of proteins and their spontaneous adsorption 3
1.3.2. Drawbacks and limitations of spontaneous adsorption 5
1.4. Preparative mass spectrometry 7
1.4.1. Soft-landing for the deposition of intact biomolecules in the gas phase 7
1.5. Gas cluster ion beams (GCIB) , with a focus on SIMS 11
1.5.1. Atomic ion beams: early developments and limitations 12
1.5.2. Origins of cluster ion beams 13
1.5.3. Gas cluster formation by supersonic adiabatic expansion 14
1.5.4. Gas cluster ion beam equipment 15
1.5.5. Unique features of cluster ion beams versus atomic ion beams 16
1.5.6. Surface processing and cluster-matter interactions 16
1.6. Time-of-Flight Secondary Ion Mass Spectrometry (ToF-SIMS) 19
1.6.1. Basic principles and static limit 19
1.6.2. The SIMS equation, sputter yield and ionization probability 22
1.6.3. Surface charging and electron flood gun 24
1.6.4. Time-of-Flight (ToF) analyzer 25
1.6.5. Primary ion sources 26
1.6.6. Operational mode of SIMS 34
1.6.7. A focus on the use of ToF-SIMS for protein analysis 36
1.7. The iBeam project 45
1.8. References 47

Chapter 2: Objectives and strategy 69
2.1. Objectives 69
2.2. Strategy 70

2.2.1. Optimizing the transfer procedure 70
2.2.2. Transfer on water-sensitive substrate, functionalized collectors, and soft substrates 71
2.2.3. Transfer of enzymes 73
2.2.4. Construction of complex multilayers 74
2.2.5. Transfer of non-covalent complexes 75

Chapter 3: General Materials & Methods 77
3.1. Instruments 77
3.1.1. ToF-SIMS 77
3.1.2. Ellipsometry 83
3.1.3. UV-Vis spectrometer (multi-well plate reader) 84
3.1.4. Spin-coater 87
3.2. Compounds and molecules 87
3.2.1. Proteins 87
3.2.2. Other organic compounds 88
3.2.3. Metal-organic compounds 88
3.3. Target and collectors preparation 88
3.4. Bioassays 89
3.4.1. Bicinchoninic acid (BCA) protein quantification assay 89
3.4.2. Lysozyme activity assay 90
3.4.3. Trypsin activity assay 92
3.5. Bibliography 92

Chapter 4: Transfer of peptides and small proteins – Optimization of the transfer parameters and characterization of the collectors 93
4.1. Introduction 95
4.2. Materials and methods 96
4.2.1. Transfer experiments 96
4.2.2. Reference samples 97
4.2.3. 3D printing of additional transfer sample holders 97
4.3. Results and discussion 97
4.3.1. Transfer of intact peptides and small proteins 97
4.3.2. Fragmentation as function of cluster's energy per atom 103
4.3.3. Determination of the thickness of the transferred thin films 106
4.3.4. Optimization of the transfer geometry 115

4.4. Conclusion 118
4.5. Bibliography 119

Chapter 5: Transfer on functionalized substrates, water-soluble materials and soft polymers 121
5.1. Introduction 122
5.2. Materials and methods 122
5.2.1. Eppendorf tubes 122
5.2.2. BCA assay on PE sheets in Eppendorfs tubes 123
5.2.3. Sugars and polymers 123
5.2.4. Preparation of the PEG-coated collectors 123
5.2.5. Preparation of the trehalose-coated collectors 124
5.2.6. SIMS depth profiles 124
5.3. Results and discussion 124
5.3.1. A note about the protein quantification challenge 124
5.3.2. Transfer on polymers 126
5.3.3. PEG self-assembled monolayers on gold-coated Si wafers 132
5.3.4. Trehalose sacrificial layer on Si wafer 137
5.3.5. Transfer on paper 146
5.4. Conclusion 148
5.5. Bibliography 149

Chapter 6: Transfer of enzymes 151
6.1. Introduction 152
6.2. Materials and Methods 152
6.2.1. SDS-PAGE gel electrophoresis 152
6.2.2. In-gel trypsin digestion 153
6.2.3. Trypsin digestion on the collector 153
6.2.4. Peptide separation using nanoUPLC 153
6.2.5. LC-IMS (Ion Mobility Separation)-ESI-QTOF-MS Analysis (HDMSE) 154
6.2.6. ESI-QTOF data processing 155
6.2.7. Activity assay protocol adapted to be performed on Si wafers 155
6.3. Results and discussion 155
6.3.1. Lysozyme 155
6.3.2. Trypsin 169
6.4. Conclusion 172
6.5. Bibliography 173

Chapter 7: Construction of multilayers 175
7.1. Introduction 176
7.2. Materials and methods 177
7.2.1. Protein and Irganox targets 177
7.2.2. Successive transfers for the multilayers construction 177
7.2.3. ToF-SIMS depth profile analysis of the multilayers 177
7.3. Results and discussion 178
7.3.1. A simple model: bradykinin/Irganox1010 multilayers 178
7.3.2. A dual protein system: bradykinin/neurotensin multilayers 181
7.3.3. Towards more complex multilayers 182
7.4. Conclusion 185
7.5. Bibliography 185

Chapter 8: Transfer of non-covalent complexes 187
8.1. Introduction 188
8.2. Materials and methods 188
8.2.1. Turbidimetry measurement 188
8.2.2. BCA assay to quantify the complexation 189
8.2.3. Enzymatic activity assay of Lys-PSS complexes 189
8.2.4. ESI-MS analyses on “vancomycin-ligand” system 189
8.3. Results and discussion 190
8.3.1. Protein-polyelectrolytes complexes to protect the proteins during transfer 190
8.3.2. Investigating the transfer of various types of non-covalent complexes 197
8.4. Conclusion 212
8.5. Bibliography 213

Chapter 9: General conclusions and future prospects 215
9.1. Conclusions 215
9.1.1. A wrap up 219
9.2. Future prospects 220
9.2.1. Instrumentation 220
9.2.2. Towards larger proteins 221

9.2.3. ToF-SIMS as an analytical tool to investigate the enzymatic activity 222
9.2.4. Detection of large proteins by conventional SIMS 226
9.2.5. Non-covalent complexes: fundamental thoughts 227
9.2.6. Towards applications 228
9.3. Bibliography 228

Chapter 1 : Introduction

1.1.On the importance of surfaces

Objects are delimited from their environment by a surface (or interface), highlighting the composition differences between the two media. The interface is where interactions take place between an object and its environment. In fact, these interactions are mostly governed by the outermost atomic layers of a solid material, equivalent to a few nanometers (nm). In other words, some properties of a material, such as its biocompatibility, wettability, adhesion, chemical activity, electrostatic behavior and corrosion resistance, rely on the chemical/molecular composition of its few external atomic/molecular layers. Often, this composition slightly or strongly differs from that of the bulk. On the one hand, the object may be prone to reorganize itself (e.g. by migration of molecules towards the surface), in order to minimize its surface energy. On the other hand, contact with the environment commonly results in either modification (physical or chemical), or in contamination of the surface. In both cases, the interface is modified, potentially altering the properties of the material. For a wide range of materials entering in everyday applications, including medical devices, batteries, polymer coatings, microelectronic devices or metallurgy, it is of utmost importance to precisely control the surface chemical and physical properties. In addition, the fact that the surface often differs from the bulk of the material justifies the need to develop analytical techniques that are surface sensitive and/or specific. Study of surfaces as well as research to handle and tune specific features and functions given to material surfaces have become disciplines of their own, namely surface analysis and engineering, respectively.

1.2.Biomaterials

“Biomaterial”, here is a word that, among others (nano-, bio-, natural, organic material), is no more restricted to one precise scientific community, and is even used in the common language. Today, people having completely different scientific backgrounds employ the word “biomaterial” for a wide variety of meanings. Therefore, it is quite a struggle to find a universal definition for the term “biomaterial”. In 2009, Williams, one of the pioneer scientist in the field of biomaterials, wrote an interesting opinion paper entitled “On the nature of biomaterials”, where he addresses existing

issues regarding the (ab)use of the word biomaterial.[1] Yet he also acknowledges that the definition must evolve as the development of the technology inevitably leads to new materials that did not exist at the time of the first accepted definition. He ends his reflection by proposing his own and updated definition, stated as follows: "*A biomaterial is a substance that has been engineered to take a form which, alone or as part of a complex system, is used to direct, by control of interactions with components of living systems, the course of any therapeutic or diagnostic procedure, in human or veterinary medicine.*"[1] This definition tends to refocus the biomaterials on their initial applications, in the biomedical domain, as was concluded in the first consensus on the nature of biomaterials.[2] Here, the goal is not to discuss further the definition of biomaterials, but rather to emphasize on the fact that no matter the definition, materials engineered to perform a targeted function have become cornerstones for countless applications. Even by sticking to Williams' definition and considering only biomedical devices, biomaterials have changed the course of human life, as they have led to an undeniable improvement in quality of life. Each year, millions of people (a number growing every year) undergo surgical procedures that involve implanted medical devices, and therefore benefit from it to compensate for a complete or partial loss of an organ's function.[3] Common medical devices are stents, orthopedic prosthesis, defibrillators, contact lenses, dental implants, etc. Historically, materials that where intended to be used with the human body had to be as inert as possible, in order to avoid any (undesired) reaction of the body towards it. However, it rapidly turned out that it was even more promising to control the resulting interactions of the biomaterial with the body, and to be able to trigger specific physiological processes. In the past decades, a myriad of methods to provide initially inert materials with specific physical and chemical properties (and hence bioactivity) have flourished, and dramatically evolved, as a result of the most simple modifications to fabrication of nanostructured functional materials.[4–7] Among others, the deposition of proteins at the surface of a material is of particular interest. Indeed, proteins are one of the building blocks of the living organisms. In the human body, they perform most of cell processes, and are key to the structure, function, and regulation of the body's tissues and organs. They represent a class of biomolecules of choice for the creation of bioactive materials. Surface engineering by immobilization of proteins has led to groundbreaking advances in many scientific fields, going beyond Williams' definition of biomaterials, including biomedical devices,[8–12] but also

cosmetics,[13] food packaging,[14–16] (bio)sensors,[17–20] drug delivery,[21–23] and biocatalysis.[24–26]

1.3. Proteins at interfaces

Proteins prefer interfaces. If one had to remember one basic principle regarding the interactions of proteins with interfaces, it could be as simple as that. In fact, it is more challenging to prevent proteins to adsorb on a material's surface than the contrary.[27] One main consequence of this attraction of proteins for interfaces is the undesired biofouling (by proteins or other biomolecules) of surfaces encountered in many applications, including biomedical devices.[28,29] However, this characteristic can be turned into a major advantage if, in opposition to prevent biofouling, one would want to biofunctionalize an object by adsorbing proteins on its surface, to provide it with a targeted biological function.

1.3.1. On the nature of proteins and their spontaneous adsorption

To understand why proteins prefer interfaces to being free in solution, we must first shortly describe them. In their native state, proteins are complex and 3D-structured biomolecules **(Fig. 1.1)**.[30,31] They are composed of 20 different amino acids, linked together to form a linear polypeptide chain, that is the primary structure. Driven by internal interactions, mostly hydrogen bonding, parts of the linear amino-acid

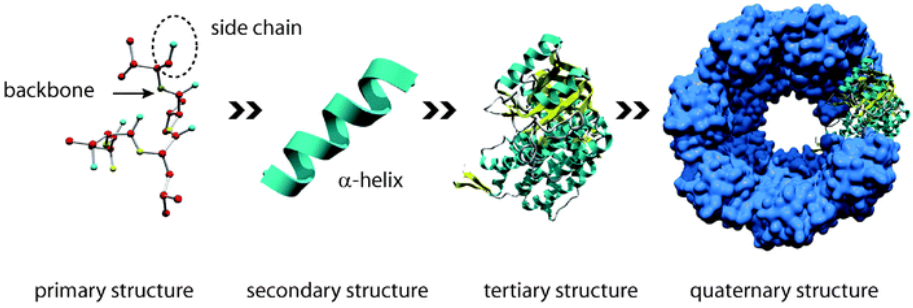


***Figure 1.1**. Illustration of the four levels of structural organization of a protein. The primary structure is the amino-acid sequence. The secondary structure corresponds to the presence of local stable arrangements, such as α-helix or β-chain (mainly stabilized by hydrogen bonding). The tertiary structure describes the folding of the protein (driven for example by hydrophobic interactions); it describes its overall shape. The quaternary structure comes into play if the protein is composed of several subunits. It describes how they are arranged one to another. Taken from Ref. 31.*

backbone may fold to adopt characteristic secondary structures, e.g. α-helices or β-sheets. These secondary structures are further precisely arranged in space, to provide the protein with its tertiary structure (protein folding). A quaternary structure may occur if two or more proteins (then called sub-units) are held together to form a larger protein complex. For future implications, it is important to note that the tertiary structure folding forces most of the hydrophobic side groups of the amino acid residues to aggregate and be buried together in the interior of the protein, to limit contact with water.[32] Consequently, polar and charged amino acid residues are predominantly present on the exterior of the molecule.

The amino-acid composition of a protein determines its physico-chemical properties, as they all display specific features, for example charge, acidity or hydrophobicity.[33] The protein's activity is closely related to its structure. When folded in its correct 3D structure, the protein is said to be in its native state, and is usually bioactive in this form. Any conformational change may affect protein activity. Hence, irrespective of the immobilization method, the process has to prevent the proteins from being structurally affected, in order to produce a bioactive coating.

When proteins in solution are in contact with a solid surface, they tend to spontaneously accumulate at the interface.[34] This observation implies that the process of protein adsorption is accompanied by a decrease of the system's Gibbs free energy (G) (**equation 1.1**):[35]

$$\Delta_{ads}G = \Delta_{ads}H - T\Delta_{ads}S < 0 \qquad (1.1)$$

Where H, S, and T are respectively the enthalpy, entropy, and absolute temperature, while Δ_{ads} is the variation of the thermodynamic functions of state resulting from the adsorption process. According to Norde, who pioneered the investigation of protein adsorption in the early 70s, three factors are predominant for the outcome of this equation, and so are key to predict the adsorption of a protein on a surface: (i) changes in the hydration state of both the protein and the surface on which the adsorption takes place, (ii) electrostatic interactions between the protein and the surface, and (iii) rearrangements in the protein's structure.[33] Based on these criteria, conditions in which the adsorption was favored or not were defined. Therefore, this made possible the prediction of the likelihood of an adsorption experiment to take place efficiently or not.[36] The conclusions of Norde's work are shown in **table 1.1**. Proteins that are prone to denaturation (labile) tend to adsorb on any surfaces, as they find a way to reorganize

themselves to minimize their surface energy. Proteins that are unlikely to unfold need to be stabilized trough favorable interactions that do not require denaturation. On hydrophobic surfaces, the entropic gain (release of water molecules) is usually sufficient to promote protein adsorption. On hydrophilic surfaces, the adsorption needs to be also driven by favorable electrostatic interactions. Even though these concepts remain valid today, protein adsorption is nonetheless still a very active field of research, and innovations are often brought so that the field is in constant evolution.

Table 1.1*. Scheme of prediction of adsorption of proteins at interfaces, by Norde. Reproduced from Ref. 36.*

Scheme to predict whether ("yes") or not ("no") proteins adsorb at surfaces				
Protein	Surface			
	Hydrophobic		Hydrophilic	
	+	-	+	-
Stable structure				
+	Yes	Yes	No	Yes
-	Yes	Yes	Yes	No
Labile structure				
+	Yes	Yes	Yes	Yes
-	Yes	Yes	Yes	Yes
The "+" and "-" signs refer to the net electric charge of the protein and the surface.				

Spontaneous adsorption is a very straightforward method to immobilize proteins on a surface, and has been widely used for multiple purposes. Yet, it has several drawbacks that prevent it to be used in certain cases of for some applications. These limitations are highlighted in the following section.

1.3.2. Drawbacks and limitations of spontaneous adsorption

As was mentioned earlier, proteins are composed of amino acid residues, whose pending groups may be either polar or non-polar. The non-polar residues usually reside in the core of the folded protein, to minimize contact with the surrounding polar water molecules. However, the main driving force that promotes adsorption is the entropic gain, originating from the removal of water molecules at the surface of the adsorbing proteins as well as at the surface of the sorbent material, as shown in **Figure 1.2**.[35] To further maximize the non-polar interactions, the protein may unfold in the

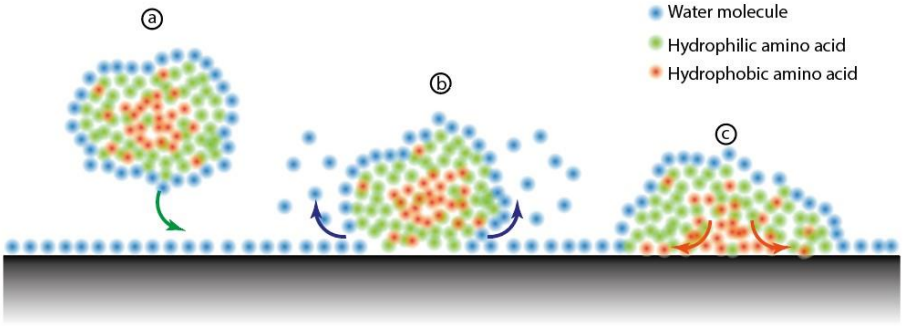


Figure 1.2. *Illustration of the three main steps leading to protein adsorption. (a) Protein diffusion to the surface. (b) Protein adsorption and dehydration. (c) Protein denaturation. Adapted from Ref. 50.*

course of the adsorption (**Fig. 1.2**), to expose its non-polar region to the surface, therefore gaining stability.[37,38] In this case, the adsorption process leads to denaturation of the proteins, which in turn may alter or completely inhibit the proteins' biological activity.[39–41] Conformational changes may also arise from dewetting when the liquid thin film resulting from the adsorption is dried. Driven by capillary forces, protein molecules may rearrange at the surface, potentially causing structural modifications. Apart from this main concern of altering the bioactivity, other difficulties may be encountered with spontaneous protein adsorption from solution such as: (i) a difficult tuning of the deposited quantity, which is usually restricted to one monolayer;[42] (ii) a lack of spatial distribution control, which mainly rely on substrate patterning approaches;[43–45] (iii) its limitation to "water-compatible" substrates; (iv) the fact that it does not work with substrates that do not spontaneously trigger the adsorption, (v) the difficulty to build complex multilayers made of different biomolecules.[46] To tackle some of these issues, a myriad of alternative adsorption techniques have been proposed. They include the so-called layer-by-layer technique[47–49], which became very popular, and a vast range of covalent immobilization approaches. The latter were originally relying on modified substrates only,[50] but more recent compelling studies report modifications of the protein itself to promote a controlled adsorption.[51–57] Other original strategies have been proposed such as the ones relying on the adsorption of protein supramolecular assemblies.[58–60] All the discoveries and contributions brought to the protein adsorption field have allowed to overcome a series of issues initially encountered with spontaneous adsorption from solution, but no method has yet appeared as the revolutionary way to immobilize proteins at interfaces. Mainly, the fact that all the proposed methods are performed

in solution presents inherent obstacles. Therefore, the development of alternative biofunctionalization methods offering a fine control over the resulting biofilm in terms of total protein amount, thickness, activity, patterning, mono- or multilayers composition and organization, and protein-surface interactions are highly desired.

1.4. Preparative mass spectrometry

Among the innovative alternatives that were suggested to circumvent the disadvantages associated with protein adsorption from solution, preparative mass spectrometry holds an important place as it rapidly proved to deliver promising results. In preparative mass spectrometry (pMS), the mass-selected ion beams that are generated, usually to perform analysis, are manipulated and directed towards a surface, where the material is collected. This process allows a controlled ion deposition on surfaces, thereby allowing the preparation of interfaces for material design and synthesis. Depending on the kinetic energy given to the ions, their interactions with the surface upon landing may considerably differ. Therefore, pMS was divided in mainly two sub-categories that are soft- and reactive landing. Soft-landing is defined as deposition that occurs with a translational kinetic energy that precludes the fragmentation of the incident species.[61] In contrast, reactive landing often implies fragmentation of the deposited species, and formation of new covalent bonds between the projectile ions or their fragments and the surface.[62] The properties of the deposited ions as well as those of the surface largely affect the efficiency of the reactive landing. Reactive landing presents advantages of its own, and as its softer alternative, has been used for highly-controlled preparation of materials for a variety of practical applications and fundamental investigations.[62–67] Yet in the case of our interest, that is the deposition of proteins, soft-landing is obviously preferred, in order to minimize the damage conferred to the biomolecules. The next section will briefly describe soft-landing, how it works, its benefits but also its limitations, with a focus on the deposition of proteins.

1.4.1. Soft-landing for the deposition of intact biomolecules in the gas phase

Soft-landing was first introduced by Cooks and co-workers in 1977.[68] Since these seminal experiments, the technical evolution of the ion sources, allowing working under milder and milder conditions, has led to

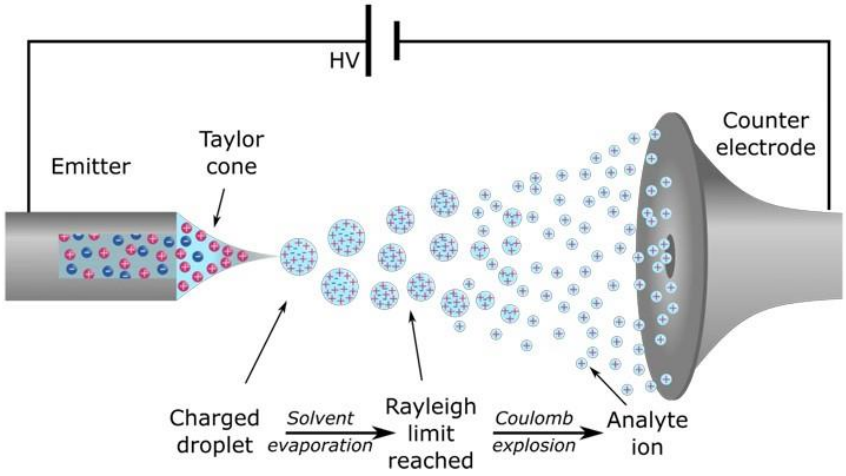


***Figure 1.3**. Schematic representation of an ESI source. Only the part between the emitter and the skimmer is shown. That is where the analyte ions are formed.*

groundbreaking progress in the field of ion soft landing. This field is vast, encompasses many applications, and therefore cannot be thoroughly discussed within this introductory section, but extensive reviews are available in the literature.[61,62,69–75] Soft-landing consists in a forced but gentle deposition at interfaces, a process wherein the integrity of the deposited ions is not to be modified. To ensure this crucial aspect of the method, the gas-phase ions have to be delivered to the surface with kinetic energies in the hyperthermal range, which is 1-100 eV.[76] To achieve such soft conditions, the most popular ion source is electrospray ionization (ESI), illustrated in **Figure 1.3.**

A schematic representation of a typical instrumental set-up to perform soft-landing is presented in **Figure 1.4**.[77] In essence, it resembles a normal ESI-MS apparatus, in which the analyzer is replaced by a material to be coated with the compound of interest. Using an ESI source made possible the transfer of intact biomolecules, and soon proteins. For the latter, it was known for a long time that they could survive the ionization process under vacuum, as their intact molecular ions could be detected in classical ESI-MS experiments. What was not clear at the time was whether the structural integrity of the proteins could be preserved during the process. In other words, the question of the biological activity of the soft-landed proteins had still to be answered. Typical mass spectrometry experiments do not deliver sufficient information on the structural aspect of the molecules to gain insights into the tridimensional conformation, and it would not be so

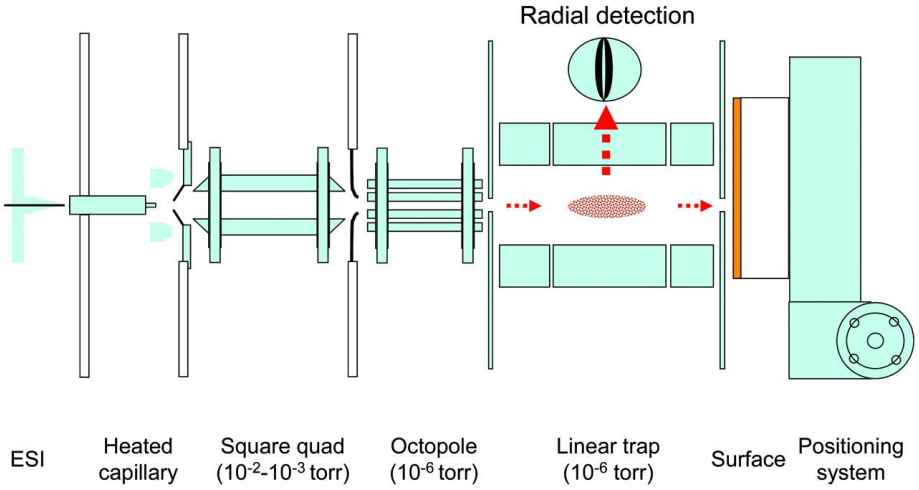


***Figure 1.4**. Instrumental set-up developed by Cooks and co-workers to use an ESI source to perform soft landing experiments. Taken from Ref. 77.*

relevant to coat surfaces with inactive proteins. In 2003, Cooks and his team shed light on the tricky structure/activity issue. They built the instrument presented in **Figure 1.4**, and used it to transfer a series of proteins. Among them were two enzymes, lysozyme and trypsin, which both retained their activity after being soft-landed.[77,78] In the following years, Volny *et al.* also demonstrated the retention of activity for soft-landed enzymes.[79] Around the same period, biological objects as large as viruses were shown to be soft-landed intact.[80] From there, ion-soft landing became a valuable alternative approach for the immobilization of proteins and other biomolecules or even biological objects at interfaces.[81] As soft-landing allows the manipulation of the ion beam, the molecules/particles of interest can be deposited at a precise location on the surface. Consequently, soft-landing was primarily used for the preparation of proteins micro-arrays, to be used in applications such as automated analysis for biological activity, biologically active protein chips, biosensors, and other functional materials.[82–89] Soft-landing is still an attractive tool under development today, and keeps on being improved over the years. Latest contributions report on the possibility to image single molecules at interfaces,[90] to soft-land huge biomolecules (>MDa),[91] but also the development of improved technologies promising for the fabrication of miniaturized instrumentation,[92,93] more efficient deposition[94] or the possibility to perform ambient soft-landing.[95] It seems that the first commercial instruments for soft-landing are about to enter the market.[96]

Vacuum-based approaches offer the possibility to largely expand the scope of applications related to protein deposition at interfaces, and are a valuable alternative to traditional adsorption-based techniques. They allow some of the barriers imposed by the presence of water to be overcome, and further lead to a more controlled deposition. In particular, owing to their outstanding mass resolution, mass spectrometry instruments are of great interest as they allow the deposition of precisely mass-filtered ions, even starting from complex mixtures, yielding pure coatings. In addition, the ion beam can be precisely focused, so that micro-arrays of ions can be deposited with a very good spatial resolution. Nonetheless, ion soft-landing has not yet become a widespread technique for the preparation of bioactive surfaces. The reasons for that is that it still suffers a few drawbacks. The main issue is the relatively low efficiency inherent to the ionization (especially true for large biomolecules such as proteins), the ion transport and ion collection processes. This leads to beams with poor current intensity and thus extremely low deposition rates, making difficult the construction of mono- and multilayers on large surface areas within reasonable experimental time. In addition, the accumulation of like-charges at the interface may induce undesired charging effects, notably with insulating collectors, and for proteins, ions with multiple charges may lead to denaturation during or upon deposition. It is expected that overcoming these barriers will lead to the emergence of numerous unforeseen applications. While improvement of soft-landing capabilities are expected in the future with the advent of novel technologies,[97] it remains highly desired to explore other new horizons for the deposition of proteins.

The development of an innovative solvent-free approach for the immobilization of proteins at interfaces is the core work of this thesis. A vacuum-based soft-landing alternative is proposed, in which ions as well as neutral species are deposited on the surface. Before getting into more details regarding this new approach, and to allow the reader a smooth reading and understanding, a few theoretical bases must first be laid. On the one hand, the proposed technique relies on the use of large cluster ion beams, and on the other hand, a time-of-flight secondary ion mass spectrometry instrument was the key equipment to develop the method. It was used for both the deposition of the biomolecules and the subsequent analysis/characterization of the coated surfaces. Gas cluster ion beams and time-of-flight secondary ion mass spectrometry will therefore be detailed in the following sections.

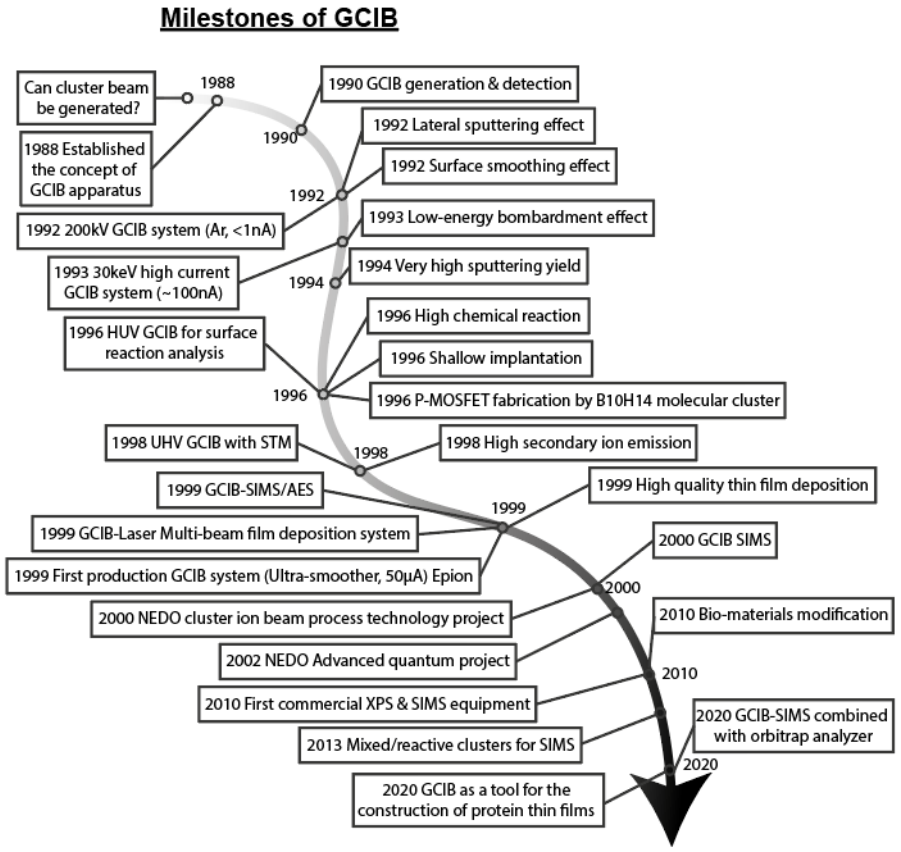


Figure 1.5. *Time line of some of the main contributions to the field of GCIB. Adapted from Ref. 130.*

1.5.Gas cluster ion beams (GCIB), with a focus on SIMS

Since the first observation of particles moving through a discharge tube at the end of the nineteenth century, the field of ion beams has evolved dramatically (**Fig. 1.5**). Driven by the potential applications that could arise from manipulation of ion beams with respect to the preparation and analysis of surfaces, efforts of many researchers, rapidly followed by industries, led to an extensive development of the theoretical knowledge as well as of the technologies and equipment associated to ion beams. Approximatively a century after the discovery of atomic ion beams, the field experienced quite a revolution as gas cluster ion beams (GCIB) were introduced. These clusters, consisting of a few hundreds to a few thousands of atoms, display unique features that expand the scope of conventional atomic and molecular ion beams, meeting the nanoscale requirements associated to more recent

applications. Today, both atomic and cluster ion beams are well-established technologies, with many associated applications, up to the industrial scale in some cases. They include ion implantation for doping of semiconductors, processing of surfaces, atomic level etching, sputtering, ion-assisted film deposition, shallow junction formation, ultrasmooth surface creation and other (low-damage) thin surface modifications. Research on ion beams have also permitted new advances in surface analysis techniques such as X-ray photoelectron spectroscopy (XPS) and time-of-flight secondary ion mass spectroscopy (ToF-SIMS), which have encountered great success, but also of less common analytical techniques including electrospray droplet impact (EDI) SIMS, desorption electrospray ionization (DESI) MS and massive cluster impact (MCI) SIMS.

1.5.1. Atomic ion beams: early developments and limitations

The very first experimental work related to ion beams is attributed to Goldstein, when in 1886, he observed particles moving through a discharge tube.[98] He named those beams of particles "canal rays". A few years later, Wien showed that the particles were in fact positively-charged ions, as he was able to deflect the beam using strong magnetic fields.[99,100] The ions were accelerated toward and through a perforated cathode, under low pressure conditions. These seminal observations mark the starting point of the research on ion beams. The following decades resulted in extensive advances in ion beams technology, which were made possible as the theoretical knowledge was always accompanied by crucial equipment development. In 1907, Thompson established the basic concept of an ion beam apparatus, still valid in industry nowadays.[101,102] It consisted in a gas

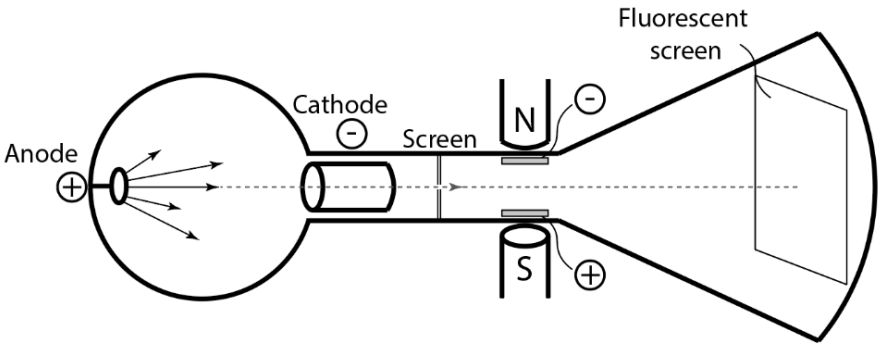


Figure 1.6. *Joseph J. Thomson's apparatus, as was depicted by George Gamow. Reproduced from Ref. 130.*

discharge ion source, an electrostatic deflection and a magnet, as depicted in **Figure 1.6**.[103]

The first applications were demonstrated by Shockley around 1950-1960, who used ion beams to perform ion implantation in semiconductors. As a consequence, changes were induced in the conductivity, and the performances of semi-conductors were improved.[104] Not long after, in 1971, Rose founded Extrion Corporation, the first company aiming at the development of ion implantation devices, initially for semiconductor doping.[105–107] Atomic and molecular ion beams proved to be very useful for a wide range of surface processing applications including hardening and improving tribological properties of surfaces, ion implantation, ion-assisted film deposition, sputtering and etching. However, recent technological advances involved miniaturization of devices to the nanoscale, and thus imply far better resolution of the surface manufacturing, to the atomic level. For examples, ultrasmooth surface fabrication, shallow junction formation, low-surface-damage processing or atomic-level etching have become basic needs for the production of advanced electronic, magnetic and optical devices. As a matter of fact, it turned out that atomic and molecular ion beams were not suited to meet such requirements. Indeed, these beams, usually operated with energies ranging from keV to MeV, penetrate quite deeply into the target material (from tens of nanometers to microns), and therefore induce in-depth modifications to the treated material. However, the field of ion beams opened up for new perspectives in the 90s, when gas cluster ion beams were introduced as a new tool for surface processing.[108] This technology has been extensively developed and made popular by Yamada and a few co-workers.[109]

1.5.2. Origins of cluster ion beams

The first milestone towards discovery and further formation of cluster ion beams dates back to 1888, and lies in the work of de Laval, who investigated the formation of supersonic gas flow through small apertures having a converging-diverging structure. Known as a de Laval nozzle, it remains widely used today in the process of gas clusters formation. Initially, these nozzles were designed to increase the speed of steam jets in turbines. In the 30s, researchers observed supersaturation and subsequent condensation of gas and vapor upon investigation of supersonic expansion through such nozzles.[110,111] In 1956, Becker *et al.* reported for the first time the observation of clusters formation by the condensation of vapor as it

expands through a miniature nozzle into vacuum.[112] A few years later, Henkes published the first cluster ion mass spectrum, demonstrating the existence of ionized species.[113] These experiments represent the beginning of research about gas clusters.[114] Since then, their unique features and promising properties regarding surface processing led to a steady growth in the enthusiasm surrounding cluster beams. Other cluster source candidates were at some point considered,[115–118] but were systematically discarded in favor of more efficient supersonic expansion.

1.5.3. Gas cluster formation by supersonic adiabatic expansion

When a gas expands from a high pressure source into vacuum through a small orifice, its random thermal energy is converted into directed kinetic energy, yielding a supersonic flow. As it accelerates, the gas cools adiabatically. Under optimal pressure and temperature conditions, the expanding gas becomes supersaturated. At that point, homogeneous condensation of the gas occurs, leading to the formation of clusters, and so-called cluster beams.[112,119] The mathematical/physical details associated to cluster formation are beyond the scope of this introductory section, but have been described in multiple publications, review articles and books.[120–126] In the course of the adiabatic expansion, and within the supersaturated gas flow, cluster generation is initiated by dimer formation, which takes place during tri-atomic collisions, due to energy and momentum conservation.[120] Once initial dimers are formed, further cluster growth may arise following two distinct pathways that usually follow each other in time: 1) monomer addition, which occurs as long as the ratio of atoms to clusters is high, and 2) cluster aggregation, which becomes dominant when the ratio is switched in favor of clusters. In a cluster, atoms (or molecules) are held together by van der Waals forces. The four most important parameters to ensure a proper cluster formation are stagnation pressure and temperature conditions, as well as the nozzle diameter and geometry. Regarding the first two parameters, it was demonstrated that the condensation

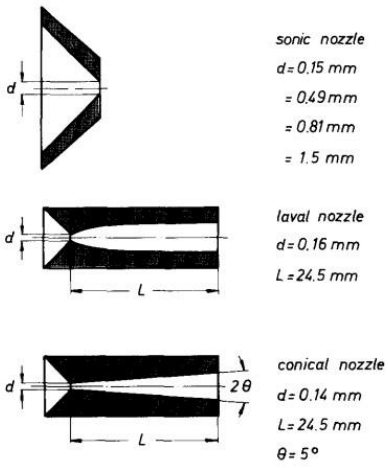


Figure 1.7. *Examples of nozzles that were used to generate large gas clusters.*[118]

process is favored (producing higher current intensity beams, with clusters having higher number of constituent atoms) when the pressure of the source is kept highest, and its temperature lowest.[127] Regarding the nozzle, several studies were conducted to determine the most efficient diameter and size.[119,120,128,129] To generate large clusters, nozzles with a converging-diverging shape, such as conical or de Laval nozzles (**Fig. 1.7**) are preferred. The orifice diameter can vary between 0.01 and 0.6 mm but is usually maintained rather small. With such nozzles, the neutral cluster beam intensity (*I*) can be described by **equation 1.2**:[119]

$$(I) \propto P_0 D \left(\frac{T_b}{T_0}\right)^{(\gamma/(\gamma-1))} \qquad (1.2)$$

Where γ and T_b are the specific heat ratio and the boiling point of source gas, respectively, P_0 and T_0 are the source pressure and temperature, respectively, D is the nozzle throat diameter. In the 90s, Yamada (Kyoto University) incorporated these nozzles in equipment that had capabilities for cluster ionization and transport, and marked the emergence of the gas cluster ion beam (GCIB) concept.[130]

1.5.4. Gas cluster ion beam equipment

A typical GCIB apparatus is shown in **Figure 1.8**. To ensure optimal vacuum conditions throughout the entire process, it is composed of several chambers, with multiple pumping devices. In the first place, a neutral gas cluster beam is formed in the nozzle chamber, as previously described. The beam then goes through a skimmer, another small orifice, whose role is to keep only the cluster-containing core of the gas stream, and to filter the more

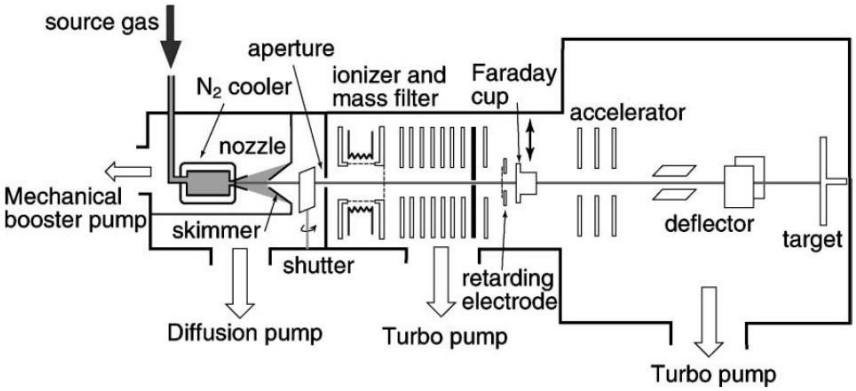


***Figure 1.8**. Typical set-up of a GCIB instrument. Taken from Ref. 130.*

external atomic/molecular flow. To further allow beam manipulation (acceleration, focusing), the neutral clusters have to be ionized. This is achieved by electron impact, after the electrons were emitted from a tungsten filament and accelerated towards a cylindrical anode. Once ionized, clusters can be extracted and accelerated using a series of electrodes with typical potentials of 2-30 kV. They can also be mass-filtered, which is most often achieved with a Wien filter.[131–133] Finally, electrostatic lenses are employed as deflectors to focus and raster the cluster beam.

1.5.5. Unique features of cluster ion beams versus atomic ion beams

Cluster ion beams present many advantages over atomic ion beams in terms of beam handling. Indeed, to reach the realm of low-energy ion-solid interactions (sub 1 eV < E < few hundreds eV), atomic ions must be accelerated using very low extraction voltages (or slowed down). However, extracting ions with energies of only a few hundreds of eV is very difficult, and further manipulation of the beam is challenging.[134–136] In order to prevent undesired space-charge effect, a balance has to be found between the beam current intensity and the beam energy, or space-charge compensation must be implemented.[137,138] In fact, as the energy of the beam is lowered, coulombic repulsion among ions in the beams becomes significant, resulting in beam expansion, and ultimately beam blow-up. Beam expansion induces ion loss on walls and electrodes, and thus loss of current intensity, as well as poor focusing. The use of cluster ion beams solves most of these problems resulting from space-charge effect.[109,139] As will be discussed later, the important parameter that governs the interactions of a cluster with a solid is the energy of each individual constituent atom of the cluster. Therefore, to keep the same energy per atom in a cluster of size N as in an atomic beam, the extraction voltage can be N times higher. Another unneglectable advantage ensuing from cluster ion beams is a less pronounced surface charging effect when a material is bombarded. For each charge, a cluster transports N atoms, so that an N-fold reduced current intensity is required to bombard the surface with the same number of atoms.

1.5.6. Surface processing and cluster-matter interactions

In a cluster, the total kinetic energy is distributed over each constituent atom. According to **equation 1.3**, each individual atom in the

cluster is bearing a small fraction of the beam energy, so that it can be considered as a low energy particle.[140]

$$E_c = E_0\left(\frac{M_c}{M_t}\right) \tag{1.3}$$

Where E_c is the resulting energy of the atom/small cluster after impact with the surface, E_0 is the total energy of the initial cluster prior to impact, M_c is the mass of the fragment/atom, and M_t is the total mass of the initial cluster. Therefore, when a cluster impacts a surface, it results in a multitude of interactions between low energy constituents and the surface, providing polyatomic ions their unique cluster-matter interactions. To visualize what happens in the event of a cluster impinging on a solid surface at the microscopic scale, Yamada compared it to the event of a meteor hitting the earth surface at the macroscopic scale (**Fig. 1.9**).[130] In fact, in both cases, similar craters are formed, with a rim from which material is ejected.[141] This observation reveals how much cluster ion impacts and interactions with solid materials differ from that of atomic ion impacts. For an equivalent total beam energy, the penetration depth is greatly reduced, as each resulting atom from the cluster retains a small amount of energy. This is confirmed by molecular dynamic simulations, as can be seen in **Figure 1.10**.[142–144] The energy, and consequently the induced damage are confined in the first nanometers of the solid surface, leaving the subsurface region unperturbed. Other molecular dynamic simulations calculated that during crater formation, transient temperature and pressure could reach values of respectively thousands of degrees and tens of gigapascals.[141] Such high temperature and pressure induce the generation of a shock wave in the material upon cluster impact.[145] This

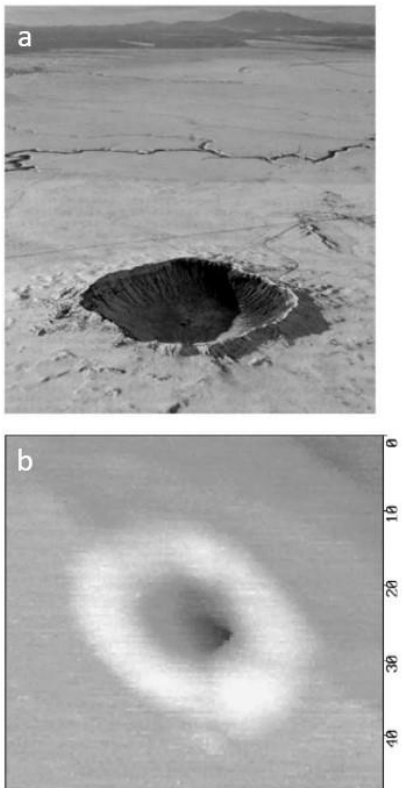


***Figure 1.9**. Macroscopic and microscopic views of craters: (a) meteor crater in northern Arizona (1.2 km in diameter) and (b) STM image of a crater on a gold surface after Ar cluster ion impact (30 nm in diameter). Taken from Ref. 130.*

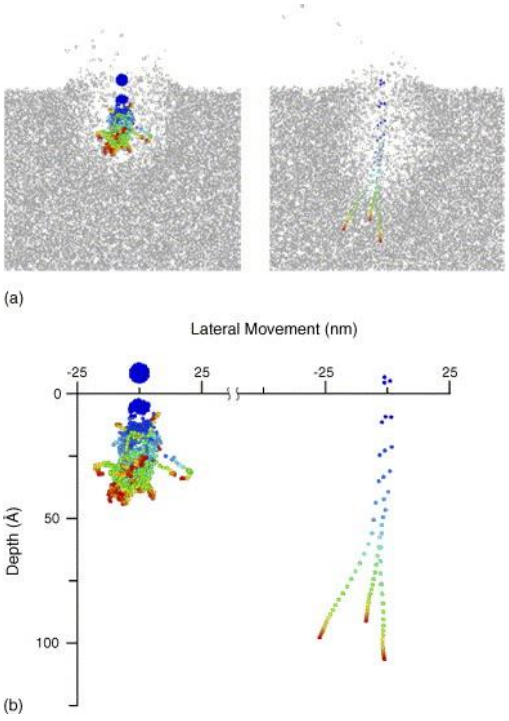


Figure 1.10. *Gold cluster and fullerene impacts. Vertical cross-sections (2 nm) of a water ice sample bombarded by Au_3 and C_{60} showing the successive positions of the projectile constituents up to 1 ps. (a) Left, C_{60} and right, Au_3, impacts on the water ice sample. (b) Representation of their lateral and depth movement in the sample. The more energetic gold atoms penetrate deeper in the solid. By Russo and Garrison.*[144]

phenomenon leads to physical processes that were not observed in the case of atomic bombardment of surfaces, and paved the way to a series of applications that could not be envisioned before. Among others, the low energy collisions and small penetration depths led to shallow implantation, directional high sputtering yield led to dry etching and surface cleaning/smoothing, and dense energy deposition facilitated chemical reactions at the surface, leading to new opportunities for surface modification and thin film formation.[130]

Over the years, manipulation of mono- and polyatomic ion beams has led to a series of industrial applications. In particular, the sputtering of molecules from a surface upon bombardment by ion beams was rapidly seen as a potential way of investigating the chemical nature of surfaces. Indeed, the ejected atoms, fragments or molecular species emitted from a surface are characteristic of the chemical composition of the probed material. As it was presumed that the emission takes place only in the first few top layers of the material, this could provide a surface-sensitive analytical technique. As soon as it was discovered that a fraction of the emitted species was ionized during the emission process, it opened new perspectives as the desorbed ions could then be manipulated, e.g. accelerated and sent to a mass analyzer. In the early 70s, the acronym SIMS, standing for secondary ion mass spectrometry, was coined by Benninghoven, and marked the beginning of surface sensitive mass spectrometry using ion beams. SIMS is defined as the mass spectrometry of ionized particles which

are emitted when a surface is bombarded by energetic particles.[146] The following sections are describing the SIMS technique and its evolution, from the first discoveries to some of the latest technological breakthrough that make SIMS a very attractive technique and an active field of research.

1.6. Time-of-Flight Secondary Ion Mass Spectrometry (ToF-SIMS)

In the realm of surface analysis, secondary ion mass spectrometry (SIMS) has become one of the most powerful and popular method owing to its outstanding performances in terms of surface sensitivity, chemical specificity, mass and spatial resolution. The SIMS technique finds its roots in the work of Benninghoven in the late 1960s when he started investigating the emission of secondary ions from solid surfaces.[147] In the beginning, monoatomic ion beams were employed. Due to the discoveries of alternative sources inherently more efficient in many ways, monoatomic ion beams are scarcely used today. However, the basic principles of the SIMS technique will be described as they were discovered, in the case where a monoatomic beam is used to bombard the surface. Other primary ion sources including small and large clusters, polyatomic and molecular ions were later developed; they will be covered further in the introductory section.

1.6.1. Basic principles and static limit

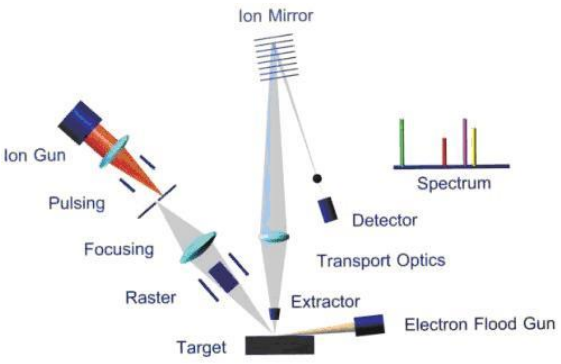


***Figure 1.11**. Schematic illustration of a SIMS experiment, from the formation of the primary ion particles to the generation of a mass spectrum. Taken from ION-TOF (https://www.iontof.com/).*

A basic SIMS experiment can be described as follows (see **Fig. 1.11**): an energetic primary ion strikes a sample surface, resulting in the desorption of so-called secondary species. Most of these ejected particles are neutral, yet a small fraction of them is ionized during the ejection process. These positive or negative secondary ions can further be analyzed via mass

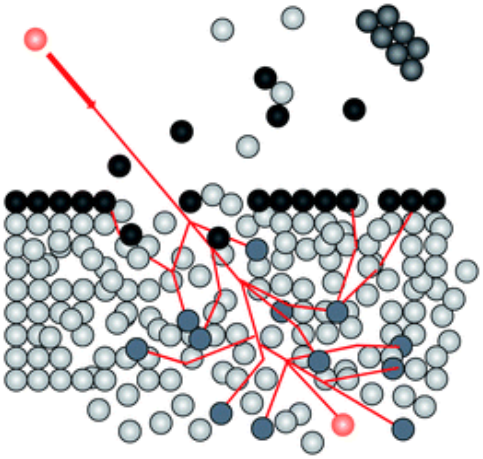


***Figure 1.12**. Representation of the billard-ball-type collision cascade occurring in the solid sample surface upon impact by the primary ion particle (red sphere). A fraction of the emitted species is ionized, and are called secondary ion particles.*

spectrometry. The key event of a SIMS measurement is undeniably the sputtering process, leading to the formation of the secondary ionized species that will further be mass analyzed. Conceptually, it can be described in a relatively simple way as a collision cascade occurring between the atoms of the solid sample being analyzed, as illustrated in **Figure 1.12**.[148] This billiard-ball-type collisional process is primarily triggered by the direct collisions between a focused ion beam (the primary ions) and the surface atoms of the solid and then extended by successive collisions between atoms in the sample. Carried through these successive collisions, a part of the energy ultimately returns to the surface. In the case where the amount of energy is sufficient, atoms and molecular fragments may very well overcome the surface binding energy, and leave the surface of the solid sample. The final collision being of relatively low energy, over 95% of the secondary particles are emitted from the top two layers of the sample, which makes ToF-SIMS a very sensitive surface analysis technique (information depth <20 Å). It is important to keep in mind that as the atoms of the sample receive energy from the collisions, they are set in motion. This causes a phenomenon called “molecular mixing”. Consequently, atoms that were initially buried deeper under the surface may end-up in the close vicinity of the surface, and *vice-versa*. This may have an influence on the surface sensitivity of the measurement. While most of the ejected particles are neutrals, a small fraction (10^{-6}-10^{-1}) is ionized in the course of leaving the surface. Depending on their electronic configuration, they are either positively or negatively charged. Mass spectra can therefore selectively be obtained in both polarities.

In SIMS, the primary ion beams usually have a high energy, typically ranging from 1 to 25 keV, which is much more than typical bond energies. The bombardment of surfaces with such energetic ions thus necessarily

induces fragmentation, not only in the first 2-3 layers, but also in the deeper ones, leading to destruction of the molecular integrity of the sample. In essence, SIMS is a destructive analysis technique. Interestingly, it was observed that in the close vicinity of the bombarded area, small fragments and (mostly) atoms resulting from an extensive fragmentation were emitted. As the collisions move away from the impact point, a fraction of their energy is dissipated in the solid, and they become less energetic, leading to emission of larger molecular fragments.[149] However, it is possible to circumvent this undesired progressive sample degradation effect and retain molecular integrity for the whole duration of a spectrum acquisition by keeping the primary ion dose very low. In fact, it was shown that when the dose of primary ions does not exceed 10^{12}-10^{13} ions/cm^2, the likelihood of a same spot to be struck by more than one primary ion drops to nearly zero. Under this so-called static limit, less than 1% of the surface receives an ion impact, and less than 10% of the uppermost layer is consumed within the time scale of an experiment. In this regime, for all practical purposes, the bombardment-induced chemical damages become negligible, and it is considered that every ion emitted from the solid sample arise from an unperturbed area. It is important to note that if 10^{13} ions/cm^2 gives a rough approximation of the static limit, the actual ion dose required to exceed the static limit may very well vary as it depends on both the primary ions used and the nature of the sample being analyzed.[150]

In contrast with “static SIMS”, higher ion doses can be operated to perform “dynamic SIMS”. In these experiments, the ion beam erodes the material surface much faster, thus penetrating the bulk of the sample being analyzed. The successively acquired mass spectra thus reflect the chemical composition of the sample layer after layer, defined as a depth profile. However, one must keep in mind that as damage is continuously generated in the sample, the molecular information is rapidly lost. Those measurements are performed when the elemental composition is investigated, and mainly concern inorganic materials. In ideal samples, atomic mixing can be attenuated to a few layers, and sub-nm depth resolutions have been reported. Yet this cannot be generalized to all samples, and these effects may have a strong influence on the resulting depth profile, to a point where it does not mirror the initial chemical distribution of the sample anymore. Molecular depth profiling of organic samples has been made possible with the emergence of polyatomic cluster ion source in the beginning of this century, as will be discussed later.

1.6.2. The SIMS equation, sputter yield and ionization probability

SIMS is concerned with the analysis of secondary ions emitted from a surface. To be analyzed, a species, either mono- or polyatomic, must be both sputtered from the material, and ionized. These two parameters are fundamental for the determination of the secondary ion yield of a species. They largely dominate the outcome of the SIMS basic equation (**eq. 1.4**), that is:

$$I_m = I_p y_m \alpha^+ \theta_m \eta \qquad (1.4)$$

Where I_m is the secondary ion current of species m, I_p is the primary particle current, y_m is the sputter yield, α^+ is the ionization probability to positive ions (it can be replaced by the ionization probability to negative ions α^-), θ_m is the fractional concentration of the species m in the analyzed layer and η is the transmission of the analysis system.

The sputter yield of a species m (y_m) is defined as the total amount of particles of the species m emitted from the surface, regardless of their charge state, per primary ion impact. The overall sputter mechanism is fairly well understood (described earlier as a collision cascade), even though quantitatively, the factors influencing it are numerous. They include the primary ion particle, and more precisely its mass, charge, and energy. The incident angle of the beam also plays an important role. Of course, the sputter yield greatly depends on the nature of the analyzed species, and on its binding strength to the surface. In the case of intact molecular species, the interactions with the surface could be weak non-covalent ones, such as hydrogen bonds, van der Waals or hydrophobic interactions. In the case of fragments, the more bonds need to be broken to free the fragment from the molecule, the less favored its desorption will be. It will then also depend on the degree to which internal energy can be stored by the molecule before it becomes fragmented.

The ionization probability is a far more complex and much less understood phenomenon that still raises many questions today. The precise time and location where ionization occurs in the course of the sputtering process remain unclear. Yet it is most likely that it takes place in the emission

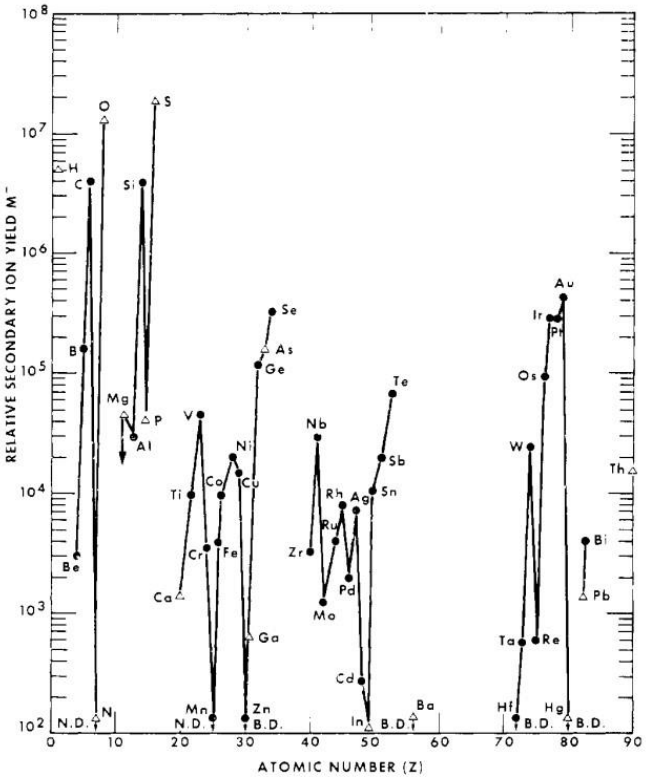


Figure 1.13*. Relative secondary ion yield of elements as a function of their atomic number. Taken from Ref. 151.*

region, within or just above the surface. The formation of secondary ions is strongly influenced by the electronic state of the surface, as it implies electron and/or cation exchange between species present at the surface. It has been shown that the positive ion yield of particular elements vary dramatically as function of their atomic number (**Fig. 1.13**)[151] and when compared to the same element in the form of their corresponding oxides (**Table 1.2**)[152] The mechanisms that lead to formation of ions are multiple, sample-dependent, and several probably take place simultaneously. They result from direct collisions either with the primary ion beam, or with energetic recoil atoms moving through the material. They encompass ejection of an odd electron, acid-base reactions, adducts formation, bond breaking with direct formation of ions (heterolysis), and probably many others. If often the exact ionization mechanism is source of controversy, it is however unanimously accepted that the chemical environment (the presence of other compounds) of the analyte drastically influences its

***Table 1.2**. Comparison of the ion yield for a series metallic elements, whether as clean metals or as metal oxides. Taken from Ref. 152.*

Metal	Clean metal M^+ yield	Oxide M^+ yield
Mg	0.01	0.9
Al	0.007	0.7
Si	0.0084	0.58
Ti	0.0013	0.4
V	0.001	0.3
Cr	0.0012	1.2
Mn	0.0006	0.3
Fe	0.0015	0.35
Ni	0.0006	0.045
Cu	0.0003	0.007
Ge	0.0044	0.02
Sr	0.0002	0.16
Nb	0.0006	0.05
Mo	0.00065	0.4
Ba	0.0002	0.03
Ta	0.00007	0.02
W	0.00009	0.035

ionization probability.[153] Known as the matrix effect, this adds a major complexity to the predictions and the understanding of the resulting mass spectrum. A compound could appear very intense in a sample in presence of another co-localized substance that promotes its ionization, or be completely suppressed in a second sample due to the presence of a substance that inhibits its ionization.[154]

1.6.3. Surface charging and electron flood gun

The bombardment of materials with ion beams (usually positive ions) may induce undesired charging effects at the surface. This happens when the probed material is intrinsically insulating, or when a conducting material is covered by a film that acts as an insulator. This is often the case when working with organic samples. Both the emission of secondary electrons and the accumulation of like-charge at the surface lead to a sudden rise of the surface potential, up to several hundred volts in few minutes. As a consequence, the positive secondary ions are emitted from the surface much faster, that is with a higher kinetic energy, which rapidly exceeds the

acceptance window of the analyzer.[155] To a lesser extent, the charging may only results in deformation of the peaks in the mass spectrum, thus degradation of the mass resolution. However, to a greater extent, it may rapidly lead to the complete loss of intensity in the spectrum. To prevent surface charging, one of the earliest solution, proposed by Briggs and co-workers, was to bombard the surface with an electron beam, in between successive secondary ion extraction pulses.[156,157] These low energy electrons allow the surface potential to return to neutral after each pulse of primary ions. The electron flood gun proved to be very successful, and is still widely used today.

1.6.4. Time-of-Flight (ToF) analyzer

Historically, the first SIMS instruments were equipped with magnetic sectors or quadrupole mass analyzers.[158] At the time, they were more affordable, and more readily incorporated into existing ultra-high vacuum (UHV) systems. However, the field rapidly evolved, and soon the quadrupole analyzers were replaced by more efficient time-of-flight (ToF) analyzers (even though quadrupoles and magnetic sectors are still in use on some instruments),[159] leading to the ToF-SIMS acronym, which is widely used throughout this manuscript. The two main advantages of ToF analyzers over their predecessors are a theoretically unlimited mass range, and a quasi-parallel mass detection that would directly improve the sensitivity.[160] Although recent efforts have led to the development of more powerful analyzers, such as the orbitrap, and their combination with a SIMS instrument, the ToF analyzer remains to date the most widespread mass analyzer on commercial SIMS equipment. Since all the experimental results presented in this work were obtained with a SIMS instrument equipped with a ToF analyzer, it will be the only described analyzer.

In reflectron-type ToF analyzers (**Fig. 1.14**), a bunch of secondary ions is accelerated near the surface region, as it enters a field-free flight tube. In this field-free region, the ions, having received the same kinetic energy, are separated based on their mass, as lighter compounds travel faster than heavier ones. Despite the identical acceleration for all ions, a spread in the flight times of ions having the same mass is usually observed, hence diminishing the mass resolution. This is due to the kinetic energy distribution of the ions leaving the surface. To reduce the impact of that kinetic energy

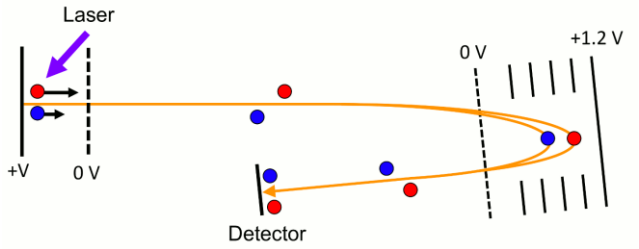


***Figure 1.14**. Schematic representation of a reflectron-type ToF analyzer.*

distribution, a reflectron was added. This two-stage mirror provides a second-order energy focusing, thereby reducing the spread in flight times and improving significantly the mass resolution.[161] In addition, this reflectron doubles the effective flight path, which also improves the mass resolution, within the same instrument size. As mentioned above, time-of-flight analyzers require a T = 0, a moment at which all ions start to travel through the field-free region. Therefore, these type of analyzers require a pulsed primary ion beam, in order to generate distinct bunches of secondary ions instead of a continuous emission. In some apparatus, the primary ion beam is continuous, and the secondary one is pulsed. The length/width of the primary ion pulses has an influence on the resulting mass resolution of the spectra. In modern ToF-SIMS instruments, the duration of the pulse may be reduced to the order of 1 ns. Yet one must keep in mind that reducing the pulse length to such values influences the experiment time (less secondary ions are generated) and may alter the spatial resolution.

1.6.5. Primary ion sources

There are tens of different primary particles that have been reported in literature for SIMS analysis. If some have not gone beyond fundamental research and preliminary experiments, other have led to groundbreaking advances and dramatically enhanced the scope of research associated with ToF-SIMS. This introduction cannot encompass all of them. Here, only a brief overview of the different available sources is given. The focus is set at presenting the most common sources that have endured over time and became popular for SIMS analysis and that are available on commercial instruments.

Initially, SIMS was developed using Ar^+ or Xe^+ as primary ion sources.[162,163] Even though far from the best candidates as primary particles, these sources yielded sufficiently promising results within two decades (70s & 80s) to generate enthusiasm around SIMS. With SIMS rapidly expanding in the surface analysis community, new types of primary sources were developed. One in particular has had a considerable success that continues today: the liquid metal ion source (LMIS, or LMIG, where G stands for "gun").[164] A typical LMIG apparatus is represented in **Figure 1.15**. It consists in a field emitter coated with the required metal. At the extremity of the tip of the reservoir, an electrode plays the role of extractor. When it is given a relatively high negative potential (-5 kV to -10 kV), an intense electric field surrounds the tip of the emitter. This field provokes the formation of a Taylor cone, from which metal ions are extracted. LMIGs became very popular as they offer a very stable and reproducible emission, with current intensities and focusing capabilities out of reach of any other type of source.[165] The first widespread LMIGs were used with gallium (Ga^+-LMIG), as for many years it provided the smallest probe size (≈10 nm) and highest current density (≈1-10 $A.cm^{-1}$). However, in the late 90s, it was discovered that secondary ion yields could be largely improved when replacing gallium by heavier atoms. Hence, Ga^+-LMIG have been supplanted by LMIGs incorporating firstly gold,

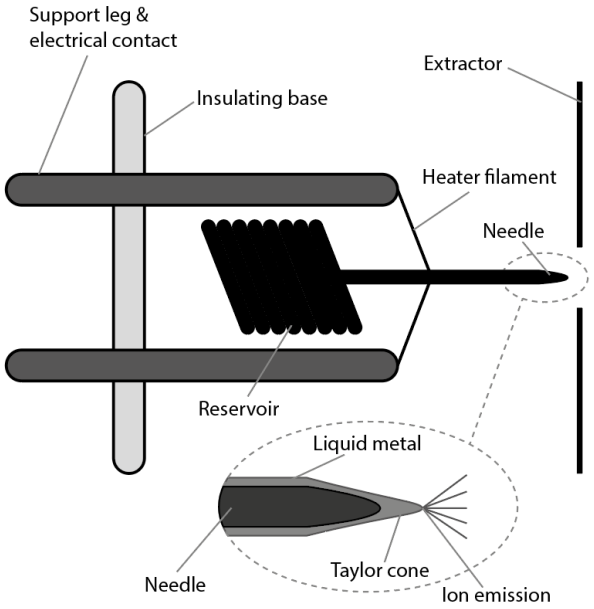


***Figure 1.15**. Schematic of a liquid metal ion source. Reproduced from Ref. 152.*

then indium, and more recently bismuth.[166] For these sources, the small decreases in focusing or current intensity are largely compensated for by the considerably improved secondary ion yield.[167] These sources remain useful today for the analysis of inorganic samples. The real drawback of LMIGs comes with the analysis of organic and hence more fragile samples, as their inherent destructive behavior when striking on a material's surface imposes some limits. In fact, the sputtering process is automatically accompanied by the destruction of the probed area, which is the topmost layer, but also the subsurface region. As previously mentioned, the energetic ions penetrate quite deeply in the material, damaging the chemical structure of the buried layers via direct hit or due to the collision cascade (**Fig. 1.16 & 1.17**). This means that as a certain ion dose is reached during the analysis (depending on the sample nature), the sample becomes extensively damaged, the molecular integrity is lost, and the sample is of no further use for qualitative analysis (see "static limit", discussed earlier).Yet, part of the solution to tackle this issue was found to lie in the LMIG itself. Indeed, it was soon demonstrated that these sources were able to generate ion beams made of small polyatomic clusters, such as Au_n^+ or Bi_n^+.[166,168] The pioneer surface analysis experiments, carried out with relatively small clusters ($n \leq 5$), clearly highlighted a non-linear enhancement of the secondary ion yield when the surface was bombarded with clusters instead of atomic ions.[168] The non-linear enhancement is defined as follows: for identical velocities or energies per atom (E/n), the sputtering or ion yield produced by one cluster ion with n atoms is larger than the cumulated yield of n separate atomic ions. The great advantage of clusters is that the increase of the secondary ion yield simultaneously comes with a decrease of the damage generated in the analyzed sample. The fragmentation of the sample during the analysis is greatly reduced, favoring the emission of larger fragments, or even intact molecular ions, in case of sufficiently small compounds ($m/z \leq 1000$). Although this represented a huge progress in the field of organic material analysis, limits were quite rapidly reached, as common LMIGs are limited to the generation of small metallic clusters. The fragmentation, as well as the damage induced to the surface and sub-surface region could only be

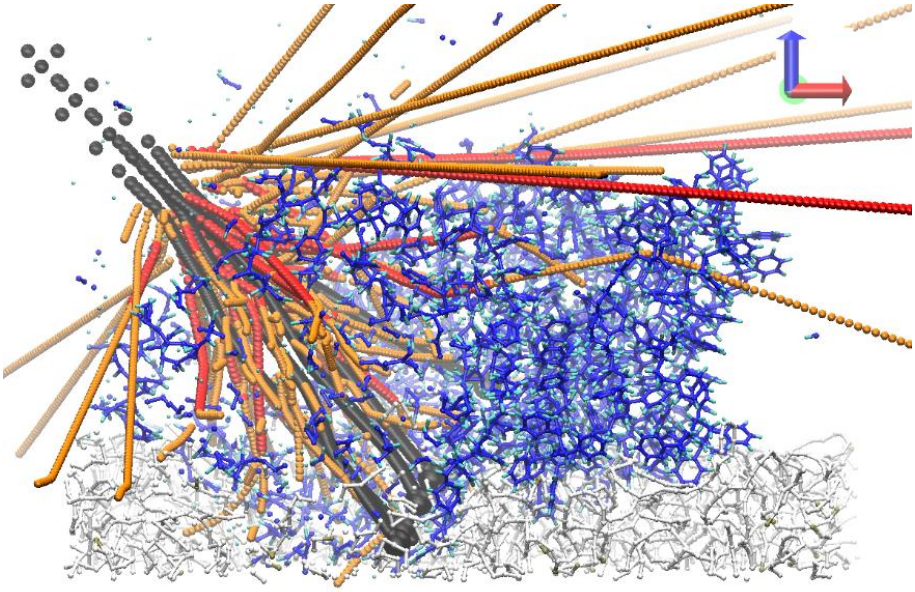


***Figure 1.16**. Result of a molecular dynamic simulation (side view). A polystyrene molecule (PS500, 60 kDa) adsorbed on amorphous polyethylene is impacted by Bi_5. Huge amount of fragmentation is observed. Color code: molecules (situation at 200 fs): blue rods / PS C-C bonds / cyan rods / PS C-H bonds / white-grey rods / PE C-C bonds. Collision cascade (successive position of the atoms between 0 et 200 fs): black spheres / Bi atoms / red spheres / molecule atoms with K>300 eV / orange spheres / molecule atoms with 300 eV>K>100 eV. Courtesy of A. Delcorte.*

decreased to a certain extent, but were far from being completely suppressed or even negligible. The emergence of larger clusters soon allowed reaching softer sputtering conditions. In the process of finding the most favorable chemical species for cluster generation, a few candidates were investigated. First, other small inorganic ionized clusters such as cesium iodide clusters, $(CsI)_nCs^+$, and ionized molecular compounds including sulfur pentafluoride, coronene, and phenylalanine were tested.[140,169–172] If these polyatomic ions have already improved the SIMS capabilities, demonstrating reduced damage cross sections and higher sputter yields, the cluster revolution in the SIMS community has been really initiated with the discovery of fullerene (C_{60}), and the use of its ions as primary particles for SIMS measurements at the beginning of the 21st century.[173–175] The first experiments designed to compare the secondary ion yields resulting from the bombardment of organic films by C_{60}^+ to that resulting from Ga^+ showed enhancement up to 50-60 (for m/z ≤ 100) in favor of the large fullerene clusters. More impressively, the enhancement could reach several hundred for larger mass fragments, or even reveal large fragments or intact

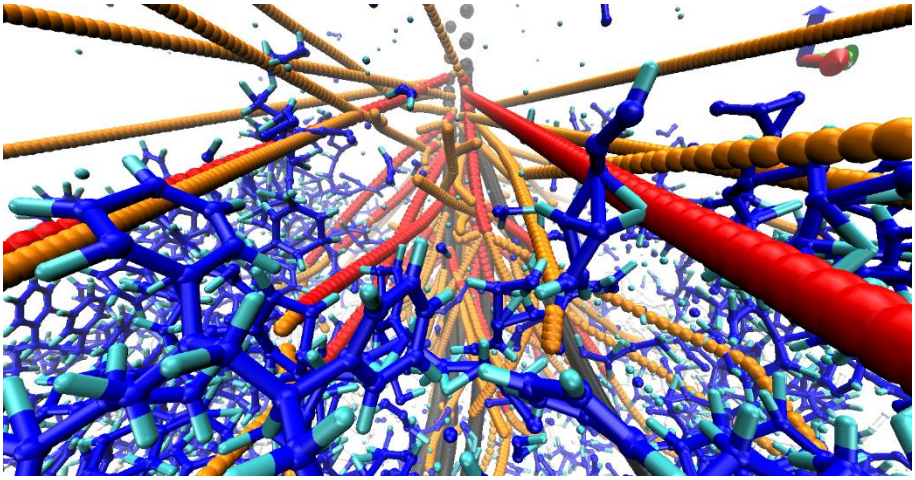


***Figure 1.17**. Close up view of the same simulation as in Fig. 16. Here again, important fragmentation induced by Bi_5 is observed. Courtesy of A. Delcorte.*

(pseudo)molecular ions that do not appear in the spectrum obtained using monoatomic ion beams. The intensity enhancement in the larger mass range illustrates the additional lowering of the fragmentation when opting for larger clusters with lower energies per atom. This was demonstrated for gramicidin (m/z = 1881), as depicted in **Figure 1.18**.[175]

The use of C_{60}^+ as primary ion source allowed SIMS to enter a new era as it finally offered possibilities for analyzing soft organic materials and biological samples, without losing the molecular information of the probed samples.[176,177] It also paved the way to molecular imaging and bulk analysis (3D-imaging, depth profiling), as the damage induced to the sample was proven to be not only much reduced, but also confined in the very outermost layers of the samples, leaving the subsurface undamaged.[178,179] As a result, it allowed performing analysis with primary ion doses exceeding that imposed by the static limit inherent to the use of monoatomic ion beams (10^{13} ions/cm^2 in best-case scenarios). Combined with the high sputtering yields associated to C_{60}^+ bombardment, it made possible to depth-profile trough organic thin films until the hard inorganic underlying substrate was reached.[179] Although C_{60}^+ has been recognized as a very efficient primary ion beam for the 2D & 3D molecular analysis of numerous organic samples, a series of other samples including fragile biological samples and tissues, polymers prone to cross-linking and organic electronic devices remained difficult to analyze with that beam due to significant damage accumulation.[180,181] Therefore, the cluster revolution in SIMS was completed

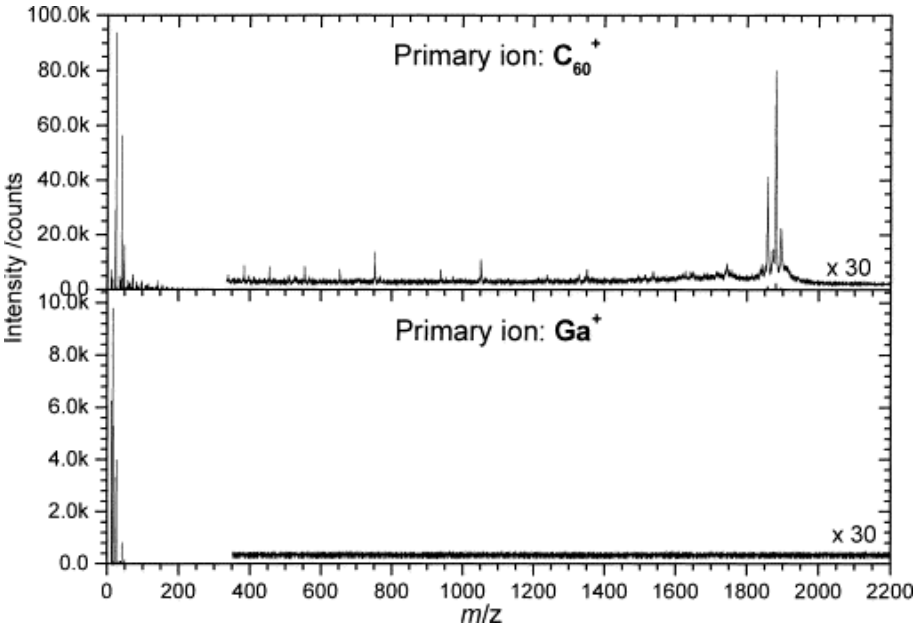


***Figure 1.18**. Negative SIMS spectrum of gramicidin using 15 keV C_{60}^+ and Ga^+. Taken from Ref. 175.*

by the end of the first decade of this century, when large argon cluster ions were incorporated into a SIMS instrument. As was previously detailed, Yamada developed the argon cluster beam technology and applied it to various applications.[109] It is however only later that Mastuo, Toyoda, Ninomiya and collaborators associated the use of large argon gas cluster ion beams (GCIBs) with a mass spectrometer to perform secondary ion mass spectrometry. It was rapidly shown that Ar-GCIBs surpass their fullerene predecessor in terms of reduced fragmentation and increased secondary ion yields in the high mass range, hence promising to broaden the scope of application of SIMS, especially to most fragile organic samples.[181] The very first use of Ar clusters for SIMS experiments was reported by Toyoda *et al*. At that time, their work comprised the use of only rather small clusters, up to 100 constituent atoms. These cluster size were however sufficient to demonstrate the potential of Ar clusters for SIMS as they observed major secondary ion yield enhancement in comparison to their atomic counterparts.[182] Thanks to the improvements of the cluster source-related instrumentation, the generation of larger Ar cluster rapidly became possible, yielding aggregates with up to a few thousands atoms.[183] It was rapidly demonstrated that by tuning the E/n of large clusters, it was possible to desorb and ionize intact biomolecules without damaging them. Since then,

Ar-GCIBs have been incorporated in many commercial SIMS instruments, and are to date the most widespread primary ion source for molecular analysis of organic samples. The non-linear effects, also called cluster effects, are originating from the same causes as those observed for smaller clusters (high density energy deposition into a very small region of the solid) but are extended to a magnitude that could previously not be envisaged. Ar-GCIB were even presented as a fragmentation-free ionization technique for mass spectrometry.[184] It was demonstrated that the decrease in the fragmentation follows that of the energy per atom in the clusters.[185] Gentle desorption conditions could be reached either by increasing the cluster's nuclearity (number of constituent atoms), or by decreasing its energy (or more efficiently by a combination of both). Ar-GCIBs have shown promising results in the analysis (especially depth profiling) of organic/biological materials which have proven difficult to analyze using C_{60}.[186] Large argon cluster ion beams became the most popular tool for low fragmentation SIMS analysis of organic samples. A schematic representation of the Ar-GCIB source mounted on a TOF.SIMS 5 spectrometer (ION-TOF GmbH, Münster, Germany), utilized during this thesis, is shown in **Figure 1.19**. It must be noted though that the gain in large mass intensities comes at the expense of mass and lateral resolution, at least in such a ToF-SIMS set-up. Indeed, the mass and lateral resolution associated to large argon clusters is significantly lower than that of LMIGs. It is therefore important to understand that the ultimate ideal source/beam, the one that would meet all requirements for all samples with any instrument unfortunately does not exist. On the one hand, LMIGs (Au_n^+ or Bi_n^+) offer the best performances in terms of spot diameter (spatial resolution), mass resolution and beam intensity, but induce high fragmentation and sub-surface damages. Hence they are more suitable for elemental analysis or high-resolution imaging, and must be used within the static limit for organic samples. On the other hand, Ar-GCIB provide soft sputtering conditions that make them suitable for molecular analysis of organic samples, but yield low mass resolution spectra.

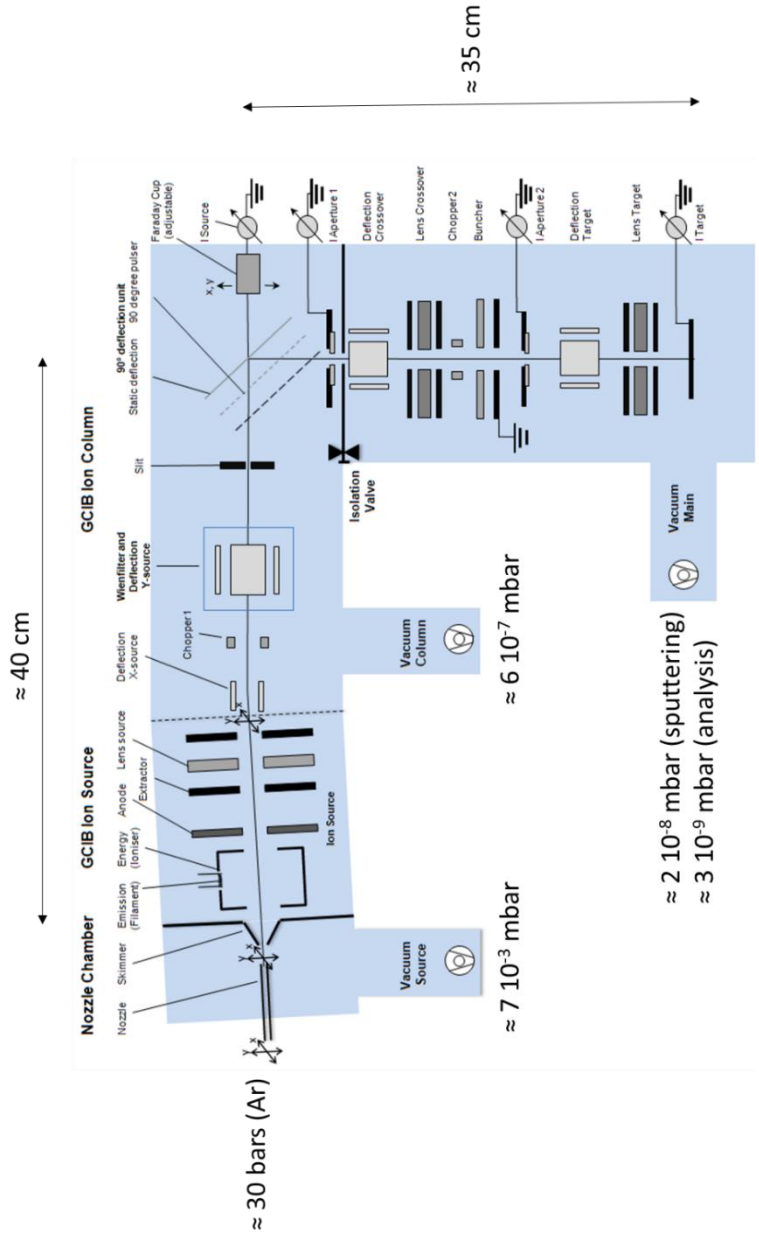


Figure 1.19. *Schematic of the GCIB source which is mounted on the ION-TOF ToF-SIMS.5 used in the framework of this thesis. Adapted from ION-TOF.*

1.6.6. Operational mode of SIMS

A SIMS instrument can be operated in various ways depending on the information to be extracted from the experiment. The typical modes of operation are surface mass spectrometry, 2D-imaging, depth-profiling and finally 3D imaging, which is a combination of the 2D-imaging and the depth-profiling modes. The different operating modes are depicted in **Figure 1.20**.

The most simple and straightforward mode is surface mass spectrometry. In this mode, the primary ion beam, that is atomic ions or clusters, is used to probe the surface (and surface only), yielding a simple mass spectrum. This mode delivers insights into the elemental composition and, under static conditions or using GCIB as primary ion beam, can provide molecular information as well. The acquisition of mass spectra using this mode presents a series of benefits such as short analysis times, high sensitivity, allowing detection of contamination even at trace concentration (ppm/ppb), high mass resolution when operating an LMIG as primary ion source (M/ΔM up to 10000 in the low-mass range), making it sensitive to isotope distributions, and a large mass-range of detectable ions, to over 10 kDa compounds.

In the 2D-imaging mode, the highly focused beam (LMIG) is raster-scanned onto a given area. The results of such experiments are chemical maps, which display the intensity distribution of selected secondary ions over small or large areas, from μm^2 up to few cm^2. In the present instrument (TOF.SIMS 5), the beam raster can be increased up to 1000 x 1000 μm^2. To obtain 2D images of larger areas, the beam moves automatically along the sample surface and gathers multiple square images that are combined as a mosaic to build the total image of the collector. The main advantage of using SIMS for 2D-imaging is the achievable lateral resolution, which in optimal conditions may be reduced to few tens of nm. The main drawback is that these experiments may become time-consuming if high lateral resolution and good sensitivity are desired. This also means that a stable primary ion beam is required, which is not always easily achieved.

SIMS also allows the analysis of the bulk material laying under the surface. As was previously mentioned, the use of clusters such as SF_5^+ or C_{60}^+, which display high sputtering yield and leave the subsurface undamaged permits to overcome the static limit and to dig in the sample with retention of the molecular information for certain classes of materials. The use of these cluster ion sources for depth profiling led to two distinct modes of analysis. In the first one, the single beam depth-profiling mode, the sputtering and the

analysis occur simultaneously. In the second one, the dual beam depth-profiling mode, the sputtering and the analysis occur sequentially, with distinct primary ion beams. A sputter beam is employed to erode the sample, while an analysis beam is chosen to probe the exposed surface in-between the sputtering events. The latter mode became even more popular with the advent of Ar-GCIB. The combined use of GCIB and LMIG allows the experimentalist to benefits from both world, with the high-mass resolution associated to LMIGs and the soft sputtering capabilities of GCIBs. Yet, it is worth emphasizing that depth profiling is still out of reach for a series of samples, notably in the case of hybrid organic-inorganic samples, where issues may be encountered because of differences in the sputtering yield of the various species present in the samples.

Finally, the two last modes presented above can be combined in order to produce 3D reconstruction of the sample being analysed. In optimal conditions, depth resolution down to 5 nm can be achieved. This mode

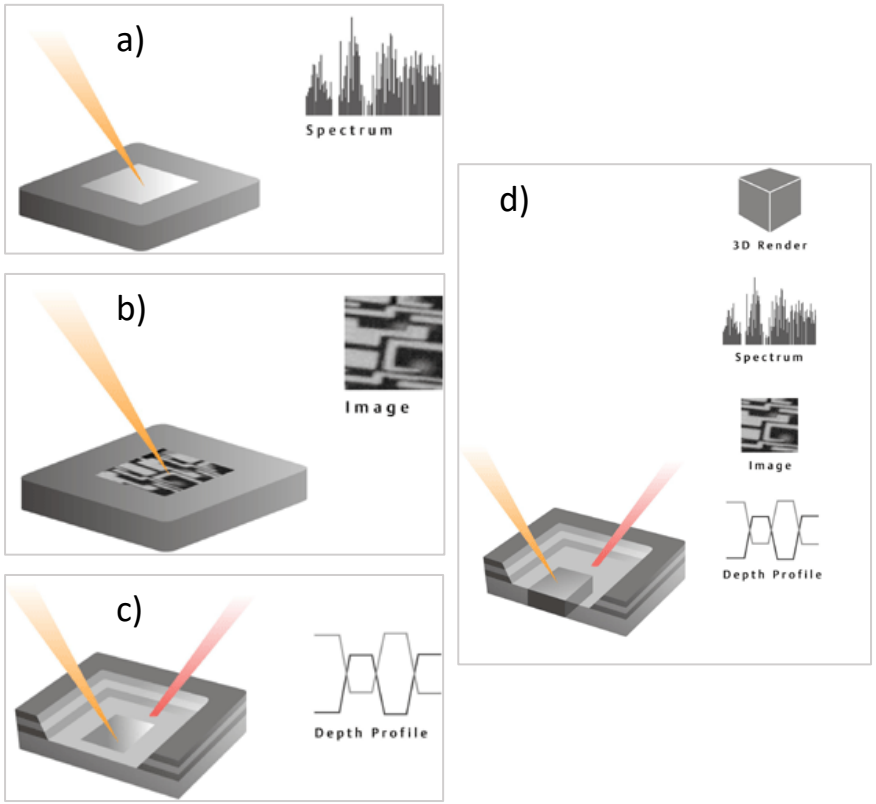


***Figure 1.20**. Illustration of the different operational modes of the ToF-SIMS instrument. (a) Simple mass spectrometry. (b) 2D imaging. (c) Depth profiling. (d) 3D imaging as a combination of 2D imaging and depth profiling. Taken from ION-TOF (https://www.iontof.com/).*

became popular for the investigation of complex biological samples due to its label-free ability to track compounds of interest diluted in complex matrices.

1.6.7. A focus on the use of ToF-SIMS for protein analysis

Initially, SIMS was essentially used for the characterization of inorganic samples. The destructive nature of the monoatomic primary ions prevented SIMS from being suitable for the analysis of complex biological samples, where molecular information is required. However, three main contributions have gradually removed the barriers standing between SIMS and fragile and complex organic/biological samples. The first contribution concerns the data treatment and the development of statistical methods. These provide a helping hand to reduce the complexity of the data contained in a SIMS spectrum, and easily extract valuable information from large and complicated data sets. Various methods have been developed, including principal component analysis, partial least squares, multivariate curve resolution and discriminant analysis. Here, only principal component analysis (PCA), one of the multivariate analysis subcategory, will be described, as it remains the most popular one when it comes to SIMS data treatment. The second contribution has already been largely developed in the previous sections, and is the advent of clusters as primary ion beams. An overview of the literature regarding the investigation of proteins using GCIBs will be given. The third contribution is related to the improvement of the ionization yield and detection efficiency. Regarding the ionization yield, various strategies have been explored, including mixed/reactive primary cluster ions, dilution of the analytes in matrices (as in MALDI-MS), or treatment of the sample with trifluoroacetic acid prior to analysis. Regarding the detection efficiency, it was mainly improved by the emergence of new mass analyzers. Moving to ToF analyzers offered a series of advantages, such as speed of analysis (through parallel detection), allowing increasing the mass range. Recently, the development of SIMS combined to an orbitrap mass analyzer allowed reaching very high mass resolution, enabling precise identification of high mass fragments.

However, despite these improvements, very heavy ions are still hardly detectable, as they reach the detector with too little kinetic energy to trigger a response and production of a signal. Tuning the post-acceleration sometimes allow overcoming this issue, but only to a certain mass range. It probably remains today one of the main limitation toward the detection of large compounds in SIMS.

1.6.7.1. Principal component analysis

In essence, a typical SIMS spectrum mirrors the surface chemistry of the probed sample. In case a complex organic or biological sample is investigated, the resulting mass spectrum can become very complex, usually containing hundreds or thousands of peaks, because of the multiplicity of ion fragments arising from even one single type of (macro)molecule. Processing of SIMS data can rapidly become a nightmare even for the most experienced scientists. PCA was developed and designed to provide researchers with an efficient tool to reduce the complexity of large data matrices to a manageable number of variables. In other words, it helps to identify relationships between different spectra. It does so by looking at the overall (co)variance within a data set.

In a SIMS spectrum, the intensity of the peaks may vary dramatically due to composition, structure, order and orientation of the surface.[187] However, there exist correlations between the relative intensities of peaks/fragments originating from the same parent molecular compounds.[188,189] An identical reflection can be made when comparing a collection of spectra. The spectral features may display a dependence, being either correlated (increasing or decreasing together) or anti-correlated (decreasing as others increase or *vice-versa*), or they may be independent. In the case where they exhibit dependence, it is said that the spectra exhibit covariance. A full description of the mathematical concepts underlying PCA is not intended in this section, but can be found elsewhere in the literature, alongside much-detailed PCA introductions.[190–192]

For a series of spectra having a defined number x of peaks, each spectrum can be represented as one data point in a space of x dimensions. The goal of PCA is to define new axes, as combinations of the original data axes, to best emphasize the dispersion of the data in this space. When PCA is applied to the case of simple static SIMS analyses, the rows of the data matrix are representative of the samples, for which a mass spectrum was acquired, while the columns contain the variables, which are the selected peaks. Each cell then contains the measured intensity of the selected peak for a given sample (or binned regions of the spectra). PCA is further carried out to find the variables that account for the majority of the covariance present in the data. For each peak, a best fit of all the measured variance is determined (the line along which the projected data display the largest spread). These fits are called the principal components (PCs). To ease the understanding, PCA can also be represented geometrically. In this respect, PCA corresponds to a

matrix rotation, or an axis rotation, applied in order to align the data set with the direction of maximal variance, as depicted in **Figure 1.21**.[193] The PCs then become the new set of axes for the reduced data. The first PC is that accounting for the highest degree of variance. The second PC is that describing the highest degree of remaining variance. The direction of this second PC is constrained to be orthogonal to the first one. The process is repeated until all the physically relevant variance is accounted for. This is usually the case with a few PCs, after which noise becomes dominant. The application of PCA to a data set generates three new matrices containing the scores, the loadings and the residuals. The scores are a projection of the original data points onto a given PC axis. They can be displayed as a score plot, and highlights the resemblance or difference between the spectra, illustrated by the clustering (resemblance) or spreading (difference) of the data points. The loadings correspond to the direction cosines between the new axes (PCs) and the initial axes. They show which variables (peaks/fragments of the mass spectrum) are responsible, and to what extent, for the dispersion of the data points observed in the scores plot (related to the same PC). The residuals represent the remaining variance in the data set.

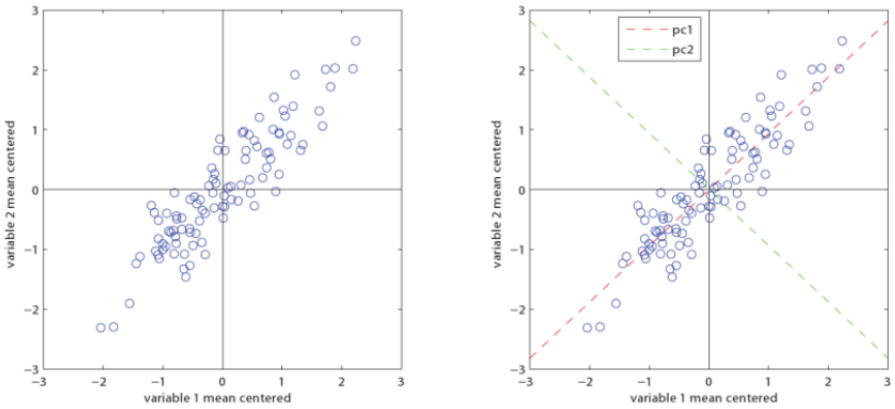


Figure 1.21. *Mean centered data (left) and the result of a matrix rotation resulting from PCA (right). The red and green dashed lines represent the new principal components axes for PC1 and PC2, respectively. Taken from Ref. 193.*

In order to perform an efficient PCA, pre-treatment of the data is crucial. A few steps are usually necessary to make sure that the variance further revealed by PCA is truly originating from physico-chemical differences of the samples and not from experimental artefacts or instrumental conditions (variance in the primary ion current intensity, charging of the sample, mean variations, etc.).[194] To provide these preliminary conditions, the data is usually normalized (to the spectrum total

intensity), and mean-centered (subtraction of a variable's mean from all values of that variable). A more exhaustive explanation as well as the precautions that are associated to this pre-processing treatment are provided elsewhere.[188,195,196]

PCA was successfully applied to the investigation of proteins by ToF-SIMS. The first reported use of PCA to treat protein-related SIMS data date back to the beginning of this century, with Castner being one of the pioneer in the field. In 2001, his group demonstrated that PCA could clearly distinguish spectra recorded on four different proteins.[197] Only two principal components were necessary to do so. This was rapidly expanded to 13 proteins, as shown in **Figure 1.22**.[198] The PCA results mirrored the amino-acid composition of the proteins. They were also able to investigate the relative concentrations of two different proteins adsorbed on the same surface. This was done by following intensity ratios of peaks related to amino acids more prevalent in either one of the two proteins. Even though it was performed on quite simple samples, this seminal work also highlighted the care that needs to be taken when performing PCA on SIMS spectra. They reported that if the peak selection was not wisely done, the PCA does not yield satisfactory results at all, as the variance is then allocated to substrate, contamination or buffer-related peaks. The same goes for the pre-processing of the data. In 2002, the same group reported a study where the detection limit of adsorbed proteins was investigated (fibrinogen in that case). PCA proved to be successful to differentiate samples with adsorbed proteins from the control samples, from a concentration of 0.1 ng/cm².[199] The same year, they reported an impressive use of PCA to probe the conformational changes that occur as the proteins are adsorbed on the surface.[200] Castner and co-workers demonstrated how combination of PCA with ToF-SIMS could provide a very promising tool to investigate the composition of adsorbed protein films on biomaterial surfaces. As they continued to work on more and more complex

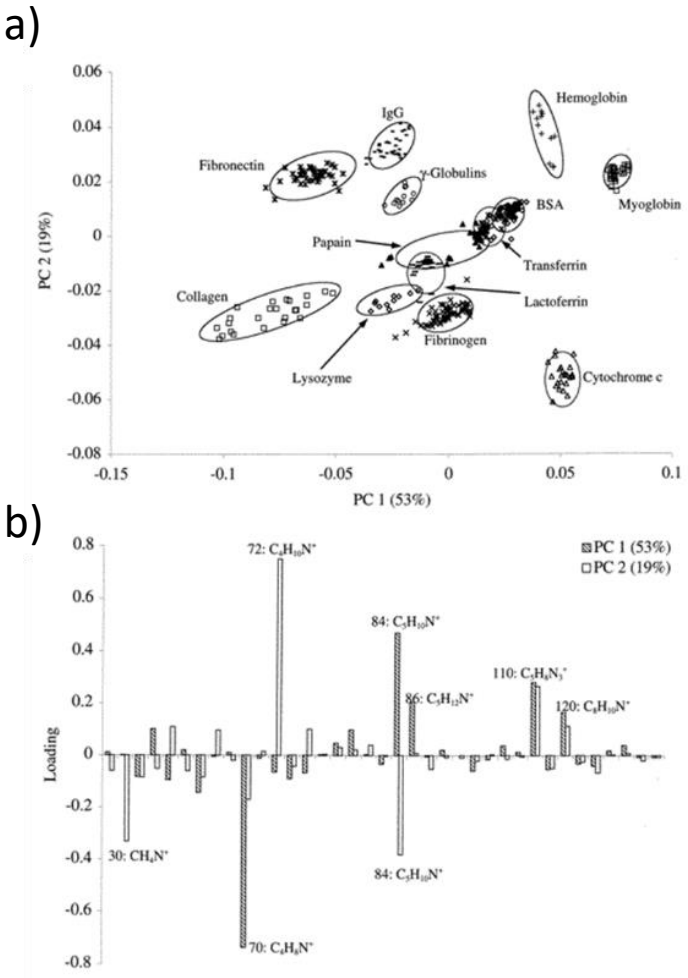


Figure 1.22. *Scores plot from PCA of the positive ion spectra of proteins adsorbed onto mica from 100 µg/mL single component protein solutions. Note the excellent separation of several of the protein spectra shown in this figure. Ellipses drawn around each of the groups represent the 95% confidence limit for that group on PCs 1 and 2. (b) Loadings plot for the first two PCs from PCA of positive ion spectra of proteins adsorbed onto mica from 100 µg/mL single component protein solutions. The loadings are ordered in increasing mass. These loadings show how the original SIMS peaks are related to the location of the spectra on the scores plot. Taken from Ref. 198.*

samples, other groups rapidly joined them, expanding the scope of applications of PCA. During the last two decades, PCA was successfully combined with SIMS analysis to yield relevant information on protein thin films. The scope encompasses conformational (denaturation)/orientational changes upon adsorption,[201–209] protein distribution (in the surface plane and in depth) when combined to SIMS 2D and 3D images,[210–212] protein

identification and quantification in complex mixtures.[213,214] SIMS combined with PCA became very popular for adsorbed antibodies analyses (surface density, orientation, denaturation).[215–219] The combination was also used for more original contributions such as investigation of protein binders in art paintings,[220] disease diagnostic,[221,222] hydration state of adsorbed proteins,[223] and characterization of biofunctional materials.[224] PCA also provided useful insights into the fragmentation pattern generated by using various primary ion sources.[225,226] Few reports were made where artificial neural networks are developed to ease the use of PCA and to allow analyzing samples that are ever more complex.[227–229] PCA still has a bright future in helping researchers with their SIMS data, especially with the advent of orbi-SIMS, which generates spectra that are even more complicated, and for SIMS imaging, which is becoming more and more popular.

1.6.7.2. Gas cluster ion beams (GCIB): towards intact proteins desorption/analysis

As soon as clusters started to be used as primary ions in SIMS instruments, their semi-destructive sputtering capabilities made them a promising tool for organic compounds analysis. As previously explained, if C_{60} initiated the cluster revolution in SIMS, it is really with the discovery that large Argon clusters beams could be used as primary ions that SIMS gained access to biomolecules. As early as in 2007, Ninomiya *et al.* showed how increasing the number of constituent atoms in the clusters (at a constant total energy, so reducing the energy per atom (E/n)) could decrease the fragmentation induced to arginine molecules.[183] They also demonstrated that at constant cluster size, increasing the total energy results in an increased fragmentation. This demonstrates that the E/n is the dominant parameter for the bombardment-induced fragmentation.[230] In 2009, Mochiji *et al.* published a groundbreaking study, in which they publish SIMS spectra containing intact molecular ions of proteins as large as insulin (MW = 5808) and cytochrome C (MW = 12 327).[231] They could obtained these results, presented in **Figure 1.23**, using a 5 keV Ar_{1400}^+ primary beam (E/n = 3.57). These results were recently (2020) reproduced by Son *et al.* using this time a 20 keV Ar_{2000}^+ beam, having an impressive energy of 10 eV per constituent atom.[232] In their study, the authors also report an innovative trypsin-digested protein analysis technique, where protein can be digested either on the surface or in solution. In 2013, Aoyagi et al. demonstrated the potential of large argon cluster beams to evaluate peptide structures.[233] The fact that

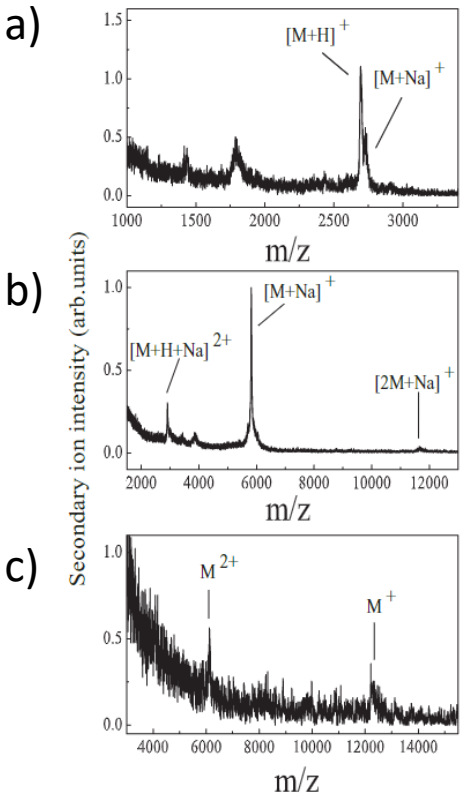


Figure 1.23. *Secondary ion mass spectra of thin film of (Pro-Hyp-Gly)$_{10}$ (a), human insulin (b), and cytochrome C (c) on silicon from the bombardment of Ar1400 at an acceleration voltage of 5 kV. Taken from Ref. 231.*

large fragments were produced under cluster bombardment allowed them to identify signature of specific amino-acid sequences in the mass spectra. This method was further developed by Aoyagi but also investigated by other groups, including those of Matsuo and Seah.[234–236] Ar-GCIB were also widely used for protein detection in biomaterials and biological tissues, improving both the generation of large molecular fragments and the imaging capabilities in two and three dimensions.[237–239] In 2017, Gilmore, in collaboration with ION-TOF and Thermo Fisher Scientific, developed the OrbiSIMS, which uses a hybrid mass analyzer.[240] The instrument is equipped with both a ToF and an Orbitrap analyzer, combining the high speed of the first one (required for example for imaging), and the mass resolution of the second one (up to 240000 at m/z 200). Very recently, Scurr and his group took advantage of such a hybrid set-up to report some outstanding results with respect to protein analysis. Using Ar clusters as primary ions and an Orbitrap analyzer, they reported the possibility to identify undigested proteins at surfaces, based on a sequencing approach.[241]

However, since 2009, to our knowledge, no one has ever reported the detection of larger proteins than cytochrome C. This is quite surprising as technological improvements permitted the generation of very large Ar clusters, with sizes reaching more than 10,000 atoms, and E/n down to 1eV/atom.[242–245] This highlights the fact that if the E/n of the clusters is the dominant parameter influencing the fragmentation observed in the spectrum, it is clearly not the only parameter to take into account to

understand the whole SIMS picture. First of all, when increasing the cluster size at a constant energy, it was shown that at some point, the sputtering yield could be dramatically decreased.[246] Second, decreasing the E/n can also greatly affect the ionization probability, which is a key parameter for ion detection in SIMS. Recent molecular dynamic simulations led by A. Delcorte tend to show that a polystyrene molecule having a mass of 60 kDa can be desorbed without fragmentation under various sputtering conditions.[247] This confirms the hypothesis that large protein molecules could be desorbed intact by large clusters, but are not ionized in the course of the desorption process, making them undetectable. It appears that ionization could be even more limiting than fragmentation when it comes to analyzing large biomolecules. In order to overcome this low inherent ionization yield, several techniques have been developed, including pre-treatment of the sample and use of mixed/reactive clusters. These strategies are briefly overviewed in the next section. Finally, even if ions are produced, they also need to be detected. It is believed that today, the main limit of the SIMS equipment with respect to large mass ions detection is the detection efficiency.

1.6.7.3. Towards improved ionization yield and detection efficiency

One of the first strategy that provided promising ionization enhancement was to blend the sample with a matrix (usually low-molecular weight organic molecules), in a similar fashion to what is done for MADLI-MS.[248–250] This matrix-enhanced (ME) SIMS delivered some impressive results. In 2006, Locklear *et al.* could obtain large enhancement of the gramicidin S molecular ion emission when it was embedded in a matrix of synaptic acid.[251] Later, ME-SIMS was specifically used by MacAleese *et al.* to perform protein identification.[252] Many MALDI matrices have been investigated, and remain the most popular molecules to perform ME-SIMS.[253] Yet other strategies, e.g. using ionic liquid matrices, have been reported.[254] More recently, ME-SIMS was used for sequencing and identification of peptides.[255–257] Another way to promote ionization of biomolecules is to work with frozen samples. Low temperature experiments offer various advantages, especially when working with biological tissues (less mixing and migrating effect, improving lateral and depth resolution, no protein denaturation, etc.).[258] In addition, it was shown that the presence of a frozen water layer/matrix on the sample acts as a proton source for further proton transfer, significantly increasing the $[M+H]^+$ signal intensity for a

series of biomolecules.[259] This effect is particularly pronounced when the water matrix is used in combination with cluster sources.[260]

Few original methods were reported in the last decades to improve the detection of organic compounds, but did not really encounter great success yet, despite yielding some very nice results. Among others, Mouhib *et al.* proposed a system to deliver water vapor closely to the sample surface, while Angerer *et al.* proposed to expose the sample to trifluoroacetic acid (TFA) vapor prior to SIMS analysis.[261–264]

Another approach encountered greater success and is still under development today. It consists in using mixed/reactive clusters, whose chemistry would trigger and promote proton-mediated reactions. In 2013, Vickerman *et al.* reported the use of water clusters as primary ions.[264] They compared the secondary ion yields in spectra of various biomolecules including amino acids and peptides recorded with 10 keV Ar_{1000}^+ or $(H_2O)_{1000}^+$ cluster beams. In all cases, the water clusters provided a 10-fold (or more) increase in secondary ion intensity with respect to their argon counterparts. Water clusters continue to be investigated, notably by the groups of Vickerman and Winograd.[265–268] As water clusters delivered quite promising results, other candidates were also tested as primary ion clusters. Clusters made of K^+, $(CH_4)_n^+$, $(CH_3OH)_n^+$, benzene and $(CO_2)_n^+$ were tested by various groups.[269–271] In addition to pure clusters, composed of one single atomic/molecular species, the group of Winograd also proposed to use mixed clusters, to benefit from the advantages of both species contained in the clusters. In 2013, they reported the use of Ar clusters doped with CH_4, which displayed significant ion yield enhancements.[272] In 2016, the same group published a study in which large Ar clusters were doped with HCl, which was intended to react with the water present at the surface of the samples, in turn favoring the ionization of molecular species.[273] The analyzed components showed 4- to 15-fold intensity increases of their protonated ions under bombardment with doped clusters. In 2022, Lockyer reported the use of water clusters that were modified by replacing the Ar carrier gas of the water GCIB by a mixture containing 12% CO_2 and 2% O_2 in Ar.[274] Under these conditions, mixed $(H_2O/CO_2)_n$ clusters are formed, which are far more reactive species, promoting the formation of secondary ions.

Mixed and reactive clusters are still in the beginning of their development, and yet they have already provided some very promising results. With the instrumental development and an infinity of possible candidates to be used as primary ions, it is believed that SIMS will keep on

being improved, especially regarding the ionization/detection of large biomolecules that remain today out of reach of SIMS, such as proteins.

1.7.The iBeam project

It is in this scientific context that the iBEAM project takes shape, project in which this thesis is embedded. With cluster ion beams as central theme, the focus of the project can be summarized by the following question: *How can cluster ion beams be engineered and used to control the transfer and ionization of complex (bio)molecules, for the design of new surface architectures and for enhanced mass spectrometry ?* To answer this question, various specific research areas have to be investigated; hence, the project is divided in four work packages (WP). To provide an overview of the whole project, each WP will briefly be presented.

In WP1, entitled "*Mass spectrometry and absorption spectroscopy of clusters",* the focus will be the study of a series of ionic molecular complexes by high-resolution mass spectrometry. The goals of this WP are multiple and encompass (i) recording and understanding the spectra of those species for their future detection in different astrophysical environments and in the Earth atmosphere; (ii) studying in detail large-amplitude vibrational motions, solvation and chemical reactivity at the molecular level, i.e. use isolated ionic clusters as ideal nano-chemical reactors to study chemical reactions in perfectly controlled conditions and (iii) providing an optimized and characterized source of clusters for molecular transfer in WP2 and SIMS analysis in WP3.

WP2, *"Cluster-induced molecular transfer for biosurface engineering"*, proposes to develop a transfer method for the construction of thin films of biomolecules. To this end, it is suggested to use various Ar_n^+ beams to sputter species from a reservoir sample (target) to the desired substrate (collector). The proposed method can be seen as to be in line with the existing soft-landing strategies, but expand their scope as neutral species are collected, together with ionized ones. The ultimate goal of this WP is to provide a tunable method that allows the controlled construction of new biosurfaces with improved control over parameters such as thickness, 3D architecture, bioactivity, etc. The experimental work related to this WP is planned to be complemented by molecular dynamics

(MD) simulations, in order to gain in-depth understanding of the phenomena occurring at each stage of the cluster-assisted deposition.

In WP3, whose title is *"Molecular ionization for secondary ion mass spectrometry"*, the tricky issue of the ionization in SIMS experiments will be tackled. As was previously mentioned in the state of the art, low ionization probabilities, especially for biological compounds of interest, are one of the main limitations when it comes to SIMS analysis of biological tissues. In addition, from the fundamental viewpoint, the mechanisms of molecular ionization upon (cluster) ion bombardment remain elusive. Here the goal is to improve our understanding of ionization via two different experimental approaches. In the first case, an alternative strategy to perform matrix-enhanced SIMS is explored. To this end, controlled quantities of molecular matrices will be deposited on organic or biological model surfaces using the same cluster-induced transfer process as in WP2. In the second case, the molecular ionization induced by specifically engineered clusters will be compared to that of reference clusters such as Ar_n^+. Once again, the experiments will be supported by MD simulations of cluster impacts.

WP4 comprises the *"Instrumental development"*. Two homemade instruments will be designed and developed in the framework of this project. A prototype mass spectrometer will be built to study the photo-dissociation of mass-selected ionic clusters and the detection of the fragments (WP1). In the meantime, a second instrument specifically dedicated to the molecular transfer and ionization studies will be entirely built. While those instruments are being developed, the experimental work described in WP2 & WP3 will be carried out using commercial cluster sources, notably the argon cluster source provided on the ToF-SIMS instrument available in the laboratory.

This PhD thesis represents the main contribution to the experimental work related to the second work package of the iBeam project.

1.8.References

(1) Williams, D. F. On the Nature of Biomaterials. *Biomaterials* **2009**.

(2) Williams, D. F. Second Consensus on Definitions in Biomaterials. *Biomater. interfaces* **1992**, *10*, 525–533.

(3) Khan, W.; Muntimadugu, E.; Jaffe, M.; Domb, A. J.; Khan, W.; Muntimadugu, • E; Jaffe, M.; Domb, A. J. Implantable Medical Devices. **2014**, 33–59.

(4) Mozetič, M. Surface Modification to Improve Properties of Materials. *Mater. 2019, Vol. 12, Page 441* **2019**, *12* (3), 441.

(5) Ratner, B. D.; Hoffman, A. S.; McArthur, S. L. Physicochemical Surface Modification of Materials Used in Medicine. *Biomater. Sci.* **2020**, 487–505.

(6) Bose, S.; Robertson, S. F.; Bandyopadhyay, A. Surface Modification of Biomaterials and Biomedical Devices Using Additive Manufacturing. *Acta Biomater.* **2018**, *66*, 6–22.

(7) Cho, Y.; Lee, M.; Park, S.; Kim, Y.; Lee, E.; Im, S. G. A Versatile Surface Modification Method via Vapor-Phase Deposited Functional Polymer Films for Biomedical Device Applications. *Biotechnol. Bioprocess Eng.* **2021**, *26*, 165–178.

(8) Tan, R. P.; Hallahan, N.; Kosobrodova, E.; Michael, P. L.; Wei, F.; Santos, M.; Lam, Y. T.; Chan, A. H. P.; Xiao, Y.; Bilek, M. M. M.; Thorn, P.; Wise, S. G. Bioactivation of Encapsulation Membranes Reduces Fibrosis and Enhances Cell Survival. *ACS Appl. Mater. Interfaces* **2020**, *12* (51), 56908–56923.

(9) Oliverio, M.; Perotto, S.; Messina, G. C.; Lovato, L.; Angelis, F. De. Chemical Functionalization of Plasmonic Surface Biosensors: A Tutorial Review on Issues, Strategies, and Costs. *ACS Appl. Mater. Interfaces* **2017**, *9* (35), 29394–29411.

(10) Yakimova, R.; Petoral, R. M.; Yazdi, G. R.; Vahlberg, C.; Spetz, A. L.; Uvdal, K. Surface Functionalization and Biomedical Applications Based on SiC. *J. Phys. D. Appl. Phys.* **2007**, *40* (20), 6435.

(11) Gharibi, R.; Agarwal, S. Favorable Antibacterial, Antibiofilm, Antiadhesion to Cells, and Biocompatible Polyurethane by Facile Surface Functionalization. *ACS Appl. Bio Mater.* **2021**, *4* (5), 4629–4640.

(12) Bilek, M. M. M.; Bax, D. V.; Kondyurin, A.; Yin, Y.; Nosworthy, N. J.; Fisher, K.; Waterhouse, A.; Weiss, A. S.; Remedios, C. G. dos; McKenzie, D. R. Free Radical Functionalization of Surfaces to Prevent Adverse Responses to Biomedical Devices. *Proc. Natl. Acad. Sci.* **2011**, *108* (35), 14405–14410.

(13) Leong, H. J.; Oh, S. G. Preparation of Antibacterial TiO2 Particles by

Hybridization with Azelaic Acid for Applications in Cosmetics. *J. Ind. Eng. Chem.* **2018**, *66*, 242–247.

(14) Tian, F.; Decker, E. A.; Goddard, J. M. Controlling Lipid Oxidation of Food by Active Packaging Technologies. *Food Funct.* **2013**, *4* (5), 669–680.

(15) Makvandi, P.; Iftekhar, S.; Pizzetti, F.; Zarepour, A.; Zare, E. N.; Ashrafizadeh, M.; Agarwal, T.; Padil, V. V. T.; Mohammadinejad, R.; Sillanpaa, M.; Maiti, T. K.; Perale, G.; Zarrabi, A.; Rossi, F. Functionalization of Polymers and Nanomaterials for Water Treatment, Food Packaging, Textile and Biomedical Applications: A Review. *Environ. Chem. Lett. 2020 191* **2020**, *19* (1), 583–611.

(16) Kian, L. K.; Jawaid, M. Surface Functionalization of Cellulose Biocomposite for Food Packaging Application. *Biopolym. Biocomposites from Agro-Waste Packag. Appl.* **2021**, 255–269.

(17) Hosseini, S.; Ibrahim, F.; Djordjevic, I.; Koole, L. H. Recent Advances in Surface Functionalization Techniques on Polymethacrylate Materials for Optical Biosensor Applications. *Analyst* **2014**, *139* (12), 2933–2943.

(18) Song, M.; Lin, X.; Peng, Z.; Xu, S.; Jin, L.; Zheng, X.; Luo, H. Materials and Methods of Biosensor Interfaces With Stability. *Front. Mater.* **2021**, *7*, 438.

(19) Di Pietrantonio, F.; Benetti, M.; Dinca, V.; Cannatà, D.; Verona, E.; D'Auria, S.; Dinescu, M. Tailoring Odorant-Binding Protein Coatings Characteristics for Surface Acoustic Wave Biosensor Development. *Appl. Surf. Sci.* **2014**, *302*, 250–255.

(20) Ménard-Moyon, C.; Bianco, A.; Kalantar-Zadeh, K. Two-Dimensional Material-Based Biosensors for Virus Detection. *ACS Sensors* **2020**, *5* (12), 3739–3769.

(21) Saurer, E. M.; Flessner, R. M.; Sullivan, S. P.; Prausnitz, M. R.; Lynn, D. M. Layer-by-Layer Assembly of DNA- and Protein-Containing Films on Microneedles for Drug Delivery to the Skin. *Biomacromolecules* **2010**, *11* (11), 3136–3143.

(22) Shah, A.; Malik, M. S.; Khan, G. S.; Nosheen, E.; Iftikhar, F. J.; Khan, F. A.; Shukla, S. S.; Akhter, M. S.; Kraatz, H. B.; Aminabhavi, T. M. Stimuli-Responsive Peptide-Based Biomaterials as Drug Delivery Systems. *Chem. Eng. J.* **2018**, *353*, 559–583.

(23) Varanko, A.; Saha, S.; Chilkoti, A. Recent Trends in Protein and Peptide-Based Biomaterials for Advanced Drug Delivery. *Adv. Drug Deliv. Rev.* **2020**, *156*, 133–187.

(24) Cheng, H. N.; Gross, R. A. Green Polymer Chemistry: Biocatalysis and Biomaterials. *ACS Symp. Ser.* **2010**, *1043*, 1–14.

(25) Zhang, G.; Johnston, T.; Quin, M. B.; Schmidt-Dannert, C. Developing

a Protein Scaffolding System for Rapid Enzyme Immobilization and Optimization of Enzyme Functions for Biocatalysis. *ACS Synth. Biol.* **2019**, *8* (8), 1867–1876.

(26) Sánchez-deAlcázar, D.; Velasco-Lozano, S.; Zeballos, N.; López-Gallego, F.; Cortajarena, A. L. Biocatalytic Protein-Based Materials for Integration into Energy Devices. *ChemBioChem* **2019**, *20* (15), 1977–1985.

(27) Brash, J. L.; Horbett, T. A. Proteins at Interfaces An Overview. **1995**.

(28) Aghajani, M.; Esmaeili, F. Anti-Biofouling Assembly Strategies for Protein & Cell Repellent Surfaces: A Mini-Review. **2021**, *32* (13), 1770–1789.

(29) Xu, J.; Lee, H. Anti-Biofouling Strategies for Long-Term Continuous Use of Implantable Biosensors. *Chemosens. 2020, Vol. 8, Page 66* **2020**, *8* (3), 66.

(30) Chothia, C. Principles That Determine the Structure of Proteins. *Annu. Rev. Biochem.* **1984**, *53* (1), 537–572.

(31) Heim, M.; Römer, L.; Scheibel, T. Hierarchical Structures Made of Proteins . The Complex Architecture of Spider Webs and Their Constituent Silk Proteins. *Chem. Soc. Rev.* **2009**, *39* (1), 156–164.

(32) Rose, G. D.; Geselowitz, A. R.; Lesser, G. J.; Lee, R. H.; Zehfus, M. H. Hydrophobicity of Amino Acid Residues in Globular Proteins. *Science (80-.).* **1985**, *229* (4716), 834–838.

(33) Mathura, V. S.; Kolippakkam, D. APDbase: Amino Acid Physico-chemical Properties Database. *Bioinformation* **2005**, *1* (1), 2.

(34) Andrade, J. D.; Hlady, V. Protein Adsorption and Materials Biocompatibility: A Tutorial Review and Suggested Hypotheses. *Biopolym. HPLC* **1986**, 1–63.

(35) Latour, R. A. Fundamental Principles of the Thermodynamics and Kinetics of Protein Adsorption to Material Surfaces. *Colloids Surfaces B Biointerfaces* **2020**, *191*, 110992.

(36) Norde, W. My Voyage of Discovery to Proteins in Flatland …and Beyond. *Colloids Surfaces B Biointerfaces* **2008**, *61* (1), 1–9.

(37) Pan, H.; Qin, M.; Meng, W.; Cao, Y.; Wang, W. How Do Proteins Unfold upon Adsorption on Nanoparticle Surfaces? *Langmuir* **2012**, *28* (35), 12779–12787.

(38) Nakanishi, K.; Sakiyama, T.; Imamura, K. On the Adsorption of Proteins on Solid Surfaces, a Common but Very Complicated Phenomenon. *J. Biosci. Bioeng.* **2001**, *91* (3), 233–244.

(39) Pan, Y.; Neupane, S.; Farmakes, J.; Bridges, M.; Froberg, J.; Rao, J.; Qian, S. Y.; Liu, G.; Choi, Y.; Yang, Z. Probing the Structural Basis and Adsorption Mechanism of an Enzyme on Nano-Sized Protein Carriers. *Nanoscale* **2017**, *9* (10), 3512–3523.

(40) Kim, Y.; Ko, S. M.; Nam, J. M. Protein–Nanoparticle Interaction-Induced Changes in Protein Structure and Aggregation. *Chem. – An Asian J.* **2016**, *11* (13), 1869–1877.
(41) Mahmoudi, M.; Lynch, I.; Ejtehadi, M. R.; Monopoli, M. P.; Bombelli, F. B.; Laurent, S. Protein-Nanoparticle Interactions: Opportunities and Challenges. *Chem. Rev.* **2011**, *111* (9), 5610–5637.
(42) Norde, W.; Horbett, T. A.; Brash, J. L. Proteins at Interfaces III: Introductory Overview. In *Proteins at Interfaces III State of the Art*; ACS Publications, 2012; pp 1–34.
(43) Liu, Q.; Zhou, X.; Wu, H.; Wu, L.; Zheng, B. A Polydopamine Patterned Perfluoropolymer-Based Substrate for Protein Microarray Applications. *Sensors Actuators B Chem.* **2019**, *287*, 306–311.
(44) Murtezi, E.; Puthukodan, S.; Jacak, J.; Klar, T. A. Biofunctionalization of Sub-Diffractionally Patterned Polymer Structures by Photobleaching. *ACS Appl. Mater. Interfaces* **2018**, *10* (38), 31850–31854.
(45) Firkowska-Boden, I.; Zhang, X.; Jandt, K. D. Controlling Protein Adsorption through Nanostructured Polymeric Surfaces. *Adv. Healthc. Mater.* **2018**, *7* (1), 1700995.
(46) Angioletti-Uberti, S.; Ballauff, M.; Dzubiella, J. Competitive Adsorption of Multiple Proteins to Nanoparticles: The Vroman Effect Revisited.
(47) Vander Straeten, A.; Bratek-Skicki, A.; Jonas, A. M.; Fustin, C. A.; Dupont-Gillain, C. Integrating Proteins in Layer-by-Layer Assemblies Independently of Their Electrical Charge. *ACS Nano* **2018**, *12* (8), 8372–8381.
(48) vander Straeten, A.; Lefèvre, D.; Demoustier-Champagne, S.; Dupont-Gillain, C. Protein-Based Polyelectrolyte Multilayers. *Adv. Colloid Interface Sci.* **2020**, *280*, 102161.
(49) vander Straeten, A.; Bratek-Skicki, A.; Germain, L.; D'Haese, C.; Eloy, P.; Fustin, C.-A.; Dupont-Gillain, C. Protein-Polyelectrolyte Complexes to Improve the Biological Activity of Proteins in Layer-by-Layer Assemblies. *Nanoscale* **2017**, *9* (44), 17186–17192.
(50) Poncin-Epaillard, F.; Vrlinic, T.; Debarnot, D.; Mozetic, M.; Coudreuse, A.; Legeay, G.; Moualij, B. El; Zorzi, W. Surface Treatment of Polymeric Materials Controlling the Adhesion of Biomolecules. *J. Funct. Biomater. 2012, Vol. 3, Pages 528-543* **2012**, *3* (3), 528–543.
(51) Williams, R. A.; Blanch, H. W. Covalent Immobilization of Protein Monolayers for Biosensor Applications. *Biosens. Bioelectron.* **1994**, *9* (2), 159–167.
(52) Gao, Y.; Kyratzis, I. Covalent Immobilization of Proteins on Carbon Nanotubes Using the Cross-Linker 1-Ethyl-3-(3-Dimethylaminopropyl)Carbodiimide—a Critical Assessment.

Bioconjug. Chem. **2008**, *19* (10), 1945–1950.

(53) Zare-Eelanjegh, E.; Bora, D. K.; Rupper, P.; Schrantz, K.; Thöny-Meyer, L.; Maniura-Weber, K.; Richter, M.; Faccio, G. Affinity-Driven Immobilization of Proteins to Hematite Nanoparticles. *ACS Appl. Mater. Interfaces* **2016**, *8* (31), 20432–20439.

(54) Li, M.; Yue, Y.; Zhang, Z. J.; Wang, Z. Y.; Tan, T. W.; Fan, L. H. Site-Specific and High-Loading Immobilization of Proteins by Using Cohesin-Dockerin and CBM-Cellulose Interactions. *Bioconjug. Chem.* **2016**, *27* (7), 1579–1583.

(55) Schneider, A.-K.; Nikolov, P. M.; Giselbrecht, S.; Niemeyer, C. M.; Schneider, A.; Nikolov, P. M.; Niemeyer, C. M.; Giselbrecht, S. DNA-SMART: Biopatterned Polymer Film Microchannels for Selective Immobilization of Proteins and Cells. *Small* **2017**, *13* (17), 1603923.

(56) Svalova, T. S.; Medvedeva, M. V.; Kozitsina, A. N. A "Clickable" Electrodeposited Polymer Films Based on 3-Ethynylthiophene for the Covalent Immobilization of Proteins. Application to a Label-Free Electrochemical Immunosensor for Escherichia Coli and Staphylococcus Aureus Determination. *Electroanalysis* **2021**, *33* (12), 2469–2475.

(57) Bednar, R. M.; Golbek, T. W.; Kean, K. M.; Brown, W. J.; Jana, S.; Baio, J. E.; Karplus, P. A.; Mehl, R. A. Immobilization of Proteins with Controlled Load and Orientation. *ACS Appl. Mater. Interfaces* **2019**, *11* (40), 36391–36398.

(58) Liu, Y.; Tao, F.; Miao, S.; Yang, P. Controlling the Structure and Function of Protein Thin Films through Amyloid-like Aggregation. *Acc. Chem. Res.* **2021**, *54* (15), 3016–3027.

(59) Wang, D.; Ha, Y.; Gu, J.; Li, Q.; Zhang, L.; Yang, P.; Wang, D.; Ha, Y.; Gu, J.; Li, Q.; Yang, P.; Zhang, L. 2D Protein Supramolecular Nanofilm with Exceptionally Large Area and Emergent Functions. *Adv. Mater.* **2016**, *28* (34), 7414–7423.

(60) Xu, Y.; Liu, Y.; Hu, X.; Qin, R.; Su, H.; Li, J.; Yang, P. The Synthesis of a 2D Ultra-Large Protein Supramolecular Nanofilm by Chemoselective Thiol–Disulfide Exchange and Its Emergent Functions. *Angew. Chemie - Int. Ed.* **2020**, *59* (7), 2850–2859.

(61) Verbeck, G.; Hoffmann, W.; Walton, B. Soft-Landing Preparative Mass Spectrometry. *Analyst* **2012**, *137* (19), 4393–4407.

(62) Grant E. Johnson,* DonGunaratne, and J. L. SOFT- AND REACTIVE LANDING OF IONS ONTO SURFACES: CONCEPTS AND APPLICATIONS. **2015**, 1–12.

(63) Mazzei, F.; Favero, G.; Frasconi, M.; Tata, A.; Pepi, F. Electron-Transfer Kinetics of Microperoxidase-11 Covalently Immobilised onto the Surface of Multi-Walled Carbon Nanotubes by Reactive Landing of

Mass-Selected Ions. *Chem. – A Eur. J.* **2009**, *15* (30), 7359–7367.
(64) Johnson, G. E.; Laskin, J. Preparation of Surface Organometallic Catalysts by Gas-Phase Ligand Stripping and Reactive Landing of Mass-Selected Ions. *Chem. – A Eur. J.* **2010**, *16* (48), 14433–14438.
(65) Johnson, G. E.; Lysonski, M.; Laskin, J. In Situ Reactivity and TOF-SIMS Analysis of Surfaces Prepared by Soft and Reactive Landing of Mass-Selected Ions. *Anal. Chem.* **2010**, *82* (13), 5718–5727.
(66) Wang, P.; Laskin, J.; Wang,] P; Laskin, J. Helical Peptide Arrays on Self-Assembled Monolayer Surfaces through Soft and Reactive Landing of Mass-Selected Ions. *Angew. Chemie* **2008**, *120* (35), 6780–6782.
(67) Wang, P.; Laskin, J. Surface Modification Using Reactive Landing of Mass-Selected Ions. In *Ion beams in nanoscience and technology*; Springer, 2009; pp 37–65.
(68) Franchetti, V.; Solka, B. H.; Baitinger, W. E.; Amy, J. W.; Cooks, R. G. Soft Landing of Ions as a Means of Surface Modification. *Int. J. Mass Spectrom. Ion Phys.* **1977**, *23* (1), 29–35.
(69) Cyriac, J.; Pradeep, T.; Kang, H.; Souda, R.; Cooks, R. G. Low-Energy Ionic Collisions at Molecular Solids. *Chem. Rev.* **2012**, *112* (10), 5356–5411.
(70) Gunaratne, K. D. D.; Prabhakaran, V.; Ibrahim, Y. M.; Norheim, R. V; Johnson, G. E.; Laskin, J. Design and Performance of a High-Flux Electrospray Ionization Source for Ion Soft Landing. *Analyst* **2015**, *140* (9), 2957–2963.
(71) Laskin, J.; Wang, P.; Hadjar, O. Soft-Landing of Peptide Ions onto Self-Assembled Monolayer Surfaces: An Overview. *Phys. Chem. Chem. Phys.* **2008**, *10* (8), 1079–1090.
(72) Lifshitz, C.; Laskin, J. *Principles of Mass Spectrometry Applied to Biomolecules*; John Wiley \& Sons, 2006.
(73) Pratihar, S.; Barnes, G. L.; Laskin, J.; Hase, W. L. Dynamics of Protonated Peptide Ion Collisions with Organic Surfaces: Consonance of Simulation and Experiment. *J. Phys. Chem. Lett.* **2016**, *7* (16), 3142–3150.
(74) Laskin, J.; Johnson, G. E.; Prabhakaran, V. Soft Landing of Complex Ions for Studies in Catalysis and Energy Storage. *J. Phys. Chem. C* **2016**, *120* (41), 23305–23322.
(75) Laskin, J.; Johnson, G. E.; Warneke, J.; Prabhakaran, V. From Isolated Ions to Multilayer Functional Materials Using Ion Soft Landing. *Angew. Chemie - Int. Ed.* **2018**, *57* (50), 16270–16284.
(76) Jacobs, D. C. The Role of Internal Energy and Approach Geometry in Molecule/Surface Reactive Scattering. *J. Phys. Condens. Matter* **1995**, *7* (6), 1023.
(77) Ouyang, Z.; Takáts, Z.; Blake, T. A.; Gologan, B.; Guymon, A. J.;

Wiseman, J. M.; Oliver, J. C.; Davisson, V. J.; Cooks, R. G. Preparing Protein Microarrays by Soft-Landing of Mass-Selected Ions. *Science (80-.).* **2003**, *301* (5638), 1351–1354.

(78) Gologan, B.; Takáts, Z.; Alvarez, J.; Wiseman, J. M.; Talaty, N.; Ouyang, Z.; Cooks, R. G. Ion Soft-Landing into Liquids: Protein Identification, Separation, and Purification with Retention of Biological Activity. *J. Am. Soc. Mass Spectrom. 2004 1512* **2004**, *15* (12), 1874–1884.

(79) Volný, M.; Elam, W. T.; Branca, A.; Ratner, B. D.; Tureček, F. Preparative Soft and Reactive Landing of Multiply Charged Protein Ions on a Plasma-Treated Metal Surface. *Anal. Chem.* **2005**, *77* (15), 4890–4896.

(80) Siuzdak, G.; Bothner, B.; Yeager, M.; Brugidou, C.; Fauquet, C. M.; Hoey, K.; Chang, C. M. Mass Spectrometry and Viral Analysis. *Chem. Biol.* **1996**, *3* (1), 45–48.

(81) Hadjar, O.; Wang, P.; Futrell, J. H.; Dessiaterik, Y.; Zhu, Z.; Cowin, J. P.; Iedema, M. J.; Laskin, J. Design and Performance of an Instrument for Soft Landing of Biomolecular Ions on Surfaces. *Anal. Chem.* **2007**, *79* (17), 6566–6574.

(82) Rinke, G.; Rauschenbach, S.; Harnau, L.; Albarghash, A.; Pauly, M.; Kern, K. Active Conformation Control of Unfolded Proteins by Hyperthermal Collision with a Metal Surface. *Nano Lett.* **2014**, *14* (10), 5609–5615.

(83) Washburn, M. P. Soft Landing for Protein Chips. *Nat. Biotechnol.* **2003**, *21* (10), 1156–1157.

(84) Pepi, F.; Ricci, A.; Tata, A.; Favero, G.; Frasconi, M.; Delle Noci, S.; Mazzei, F. Soft Landed Protein Voltammetry. *Chem. Commun.* **2007**, No. 33, 3494–3496.

(85) Pepi, F.; Tata, A.; Garzoli, S.; Giacomello, P.; Ragno, R.; Patsilinakos, A.; Fusco, M. Di; D'Annibale, A.; Cannistraro, S.; Baldacchini, C.; others. Chemically Modified Multiwalled Carbon Nanotubes Electrodes with Ferrocene Derivatives through Reactive Landing. *J. Phys. Chem. C* **2011**, *115* (11), 4863–4871.

(86) Mazzei, F.; Favero, G.; Frasconi, M.; Tata, A.; Pepi, F. Electron-Transfer Kinetics of Microperoxidase-11 Covalently Immobilised onto the Surface of Multi-Walled Carbon Nanotubes by Reactive Landing of Mass-Selected Ions. *Chem. Eur. J.* **2009**, *15* (30), 7359–7367.

(87) Mazzei, F.; Favero, G.; Frasconi, M.; Tata, A.; Tuccitto, N.; Licciardello, A.; Pepi, F. Soft-Landed Protein Voltammetry: A Tool for Redox Protein Characterization. *Anal. Chem.* **2008**, *80* (15), 5937–5944.

(88) Alvarez, J.; Futrell, J. H.; Laskin, J. Soft-Landing of Peptides onto Self-Assembled Monolayer Surfaces. *J. Phys. Chem. A* **2006**, *110* (4), 1678–1687.

(89) Rauschenbach, S.; Stadler, F. L.; Lunedei, E.; Malinowski, N.; Koltsov, S.; Costantini, G.; Kern, K. Electrospray Ion Beam Deposition of Clusters and Biomolecules. *Small* **2006**, *2* (4), 540–547.
(90) Wu, X.; Delbianco, M.; Anggara, K.; Michnowicz, T.; Pardo-Vargas, A.; Bharate, P.; Sen, S.; Pristl, M.; Rauschenbach, S.; Schlickum, U.; Abb, S.; Seeberger, P. H.; Kern, K. Imaging Single Glycans. *Nat. 2020 5827812* **2020**, *582* (7812), 375–378.
(91) Walz, A.; Stoiber, K.; Huettig, A.; Schlichting, H.; Barth, J. V. Navigate Flying Molecular Elephants Safely to the Ground: Mass-Selective Soft Landing up to the Mega-Dalton Range by Electrospray Controlled Ion-Beam Deposition. **2021**.
(92) Su, P.; Espenship, M. F.; Laskin, J. Principles of Operation of a Rotating Wall Mass Analyzer for Preparative Mass Spectrometry. *J. Am. Soc. Mass Spectrom.* **2020**, *31* (9), 1875–1884.
(93) Su, P.; Hu, H.; Unsihuay, D.; Zhang, D.; Dainese, T.; Diaz, R. E.; Lee, J.; Gunaratne, D. K.; Wang, H.; Maran, F.; Mei, J.; Laskin, J. Preparative Mass Spectrometry Using a Rotating-Wall Mass Analyzer. *Angew. Chemie* **2020**, *132* (20), 7785–7790.
(94) Su, P.; Hu, H.; Warneke, J.; Belov, M. E.; Anderson, G. A.; Laskin, J. Design and Performance of a Dual-Polarity Instrument for Ion Soft Landing. *Anal. Chem.* **2019**, *91* (9), 5904–5912.
(95) Badu-Tawiah, A. K.; Wu, C.; Cooks, R. G. Ambient Ion Soft Landing. *Anal. Chem.* **2011**, *83* (7), 2648–2654.
(96) Fremdling, P.; Esser, T. K.; Saha, B.; Makarov, A.; Fort, K.; Reinhardt-Szyba, M.; Gault, J.; Rauschenbach, S. A Preparative Mass Spectrometer to Deposit Intact Large Native Protein Complexes. **2022**.
(97) Gunaratne, K. D. D.; Prabhakaran, V.; Ibrahim, Y. M.; Norheim, R. V.; Johnson, G. E.; Laskin, J. Design and Performance of a High-Flux Electrospray Ionization Source for Ion Soft Landing. *Analyst* **2015**, *140* (9), 2957–2963.
(98) Goldstein, E. Ueber Eine Noch Nicht Untersuchte Strahlungsform an Der Kathode Inducirter Entladungen, Sitzungsbericht Der Berl. Akad., 25 Juli 1886. *Ann. Phys. Chem.* **1898**, *64* (1), 38–48.
(99) Wien, K. 100 Years of Ion Beams: Willy Wien's Canal Rays. *Braz. J. Phys.* **1999**, *29* (3), 401–414.
(100) Hedenus, M. Eugen Goldstein Und Die Kathodenstrahlen: Mit Astrophysik Im Labor Wurde Der Entdecker Der „Kanalstrahlen" Berühmt. *Phys. Blätter* **2000**, *56* (9), 71–73.
(101) Thomson, J. J. On Rays of Positive Electricity. In *Philos. Mag.*; Taylor & Francis Group, 1907; Vol. 13, pp 561–575.
(102) Thomson, J. J. Rays of Positive Electricity. In *Proc. R. Soci. of London,*

LXXXIX; The Royal Society London, 1913.
(103) Gamow, G. *The Great Physicists from Galileo to Einstein*, Dover publ.; New York, 1988.
(104) Fair, J. B. A Historical View of the Role of Ion-Implantation Defects in PN Junction Formation for Devices. *Mater. Res. Soc. Symp.* **2000**, *610*, B41.1-B41.12.
(105) Rose, P. H. A History of Commercial Implantation. *Nucl. Instruments Methods Phys. Res. Sect. B Beam Interact. with Mater. Atoms* **1985**, *6* (1–2), 1–8.
(106) Rose, P. H.; Ryding, G. Concepts and Designs of Ion Implantation Equipment for Semiconductor Processing. *Rev. Sci. Instrum.* **2006**, *77* (11).
(107) McKenna, C. M. A Personal Historical Perspective of Ion Implantation Equipment for Semiconductor Applications. In *IIt School Book (2000)*; Chester, 2000; pp 1–45.
(108) Yamada, I. Proc. 14th Symp. on Ion Sources and Ion-Assisted Technology; The Ion Engineering Society of Japan: Tokyo, 1991; pp 227–235.
(109) Yamada, I.; Matsuo, J.; Toyoda, N.; Kirkpatrick, A. Materials Processing by Gas Cluster Ion Beams. *Mater. Sci. Eng. R Reports* **2001**, *34* (6), 231–295.
(110) Yellot, J. I.; Holland, C. K. The Condensation of Flowing Steam: Condensation in Diverging Nozzles. *Engineering* **1937**, *143*, 647.
(111) Oswatitsch, K. Condensation Phenomena in Supersonic Nozzles. *Contrib. to Dev. Gasdyn.* **1980**, 397–418.
(112) Becker, E. W.; Bier, K.; Henkes, W. Strahlen Aus Kondensierten Atomen Und Molekeln Im Hochvakuum. *Zeitschrift für Phys.* **1956**, *146* (3), 333–338.
(113) Henkes, W. Massenspektroinetrische Untersuchung von Strahlen Aus Kondensiertem Wasserstoff. *Zeitschrift fur Naturforsch. - Sect. A J. Phys. Sci.* **1962**, *17* (9), 786–789.
(114) Becker, E. W. On the History of Cluster Beams. *Met. Clust.* **1986**, 1–7.
(115) McEachern, R. L.; Brown, W. L.; Jarrold, M. F.; Sosnowski, M.; Takaoka, G.; Usui, H.; Yamada, I. An Investigation of Cluster Formation in an Ionized Cluster Beam Deposition Source. *J. Vac. Sci. Technol. A Vacuum, Surfaces, Film.* **1998**, *9* (6), 3105.
(116) Brown, W. L.; Jarrold, M. F.; McEachern, R. L.; Sosnowski, M.; Takaoka, G.; Usui, H.; Yamada, I. Ion Cluster Beam Deposition of Thin Films. *Nucl. Instruments Methods Phys. Res. Sect. B Beam Interact. with Mater. Atoms* **1991**, *59–60* (PART 1), 182–189.
(117) Schaber, H.; Martin, T. P. Properties of a Cluster Source. *Surf. Sci.* **1985**, *156* (PART 1), 64–68.

(118) Dietz, T. G.; Duncan, M. A.; Powers, D. E.; Smalley, R. E. Laser Production of Supersonic Metal Cluster Beams. *J. Chem. Phys.* **1998**, *74* (11), 6511.
(119) Hagena, O. F.; Obert, W. Cluster Formation in Expanding Supersonic Jets: Effect of Pressure, Temperature, Nozzle Size, and Test Gas. *J. Chem. Phys.* **2003**, *56* (5), 1793.
(120) Wegener, P. P. Molecular Beams and Low Density Gasdynamics. *New York* **1974**, *4*.
(121) Landau, L. D.; Lifshitz, E. M. Theoretical Physics, Vol. 6, Fluid Mechanics. Pergamon, London 1987.
(122) Wegener, P. P. Gasdynamics of Expansion Flows with Condensation, and Homogeneous Nucleation of Water Vapor. *Nonequilibrium Flows* **1969**, *1*, 163–243.
(123) Springer, G. S. Advances in Heat Transfer. *Acad. Press* **1978**, *14*, 281–346.
(124) Wegener, P.; Parlange, J. Condensation by Homogeneous Nucleation in the Vapor Phase. **1970**.
(125) Wegener, P. P.; Pouring, A. A. Experiments on Condensation of Water Vapor by Homogeneous Nucleation in Nozzles. *Phys. Fluids* **2004**, *7* (3), 352.
(126) Hill, P. G. Condensation of Water Vapour during Supersonic Expansion in Nozzles. *J. Fluid Mech.* **1966**, *25* (3), 593–620.
(127) Hagena, O. F. Nucleation and Growth of Clusters in Expanding Nozzle Flows. *Surf. Sci.* **1981**, *106* (1–3), 101–116.
(128) Lu, H.; Ni, G.; Li, R.; Xu, Z. An Experimental Investigation on the Performance of Conical Nozzles for Argon Cluster Formation in Supersonic Jets. *J. Chem. Phys.* **2010**, *132* (12), 124303.
(129) Chen, G.; Kim, B.; Ahn, B.; Kim, D. E. Pressure Dependence of Argon Cluster Size for Different Nozzle Geometries. *J. Appl. Phys.* **2009**, *106* (5), 053507.
(130) Yamada, I. *Materials Processing by Cluster Ion Beams: History, Technology, and Applications*, CRC Press.; 2015.
(131) Wien, W. Untersuchungen Über Die Elektrische Entladung in Verdünnten Gasen. *Ann. Phys.* **1902**, *313* (6), 244–266.
(132) Yano, K.; Be, S. H. Mass Analyses of Cluster Ion Beams by Wien Filter. *Jpn. J. Appl. Phys.* **1980**, *19* (6), 1019–1025.
(133) Wrenger, B.; Meiwes-Broer, K. H. The Application of a Wien Filter to Mass Analysis of Heavy Clusters from a Pulsed Supersonic Nozzle Source. *Rev. Sci. Instrum.* **1998**, *68* (5), 2027.
(134) Wilson, R. G.; Brewer, G. R. *Ion Beams: With Applications to Ion Implantation*; Wiley, 1973.
(135) Hirohata, S.; Kosugi, T.; Sawaragi, H.; Aihara, R.; Gamo, K. Aberration

Properties of Focused Ion-beam Induced by Space Charge Effect. *J. Vac. Sci. Technol. B Microelectron. Nanom. Struct. Process. Meas. Phenom.* **1998**, *10* (6), 2814.

(136) Tanner, S. D. Space Charge in ICP-MS: Calculation and Implications. *Spectrochim. Acta Part B At. Spectrosc.* **1992**, *47* (6), 809–823.

(137) Chauvin, N.; Delferrière, O.; Duperrier, R.; Gobin, R.; Nghiem, P. A. P.; Uriot, D. Transport of Intense Ion Beams and Space Charge Compensation Issues in Low Energy Beam Lines (Invited)A). *Rev. Sci. Instrum.* **2012**, *83* (2), 02B320.

(138) Ishikawa, J.; Sano, F.; Takagi, T. Ion Beam Extraction with Ion Space-charge Compensation in Beam-plasma Type Ion Source. *J. Appl. Phys.* **1998**, *53* (9), 6018.

(139) Yamada, I.; Jones, J. M. E. C.; Takeuchi, D.; Aoki, T.; Goto, K.; Sugii, T. Materials Research Society Symposium Proceedings, Vol. 438,"Materials Modification and Synthesis by Ion Beam Processing", Eds. D. Alexander, B. Park, N. Cheung, and W. Skorupa, 1996. *Mater. Res. Soc. Pittsburgh* **1997**, 368.

(140) Gillen, G.; Roberson, S. Preliminary Evaluation of an SF 5 ‡ Polyatomic Primary Ion Beam for Analysis of Organic Thin Films by Secondary Ion Mass Spectrometry †.

(141) American, T. G.-S.; 1996, undefined. Collisions with Comets and Asteroids. *JSTOR* **1996**, *274* (3), 54–59.

(142) Delcorte, A.; Poleunis, C. Mechanistic Insight into Gas Cluster-Induced Sputtering of Kilodalton Molecules Using Kinetic Energy Distribution Measurements. *J. Phys. Chem. C* **2019**, *123* (32), 19704–19714.

(143) Delcorte, A.; Debongnie, M. Macromolecular Sample Sputtering by Large Ar and CH4 Clusters: Elucidating Chain Size and Projectile Effects with Molecular Dynamics. *J. Phys. Chem. C* **2015**, *119* (46), 25868–25879.

(144) Russo, M. F.; Wojciechowski, I. A.; Garrison, B. J. Sputtering of Amorphous Ice Induced by C60 and Au3 Clusters. *Appl. Surf. Sci.* **2006**, *252* (19), 6423–6425.

(145) Delcorte, A.; Garrison, B. J.; Hamraoui, K. Dynamics of Molecular Impacts on Soft Materials: From Fullerenes to Organic Nanodrops. *Anal. Chem.* **2009**, *81* (16), 6676–6686.

(146) Benninghoven, A.; Rudenauer, F. G.; Werner, H. W. Secondary Ion Mass Spectrometry: Basic Concepts, Instrumental Aspects, Applications and Trends. **1987**.

(147) Benninghoven, A. Untersuchungen Zum Spektrum Und Den Anfangsenergien Negativer Sekundärionen. *Zeitschrift für Phys. 1967 1991* **1967**, *199* (1), 141–156.

(148) Senoner, M.; Unger, W. E. S. SIMS Imaging of the Nanoworld:

Applications in Science and Technology. *J. Anal. At. Spectrom.* **2012**, *27* (7), 1050–1068.
(149) Belu, A. M.; Graham, D. J.; Castner, D. G. Time-of-Flight Secondary Ion Mass Spectrometry: Techniques and Applications for the Characterization of Biomaterial Surfaces. *Biomaterials* **2003**, *24* (21), 3635–3653.
(150) Hearn, M. J.; Briggs, D. Ion Beam Damage Effects in Poly(Methyl Methacrylate). *Surf. Interface Anal.* **1986**, *9* (1–6), 411.
(151) Storms, H. A.; Brown, K. F.; Stein, J. D. Evaluation of a Cesium Positive Ion Source for Secondary Ion Mass Spectrometry. *Anal. Chem.* **1977**, *49* (13), 2023–2030.
(152) Vickerman, J. C.; Briggs, D. *ToF-SIMS: Materials Analysis by Mass Spectrometry*; im publications, 2013.
(153) Jones, E. A.; Lockyer, N. P.; Vickerman, J. C. Depth Profiling Brain Tissue Sections with a 40 KeV C60+ Primary Ion Beam. *Anal. Chem.* **2008**, *80* (6), 2125–2132.
(154) Jones, E. A.; Lockyer, N. P.; Vickerman, J. C. Suppression and Enhancement of Non-Native Molecules within Biological Systems. *Appl. Surf. Sci.* **2006**, *252* (19), 6727–6730.
(155) Brown, A.; Vickerman, J. C. A Comparison of Positive and Negative Ion Static SIMS Spectra of Polymer Surfaces. *Surf. Interface Anal.* **1986**, *8* (2), 75–81.
(156) Briggs, D.; Wootton, A. B. Analysis of Polymer Surfaces by SIMS 1. An Investigation of Practical Problems. *Surf. Interface Anal.* **1982**, *4* (3), 109–115.
(157) Hagenhoff, B.; Leyen, D. van; Niehuis, E.; Benninghoven, A. Time-of-flight Secondary Ion Mass Spectrometry of Insulators with Pulsed Charge Compensation by Low-energy Electrons. *J. Vac. Sci. Technol. A Vacuum, Surfaces, Film.* **1998**, *7* (5), 3056.
(158) Benninghoven, A.; Loebach, E. Tandem Mass Spectrometer for Secondary Ion Studies. *Rev. Sci. Instrum.* **2003**, *42* (1), 49.
(159) Benninghoven, A. Some Aspects of Secondary Ion Mass Spectrometry of Organic Compounds. *Int. J. Mass Spectrom. Ion Phys.* **1983**, *53* (C), 85–99.
(160) Niehuis, E.; Heller, T.; Feld, H.; Benninghoven, A. Design and Performance of a Reflectron Based Time-of-flight Secondary Ion Mass Spectrometer with Electrodynamic Primary Ion Mass Separation. *J. Vac. Sci. Technol. A Vacuum, Surfaces, Film.* **1998**, *5* (4), 1243.
(161) Mamyrin, B.; Karataev, V.; Shmikk, D.; Fiz, V. Z.-Z. E. T.; 1973, undefined. The Mass-Reflectron, a New Nonmagnetic Time-of-Flight Mass Spectrometer with High Resolution. *jetp.ras.ru* **1973**.
(162) Briggs, D. Polymer Surface Analysis by XPS and Static SIMS. In

Cambridge Solid State Science; Cambridge University Press Cambridge, 1998.

(163) Barber, M.; Vickerman, J. C.; Wolstenholme, J. Adsorption and Surface Reactivity of Metals by Secondary Ion Mass Spectrometry. Part 1.—Adsorption of Carbon Monoxide on Nickel and Copper. *J. Chem. Soc. Faraday Trans. 1 Phys. Chem. Condens. Phases* **1976**, *72* (0), 40–50.

(164) Prewett, P. D.; Mair, G. L. R. *Focused Ion Beams from Liquid Metal Ion Sources*; Research Studies PressLtd, 1991; Vol. 1.

(165) Hill, R. Analysis Beams Used in ToF-SIMS. *TOF-SIMS Surf. Anal. by Mass Spectrom.* **2013**, 271–275.

(166) Touboul, D.; Kollmer, F.; Niehuis, E.; Brunelle, A.; Laprévote, O. Improvement of Biological Time-of-Flight-Secondary Ion Mass Spectrometry Imaging with a Bismuth Cluster Ion Source. *J. Am. Soc. Mass Spectrom.* **2005**, *16* (10), 1608–1618.

(167) Walker, A. V. Secondary Ion Mass Spectrometry. *Encycl. Spectrosc. Spectrom.* **2016**, 44–49.

(168) Benguerba, M.; Brunelle, A.; Della-Negra, S.; Depauw, J.; Joret, H.; Le Beyec, Y.; Blain, M. G.; Schweikert, E. A.; Assayag, G. Ben; Sudraud, P. Impact of Slow Gold Clusters on Various Solids: Nonlinear Effects in Secondary Ion Emission. *Nucl. Instruments Methods Phys. Res. Sect. B Beam Interact. with Mater. Atoms* **1991**, *62* (1), 8–22.

(169) Blain, M. G.; Della-Negra, S.; Joret, H.; Le Beyec, Y.; Schweikert, E. A. Secondary-Ion Yields from Surfaces Bombarded with KeV Molecular and Cluster Ions. *Phys. Rev. Lett.* **1989**, *63* (15), 1625.

(170) Andersen, H. H.; Brunelle, A.; Della-Negra, S.; Depauw, J.; Jacquet, D.; Le Beyec, Y.; Chaumont, J.; Bernas, H. Giant Metal Sputtering Yields Induced by 20--5000 KeV/Atom Gold Clusters. *Phys. Rev. Lett.* **1998**, *80* (24), 5433.

(171) Kötter, F.; Benninghoven, A. Secondary Ion Emission from Polymer Surfaces under Ar+, Xe+ and SF5+ Ion Bombardment. *Appl. Surf. Sci.* **1998**, *133* (1–2), 47–57.

(172) Biddulph, G. X.; Piwowar, A. M.; Fletcher, J. S.; Lockyer, N. P.; Vickerman, J. C. Properties of C84 and C24H12 Molecular Ion Sources for Routine TOF-SIMS Analysis. *Anal. Chem.* **2007**, *79* (19), 7259–7266.

(173) Kroto, H. W.; Heath, J. R.; O'Brien, S. C.; Curl, R. F.; Smalley, R. E. C60: Buckminsterfullerene. *Nature* **1985**, *318* (6042), 162–163.

(174) Scheier, P.; Dünser, B.; Wörgötter, R.; Lezius, M.; Robl, R.; Märk, T. D. Appearance and Ionization Energies of Singly, Doubly and Triply Charged C60 and Its Fragment Ions Produced by Electron Impact Ionization. *Int. J. Mass Spectrom. Ion Process.* **1994**, *138*, 77–93.

(175) Wong, S. C. C.; Hill, R.; Blenkinsopp, P.; Lockyer, N. P.; Weibel, D. E.; Vickerman, J. C. Development of a C60+ Ion Gun for Static SIMS and

Chemical Imaging. *Appl. Surf. Sci.* **2003**, *203*, 219–222.
(176) Fletcher, J. S.; Lockyer, N. P.; Vickerman, J. C. Ce60 Buckminsterfullerene: Its Impact on Biological ToF-SIMS Analysis. *Surf. Interface Anal.* **2006**, *38* (11), 1393–1400.
(177) Weibel, D. E.; Lockyer, N.; Vickerman, J. C. C60 Cluster Ion Bombardment of Organic Surfaces. *Appl. Surf. Sci.* **2004**, *231–232*, 146–152.
(178) Delcorte, A.; Garrison, B. J. Sputtering Polymers with Buckminsterfullerene Projectiles: A Coarse-Grain Molecular Dynamics Study. *J. Phys. Chem. C* **2007**, *111* (42), 15312–15324.
(179) Fletcher, J. S.; Lockyer, N. P.; Vaidyanathan, S.; Vickerman, J. C. TOF-SIMS 3D Biomolecular Imaging of Xenopus Laevis Oocytes Using Buckminsterfullerene (C60) Primary Ions. *Anal. Chem.* **2007**, *79* (6), 2199–2206.
(180) Czerwinski, B.; Delcorte, A. Molecular Dynamics Study of Fullerite Cross-Linking under KeV C 60 and Arn Cluster Bombardment. *J. Phys. Chem. C* **2013**, *117* (7), 3595–3604.
(181) Rabbani, S.; Barber, A. M.; Fletcher, J. S.; Lockyer, N. P.; Vickerman, J. C. TOF-SIMS with Argon Gas Cluster Ion Beams: A Comparison with C 60. *Anal. Chem* **2011**, *83*, 3793–3800.
(182) Toyoda, N.; Matsuo, J.; Aoki, T.; Yamada, I.; Fenner, D. B. Secondary Ion Mass Spectrometry with Gas Cluster Ion Beams. *Nucl. Instruments Methods Phys. Res. Sect. B Beam Interact. with Mater. Atoms* **2002**, *190* (1–4), 860–864.
(183) Ninomiya, S.; Nakata, Y.; Ichiki, K.; Seki, T.; Aoki, T.; Matsuo, J. Measurements of Secondary Ions Emitted from Organic Compounds Bombarded with Large Gas Cluster Ions. *Nucl. Instruments Methods Phys. Res. Sect. B Beam Interact. with Mater. Atoms* **2007**, *256* (1), 493–496.
(184) Ninomiya, S.; Nakata, Y.; Honda, Y.; Ichiki, K.; Seki, T.; Aoki, T.; Matsuo, J. A Fragment-Free Ionization Technique for Organic Mass Spectrometry with Large Ar Cluster Ions. *Appl. Surf. Sci.* **2008**, *255* (4), 1588–1590.
(185) Delcorte, A.; Cristaudo, V.; Lebec, V.; Czerwinski, B. Sputtering of Polymers by KeV Clusters: Microscopic Views of the Molecular Dynamics. *Int. J. Mass Spectrom.* **2014**, *370*, 29–38.
(186) Ninomiya, S.; Ichiki, K.; Yamada, H.; Nakata, Y.; Seki, T.; Aoki, T.; Matsuo, J. Molecular Depth Profiling of Multilayer Structures of Organic Semiconductor Materials by Secondary Ion Mass Spectrometry with Large Argon Cluster Ion Beams. *Rapid Commun. Mass Spectrom.* **2009**, *23* (20), 3264–3268.
(187) Michel, R.; Castner, D. G. Advances in Time-of-Flight Secondary Ion

Mass Spectrometry Analysis of Protein Films. *Surf. Interface Anal.* **2006**, *38* (11), 1386–1392.
(188) Wagner, M. S.; Graham, D. J.; Ratner, B. D.; Castner, D. G. Maximizing Information Obtained from Secondary Ion Mass Spectra of Organic Thin Films Using Multivariate Analysis. *Surf. Sci.* **2004**, *570* (1–2), 78–97.
(189) Graham, D. J.; Wagner, M. S.; Castner, D. G. Information from Complexity: Challenges of TOF-SIMS Data Interpretation. *Appl. Surf. Sci.* **2006**, *252* (19), 6860–6868.
(190) Wold, S.; Esbensen, K.; Geladi, P. Principal Component Analysis. *Chemom. Intell. Lab. Syst.* **1987**, *2* (1–3), 37–52.
(191) Bro, R.; Smilde, A. K. Principal Component Analysis. *Anal. Methods* **2014**, *6* (9), 2812–2831.
(192) Abdi, H.; Williams, L. J. Principal Component Analysis. *Wiley Interdiscip. Rev. Comput. Stat.* **2010**, *2* (4), 433–459.
(193) Henderson, A. Multivariate Analysis of SIMS Spectra. *TOF-SIMS Mater. Anal. by Mass Spectrom.* **2013**, 449–484.
(194) Wagner, M. S.; Graham, D. J.; Castner, D. G. Simplifying the Interpretation of ToF-SIMS Spectra and Images Using Careful Application of Multivariate Analysis. *Appl. Surf. Sci.* **2006**, *252* (19), 6575–6581.
(195) Field, A. *Discovering Statistics Using IBM SPSS Statistics*; sage, 2013.
(196) Graham, D. J.; Castner, D. G. Multivariate Analysis of ToF-SIMS Data from Multicomponent Systems: The Why, When, and How. *Biointerphases* **2012**, *7* (1), 49.
(197) Lhoest, J.-B.; Wagner, M. S.; Tidwell, C. D.; Castner, D. G. Characterization of Adsorbed Protein Films by Time of Flight Secondary Ion Mass Spectrometry. *J. Biomed. Mater. Res.* **2001**, *57* (3), 432–440.
(198) Wagner, M. S.; Castner, D. G. Characterization of Adsorbed Protein Films by Time-of-Flight Secondary Ion Mass Spectrometry with Principal Component Analysis. *Langmuir* **2001**, *17* (15), 4649–4660.
(199) Wagner, M. S.; McArthur, S. L.; Shen, M.; Horbett, T. A.; Castner, D. G. Limits of Detection for Time of Flight Secondary Ion Mass Spectrometry (ToF-SIMS) and X-Ray Photoelectron Spectroscopy (XPS): Detection of Low Amounts of Adsorbed Protein. *J. Biomater. Sci. Polym. Ed.* **2002**, *13* (4), 407–428.
(200) Xia, N.; May, C. J.; McArthur, S. L.; Castner, D. G. Time-of-Flight Secondary Ion Mass Spectrometry Analysis of Conformational Changes in Adsorbed Protein Films. *Langmuir* **2002**, *18* (10), 4090–4097.
(201) Gajos, K.; Awsiuk, K.; Budkowski, A. Controlling Orientation,

Conformation, and Biorecognition of Proteins on Silane Monolayers, Conjugate Polymers, and Thermo-Responsive Polymer Brushes: Investigations Using TOF-SIMS and Principal Component Analysis. *Colloid Polym. Sci. 2020 2993* **2020**, *299* (3), 385–405.

(202) Gajos, K.; Budkowski, A.; Petrou, P.; Kakabakos, S. A Perspective on ToF-SIMS Analysis of Biosensor Interfaces: Controlling and Optimizing Multi-Molecular Composition, Immobilization through Bioprinting, Molecular Orientation. *Appl. Surf. Sci.* **2022**, *594*, 153439.

(203) Foster, R. N.; Harrison, E. T.; Castner, D. G. ToF-SIMS and XPS Characterization of Protein Films Adsorbed onto Bare and Sodium Styrenesulfonate-Grafted Gold Substrates. *Langmuir* **2016**, *32* (13), 3207–3216.

(204) Lebec, V.; Landoulsi, J.; Boujday, S.; Poleunis, C.; Pradier, C. M.; Delcorte, A. Probing the Orientation of β-Lactoglobulin on Gold Surfaces Modified by Alkyl Thiol Self-Assembled Monolayers. *J. Phys. Chem. C* **2013**, *117* (22), 11569–11577.

(205) Dupont-Gillain, C. C.; Mc Evoy, K. M.; Henry, M.; Bertrand, P. Surface Spectroscopy of Adsorbed Proteins: Input of Data Treatment by Principal Component Analysis. *J. Mater. Sci. Mater. Med.* **2010**, *21* (3), 955–961.

(206) Kempson, I. M.; Martin, A. L.; Denman, J. A.; French, P. W.; Prestidge, C. A.; Barnes, T. J. Detecting the Presence of Denatured Human Serum Albumin in an Adsorbed Protein Monolayer Using TOF-SIMS. *Langmuir* **2010**, *26* (14), 12075–12080.

(207) Kim, Y. P.; Hong, M. Y.; Kim, J.; Oh, E.; Shon, H. K.; Moon, D. W.; Kim, H. S.; Lee, T. G. Quantitative Analysis of Surface-Immobilized Protein by TOF-SIMS: Effects of Protein Orientation and Trehalose Additive. *Anal. Chem.* **2007**, *79* (4), 1377–1385.

(208) Wagner, M. S.; Castner, D. G. Analysis of Adsorbed Proteins by Static Time-of-Flight Secondary Ion Mass Spectrometry. *Appl. Surf. Sci.* **2004**, *231–232*, 366–376.

(209) Henry, M.; Dupont-Gillain, C.; Bertrand, P. Conformation Change of Albumin Adsorbed on Polycarbonate Membranes as Revealed by ToF-SIMS. *Langmuir* **2003**, *19* (15), 6271–6276.

(210) Massonnet, P.; Heeren, R. M. A. A Concise Tutorial Review of TOF-SIMS Based Molecular and Cellular Imaging. *J. Anal. At. Spectrom.* **2019**, *34* (11), 2217–2228.

(211) Tyler, B. J.; Rayal, G.; Castner, D. G. Multivariate Analysis Strategies for Processing ToF-SIMS Images of Biomaterials. *Biomaterials* **2007**, *28* (15), 2412–2423.

(212) Wickes, B. T.; Kim, Y.; Castner, D. G. Denoising and Multivariate Analysis of Time-of-Flight SIMS Images. *Surf. Interface Anal.* **2003**, *35*

(8), 640–648.
(213) Gajos, K.; Budkowski, A.; Petrou, P.; Pagkali, V.; Awsiuk, K.; Rysz, J.; Bernasik, A.; Misiakos, K.; Raptis, I.; Kakabakos, S. Protein Adsorption/Desorption and Antibody Binding Stoichiometry on Silicon Interferometric Biosensors Examined with TOF-SIMS. *Appl. Surf. Sci.* **2018**, *444*, 187–196.
(214) Brüning, C.; Hellweg, S.; Dambach, S.; Lipinsky, D.; Arlinghaus, H. F. Improving the Interpretation of ToF-SIMS Measurements on Adsorbed Proteins Using PCA. *Surf. Interface Anal.* **2006**, *38* (4), 191–193.
(215) Welch, N. G.; Madiona, R. M. T.; Scoble, J. A.; Muir, B. W.; Pigram, P. J. ToF-SIMS and Principal Component Analysis Investigation of Denatured, Surface-Adsorbed Antibodies. *Langmuir* **2016**, *32* (42), 10824–10834.
(216) Harrison, E. T.; Wang, Y.-C.; Carter, L.; Castner, D. G. Characterizing Protein G B1 Orientation and Its Effect on Immunoglobulin G Antibody Binding Using XPS, ToF-SIMS, and Quartz Crystal Microbalance with Dissipation Monitoring. *Biointerphases* **2020**, *15* (2), 021002.
(217) Welch, N. G.; Madiona, R. M. T.; Payten, T. B.; Easton, C. D.; Pontes-Braz, L.; Brack, N.; Scoble, J. A.; Muir, B. W.; Pigram, P. J. Surface Immobilized Antibody Orientation Determined Using ToF-SIMS and Multivariate Analysis. *Acta Biomater.* **2017**, *55*, 172–182.
(218) Madiona, R. M. T.; Welch, N. G.; Muir, B. W.; Winkler, D. A.; Pigram, P. J. Rapid Evaluation of Immobilized Immunoglobulins Using Automated Mass-Segmented ToF-SIMS. *Biointerphases* **2019**, *14* (6), 061002.
(219) Gajos, K.; Szafraniec, K.; Petrou, P.; Budkowski, A. Surface Density Dependent Orientation and Immunological Recognition of Antibody on Silicon: TOF-SIMS and Surface Analysis of Two Covalent Immobilization Methods. *Appl. Surf. Sci.* **2020**, *518*, 146269.
(220) Benetti, F.; Perra, G.; Damiani, D.; Atrei, A.; Marchettini, N. ToF-SIMS Characterization of Proteinaceous Binders in the Wall Painting "Madonna and Child Enthroned with Saints" by Ambrogio Lorenzetti in the St. Augustine Church (Siena, Italy). *Int. J. Mass Spectrom.* **2015**, *392*, 111–117.
(221) Park, J. W.; Min, H.; Kim, Y. P.; Shon, H. K.; Kim, J.; Moon, D. W.; Lee, T. G. Multivariate Analysis of ToF-SIMS Data for Biological Applications. *Surf. Interface Anal.* **2009**, *41* (8), 694–703.
(222) Urbini, M.; Petito, V.; de Notaristefani, F.; Scaldaferri, F.; Gasbarrini, A.; Tortora, L. ToF-SIMS and Principal Component Analysis of Lipids and Amino Acids from Inflamed and Dysplastic Human Colonic Mucosa. *Anal. Bioanal. Chem.* **2017**, *409* (26), 6097–6111.

(223) Yu, J.; Zhou, Y.; Engelhard, M.; Zhang, Y.; Son, J.; Liu, S.; Zhu, Z.; Yu, X. Y. In Situ Molecular Imaging of Adsorbed Protein Films in Water Indicating Hydrophobicity and Hydrophilicity. *Sci. Reports 2020 101* **2020**, *10* (1), 1–8.
(224) Wald, J.; Müller, C.; Wahl, M.; Hoth-Hannig, W.; Hannig, M.; Kopnarski, M.; Ziegler, C. ToF-SIMS Investigations of Adsorbed Proteins on Dental Titanium. *Phys. status solidi* **2010**, *207* (4), 831–836.
(225) Michel, R.; Castner, D. G. Advances in Time-of-Flight Secondary Ion Mass Spectrometry Analysis of Protein Films. *Surf. Interface Anal.* **2006**, *38* (11), 1386–1392.
(226) Muramoto, S.; Graham, D. J.; Wagner, M. S.; Lee, T. G.; Moon, D. W.; Castner, D. G. ToF-SIMS Analysis of Adsorbed Proteins: Principal Component Analysis of the Primary Ion Species Effect on the Protein Fragmentation Patterns. *J. Phys. Chem. C* **2011**, *115* (49), 24247–24255.
(227) Matsuda, K.; Aoyagi, S. Time-of-Flight Secondary Ion Mass Spectrometry Analysis of Hair Samples Using Unsupervised Artificial Neural Network. *Biointerphases* **2020**, *15* (2), 021013.
(228) Welch, N. G.; Madiona, R. M. T.; Payten, T. B.; Jones, R. T.; Brack, N.; Muir, B. W.; Pigram, P. J. Surface Adsorbed Antibody Characterization Using ToF-SIMS with Principal Component Analysis and Artificial Neural Networks. *Langmuir* **2016**, *32* (34), 8717–8728.
(229) Sanni, O. D.; Wagner, M. S.; Briggs, D.; Castner, D. G.; Vickerman, J. C. Classification of Adsorbed Protein Static ToF-SIMS Spectra by Principal Component Analysis and Neural Networks. *Surf. Interface Anal.* **2002**, *33* (9), 715–728.
(230) Matsuo, J.; Ninomiya, S.; Nakata, Y.; Honda, Y.; Ichiki, K.; Seki, T.; Aoki, T. What Size of Cluster Is Most Appropriate for SIMS? *Appl. Surf. Sci.* **2008**, *255* (4), 1235–1238.
(231) Mochiji, K.; Hashinokuchiy, M.; Moritani, K.; Toyoda, N. Matrix-Free Detection of Intact Ions from Proteins in Argon-Cluster Secondary Ion Mass Spectrometry. *Rapid Commun. Mass Spectrom.* **2009**, *23* (5), 648–652.
(232) Son, J. G.; Yoon, S.; Shon, H. K.; Moon, J. H.; Joh, S.; Lee, T. G. Ar-Gas Cluster Ion Beam in ToF-SIMS for Peptide and Protein Analysis. *Biointerphases* **2020**, *15* (2), 021011.
(233) Aoyagi, S.; Fletcher, J. S.; Sheraz, S.; Kawashima, T.; Berrueta Razo, I.; Henderson, A.; Lockyer, N. P.; Vickerman, J. C. Peptide Structural Analysis Using Continuous Ar Cluster and C60 Ion Beams. *Anal. Bioanal. Chem.* **2013**, *405* (21), 6621–6628.
(234) Gnaser, H.; Fujii, M.; Nakagawa, S.; Seki, T.; Aoki, T.; Matsuo, J.

Peptide Dissociation Patterns in Secondary Ion Mass Spectrometry under Large Argon Cluster Ion Bombardment. *Rapid Commun. Mass Spectrom.* **2013**, *27* (13), 1490–1496.

(235) Aoyagi, S.; Kawashima, T.; Yokoyama, Y. Peptide Fragmentation Caused by Ar Cluster Ions Depending on Primary Ion Energy. *Rapid Commun. Mass Spectrom.* **2015**, *29* (18), 1687–1695.

(236) Yokoyama, Y.; Aoyagi, S.; Fujii, M.; Matsuo, J.; Fletcher, J. S.; Lockyer, N. P.; Vickerman, J. C.; Passarelli, M. K.; Havelund, R.; Seah, M. P. Peptide Fragmentation and Surface Structural Analysis by Means of ToF-SIMS Using Large Cluster Ion Sources. *Anal. Chem.* **2016**, *88* (7), 3592–3597.

(237) lshikawa, K.; Okamoto, M.; Aoyagi, S. Structural Analysis of the Outermost Hair Surface Using TOF-SIMS with Gas Cluster Ion Beam Sputtering. *Biointerphases* **2016**, *11* (2), 02A315.

(238) Winograd, N. Gas Cluster Ion Beams for Secondary Ion Mass Spectrometry. **2018**, *11*, 29–48.

(239) Angerer, T. B.; Velickovic, D.; Nicora, C. D.; Kyle, J. E.; Graham, D. J.; Anderton, C.; Gamble, L. J. Exploiting the Semi-Destructive Nature of GCIB-ToF-SIMS Imaging for Simultaneous Localization and Confident Lipid Annotations. *Anal. Chem.* **2019**, *91* (23), 15073.

(240) Passarelli, M. K.; Pirkl, A.; Moellers, R.; Grinfeld, D.; Kollmer, F.; Havelund, R.; Newman, C. F.; Marshall, P. S.; Arlinghaus, H.; Alexander, M. R.; West, A.; Horning, S.; Niehuis, E.; Makarov, A.; Dollery, C. T.; Gilmore, I. S. The 3D OrbiSIMS - Label-Free Metabolic Imaging with Subcellular Lateral Resolution and High Mass-Resolving Power. *Nat. Methods* **2017**, *14* (12), 1175–1183.

(241) Kotowska, A. M.; Trindade, G. F.; Mendes, P. M.; Williams, P. M.; Aylott, J. W.; Shard, A. G.; Alexander, M. R.; Scurr, D. J. Protein Identification by 3D OrbiSIMS to Facilitate in Situ Imaging and Depth Profiling. *Nat. Commun. 2020 111* **2020**, *11* (1), 1–8.

(242) Fu, T.; Della-Negra, S.; Touboul, D.; Brunelle, A. Internal Energy Distribution of Secondary Ions Under Argon and Bismuth Cluster Bombardments: “Soft” Versus “Hard” Desorption–Ionization Process. *J. Am. Soc. Mass Spectrom.* **2019**, *30* (2), 321–328.

(243) Toyoda, N.; Yamada, I. Reduction of Irradiation Damage Using Size-Controlled Nitrogen Gas Cluster Ion Beams. *Nucl. Instruments Methods Phys. Res. Sect. B Beam Interact. with Mater. Atoms* **2012**, *273*, 11–14.

(244) Toyoda, N.; Yamada, I. Cluster Size Dependence of Surface Morphology after Gas Cluster Ion Bombardments. *Nucl. Instruments Methods Phys. Res. Sect. B Beam Interact. with Mater. Atoms* **2008**, *266* (10), 2529–2532.

(245) Toyoda, N.; Yamada, I. Low-Damage Processing Using Size-Controlled Gas Cluster Ion Beams. *Nucl. Instruments Methods Phys. Res. Sect. B Beam Interact. with Mater. Atoms* **2007**, *261* (1–2), 643–646.
(246) Ichiki, K.; Ninomiya, S.; Seki, T.; Aoki, T.; Matsuol, J. Sputtering Yield Measurements with Size-Selected Gas Cluster Ion Beams. *MRS Online Proc. Libr.* **2009**, *1181*, 135–140.
(247) Delcorte, A. A Microscopic View of Macromolecule Transfer in the Vacuum Using Gas and Bismuth Clusters. *J. Phys. Chem. C* **2022**, *126* (16), 7307–7318.
(248) Adriaensen, L.; Vangaever, F.; Lenaerts, J.; Gijbels, R. Matrix-Enhanced Secondary Ion Mass Spectrometry: The Influence of MALDI Matrices on Molecular Ion Yields of Thin Organic Films. *Rapid Commun. Mass Spectrom.* **2005**, *19* (8), 1017–1024.
(249) Heeren, R. M. A.; McDonnell, L. A.; Amstalden, E.; Luxembourg, S. L.; Altelaar, A. F. M.; Piersma, S. R. Why Don't Biologists Use SIMS?: A Critical Evaluation of Imaging MS. *Appl. Surf. Sci.* **2006**, *252* (19), 6827–6835.
(250) Delcorte, A. Matrix-Enhanced Secondary Ion Mass Spectrometry: The Alchemist's Solution? *Appl. Surf. Sci.* **2006**, *252* (19), 6582–6587.
(251) Locklear, J. E.; Guillermier, C.; Verkhoturov, S. V.; Schweikert, E. A. Matrix-Enhanced Cluster-SIMS. *Appl. Surf. Sci.* **2006**, *252* (19), 6624–6627.
(252) MacAleese, L.; Duursma, M. C.; Klerk, L. A.; Fisher, G.; Heeren, R. M. A. Protein Identification with Liquid Chromatography and Matrix Enhanced Secondary Ion Mass Spectrometry (LC-ME-SIMS). *J. Proteomics* **2011**, *74* (7), 993–1001.
(253) Dowlatshahi Pour, M.; Malmberg, P.; Ewing, A. An Investigation on the Mechanism of Sublimed DHB Matrix on Molecular Ion Yields in SIMS Imaging of Brain Tissue. *Anal. Bioanal. Chem.* **2016**, *408* (12), 3071–3081.
(254) Fitzgerald, J. J. D.; Kunnath, P.; Walker, A. V. Matrix-Enhanced Secondary Ion Mass Spectrometry (ME SIMS) Using Room Temperature Ionic Liquid Matrices. *Anal. Chem.* **2010**, *82* (11), 4413–4419.
(255) Ogrinc Potočnik, N.; Fisher, G. L.; Prop, A.; Heeren, R. M. A. Sequencing and Identification of Endogenous Neuropeptides with Matrix-Enhanced Secondary Ion Mass Spectrometry Tandem Mass Spectrometry. *Anal. Chem.* **2017**, *89* (16), 8223–8227.
(256) Korsgen, M.; Pelster, A.; Dreisewerd, K.; Arlinghaus, H. F. 3D ToF-SIMS Analysis of Peptide Incorporation into MALDI Matrix Crystals with Sub-Micrometer Resolution. *J. Am. Soc. Mass Spectrom.* **2016**, *27* (2), 277–284.

(257) Körsgen, M.; Tyler, B. J.; Pelster, A.; Lipinsky, D.; Dreisewerd, K.; Arlinghaus, H. F. Changes in the Molecular Ion Yield and Fragmentation of Peptides under Various Primary Ions in ToF-SIMS and Matrix-Enhanced ToF-SIMS. *Biointerphases* **2016**, *11* (2), 02A318.
(258) Piwowar, A. M.; Keskin, S.; Delgado, M. O.; Shen, K.; Hue, J. J.; Lanekoff, I.; Ewing, A. G.; Winograd, N. C60-ToF SIMS Imaging of Frozen Hydrated HeLa Cells. *Surf. Interface Anal.* **2013**, *45* (1), 302–304.
(259) Piwowar, A. M.; Fletcher, J. S.; Kordys, J.; Lockyer, N. P.; Winograd, N.; Vickerman, J. C. Effects of Cryogenic Sample Analysis on Molecular Depth Profiles with TOF-Secondary Ion Mass Spectrometry. *Anal. Chem.* **2010**, *82* (19), 8291–8299.
(260) Conlan, X. A.; Lockyer, N. P.; Vickerman, J. C. Is Proton Cationization Promoted by Polyatomic Primary Ion Bombardment during Time-of-Flight Secondary Ion Mass Spectrometry Analysis of Frozen Aqueous Solutions? *Rapid Commun. Mass Spectrom.* **2006**, *20* (8), 1327–1334.
(261) Mouhib, T.; Delcorte, A.; Poleunis, C.; Bertrand, P. Organic Secondary Ion Mass Spectrometry: Signal Enhancement by Water Vapor Injection. *J. Am. Soc. Mass Spectrom.* **2011**, *21* (12), 2005–2010.
(262) Mouhib, T.; Delcorte, A.; Poleunis, C.; Bertrand, P. Organic Ion Yield Enhancement in Secondary Ion Mass Spectrometry Using Water Vapour Injection. *Surf. Interface Anal.* **2013**, *45* (1), 46–49.
(263) Angerer, T. B.; Dowlatshahi Pour, M.; Malmberg, P.; Fletcher, J. S. Improved Molecular Imaging in Rodent Brain with Time-of-Flight-Secondary Ion Mass Spectrometry Using Gas Cluster Ion Beams and Reactive Vapor Exposure. *Anal. Chem.* **2015**, *87* (8), 4305–4313.
(264) Angerer, T. B.; Mohammadi, A. S.; Fletcher, J. S. Optimizing Sample Preparation for Anatomical Determination in the Hippocampus of Rodent Brain by ToF-SIMS Analysis. *Biointerphases* **2016**, *11* (2), 02A319.
(265) Sheraz Née Rabbani, S.; Razo, I. B.; Kohn, T.; Lockyer, N. P.; Vickerman, J. C. Enhancing Ion Yields in Time-of-Flight-Secondary Ion Mass Spectrometry: A Comparative Study of Argon and Water Cluster Primary Beams. *Anal. Chem.* **2015**, *87* (4), 2367–2374.
(266) Tian, H.; Sheraz Née Rabbani, S.; Vickerman, J. C.; Winograd, N. Multiomics Imaging Using High-Energy Water Gas Cluster Ion Beam Secondary Ion Mass Spectrometry [(H2O)n-GCIB-SIMS] of Frozen-Hydrated Cells and Tissue. *Anal. Chem.* **2021**, *93* (22), 7808–7814.
(267) Tian, H.; Sparvero, L. J.; Anthonymuthu, T. S.; Sun, W. Y.; Amoscato, A. A.; He, R. R.; Bayır, H.; Kagan, V. E.; Winograd, N. Successive High-Resolution (H2O)n-GCIB and C60-SIMS Imaging Integrates Multi-Omics in Different Cell Types in Breast Cancer Tissue. *Anal. Chem.*

2021, *93* (23), 8143–8151.

(268) Sheraz, S.; Barber, A.; Razo, I. B.; Fletcher, J. S.; Lockyer, N. P.; Vickerman, J. C. Prospect of Increasing Secondary Ion Yields in ToF-SIMS Using Water Cluster Primary Ion Beams. *Surf. Interface Anal.* **2014**, *46* (S1), 51–53.

(269) Dimovska Nilsson, K.; Karagianni, A.; Kaya, I.; Henricsson, M.; Fletcher, J. S. (CO2)N+, (H2O)N+, and (H2O)N+ (CO2) Gas Cluster Ion Beam Secondary Ion Mass Spectrometry: Analysis of Lipid Extracts, Cells, and Alzheimer's Model Mouse Brain Tissue. *Anal. Bioanal. Chem.* **2021**, *413* (16), 4181.

(270) Moritani, K.; Nagata, S.; Tanaka, A.; Goto, K.; Inui, N. Large Molecular Cluster Formation from Liquid Materials and Its Application to ToF-SIMS. *Quantum Beam Sci. 2021, Vol. 5, Page 10* **2021**, *5* (2), 10.

(271) Moritani, K.; Kanai, M.; Goto, K.; Ihara, I.; Inui, N.; Mochiji, K. Secondary Ion Emission from Insulin Film Bombarded with Methane and Noble Gas Cluster Ion Beams. *Nucl. Instruments Methods Phys. Res. Sect. B Beam Interact. with Mater. Atoms* **2013**, *315*, 300–303.

(272) Wucher, A.; Tian, H.; Winograd, N. A Mixed Cluster Ion Beam to Enhance the Ionization Efficiency in Molecular Secondary Ion Mass Spectrometry. *Rapid Commun. Mass Spectrom.* **2014**, *28* (4), 396–400.

(273) Tian, H.; Wucher, A.; Winograd, N. Reducing the Matrix Effect in Organic Cluster SIMS Using Dynamic Reactive Ionization. *J. Am. Soc. Mass Spectrom.* **2016**, *27* (12), 2014–2024.

(274) Lagator, M.; Berrueta Razo, I.; Royle, T.; Lockyer, N. P. Sensitivity Enhancement Using Chemically Reactive Gas Cluster Ion Beams in Secondary Ion Mass Spectrometry (SIMS). *Surf. Interface Anal.* **2022**, *54* (4), 349–355.

Chapter 2 : Objectives and strategy

2.1. Objectives

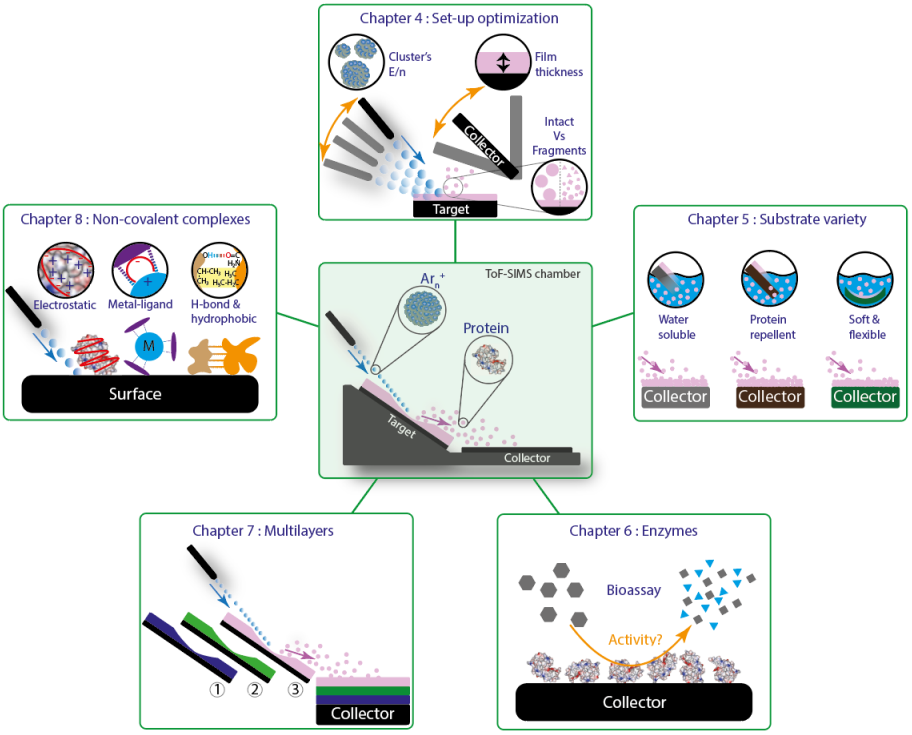


Figure 2.1. *Schematic illustration of the main goals that were pursued in this work.*

This thesis aims at **the development of an innovative solvent-free method for the construction of protein thin films**. Relying on the use of a time-of-flight secondary ion mass spectrometer, it is proposed to utilize large argon cluster ion beams to transfer a plume of pure protein molecules from a target sample to a collector surface. In principle, this technique should offer a series of advantages in comparison to existing methods, and help overcoming a few obstacles still encountered today with respect to protein thin films preparation. The developed approach could possibly enable the controlled construction of complex multilayers that are out of reach of current techniques. This should significantly expand the scope of applications of protein thin films. The developed method should allow i) **the deposition of intact proteins**, and in the case of enzymes, with retention of their enzymatic activity; ii) **a controlled biointerface construction**, in terms of thickness and spatial distribution; iii) the deposition on a multitude of **different substrates**;

iv) the **construction of mixed multilayers** made of different proteins or other compounds, including in the form of alternated layers. Transferring intact proteins involves desorbing objects whose 3D structure is mainly defined by weak non-covalent interactions. In order to gain more insights into the ability of ToF-SIMS to desorb such compounds held together by weak interactions without breaking them, **the desorption and the transfer of a few model non-covalent complexes** will also be investigated.

2.2. Strategy

2.2.1. Optimizing the transfer procedure

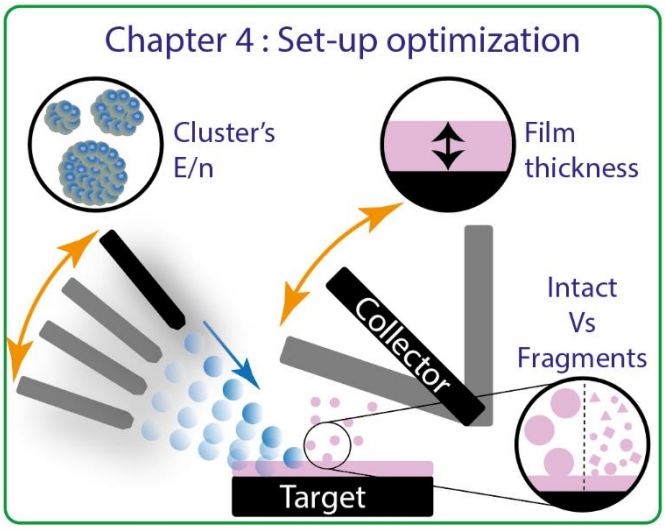


Figure 2.2. *Graphical abstract of Chapter 4.*

In **Chapter 4**, peptides and small proteins will be used as model molecules to assess the feasibility of the proposed transfer method. Angiotensin and bradykinin will be the first protein-like candidates to be transferred. Having both a mass around 1 kDa, their molecular ions are easily detectable in SIMS. That is very convenient as *in situ* SIMS analysis of the collector can then immediately provide relevant information regarding the fragmentation of the peptide molecules upon transfer. These two peptides will be used to further optimize the transfer conditions. The preliminary experiments should answer a few technical questions such as “how to prepare the target?” or “what size should the target and collector substrates have?”. A more in depth study should lead to optimized transfer conditions in terms of cluster size and energy (thus *in fine* defining the optimal E/n of the constituent atoms), and in terms of transfer geometry (primary ion impinging angle on the target

and collecting angle). Bradykinin will also be used to investigate the possibility to finely control the thickness and the homogeneity of the deposited layer. To this end, it is envisaged to develop an *in situ* method for the measurement of the thickness directly using the ToF-SIMS instrument. Once the optimized transfer parameters will have been determined, it will be time to investigate the transfer of larger molecules. To this end, a small protein, insulin (6 kDa), is planned to be the first selected protein. If the transfer is a success, the next step will be to transfer enzymes (inherently larger) and to investigate whether the transfer conditions allow the deposition of intact and bioactive proteins (e.g. without alteration of their 3D structure that would affect their activity).

2.2.2. Transfer on water-sensitive substrate, functionalized collectors, and soft substrates

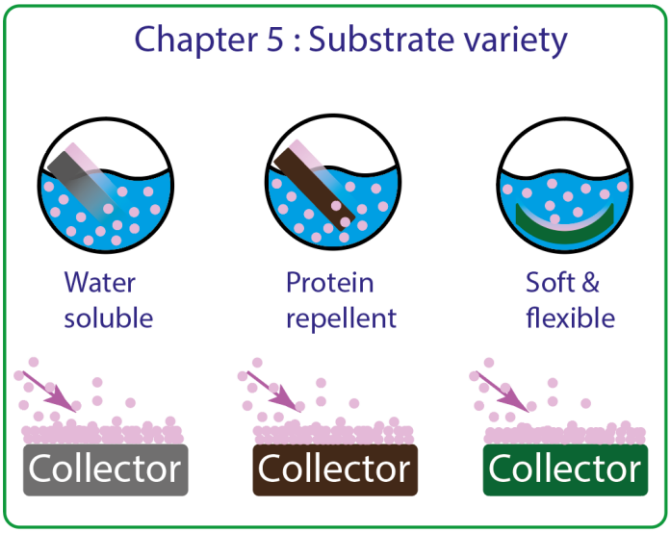


***Figure 2.3**. Graphical abstract of Chapter 5.*

One of the main limitations of the well-established solution-based protein adsorption methods is that they can only be considered for substrates that are water compatible/resistant. With the present solvent-free approach, it is hoped to expand the scope of accessible substrates to theoretically any solid material that can withstand vacuum. In **Chapter 5**, to demonstrate this promising feature, the transfer of proteins on paper, a common material whose properties are altered when placed in contact with water, will be investigated. The result of a deposition achieved with our transfer method will be compared to that obtained by spin-coating.

This study will also explore the possibility to transfer the proteins on "functionalized" collectors. The focus will be on finding a way to trigger a rapid and complete release of the proteins from the surface once the latter is placed into solution. In a practical sense, it could really help in the quantification of the proteins deposited on the collectors, as well as for the other analyses that require having the proteins in solution. In addition, on a long-term perspective, this could be beneficial for applications where the proteins need to be delivered at once in solution (delivery applications). Two strategies will be considered in this work, employing a collector coated either with a protein-repulsive material, a polyethylene glycol (PEG) self-assembled monolayer (SAM), or with a sacrificial layer, prepared with sugar, trehalose or fructose. In the case of the PEG coating, it was decided to work with thiol-terminated PEG. Combined with gold-coated silicon wafers, it allows the spontaneous grafting of the PEG to the substrate. For both the PEG and the sugar layers, it will first be necessary to control that the molecules of the layer do not interfere with the bioassays that will be used for to quantify and to probe the activity of the proteins. The work will then be focused on the preparation of the collectors. Once the functionalized collectors are prepared, proteins will be transferred, and the release of the proteins in solution will be investigated.

Finally, proteins will be transferred on a soft material, in this case polyethylene (PE) films. The strong benefit of working with flexible collectors is that they are ultimately easier to handle to perform any type of analysis after protein deposition. In this case, the goal is to work with a type of collector that could fit into small Eppendorf tubes. These are extremely handy to carry out bioassays in small solution volumes, without experiencing evaporation problems. It will be investigated how these flexible collectors could help to overcome technical issues encountered with solid substrates. In addition to the analytical advantages, the ability to transfer the proteins on soft substrates could be exploited to develop various applications, such as biomedical implants and miniaturized sensors.

2.2.3. Transfer of enzymes

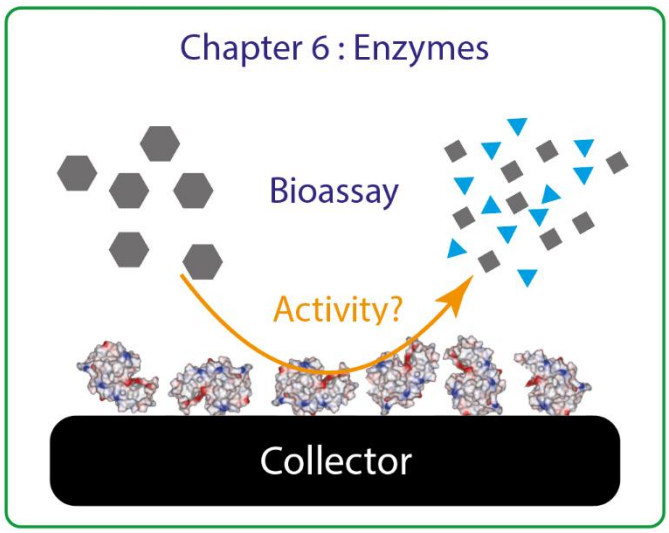


***Figure 2.4**. Graphical abstract of Chapter 6.*

Chapter 6 aims at investigating whether the 3D structure of the transferred proteins is altered or not in the course of the transfer. Even though optimized to be as soft as possible, the bombardment by the energetic clusters, the flight in vacuum and the landing on hard substrates are so many steps that can still trigger partial (or total) denaturation of the proteins, which may in turn affect their bioactivity. To study to what end this could be an issue, a model enzyme, lysozyme (14.3 kDa), will be used as first candidate. Once transferred, protocols will be developed to probe the integrity of the biomolecules in terms of both primary and tertiary structure. In fact, lysozyme is too big to be detected by SIMS, hence alternative procedures will be required. The primary structure (integrity of the amino-acids chain) will be investigated by means of electrophoresis, while the tertiary structure will be indirectly assessed by means of enzymatic activity assay (*via* the structure-activity relationship). If everything goes along the plan, larger enzymes should be investigated as well. The potential larger candidates are trypsin and chymotrypsin (both around 24 kDa), horseradish peroxidase (44 kDa) and glucose oxidase (160 kDa).

2.2.4. Construction of complex multilayers

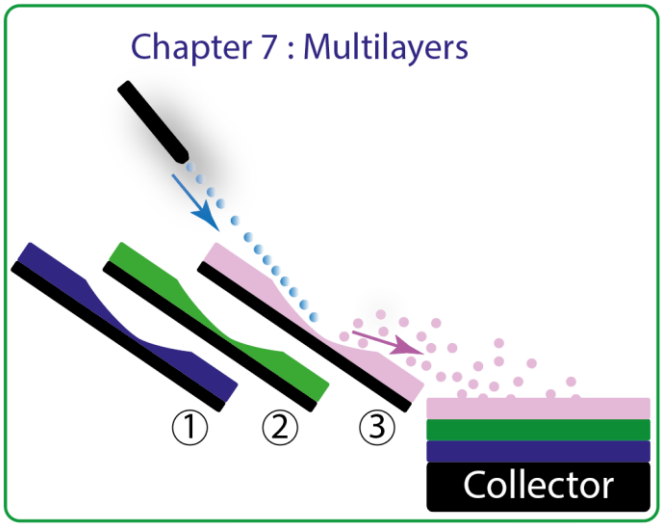


Figure 2.5. *Graphical abstract of Chapter 7.*

Another feature that should be made possible by the proposed approach is the construction of multilayers. That is either multiple layers of the same molecule, but also constructions that are more complex, starting with alternated layers of different molecules. This can turn out to be tricky to achieve by solution-based approaches as at each additional step, solubilization of the previously deposited layers may occur. As a consequence, all the molecules would then mix as the multilayer is constructed. At this point, multilayers of a single protein should have been already prepared. Therefore, **Chapter 7** will aim at the construction of multilayers made of two different molecules. To facilitate the subsequent analysis of the multilayer, it is decided to first work with a peptide, namely bradykinin, and a second non-protein compound, here Irganox 1010. The bradykinin and the Irganox molecules can be readily differentiated using their respective SIMS signatures, so it is quite simple to identify them in the SIMS depth profile of the sample, especially as both molecular ions are visible in the spectra. The more complex step will be to build multilayers of two distinct proteins. Here three levels of difficulty, with respect to the subsequent analysis and characterization of the multilayer, can be identified: first, two peptides/small proteins for which the molecular ion is detectable. Second, two proteins out of which only one molecular ion is detectable. Finally, multilayers comprised of two large proteins neither of which displays

a molecular ion in the spectra. In that case, the identification of each protein in the depth profile may require the use of multivariate analysis such as PCA.

2.2.5. Transfer of non-covalent complexes

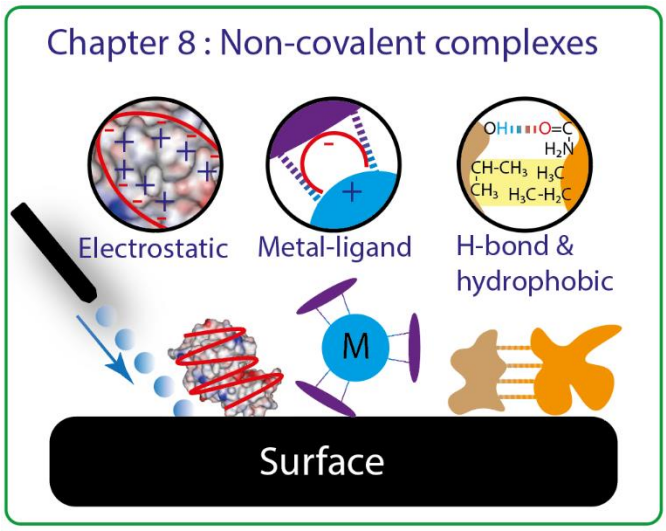


Figure 2.6. *Graphical abstract of Chapter 8.*

Finally, in **Chapter 8**, the goal is to investigate the transfer of weakly bound molecular entities. This chapter will be more exploratory, and can be divided in two parts. On the one hand, protein-polyelectrolyte complexes (PPCs) will be prepared. It was previously demonstrated that these complexes could be useful for the immobilization of proteins at interfaces, as they tend to keep the proteins in a hydrated environment. The investigation will focus on finding whether such complexes can be transferred. If successful deposition can be achieved, it will be investigated to what end the proteins can be protected in the complexes with respect to the risk of fragmentation and denaturation. Once again, lysozyme will be the model protein, while polystyrene sulfonate (PSS) will be the polymeric counterpart. In addition, the possibility to transfer organometallic complexes, of general formula M_xL_y (M being a metallic species, while L represents an organic ligand) will be investigated.

Chapter 3 : General Materials & Methods

3.1. Instruments

3.1.1. ToF-SIMS

3.1.1.1. Instrument description and transfer experiments

The core instrument of this thesis is a time-of-flight secondary ion mass spectrometer. A TOF.SIMS 5 (ION-TOF GmbH, Münster, Germany), depicted in **Figure 3.1** was used both for transfer experiments and for analysis of collectors and other samples. A ToF-SIMS is composed of several pulsed primary ion sources, a sample stage that can be manipulated, and a secondary ions analyzer. The instrument used for this work is equipped with a Bismuth source (Bi Nanoprobe) and an Argon gas cluster ion beam (Ar-GCIB), both mounted at 45° with respect to the sample surface. The instrument also offers a Dual Source Column that can be operated with O_2 or Cs but this source was not used in the framework of this thesis. The time-of-flight mass analyzer is perpendicular to the sample surface.



***Figure 3.1**. ToF-SIMS.5 (ION-TOF).*

For the transfer experiments, and regardless of the geometry, the sample holder with target and collector plates was aligned with the GCIB. The alignment was done by sight for the x and y coordinates, and using the laser that is coaxial with the analyzer for the height z. The Ar-GCIB source was operated at 5 or 10 keV and the cluster distribution was centred selectively on Ar_{1500}^+, Ar_{3000}^+, Ar_{5000}^+ or Ar_{7000}^+. The cluster distribution was controlled and recorded prior to any deposition. Throughout the manuscript, the chosen cluster size, as well as the transfer ion dose are always given where necessary. The GCIB was used in interlaced sputter mode, with the analysis beam shut down during the entire transfer. The analyzer was also turned off during the transfer. The current intensity was measured each time prior to

experiment and is specified where relevant. The beam raster was always fixed at 128 x 128 data points over an area of 700 x 700 μm^2.

3.1.1.2. Types of analysis

For the analysis of the collectors and other samples such as spin-coated references, a few types of analyses were carried out and are worth being described.

First, simple mass spectra were recorded, with various primary ion beams. Most of the time, to perform these static analyses, the 30 keV Bismuth Nanoprobe-LMIG was employed. The source can selectively produce monoatomic ions, Bi_1^+, and a range of clusters such as Bi_3^+, Bi_3^{++}, and Bi_5^+. In this study, a 30 keV Bi_5^+ cluster ion beam (current intensity of about 0.1 pA) was preferentially used. This beam offers both high total secondary ion yields and somewhat high intensities for relatively high mass secondary ions, allowing for example the detection of the molecular ions of angiotensin and bradykinin at a m/z of around 1 kDa. Except otherwise stated, the static spectra were acquired during 60 s, ensuring that the static limit was not overreached. The beam was operated in "high current bunched" mode, to achieve high mass resolution ($m/\Delta m \approx 4300$ at 30 m/z, corresponding to CH_4N^+, was maintained for spectra acquisition). In this mode, the final diameter of the beam reaching the sample is about 2 to 3 µm. The cycle time was varied according to the highest mass to be detected, but remained between 100 and 200 µs.

In the particular scenario where ToF-SIMS was used to measure the protein film thickness, the 30 keV Bi^+ was employed. The method, fully described in **Chapter 4**, relies on the intensity measurement of the underlying Si substrate. In the monoatomic beam, each individual Bi atom has a much larger energy than in the clusters (30 keV vs 6 keV in comparison to Bi_5^+). Thus, the ions penetrate deeper in the sample and allow reaching the Si substrate with a larger range of protein thicknesses deposited on top.[1] Mass spectra were also recorded for 60 s, but the current intensity of the beam was much larger, around 1.4 pA. The monoatomic ion beam also generates high secondary ion yields, but due to a larger E/n, produces far less ions of large mass. However, for thickness measurements, only the Si signal intensity is relevant in the spectra, which is at m/z of 28. The resolving power was maintained around 6000 at 30 m/z.

In the case where secondary ions larger than 1 kDa had to be generated, for example to detect the molecular ion of insulin (5.8 kDa), the Ar-GCIB could be operated in analysis mode. In the latter, the beam was bunched just as the LMIG, to allow combination with the ToF analyzer. The Ar-GCIB generates far less secondary ions than the Bi-LMIG, but also induces much less fragmentation to the sample molecules. Therefore, the relative intensity of high-mass secondary ions is much higher when massive clusters are used as primary particles (due to a reduced E/n, as described in the introductory section). In this study, 10 keV Ar_{3000}^+ was selected as it provides a good compromise between the secondary ion yield, the fragmentation and the mass resolution. Its current intensity was kept below 1 pA, while the mass resolution was around 200 at m/z = 41 ($C_5H_5^+$).

Second, large 2D images of the collectors were acquired. This type of analyses yields pertinent information regarding the spatial distribution of the species of interest at the surface. They can be seen as chemical images of the surface of the sample. In our case, this mode was used on the collectors after the transfer, to make sure that the transfer was efficient and that proteins were present on the collectors. It further allowed to investigate the deposition pattern of the proteins at the surface. The 2D imaging mode is provided as an automated procedure by ION-TOF. In this operating mode, only possible in a typical backmount sample holder (**see Figure 3.2**), the beam moves automatically along the sample surface and gathers multiple square images to build the total image of the collector. Here, 30 keV Bi_5^+ was employed, with a current intensity of about 0.1 pA and with a raster of 128 x 128 data points over an area of 500 x 500 μm^2. A single scan was performed, but two frames were taken on every 500 x 500 μm^2 patch to increase signal intensity. Only positive secondary ion species were analyzed. A mass resolution of $m/\Delta m \approx 4300$ at 30 m/z (corresponding to CH_4N^+) was maintained for spectra acquisition. When performing large images, the spatial resolution lies around 3-4 µm. Images were also performed using 30 keV Bi^+ in order to generate thickness maps of the collectors. These being quite original experiments, they will be fully detailed in **Chapter 4**.

Third, depth profiles were acquired on some samples. Depth profiles are recorded as successive static spectra, interspersed with periods during which a sputter beam is turned on to progressively erode the surface and penetrate into the bulk of the sample. The depth profiles allow investigating the changes in the chemistry and so in composition of the material as a function of depth in the sample. They are very useful to study multilayers and other

complex samples. The sputter beam is a massive argon cluster ion beam, whose size can be varied (Ar_n, with n usually ranging from 1000 to 5000) to find the best suitable conditions for the analysis. The depth profile can be achieved in single or dual beam mode, depending on the ion beam used for the analysis. On the one hand, if low fragmentation is desired, the Ar-GCIB can be used both for sputtering and for analysis (single beam mode). On the other hand, if high secondary ion yield and high mass resolution are required, then the Ar sputter beam can be alternated with the Bi-LMIG (dual beam mode). This latter was mainly used for the purpose of this work. In typical experimental set-ups, the sputter beam would be rastered on a relatively large area on the surface, e.g. 600 x 600 µm², while the analysis beam would be rastered on a much smaller area, centred on the sputtered one (for example 200 x 200 µm²). This prevents the appearance of crater side effects on the analysis, as the sample is depth profiled. Parameters such as sputter beam size, energy, current intensity, and analysis beam current intensity must be finely tuned to best suit the undergoing analysis. The eroding speed is important, as it will influence the depth resolution. Yet eroding the sample too slowly may result in undesired effect induced by the energetic analysis beam, such as damage accumulation and loss of molecular information. The conditions being different for each sample, they will be given alongside the results of the depth profiles were necessary.

3.1.1.3. Charge compensation

During a ToF-SIMS analysis, insulating samples may suffer from charging effect. This like-charge accumulation at the surface may result from two contributions: the accumulation of positive charges originating from the primary ions impinging on the surface and the imbalance between the emitted fluxes of secondary ions (positive and negative) and electrons. The charge build-up at the surface may cause instability of the signals and lead to peak broadening or shifting. Proteins, as well as most organic compounds, find themselves to be insulators. In case relatively thick layers are deposited, charge compensation will be necessary. For this work, mainly (ultra)-thin layers (< µm) were prepared, and were shown not to suffer from any charging effect. However, in few cases (long deposition, construction of multilayers), charging effect were observed, and charge compensation was used. The electron flood gun provided on the instrument was operated between 5 and 20 eV. The use of the charge compensation will be specified where needed.

3.1.1.4. Time-of-flight mass analyzer

The SIMS instrument of the lab is equipped with a time-of-flight (ToF) mass analyzer. The extracting lens is placed at 1.5 mm of the sample surface, and set at an electric potential of 2 kV. When positive polarity spectra are recorded, negative extracting potentials are applied, and *vice versa*. Once extracted, the secondary ions enter a field-free drift tube of 2 m length (L). Ideally, the secondary ions possess a constant kinetic energy (product of their charge z, typically equal to 1, by the extraction potential (V)). Once in the field-free region, the ions migrate at a speed that is inversely proportional to their mass (lighter ions travel faster than heavier ones). Therefore, measuring the flight time (t) of an ion allows the determination of its mass to charge ratio (m/z), as given by **equation 3.1**:

$$\frac{m}{z} = \frac{2.V.t^2}{L^2} \tag{3.1}$$

It must be noted that the ideal scenario where all the ions of an identical mass have the same velocity as they travel in the field-free region is illusory. Indeed, the sputtering process is inherently accompanied by an angular distribution of the emitted species, as well as a relatively large energy distribution. These two facts may cause a diminution of the mass resolution, as ions of the same mass are detected at different times. To get rid of this issue, the ions are forced to travel through a reflectron, as described in the **introductory section** (**Chapter 1**).

3.1.1.5. Secondary ion detector

The instrument is equipped with a single ion counting device. It is composed of a single microchannel plate (MCP), combined with a scintillator and a photomultiplier. The microchannel plate is closely related to an electron multiplier, as both allow increasing an original signal (here the impact of a secondary ion) by multiplying electrons via secondary emission. The main advantage of the MCP is that thanks to its vast number of separate channels, it can provide an additional spatial resolution. The efficiency of the process greatly depends of the velocity of the particles. In order to maximize the signal, hence improving the detection limit, the secondary ions are post-accelerated just before reaching the MCP. The post-acceleration is typically done by a 10 kV potential, but can be increased to favor the detection of high mass (thus low velocities) ions. In this study, nearly all measurements were performed at 10 kV. In the particular case where detection of large intact

molecular ions of proteins was intended, the post-acceleration was boosted to 20 kV. The electrons generated in the MCP are then directed towards the scintillator plate. The latter transforms the electron current into photons, via production of fluorescent flashes. The photons are finally detected and counted by the photomultiplier tube.

3.1.1.6. Sample holders

Various samples holders were used during this work, depending on the experiment to be carried out. ION-TOF commercializes a set of sample holders, displayed in **Figure 3.2**. The Backmount is the typical sample holder used to perform analyses on classic samples, such as small Si wafers. The topmount is a flat steel plate, with screw holds, that allows fixing a multitude of samples having unorthodox shapes or too large to fit in the backmount. ION-TOF also offers more specific sample holders such as the holder G, allowing heating and cooling of the sample or a spinning sample holder to

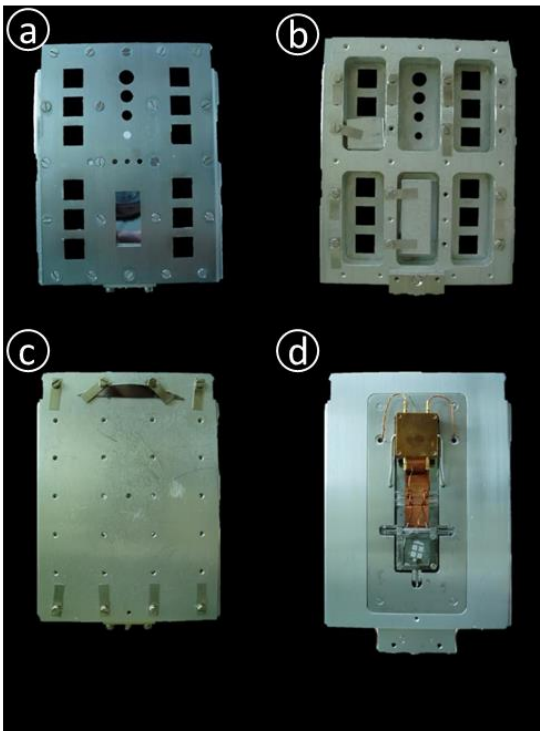


Figure 3.2. *The three sample holders provided by with the ToF-SIMS instrument. Bottom (a) and top (b) views of the backmount sample holder, used for all basic analyses. Topmount sample holder (c), on which were fixed the specific transfer sample holders, and sample holder G (d), which allows control of the temperature.*

enhance the performances of the instrument during depth profile analyses. In the framework on this thesis, both the backmount and the topmount were used. The backmount was used for all analyses, while the topmount was used for all the transfer experiments. Indeed, specific sample holders were designed and manufactured in-house to allow transfer in various geometries. These samples holders were fixed on the topmount. They are fully described in the related section of the results.

3.1.2. Ellipsometry

3.1.2.1. Basic principle

Ellipsometry is an optical technique widely used to derive a series of information about surfaces. It relies on the change of polarization state of light upon reflection from a thin film. Information that can be delivered by ellipsometry encompasses the composition, roughness, thickness, electrical conductivity, optical constants and other properties of the probed material. Ellipsometry became especially popular for thickness measurements, as it proved to be very precise for film thicknesses ranging from less than a nanometer to several microns. Ellipsometry presents the main advantage of being non-destructive. Therefore, samples that are studied by ellipsometry can further be used for other types of analyses such as SIMS experiments. In this work, ellipsometry was used for protein thin films thickness measurement only.

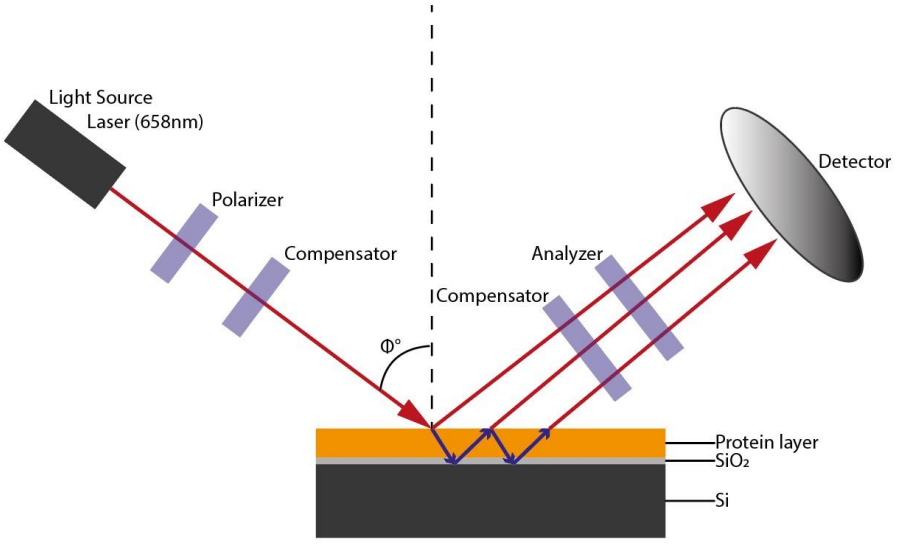


***Figure 3.3**. Schematic representation of an ellipsometry experimental set-up.*

The experimental work was carried out on an Accurion EP3+ SW (Accurion GmbH, Göttingen). A schematic representation of an ellipsometry set-up is given in **Figure 3.3**. The principle of ellipsometry will be briefly explained without detailing the underlying complex mathematical theory, which is believed to be out of the scope of this work. In a simple experiment, electromagnetic radiation is emitted by a light source (usually a laser, allowing the generation of a single wavelength). The light is then linearly polarized by a polarizer, and passes through a compensator before reaching the surface. As it goes through the thin film and is reflected by the film and by the substrate, the polarization of the light changes. The polarization goes from linear to elliptical. The change is represented and measured as an amplitude ratio, Ψ, and a phase difference, Δ. These are measured by other optical devices such as a compensator, an analyzer and a detector.

3.1.2.2. Sample model and fixed parameters

Ellipsometry is an indirect technique, as it relies on the use of known models, and regression-based data fitting procedures. In this work, all the samples were similar, that is a protein layer spin-coated on a Si wafer. The Si wafer is described as two distinct layers with respect to an ellipsometry experiment. In fact, the elemental Si bulk is covered by an oxidized layer of SiO_2. The model of the sample is then described as follows: Si/SiO_2/protein, as shown in **Figure 3.3**. To measure the thickness of a thin film, one must enter in the model the refractive index (n) of each constituent of the sample, as well as its absorption coefficient (k). In the case of proteins, the refractive index was set at 1.5 and the absorption coefficient was set at 0. In the precise case of the samples investigated in this work, the protein layer cannot be measured independently from the SiO_2 layer. Indeed, SiO_2 also displays a refractive index around 1.5, and so they are taken as one single layer by the instrument. To measure the thickness of the protein layer only, the thickness of the SiO_2 was measured on clean Si wafers, then always subtracted from the total thickness measured on the samples with the spin-coated protein layer. The SiO_2 layer was measured to be 1.5 nm.

3.1.3. UV-Vis spectrometer (multi-well plate reader)

3.1.3.1. Instrument description

For all quantification and activity bioassays, a multi-mode microplate reader from Molecular Devices (San Jose, California, US) was used for both absorbance and fluorescence measurements. The instrument is a

SpectraMax iD3, supporting multi-well plates ranging from 6 to 384 wells, and featuring several reading modes: endpoint, kinetic, well scan and spectrum. For this study, mainly the endpoint mode was utilized, defined as when a reading of each plate well is taken in the center of each well at a given time. This can be achieved at a single or at multiple wavelengths. Whatever the mode, the instrument can be operated from 15°C to 60°C. All measurements were performed in 96-wells plates, either clear, for absorbance, or black, for fluorescence. The plates were purchased at Greiner Bio-One nv/sa (Vilvoorde, Belgium). When the reaction was carried out in Eppendorf tubes, or in other vials, the resulting mixture was transferred into 96-wells plate to further be measured. (NB: all the instrument specifications were provided by the manufacturer).

3.1.3.2. Absorbance mode

The absorbance represents the quantity of light absorbed by a solution. It is given by **equation 3.2**:

$$A = log_{10}\left(\frac{I_0}{I}\right) = -log_{10}\left(\frac{I}{I_0}\right) \quad (3.2)$$

where I_0 is the intensity of the light before it enters the sample, and I is the intensity of the light after it passes through the sample. For a given substrate, it can also be given by **equation 3.3**:

$$A = \varepsilon l c \quad (3.3)$$

where ε is the molar attenuation coefficient of the probed species (L x mol^{-1} x cm^{-1}), l is the optical path length in cm, and c is the concentration of the attenuating species (mol x L^{-1}).

The absorbance wavelength range of the instrument goes from 230 to 1000 nm. The monochromator allows fine-tuning of the wavelength in 1 nm increments, with given bandwidth of 4 nm. Photometric range goes from 0 to 4 OD. OD stands for optical density, and is equivalent to the absorbance.

3.1.3.3. Fluorescence mode

Fluorescence occurs when a radiative relaxation is observed after that light was absorbed. The fluorescence excitation (EX) and emission (EM) wavelength ranges of the instrument are respectively 250 - 830 nm and 270 - 850 nm. The wavelength selection is done by a monochromator, tunable in 1 nm increments, with given bandwidths of 15 nm and 25 nm for EX and EM respectively. The dynamic range covers more than 6 logs. The instrument

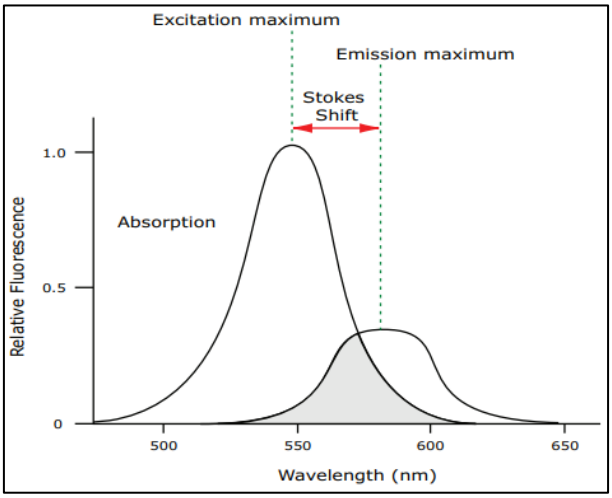


***Figure 3.4**. Illustration of the fluorescence mechanism, and the problem that may occur if the excitation and emission maximums are too close one from another.*

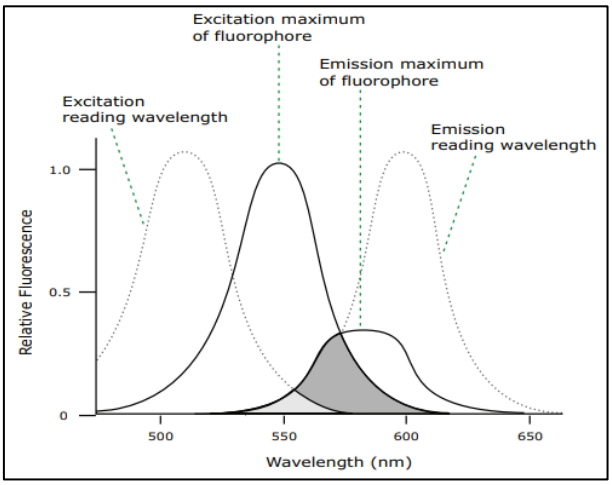


***Figure 3.5**. Illustration of the automated protocol that finds the best suitable excitation and emission wavelengths to avoid overlap.*

expresses the results in relative fluorescence units (RFU). For some fluorophores, it can be observed that the excitation and emission wavelengths are relatively close one to another, corresponding to a small Stokes shift (**Figure 3.4**). In that case, it is likely that an interference occurs, as the excitation light will be detected alongside the emitted light. To overcome this issue, the instrument offers an automated procedure to find the optimal EX and EM wavelengths. The outcome is a compromise between being still able to stimulate the fluorophore and detect emitted light, while being as far away from each other as possible to reduce the overlap between the EX and the EM spectra (**Figure 3.5**). This procedure was used to optimize some of the bioassays protocols.

For both absorbance and fluorescence measurements, the samples containing the compound of interest, to be quantified, were always measured alongside blank wells. These contained everything (water, buffer, salt, detergent or other additives) used within the sample wells, with the exception of the chromophore/fluorophore. This procedure allows compensating for the background signals. When possible (that is always except for some transferred samples), the measurements were done in triplicates. Statistical calculations were then performed to present the results as means of three measurements, accompanied with a value of standard deviation.

3.1.4. Spin-coater

Thin films of different compounds were prepared to record SIMS reference spectra. These samples were prepared using a spin-coater instrument (WS-400B-6NPP/LITE, Laurell, USA). After cleaning, a drop of 150 µL of a solution of fresh proteins or other molecules (1g/L) was deposited on the substrate, which was then spun at 3000 RPM for 1 min.

3.2. Compounds and molecules

3.2.1. Proteins

All proteins (human angiotensin II, bradykinin, insulin, lysozyme, cytochrome C, trypsin, glucose oxidase) were purchased from Sigma-Aldrich (Steinheim, Germany) and used without further purification. For each protein, a concentrated aqueous stock solution at 20 g/L was prepared using ultra-pure water (resistivity > 18 ohm) and stored at -20°C. When needed, the stock solution was diluted to 1 or 0.1 gL^{-1}.

3.2.2. Other organic compounds

Irganox1010 was purchased at Ciba (now BASF, Antwerpen, Belgium). Vancomycin hydrochloride, D-Alanine-D-Alanine and Acetyl-Lysine-D-Alanine-D-Alanine were all purchased from Sigma-Aldrich (Steinheim, Germany). Sodium polystyrene sulfonate (Mw = 8 kDa) was purchased from Scientific Polymer product (Ontario, NY, United States). Poly (acrylic acid) (Mw = 1.8 kDa) was purchased from Sigma-Aldrich (Steinheim, Germany). Deacetylated Chitosan (95/5, Mw = 10-50 kDa) was purchased from Heppe Medical Chitosan Gmbh (Halle, Germany). Trehalose and fructose were both purchased from Sigma-Aldrich (Steinheim, Germany). Poly(ethylene glycol) methyl ether, ω-thiol-terminated (Mn = 1.1 x 10^3, PDI = 1.08, SH functionality >95%) was purchased from Polymer Source, Inc (Dorval, Canada).

3.2.3. Metal-organic compounds

Chromium, cobalt, copper and nickel trifluoroacetylacetonates (tfac) were all kindly provided by Pr. Sophie Hermans (SST/IMCN/MOST). They were synthesized by master students during practical works.

3.3. Target and collectors preparation

The targets are thick (0.73 mm) rectangular silicon (Si) wafers. Depending on the transfer set-up/geometry, the dimensions of the targets are either 1 x 0.3 cm^2 (15° geometry) or 0.4 x 0.6 cm^2 (45° geometry). Prior to protein deposition, wafers were cleaned for 15 min in piranha mixture (sulfuric acid/hydrogen peroxide, 4:1) then underwent a UV-ozone treatment for 15 min. Targets were prepared by three consecutive depositions of a 10 - 20 µL drop (depending on the target size) of the protein stock solution (20 gL^{-1}), resulting in a thick dry protein layer of about 23 µm in thickness. Thickness data were obtained by measuring the depth of the crater by profilometry (Bruker Dektak XT 0.7 µm, Bruker UK Ltd) after sputtering the target until the Si substrate was reached. The target is rather uniform in terms of thickness, yet the surface roughness of these drop-dried thick layers is relatively important. The topography was measured with the profilometer prior to the transfer experiment, and revealed a peak-to-valley value of about 200 nm. Targets were kept at room temperature for no longer than 7 days before use.

Various types of collectors were used. Typical materials such as Si wafer and PE sheets will be described in this section. Functionalized collectors will be

described in the results section dedicated to them. For each transfer experiment throughout this manuscript, the collector that was used will be specified. For ToF-SIMS imaging and some SDS-PAGE experiments, collector were thin (0.28 mm) 1 x 1 cm² square Si wafers. Si wafers are purchased as disks of 5.08 cm in diameter at Neyco (Vanves, France), then cut into smaller pieces using a diamond tip. For some enzymatic activity assays, collectors were 1.4 x 1.4 cm² thin Si wafers. Si collectors were cleaned just before being inserted in the SIMS, following the same cleaning procedure as for targets. Soft PE sheets were also used as collectors to allow bioassays to be carried out easily in Eppendorf tubes. A large roll of PE low density film was purchased at Goodfellow (Cambridge, England). The film is 0.05 mm thick, and is reported as additive free. To prepare the collectors, small 1 x 1 cm² sheets were cut, and cleaned in ethanol for 15 min, while placed in the sonicator, then dried under N_2.

3.4. Bioassays

3.4.1. Bicinchoninic acid (BCA) protein quantification assay

The BCA assay is one of the most popular assays when it comes to protein quantification. It is a colorimetric assay, relying on a two-stage reaction (**Figure 3.6**). It combines the well-known Biuret reaction, which is the reduction of Cu^{2+} to Cu^{+} by proteins, and the chelation of two BCA molecules with one Cu^{+}. The formation of the latter water-soluble complex yields a purple-colored solution, whose concentration can be monitored by measuring the absorbance at 562 nm.

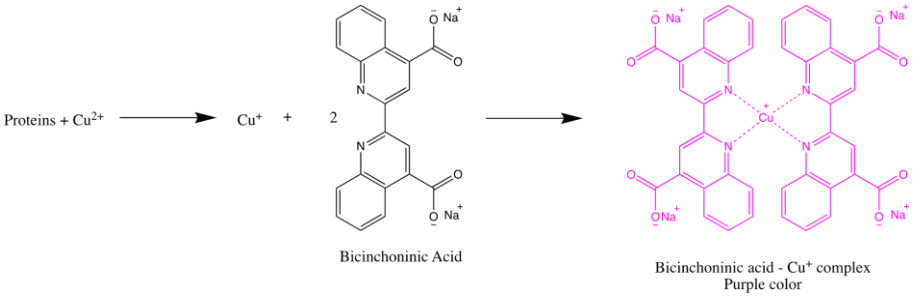


***Figure 3.6**. Chemical reactions involved in the BCA assay.*

It was shown that the reduction of Cu^{2+}, the subsequent complexation with BCA and hence the absorbance at 562 nm increase linearly with increasing protein concentration in the initial sample. This was verified for quite a broad protein concentration range, from 20 to 2000 µg/mL. It was reported that

the results of a BCA assay could be influenced by the protein structure, the number of peptides bonds or the presence of particular amino-acids (cysteine, tryptophan and tyrosine). However, the BCA assay is known to be very consistent from one protein to another, allowing comparison between solutions of different compositions. In practice, protein concentration are always determined in reference to a standard calibration line, which consists in a series of dilutions of known concentration. In practice, to ensure a minimal error due to different amino-acids composition, the calibration line is prepared with the same protein than that in the unknown concentration samples. For this work, BCA assay reagents were all bought as a kit at ThermoFisher Scientific (PierceTM BCA Protein Assay Kit, cat. numb. 23225).

3.4.1.1. General protocol to perform the BCA assay in a 96-wells plate

20 µL of a protein solution of known (for the calibration line) or unknown (samples to be quantified) concentration are added to each well. Afterwards, 200 µL of BCA working reagent were added in each well. The plate was then incubated for 1 hour at 60°C before absorbance was measured at 562 nm. Measurements were performed in triplicate.

This standard protocol was further adapted to be performed directly at the surfaces of collectors. The adapted procedures will be described in the section dedicated to the transfer on collectors different than Si wafers.

3.4.2. Lysozyme activity assay

Lysozyme activity was tested using the 4-Methylumbelliferyl β-D-N,N',N''-triacetylchitotrioside compound as substrate (**Figure 3.7**). This substrate consists in a tri-sugar linked to a 4-Methylumbelliferyl moiety. When native lysozyme (intact and active) is in presence of the substrate, it will randomly hydrolyze one or more glycosidic bonds of the molecule. When the bond linking the 4-Methylumbelliferyl moiety to the rest of the substrate is digested, fluorescent 4-Methylumbelliferone is released in the medium. The amount of fluorescence is linearly proportional to the quantity of active lysozyme in the sample. Fluorescence of the 4-Methylumbelliferone can be measured with an excitation wavelength of 360 nm and an emission wavelength of 450 nm.

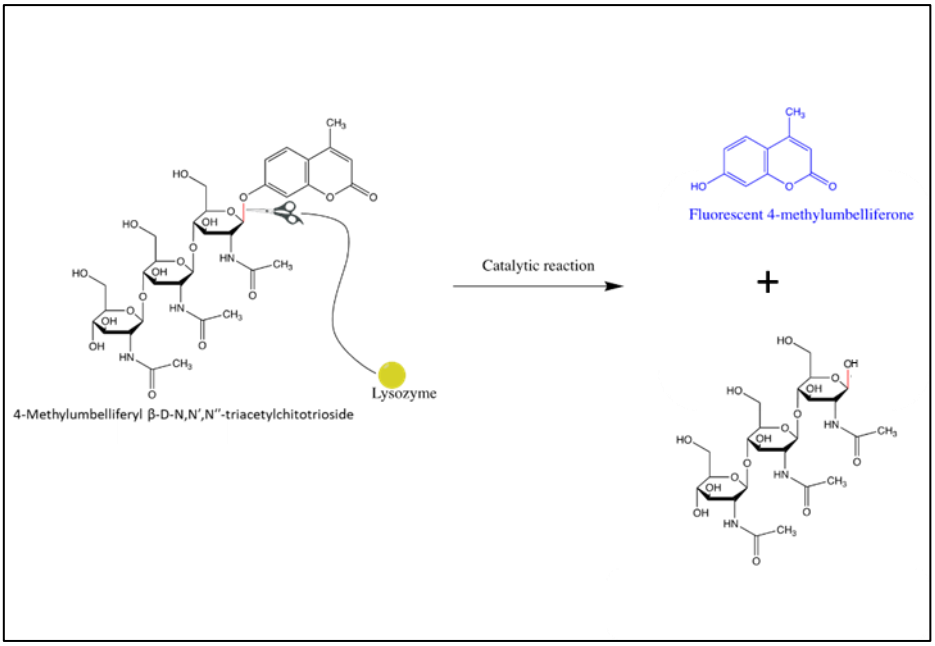


Figure 3.7. Chemical reaction involved in the activity assay of lysozyme.

3.4.2.1. General protocol to perform the lysozyme activity assay in a 96-wells plate

20 µL of a lysozyme solution of known (for the calibration line) or unknown (samples to be quantified) concentration are added to each well. Then 180 µL of acetate buffer (10 mM) at pH 5 and ionic strength adjusted to 10 mM with NaCl were added to each well. Finally 20 µL of 4-methylumbelliferyl β-D-N,N′,N′′-triacetylchitotrioside (0.1 g L^{-1}, Steinheim, Germany) in dimethyl sulfoxide (DMSO)/water 2:1 (v:v) were added in each well. The plate was kept under agitation (250 rpm) for 24 h at 40 °C. 180 µL of reactional media were then transferred to a black 96-well plate and mixed with 50 µL of 50 mM glycine buffer at pH 10.6 (adjusted with NaOH). Fluorescence was then measured with excitation and emission wavelengths respectively set at 360 nm and 450 nm.

This standard protocol was further adapted to be performed directly at the surface of collectors. The adapted procedures will be described in the section dedicated to the transfer of enzymes.

3.4.3. Trypsin activity assay

The Thermo Scientific™ Pierce™ Fluorescent Protease Assay Kit was chosen to probe the activity of the transferred trypsin molecules. Fluorescein-labeled casein is used as a substrate. Fluorescence properties of this heavily-labeled, intact protein substrate change dramatically upon digestion by proteases, resulting in a measurable indication of proteolysis (**Figure 3.8**). FRET-based measurement detects the decrease in fluorescence quenching (= increased total fluorescence) that occurs as the FTC-Casein substrate (casein labeled with fluorescein isothiocyanate) is digested into smaller fluorescein-labeled fragments.

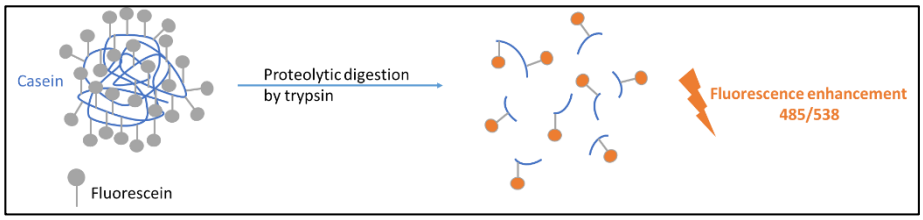


Figure 3.8. Schematic representation of the trypsin activity assay based on the use of fluorescein-labeled casein.

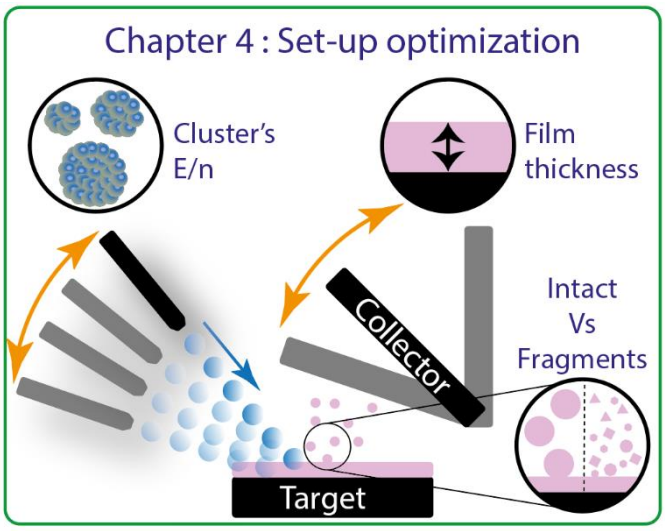
3.4.3.1. General protocol to perform the trypsin activity assay in a 96-wells plate

100 µL of a trypsin solution of known (for the calibration line) or unknown (samples to be quantified) concentration were added to each well. 100 µL of the working reagent solution were then added. The plate was incubated at room temperature between 5 and 60 min. Fluorescence was finally measured with excitation and emission wavelengths respectively set at 485 nm and 538 nm.

3.5. Bibliography

(1) Szakal, C.; Kozole, J.; Russo, M. F.; Garrison, B. J.; Winograd, N. Surface Sensitivity in Cluster-Ion-Induced Sputtering. *Phys. Rev. Lett.* **2006**, *96* (21), 3–6.

Chapter 4 : Transfer of peptides and small proteins – Optimization of the transfer parameters and characterization of the collectors



In this chapter, a solvent-free method for the controlled construction of protein thin films is reported. Using large argon gas cluster ion beams, proteins are sputtered from a target (a pool of pure proteins), and collected on Si wafers. ToF-SIMS revealed the presence of intact protein molecules on the collectors. Furthermore, lowering the energy per atom in the cluster projectiles down to 1 eV/atom allowed more than 60% of bradykinin molecules to be transferred intact. This protein deposition method offers a precise control of the film thickness as the transferred protein quantity is proportional to the argon clusters ion dose reached for the transfer. This major feature enables building protein films from (sub)mono- to multilayers, without upper limitation of the thickness. A procedure was developed to measure the film thickness using the ToF-SIMS instrument. Finally, the transfer geometry was optimized in terms of cluster ions impinging angle and collecting angle by building different sample holders and comparing their efficiency.

A paper closely related to this chapter is published: ***V. Delmez[$], B. Tomasetti[$], T. Daphnis, C. Poleunis, C. Lauzin, C. Dupont-Gillain*, A. Delcorte*. ACS Applied Bio Materials 2022 5 (7), 3180-3192***

Benjamin Tomasetti is especially acknowledged for his contribution related to the optimization of the transfer geometry, for which he performed the sample holder designs in Solidworks as well as the 3D printing. He also developed the application to easily transform the SIMS intensity images into thickness maps.

4.1. Introduction

In 2016, Lorenz *et al.* showed that large argon clusters could be used to transfer organic material from one surface onto another.[1] Indeed, they reported a protocol in which the Ar-GCIB of a time-of-flight secondary ion mass spectrometer (ToF-SIMS) was derived from its usual analytical function to be used for the transfer of organic material, here antioxidant molecules. In fact, such a transfer strategy had been envisioned before, in 2008, when Wirtz *et al*. reported the "storing matter" technique, which was designed to improve the SIMS analytical performances.[2–5] However, a monoatomic beam was used for transfer, ultimately leading to low deposition rate and high fragmentation of the transferred molecules. Using large argon cluster ion beams, Lorenz *et al.* showed that a large fraction of the transferred molecules was intact after deposition. Later, they developed an *in situ* matrix-enhanced SIMS based on this transfer mechanism,[6] which was further exploited in our group.[7] Inspired by these promising results, we took advantage of the outstanding characteristics of Ar-GCIB to develop a soft-landing technique carried out within a ToF-SIMS instrument. This method, consisting of bombarding a sample with an Ar-GCIB and collecting all ejected material on a desired surface, differs from other soft-landing methods mainly on two points: first, the target consists in a pure solid pool of molecules, and second, neutral molecules are transferred together with the ionized species. This latter evolution overcomes the low ionization yield inherent to existing soft-landing techniques.

In this first chapter, peptides, to start with, and larger proteins, are used to evaluate the feasibility of the method. One straightforward way to confirm that the peptides and proteins can be transferred intact would be to detect their intact molecular ion on the collectors as they are analyzed by ToF-SIMS. As the proof of concept experiments were performed, an optimization of the transfer experimental set up and conditions was carried out, by investigating the influence of various experimental parameters (Ar clusters size and energy, primary ions impinging angle and collecting angle, size of transferred biomolecule) on the efficiency of the transfer. This chapter is therefore divided into four sub-sections. In the first one, the possibility to transfer intact peptides and proteins will be investigated. In the second one, the influence of the cluster's energy per atom on the fragmentation of the transferred proteins will by studied using bradykinin as a model protein-like molecule. In the third one, the newly formed peptide and protein thin films will be characterized, in terms of the deposited thickness, and film

homogeneity. In this section, the influence of the mass of the protein on its transfer efficiency will also be examined. Finally, in the fourth section, the transfer geometry will be optimized. To this end, several new samples holders will be built.

4.2. Materials and methods

4.2.1. Transfer experiments

The procedures regarding the cleaning and the preparation of the targets and the collectors, as well as detailed description of the transfer procedure and general experimental conditions were provided in the **General materials and methods section** (**Chapter 3**). Here, key points are reminded to allow a clear understanding of the Chapter. Transfer experiments were conducted in a commercial ToF-SIMS instrument. However, a homemade sample holder was designed and built to carry out the transfer experiments (**Figure 4.1**)**.** The transfer consists of bombarding a reservoir of proteins (the target) with large Ar cluster ions and collecting the ejected particles onto a clean solid sample (the collector). In the initial setup, inspired by that of Lorenz et al.,[1] the target is placed with an angle of 30° with respect to the collector (which is itself horizontal), so that the Ar cluster ions impinge the target with a grazing angle of 15°. The targets are relatively thick solid layers of proteins (approximatively 20 µm thick, measured by profilometry). They were

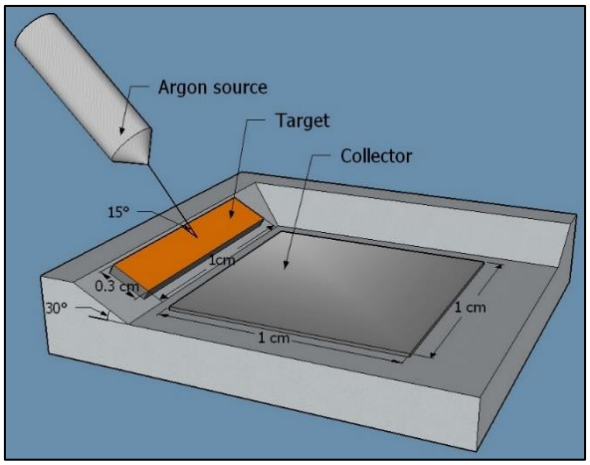


Figure 4.1*. Schematic representation of the initial transfer geometry. The protein target is represented in orange, and the collector in grey. The collector is horizontal, and the target is placed at 30° with respect to the collector. The cluster beams impinge on the target with an angle of 15°.*

prepared by drop-casting, usually using three successive evaporations of a few µL of a protein stock solution. Throughout this chapter, the collectors were always clean Si wafers.

4.2.2. Reference samples

Reference samples of proteins refer to fresh protein solutions spin-coated on Si wafers.

4.2.3. 3D printing of additional transfer sample holders

In the third section of this chapter, different transfer geometries and associated samples holders were envisaged. In order to be tested, the sample holders were 3D printed in polylactic acid (PLA) (MakerBot Filament, MakerBot Industries, Brooklyn, USA). The design was made with Solidworks and a Makerbot 2X Replicator (MakerBot Industries, Brooklyn, USA) was used for printing by fused-deposition modeling. Small 3D printed sample holders in PLA did not require additional pumping time in the ToF-SIMS instrument, were stable under vacuum and allowed to quickly adapt to any type of substrate and geometry.

4.3. Results and discussion

4.3.1. Transfer of intact peptides and small proteins

To assess the feasibility to transfer intact proteins using large argon clusters, peptides were chosen as first candidates, namely human angiotensin II (further referred to as angiotensin) and bradykinin, with respective masses of 1046 and 1060 Da. The molecular ion of these two peptides is easily detected by ToF-SIMS within regular surface analysis experiments, easing their detection on the collector after transfer.

In this first section, transfers were achieved with a 10 keV Ar_{5000}^+ beam. After transfer, the collectors were placed in the classical analysis sample holder to perform ToF-SIMS analysis. First, mass spectrometric images of the collector were acquired by operating the ToF-SIMS instrument in the 2D mosaic imaging mode with a highly focused Bi_5^+ analysis beam. It can be seen on the angiotensin and bradykinin collector images presented in **Figure 4.2** that material was efficiently transferred from the target onto the collector. Indeed, the substrate signal intensity (**Fig. 4.2, top images**), characterized by Si^+ and $SiOH^+$ (respectively at m/z = 28 and 45), is attenuated on the collector, showing that an overlayer was deposited on top of it. The image of

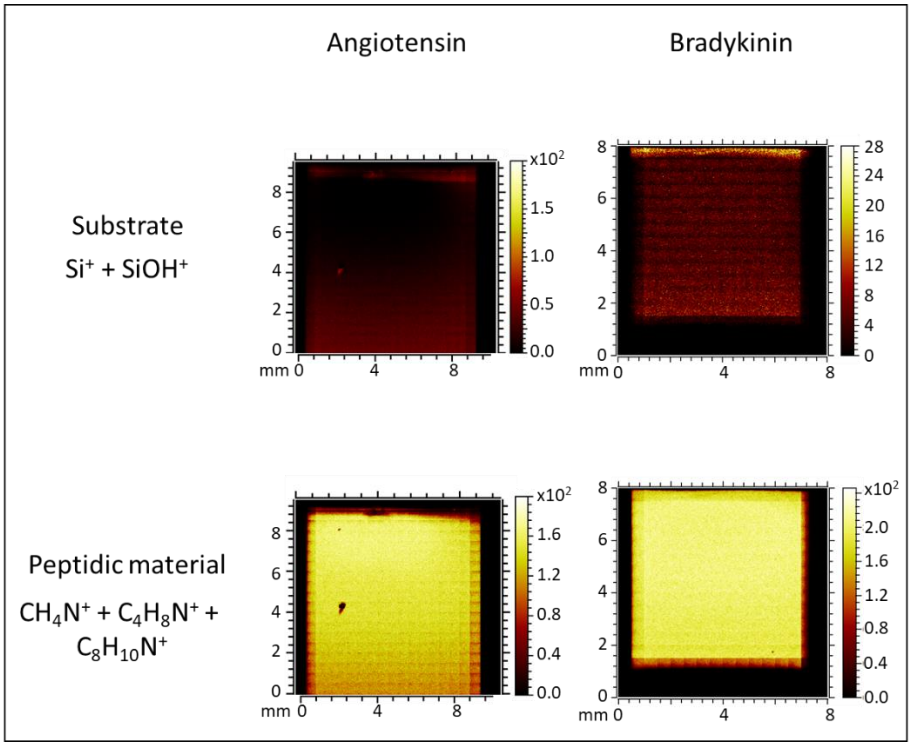


***Figure 4.2**. Angiotensin and bradykinin collector ion images. **Top:** substrate intensity images, represented by the summed intensities of Si^+ and $SiOH^+$ (respectively at m/z = 28 and 45). **Bottom:** amino acid material image, represented by the summed intensities of CH_4N^+, $C_4H_8N^+$ and $C_8H_{10}N^+$ (respectively at m/z = 30, 70, 120).*

characteristic fragments of amino acids (**Fig. 4.2, bottom images**), that are CH_4N^+, $C_4H_8N^+$ and $C_8H_{10}N^+$ or $C_9H_8N^+$ (respectively at m/z = 30, 70, 120 and 130), confirms the protein nature of the deposited film. These specific fragments were selected as they display a high intensity in the SIMS spectra in comparison with the molecular ion (depending on the protein, the most intense peak of either $C_8H_{10}N^+$ or $C_9H_8N^+$ was selected to be part of the peptidic material image; $C_8H_{10}N^+$ for angiotensin, bradykinin and insulin, and $C_9H_8N^+$ for lysozyme). Similar results were obtained for the larger proteins, insulin and lysozyme, that were transferred later (**Fig. 4.3**). These chemical images also shed light on the deposition pattern of the proteins at the surface of the collector. Indeed, when the transferred quantity is relatively small, the collector is not completely covered, and the SIMS intensity image of the substrate provides information about the area covered with proteins (as can be seen on the images recorded for insulin and lysozyme in **Fig. 4.3**). It is observed that proteins are deposited in an ellipsoidal shape pattern mirroring the angular distribution of the ejecta.[6] The substrate image

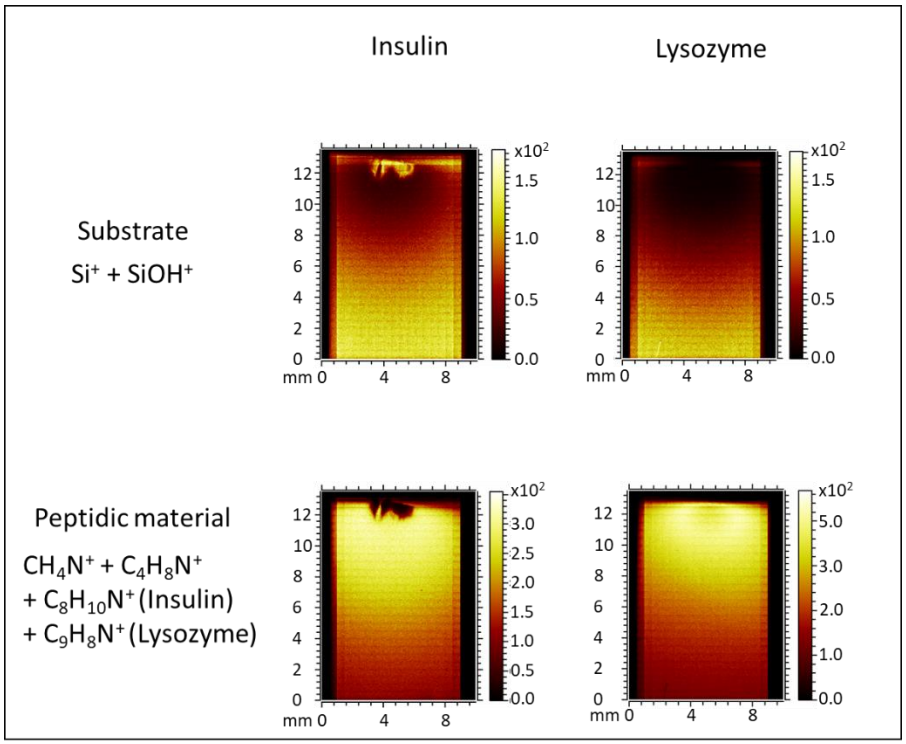


Figure 4.3. *Insulin and lysozyme collector ion images.* ***Top:*** *substrate intensity images, represented by the summed intensities of Si^+ and $SiOH^+$ (respectively at m/z = 28 and 45).* ***Bottom:*** *amino acid material image, represented by the summed intensities of CH_4N^+, $C_4H_8N^+$ and $C_8H_{10}N^+$ or $C_9H_8N^+$ (respectively at m/z = 30, 70, 120 and 130).*

displays a shading with a similar pattern. These images already point out one of the inconvenient aspects of this transfer geometry, which is that a relatively strong thickness gradient is present on the collector. In fact, the substrate signal provides an indirect estimate of the transferred protein thickness variation, since it is expected to decrease exponentially with the overlayer thickness.[8,9] In the cases where longer transfers were achieved and the entire collector is covered with a relatively thick protein layer (more than 5-6 nm), the SIMS images tend to display homogeneous intensity, that could be attributed to homogeneous protein thickness across the collector. However, the thickness gradient is still present, but no more visible on the SIMS images, due to the small information depth of SIMS (loss of the substrate signal) and lack of quantitative information. Homogeneity issues will be discussed more in depth in **section 4.3.3**. Static spectra (60s, 30 keV Bi_5^+) were further acquired on the collectors to investigate the presence or absence of the molecular ion, and thus of intact peptides/proteins. Note

that, from here onwards, “intact peptide/proteins” refers to the integrity of the primary structure (the amino acid chain), and should not be extrapolated to the secondary and tertiary structure, as SIMS does not yield any direct information one those properties. For angiotensin and bradykinin, the intact molecular ion was readily detected on the collector using the typical 30 keV Bi_5^+ analysis beam, as shown in **Figure 4.4 a & b**, with the usual isotopic distribution. In addition, if one compares the small mass region (<100m/z) of the spectrum obtained on the collector with that of a reference spin-coated sample (**Figure 4.5**), one can observe very close resemblance in the fragmentation pattern and relative peak intensities. An exception is found for the sodium peak at m/z = 23, which sometimes displays a massive enhancement on the collector (yet never at the point where it would dominate the spectrum). In most cases, it is likely due to surface contamination of the collector prior to the protein deposition, or arises from contamination occurring between the deposition and the analysis as the samples are exposed to air when transferred to the analysis sample holder.

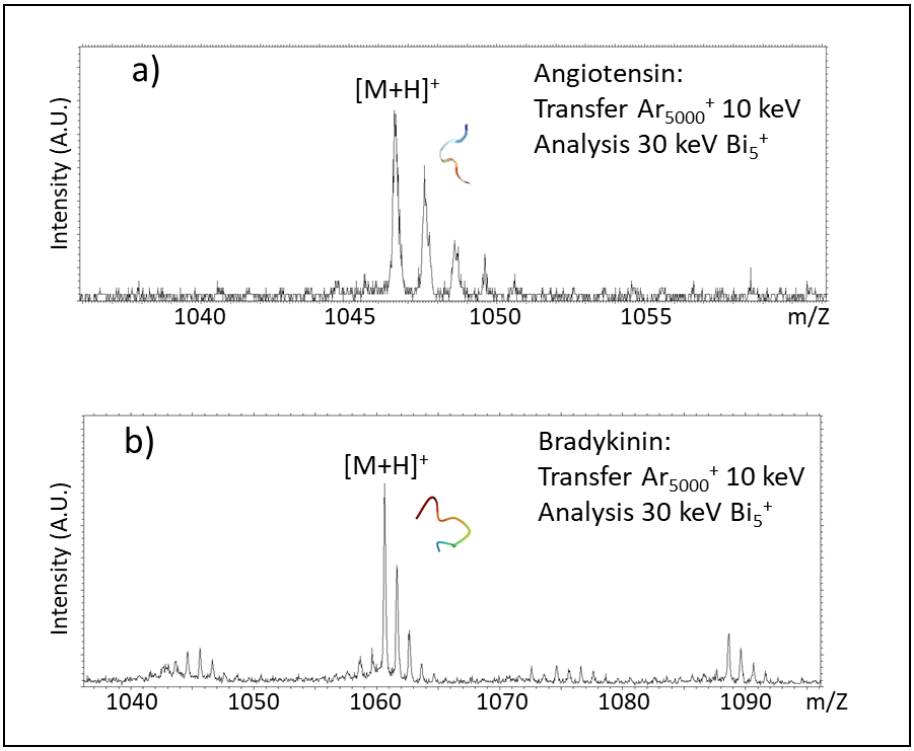


Figure 4.4. *ToF-SIMS spectra recorded on collectors after transfer of respectively* ***a)*** *Angiotensin and* ***b)*** *Bradykinin. In each case, the molecular ion is detected, demonstrating that at least a fraction of the peptides/proteins is transferred intact.*

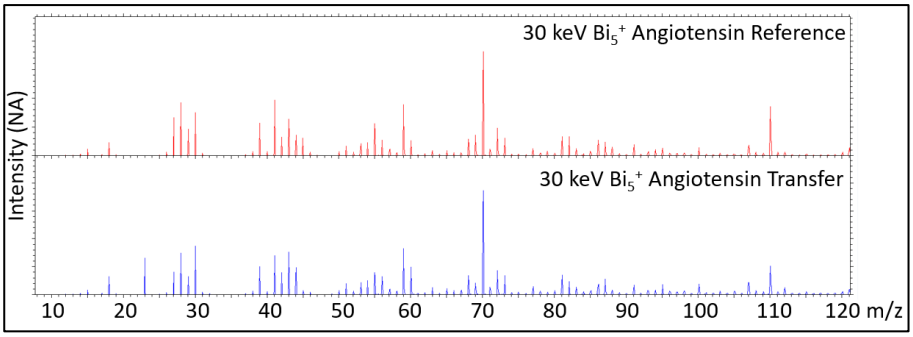


Figure 4.5. *Low-mass range of the ToF-SIMS spectra of angiotensin. In red, reference spin-coated sample. In blue, the transferred angiotensin sample. Close resemblance in the fragmentation patterns and in the peak relative intensities are observed. Only one peak differs significantly, that is the one at m/z = 23, corresponding to sodium.*

Indeed, a random distribution of the sodium signal is usually observed on the collectors. Yet, for some proteins, the sodium seems to originate from the target (sodium distribution mirroring that of the protein material). In these cases, the contamination may have occurred during the preparation of the protein stock solution. Other effects typically encountered in SIMS such as thickness, diffusion or matrix effects may play a role in the sodium intensity variations that were observed. An example is shown for angiotensin in **Figure 4.5**. For the larger protein, insulin (5808 Da) and lysozyme (roughly 14.3 kDa), ToF-SIMS analysis using 30 keV Bi_5^+ failed at demonstrating the presence of intact molecular ion at the surface of the collector. However, this was expected and should not be taken as an indication that these proteins cannot be transferred intact. Indeed, even on reference samples, small energetic clusters such as those of the Bi-LMIG are inherently too destructive to desorb such large biomolecules intact. As demonstrated previously,[10] insulin can however be detected upon bombardment by large argon clusters. In the case of insulin, an Ar_{5000}^+ 10 keV beam was used for the transfer, and the collector was analyzed with Ar_{3000}^+ 10 keV. With these soft analysis conditions, just as for angiotensin and bradykinin, the molecular ion, corresponding to the intact protein could be detected on the collector, as depicted in **Figure 4.6**. Similarly as for references, the fragment corresponding to the β-chain of insulin is present. The very low intensity of the intact insulin peak in the SIMS spectrum may be due to various causes, and raises several comments and questions. At first glance, one may be tempted to attribute that simply to a larger fragmentation upon transfer than that observed for smaller proteins. If this is very likely to have an impact, it is certainly not the only effect to take into account. First, it should be kept in mind that even on thick reference

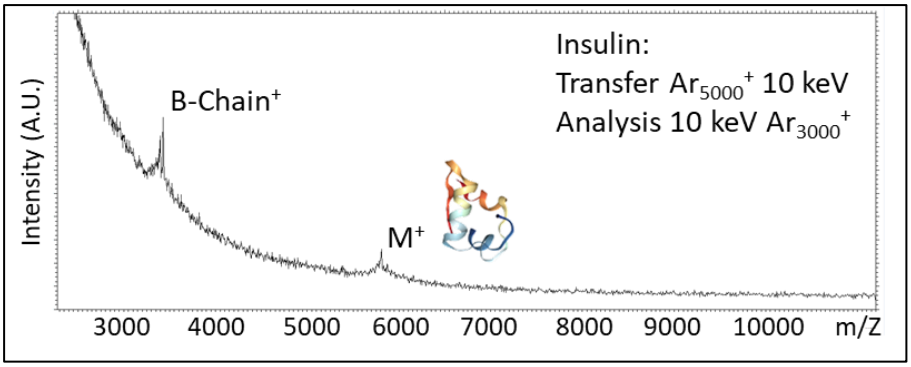


***Figure 4.6**. Static SIMS spectrum recorded on a collector after transfer of insulin. The analysis was performed using a 10 keV Ar_{3000}^+ beam.*

samples, insulin is quite poorly detected in ToF-SIMS due to its mass. Second, as will be discussed later in this chapter, larger molecules are transferred with less efficiency than smaller ones, thus the amount of material available for analysis was probably much smaller in the case of insulin. More experimental work would be required to precisely attribute the influence of each parameter. However, this illustrates the difficulties and limitations that are imposed by the analytical constraints of ToF-SIMS when working with larger molecules. Lysozyme for example could not be detected intact on the collector whatever the routine experimental conditions that were tested. To evaluate the integrity of larger transferred proteins, other methods will be required, as will be demonstrated in **Chapter 6**.

To summarize, the two most important results were that the 2D chemical images demonstrated that peptidic material could be efficiently transferred on the collector, at least as fragmented species. Longer spectrum acquisition further revealed the presence of the molecular ions of angiotensin, bradykinin and insulin. These results can be seen as the proof of concept that peptides and small proteins can be deposited intact using large argon clusters under UHV conditions. The case of larger proteins and enzymes will be investigated in depth in **Chapter 6**. Meanwhile, the small peptides that are easily detected by SIMS will be used as model compounds to study the influence of various parameters on the efficiency of transfer, and to find optimized conditions that could be further used for the construction of more complex multilayers or for the transfer of larger and more complex molecules.

4.3.2. Fragmentation as function of cluster's energy per atom

Argon clusters have been widely investigated and characterized for the analysis of proteins and other organic materials. It has been demonstrated on numerous occasions that fragmentation induced during sputtering is mainly function of the energy per atom ratio (E/n) in the clusters.[11,12] These experimental results are supported by molecular dynamic simulations.[13] Making the link now with molecular transfer using such clusters, it is thus expected that bombarding the target with clusters having a lower E/n would prevent fragmentation and favor the transfer of intact peptides and proteins. Here, bradykinin (1060 Da) was transferred using Ar beams of various sizes and energies (**Table 4.1**). The cluster beams are ordered by decreasing E/n, which is believed to be the most important parameter. All argon cluster beam distributions are shown in **Figure 4.7**. From this figure, it must be noted that the distributions are quite wide, whatever the desired cluster size. This aspect should be kept in mind as it is likely to have a significant effect on the observed fragmentation.

***Table 4.1**. Summary of the different cluster beams used to investigate the influence of the E/n on the fragmentation during transfer.*

Cluster beam	Beam energy (keV)	Energy per atom (eV/atom)	Beam current intensity (nA)
Ar_{1500}^+	10	6.67	≈ 11
Ar_{3000}^+	10	3.33	≈ 8.5
Ar_{5000}^+	10	2.00	≈ 1.4
Ar_{3000}^+	5	1.67	≈ 1.4
Ar_{7000}^+	10	1.43	≈ 0.3
Ar_{5000}^+	5	1.00	≈ 0.2

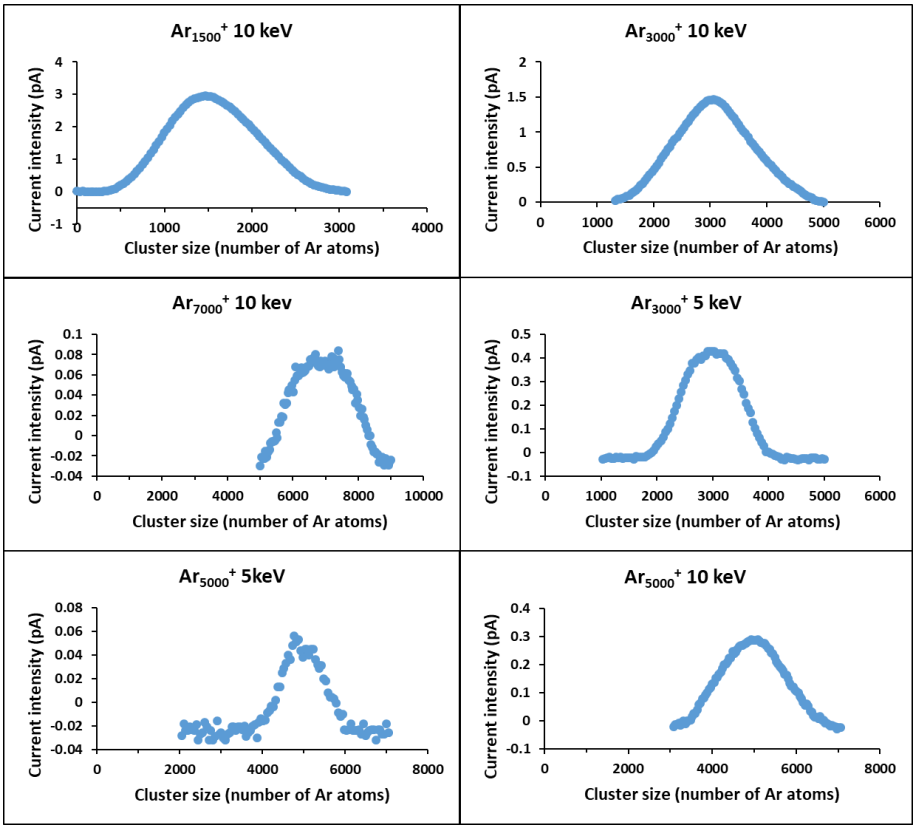


Figure 4.7*. Size distribution of argon cluster beams used for transfer experiments (see Table 1 for their description).*

The collectors were then analyzed by ToF-SIMS using the 30 keV Bi_5^+ beam. In **Figure 4.8**, the normalized percentage of intact peptide molecules detected on the collectors is plotted in blue for each transfer condition (the reference is plotted in green). This fraction of intact peptide is measured as the ratio "molecular ion intensity to total ion intensity" and normalized to the reference, a fresh bradykinin spin-coated sample, that is considered as made of 100% of intact peptides molecules. Note that the higher this percentage, the lower the fragmentation upon transfer. The orange bars represent the E/n of the clusters used for transfer. In good agreement with literature, fragmentation of the transferred material is maximal when E/n is high (here highest for 10 keV Ar_{1500}^+, 6.67 eV/atom), and then decreases with decreasing E/n, being minimal for 5 keV Ar_{5000}^+ (1 eV/atom). For the latter argon beam, it can be concluded from the comparison with the analysis of the reference that more than 60% of the material transferred to the collector is made of intact peptide molecules. It is more important to focus and

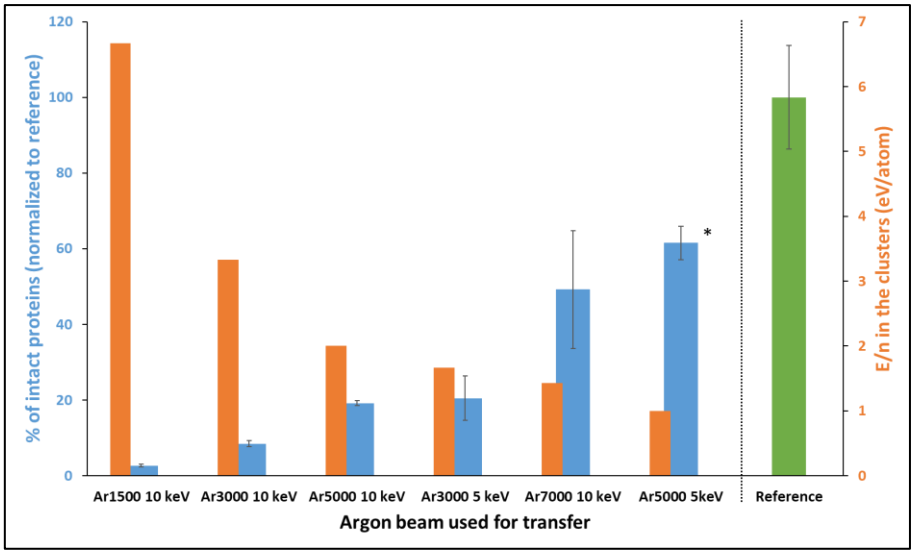


Figure 4.8. *Fragmentation induced during transfer. For each Argon beam used for transfer, the relative percentage of intact peptides is plotted in blue. The E/n of each Argon beam is plotted in orange. It is observed that the percentage of intact peptides on the collector increases as E/n decreases. *The sample Ar_{5000} 5 keV was prepared using a transfer geometry in which the target is bombarded at 45° instead of 15°.*

emphasize on the trend rather than on the exact values. Indeed, the trend clearly highlights that a reduced fragmentation can be reached by using less energetic clusters. The values however should be taken as rough estimations, as they could be biased due to different sticking coefficients of small fragments versus intact peptides (smaller fragments having a higher probability of being volatile under vacuum, and so leave the surface) or by fragmentation induced on the collector by backscattered Ar atoms, especially intense at low impinging angles such as 15° (to be discussed in Chapter 4, section 4.3.3). Other typical SIMS effects such as thickness or matrix effects may influence the ionization probabilities during the analysis. In addition, an important comment must be made regarding the 5 keV Ar_{5000}^{+} sample. It turns out that reducing the clusters total energy and therefore the energy per atom to such a low value significantly deteriorates the transfer efficiency at this grazing impinging angle. This observation is in line with the results obtained by Seah *et al.*[14] in their study of angle dependence of argon gas cluster sputtering. They showed that sputtering yields of clusters with low E/n values were much more sensitive to impinging angle variations, leading to much reduced sputtering yields at angles away from 45°. In our case, this leads to transferred quantities that are too small to be analyzed quantitatively within reasonable transfer durations. In fact, a minimum layer

thickness is required to avoid bias in the fragmentation measurements due to the influence of the underlying hard Si substrate. As detailed by Cristaudo et al.,[15] fragmentation of organic molecules induced during analysis is favored on hard substrates for ultrathin films. To tackle this issue and improve the transfer efficiency for low energy clusters, other transfer geometries in which targets are bombarded at higher angles were developed and are investigated further in this chapter. One of these geometries showed significant improvement of the transfer efficiency, and allowed a sufficient amount of proteins to be transferred using Ar_{5000}^{+} 5 keV. This specific sample was therefore prepared using another geometry, which is believed to have a negligible effect on fragmentation itself. Another point worth mentioning is the shape and width of the different cluster size distributions. Indeed, a relatively large width at half maximum can be observed for each of the distribution (**Fig. 4.7**). The left side of each distribution is composed of smaller clusters (having less constituent atoms), yet also accelerated at 10 keV. Therefore, in this so-called energetic tail of the distribution, the clusters contain atoms of higher energy than those at the desired mass. Even though their proportion decreases as their energy per atom increases, these energetic clusters are believed to play an important role in the measured fragmentation. Despite these technical and geometrical details, the data show that lowering the E/n of the clusters largely favors the deposition of intact bradykinin molecules, up to >60% in the mildest investigated conditions (Ar_{5000}^{+} 5 keV, 1eV/atom). Knowing that a large fraction of peptide/protein molecules can be transferred intact, the next section aims at controlling the amount of protein molecules that is transferred, and so the resulting film thickness.

4.3.3. Determination of the thickness of the transferred thin films

4.3.3.1. Measuring and finely tuning the deposited film thickness

As was briefly mentioned in the **Introduction section** (**Chapter 1**), controlling the quantity of deposited proteins is among the main limitations of other existing protein deposition techniques. Roughly speaking, the ones relying on spontaneous adsorption are usually restricted to construction of maximum one monolayer, while the ones relying on soft landing display a very low deposition rate as only ionized species are deposited. The transfer technique proposed here should allow overcoming limitations inherent to

both existing methodologies. First, it is expected that the amount of transferred peptides/proteins will be linearly correlated to the primary ion dose used for transfer. As long as the target is not depleted, there should not be a limit to the thickness that can be reached on the collector. Second, in contrast with ESI-based soft-landing, the transferred molecules are not selected in mass, and therefore do not require to be ionized. All emitted species are transferred and collected, regardless of their charge state. This substantially enhances the deposition rate, enabling the construction of mono- to multilayers within a reasonable experimental time and in a controlled way.

To ease and accelerate the thickness measurement of the deposited layer, a protocol to measure the protein thickness directly using ToF-SIMS was devised. It has been previously demonstrated in the literature that when a layer of polyelectrolytes or frozen water was deposited on top of a flat inorganic substrate, the SIMS substrate signal intensity showed an exponential decay with increasing layer thickness.[8,9] To our knowledge, this has not yet been generalized to all organic materials. Therefore, we first demonstrated that this relationship was verified in the case of peptides and proteins. For this purpose, fresh lysozyme solutions of increasing concentrations were spin-coated on silicon wafers (see **General materials and methods section, Chapter3**). Their thickness was measured using

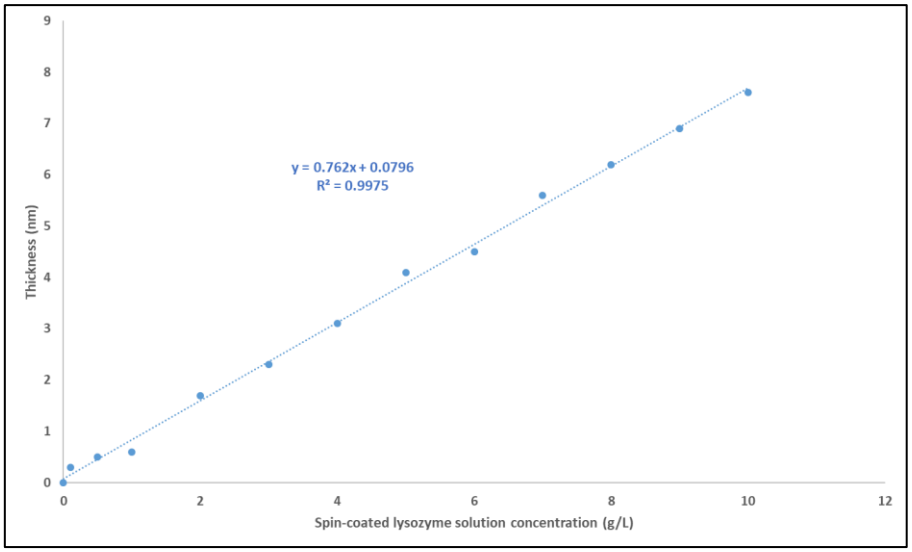


***Figure 4.9**. Ellipsometry measurements. The thickness of protein (lysozyme) reference samples was measured. Linear correlation is obtained between the concentration of the spin-coated solution and the resulting thin film thickness.*

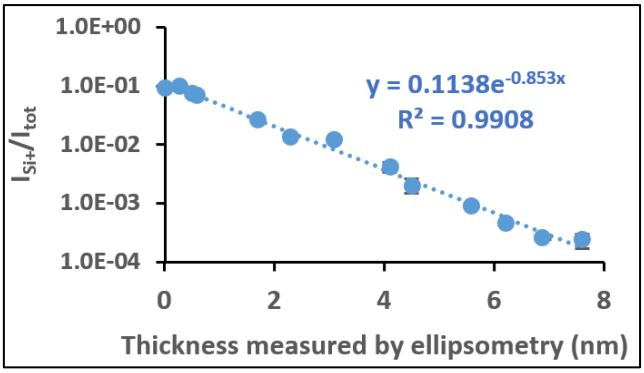


***Figure 4.10**. Exponential decay of the ToF-SIMS Si^+ substrate intensity as function of the protein layer thickness deposited on top of it. In this case, the Si^+ intensity was normalized to the spectrum total intensity to further avoid bias due to differences in the analysis conditions.*

ellipsometry (**Fig. 4.9**). As expected, linear correlation is observed between the concentration of the spin-coated solution and the deposited film thickness. These samples were then analyzed by ToF-SIMS, using the monoatomic 30 keV Bi_1^+ beam. For these measurements, Bi_1^+ was selected over Bi_5^+ mainly because it offers a larger information depth. In fact, in a Bi_5^+ beam, the atoms are less energetic, which means that they penetrate less into the sample.[8] Therefore, the substrate signal intensity was rapidly lost, even with very thin protein layers (5 nm), making the protein thickness range very small. In addition, the cluster effect already observed in the desorption mechanism of Bi_5^+ did not seem to be compatible with such measurements. **Figure 4.10** shows the relative Si^+ peak intensity as a function of protein layer thickness. In good agreement with previous results, an exponential decay is observed, covering three orders of magnitude. Nonetheless, one may notice that at both ends of this calibration, the data points are somewhat out of the exponential decay line. At very low thicknesses, this is explained by specific substrate effects on sputtering, fragmentation and ionization, which ultimately affect the ion fractions. At thicknesses above 8 nm, the data points tend to form a plateau (not shown on the graph), mirroring the loss of the silicon signal in the noise of the spectra. Therefore, the method is not valid for thicknesses below 0.2 nm or above 7 nm. Yet this range is sufficient to demonstrate our hypothesis that the deposited thickness is linearly correlated with the transfer ion dose, and therefore can be precisely controlled. To demonstrate this hypothesis, we proceeded as follows. For each specific cluster size, large numbers of transfers were achieved with various transfer ion doses. The collectors were then first imaged with 30 keV Bi_5^+ to control that deposition was efficient. Then, in the middle of the

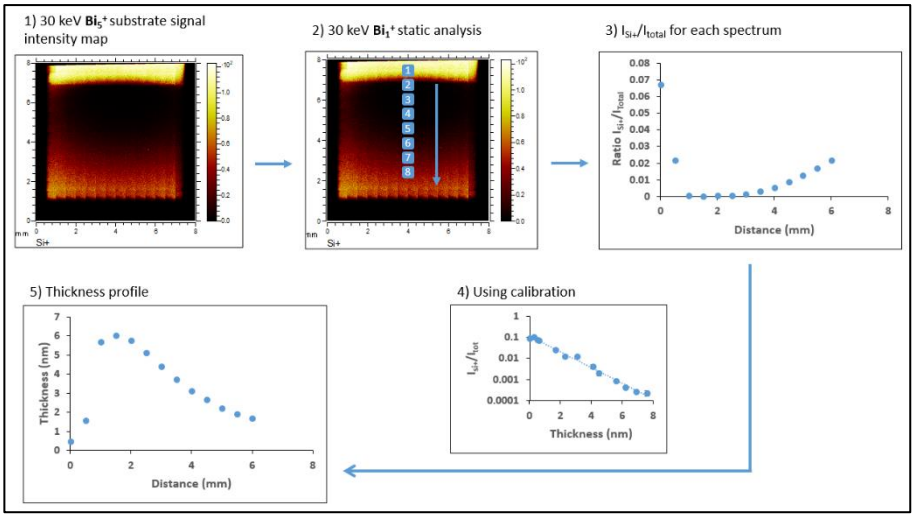


***Figure 4.11**. Strategy proposed for the direct measurement of the deposited films thickness using ToF-SIMS. 1) After the transfer, the collector is imaged by 30 keV Bi_5^+ to confirm the transfer success. 2) In the middle of the collector, successive 30 keV Bi_1^+ spectra are recorded on a straight line, starting from the top (close from the target) to the bottom. 3) For each data point, the Si^+ intensity is normalized to the spectrum total intensity. 4) Using the calibration (exponential function), each normalized intensity can be converted into a thickness value. 5) A thickness profile of the deposited film can be drawn.*

collector, successive 30 keV Bi_1^+ static spectra were acquired on a straight line, starting from the top (close to the target) to the bottom (procedure depicted in **Fig. 4.11**). At each point on the collector, the Si^+ intensity of the recorded spectrum can be transformed into protein thickness, ultimately yielding a thickness profile of the collector, as can be seen in **Figure 4.11**. As could be already observed in the simple 2D images, the initial transfer geometry leads to a non-uniform film thickness on the collector as more material is deposited close to the target. Therefore, to compare the transferred quantity on different samples, we based our study on the maximum thickness measured on each collector (example given for lysozyme transferred with 10 keV Ar_{3000}^+ in **Fig. 4.12**).

Transfers were performed for bradykinin with various Ar_n^+ beams (n = 1500, 3000 and 5000), and different transfer ion doses for each beam. All collectors were studied as described above, and finally the maximum thicknesses measured on each collector were plotted as a function of transfer ion dose, as shown in **Figure 4.13** (yellow, orange and gray lines). One can observe that for each cluster beam, the maximum thickness of the deposited films is increasing with a quite good linearity with the transfer ion dose. This demonstrates that by controlling the transfer ion dose, it is possible to finely

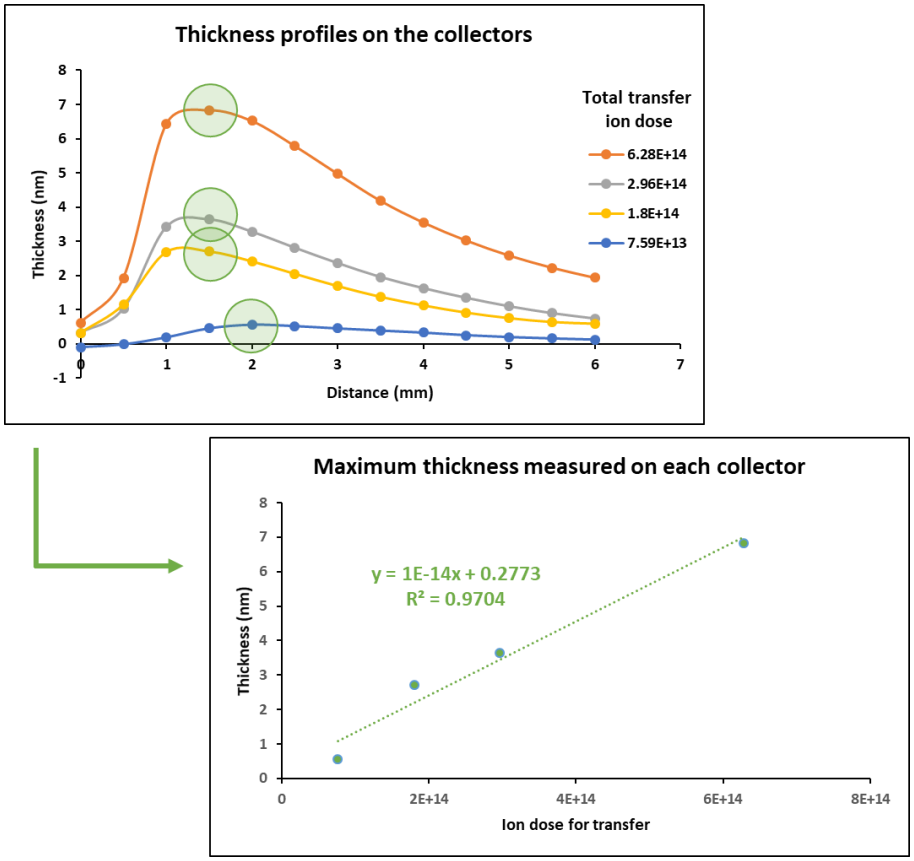


***Figure 4.12**. Example of how a graph "transferred thickness as a function of the transfer ion dose" is constructed. For a given protein and transfer Ar beam, here lysozyme and 10 keV Ar_{3000}^{+}, transfers of various total ion doses are achieved. For each transfer, the deposited film thickness profile is plotted (top image). For each transfer, the maximum thickness of the profile is then plotted as function of the transfer ion dose (bottom image).*

tune the thickness of the deposited films, from sub mono- to multilayers of proteins. Lysozyme and bradykinin have respectively a size of roughly 3.5 and 1.1 nm, so that when a 7 nm film is deposited, it corresponds to approximately 2 and 6 layers of each protein. The green point on the y-axis is the experimental "zero" (no transfer) sample, common to all curves. It does not appear at zero nm because of the offset of the calibration line at very thin protein thicknesses. Regarding the efficiency of the transfer between different cluster sizes at an equivalent total energy of 10 keV (and therefore different E/n), it was expected that higher E/n clusters would favor desorption and thus display a higher deposition rate. If this was verified for the transfer of bradykinin with Ar_{5000}^{+} and Ar_{3000}^{+}, the deposition rate observed for Ar_{1500}^{+} was surprisingly low. Taking a closer look at the amino

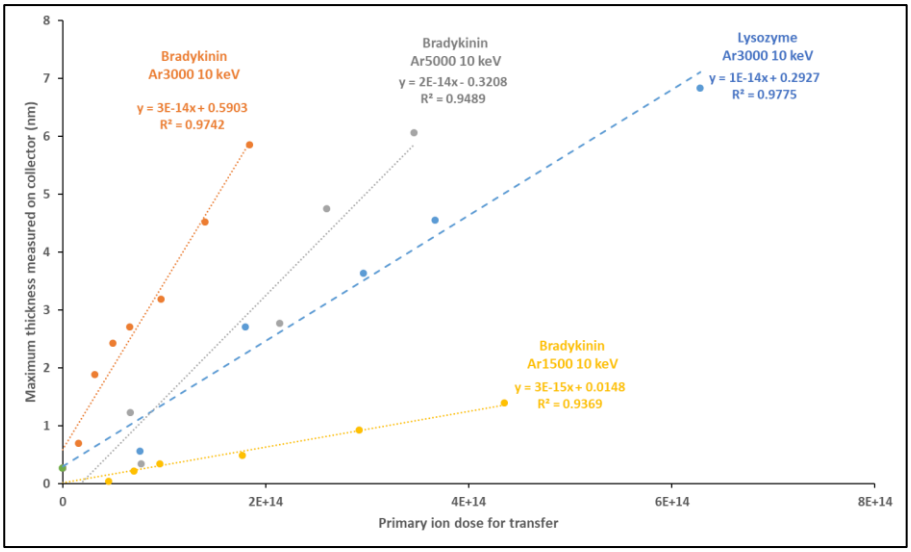


***Figure 4.13**. Relationship between the transfer ion dose and the amount of deposited protein. The maximum thickness measured on each collector is plotted as function of the transfer ion dose. In fact, each data point represents an individual transfer. In orange, grey and yellow, bradykinin was transferred using respectively a 10 keV Ar_{3000}^+, Ar_{5000}^+ and Ar_{1500}^+. In blue, lysozyme was transferred using a 10 keV Ar_{3000}^+. In each case, a linear fit was applied to relate the maximum transferred thickness to the transfer ion dose.*

acid material images of the collector, as shown for example for the molecular ion image of angiotensin transferred by 10 keV Ar_{5000}^+, Ar_{3000}^+ and Ar_{1500}^+ (**Figure 4.14a**), one notices that an area in the center top of the collector is shadowed, as if less material was deposited in that spot. This effect may be attributed to the backscattered argon atoms and small clusters, resulting from the dissociation of the large primary clusters upon impact with the target surface. Indeed, under this grazing angle impact, the backscattered particles tend to keep a forward direction, and so are sent towards the collector, as illustrated in **Figure 4.14b**. This is supported by molecular dynamic simulations.[16] The shadowed area becomes larger from Ar_{5000}^+ to Ar_{1500}^+, mirroring the increase of the E/n of the clusters. Most likely, backscattered projectile atoms that reach the collector with sufficient energy may lead to degradation and further sputtering of the protein fragments from the collector. The final deposited amount of material and the deposition rate would then depend on the balance between the total transferred quantity and the fraction desorbed from the collector for each cluster impact. If the deposition is largely favored for Ar_{5000}^+ and Ar_{3000}^+ due

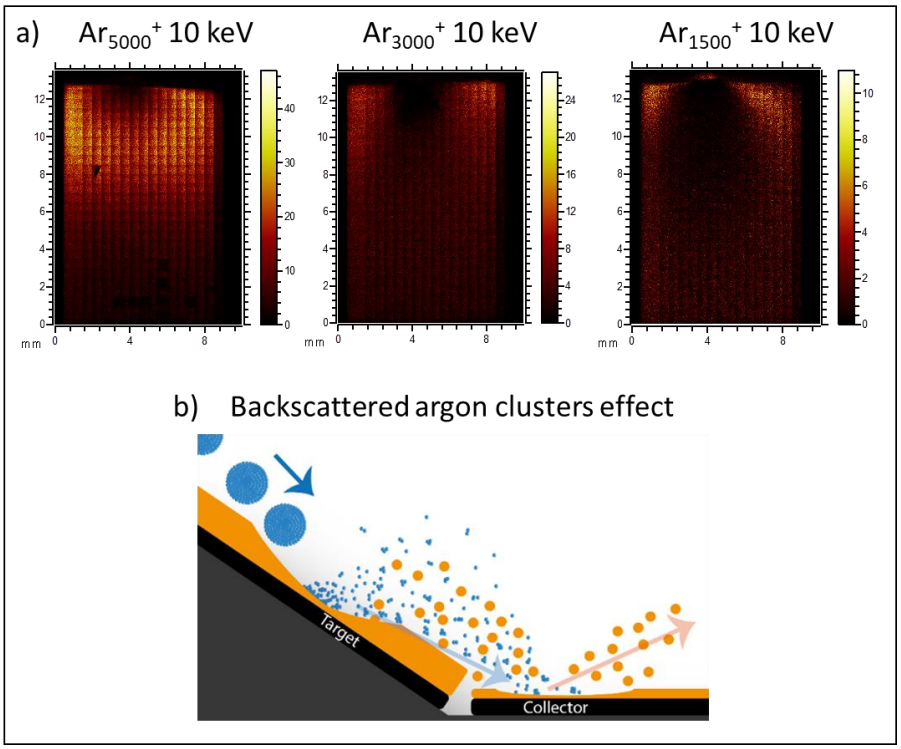


***Figure 4.14**. **a)** Molecular ion images (ToF-SIMS) of angiotensin, transferred with various 10 keV Ar_n^+ beams. A shadowed area where fewer peptides were deposited is observed for each transfer condition, and is gradually increasing with increasing E/n in the clusters. **b)** Schematic illustration of the backscattering of argon particles (atoms and small clusters) to explain the presence of the shadowed areas shown in **a)**. Peptides/protein material is represented is orange while the Argon atoms are represented in blue.*

to their low E/n, deposition and desorption seem to be more balanced for Ar_{1500}^+, explaining the low deposition rate observed in **Figure 4.13**.

The same procedure was applied to lysozyme, a much larger protein, with 10 keV Ar_{3000}^+. Here again, a linear correlation could be established between the deposited thickness and the transfer ion dose (**Fig. 4.13,** blue line). As expected, the deposition rate is lower for lysozyme than for bradykinin, as lysozyme is roughly 14 times larger. This gives a first insight into a potential limitation of the technique, if much larger molecules with lower sputtering yields need to be deposited. Nevertheless, this drawback could be compensated for by optimizing the transfer geometry and consequently substantially enhancing the deposition rate. This will be investigated in the section 4 of this chapter.

4.3.3.2. Homogeneity of the deposited thin films

Insights of the deposition pattern could be already gained simply from observation of the different 2D images of the collectors and was confirmed by the thickness profiles that were measured and presented above (**Fig. 4.12**). It is clear that material is deposited in an ellipsoidal fashion, mostly close from the target, and centered on the impact point of the primary ions. However, these rapid 30 keV Bi_5^+ images do not allow an accurate quantification to be performed. To investigate further the thickness homogeneity of the deposited thin films across the entire collector, we combined both the 2D imaging mode and the SIMS-based thickness measurement method that was developed. In fact, if one records an entire image of the collector with the 30 keV Bi_1^+ beam, it is then possible to transform each pixel into a thickness value using the calibration line, ultimately leading to a complete thickness map of the collector (**Figure 4.15**). This type of analysis is very time-consuming and generates a huge quantity of data. To facilitate the data analysis and allow a rapid conversion of the Si^+ signal intensity into protein thickness, an application was developed in both PYTHON (pyTBB1) and MATLAB (AppTBB1). These platforms, named "Thickness By Bi1", allow to load the raw substrate intensity image, perform normalization, transform the Si^+ intensity into protein thickness using the calibration, and offer a multitude of options to display the resulting thickness maps in a user-friendly way, as shown in **Figure 4.15**. These tools could easily be used for thickness measurements of other materials as parameters of the calibration can be tuned directly in the app. The app and a discussion of the methods and analyses are made available in the extensive Github platform *https://github.com/Benjamin-sc/TBB1*.

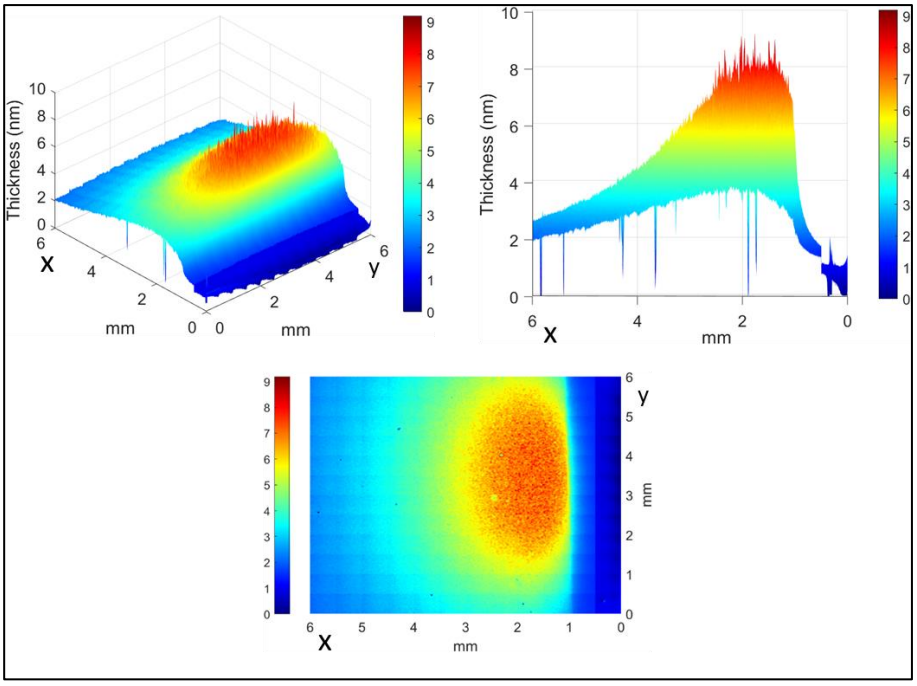


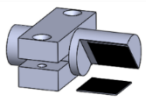
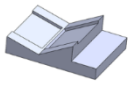
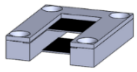
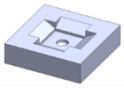
***Figure 4.15**. Three ways to display a thickness map of an entire collector. Here a collector, resulting of the transfer of lysozyme with Ar_{3000}^{+} with a total ion dose of $6.28x10^{14}$ ions, is shown as an example.*

All the results regarding the thickness uniformity across the collector go in the same direction, that is that the 15° transfer geometry does not yield very homogenous thin films. Indeed, a maximum of the deposited thickness is observed relatively close from the target, and then a relatively strong gradient is observed in all directions. The deposition pattern mirrors the angular distribution of the ejecta. In addition to that inhomogeneous deposition, and as was mentioned earlier, this initial transfer geometry might not be optimal (as can be concluded from reported experimental results,[14,17] and from MD simulation[16]). In order to improve both the efficiency of the transfer and the thickness uniformity of the newly fabricated films, several other transfer geometries were investigated. The next section is dedicated to the optimization of the transfer geometry.

4.3.4. Optimization of the transfer geometry

Regarding the transfer geometry, two parameters play an important role with respect to the outcome of a transfer experiment. These are the impinging angle of the clusters on the target, and the collecting angle. A third and crucial parameter is that of the ease of use each sample holder, as the Tof-SIMS analysis chamber imposes restrictions on the geometry and size of the sample holder, but also on the visibility, through the camera and the portholes, which is necessary for placing the sample in the right position and focusing the ions beams. Few geometries were envisaged, and for each, a specific sample holder was 3D-printed in polylactic acid (PLA). Among all 3D-printed transfer sample holders, one stands out by its simplicity of use, the versatility in the angles it allows, and the results it yielded. This sample holder (the top one in **Table 4.2**) will be described in more detail and was used to gather all data showed in the following discussion. The others are also presented in **Table 4.2**, with a short description and their advantages/disadvantages. If they were not further used in this work, they could very well be useful in the future, as they could allow different features, such as loading several different targets on the same sample holder.

***Table 4.2**. Overview of the transfer sample holders printed in PLA and tested for the molecular transfer. For each one of them, the Solidworks design is shown, as well as the Ar beam incident angle and the ejected material collection angle. A short summary of their pros and cons is given.*

Printed sample holders	Incident angle	Collection angle	Pros and cons
	0° to 90°	0° to 90°	➢ All angles possible ➢ Incident angle optimal (45°) ➢ Large collector and multilayers possible ➢ The collector needs to be attached with tape
	30°	60°	➢ Easily attached collector and target ➢ Charging effect due to PLA insulated target => needs to be compensated by conductive tape or electron floodgun
	45°	180°	➢ Easily attached collector and target ➢ Incident angle optimal (45°) ➢ Large collectors and multilayers possible
	15°	0°	➢ Multi-target to build multilayers ➢ Charging effect due to PLA insulated target => needs to be compensated by conductive tape or electron floodgun ➢ Not optimal incident and collection angles

In the best and most versatile set-up, depicted in **Figure 4.16 a & b**, the target is horizontal, for an optimal Ar beam incidence angle (45°), and a rotating

part allows the collection angle to be varied. In a first experiment, in order to observe the angular distribution of the proteins, the collector was placed at 90° from the target. As reported by Lorentz et al. for Irganox,[1] the sputtered proteins are ejected at average polar angles smaller than 45° with respect to the horizontal target surface. **Figure 4.16c** illustrates this for lysozyme sputtered with 10 keV Ar_{3000}^{+}, with the maximum of the deposition detected at 25°. As observed is **Figure 4.16c**, all sputtered molecules are collected, as the collector is larger than the ejection cone at the collecting distance. This implies that the collecting angle (fixed angle of the collector on the sample holder) does not have a major impact. In the following, and strictly for technical reasons (ease of focusing the Ar cluster beam impact point on the target), the collector was systematically placed at 45° from the target.

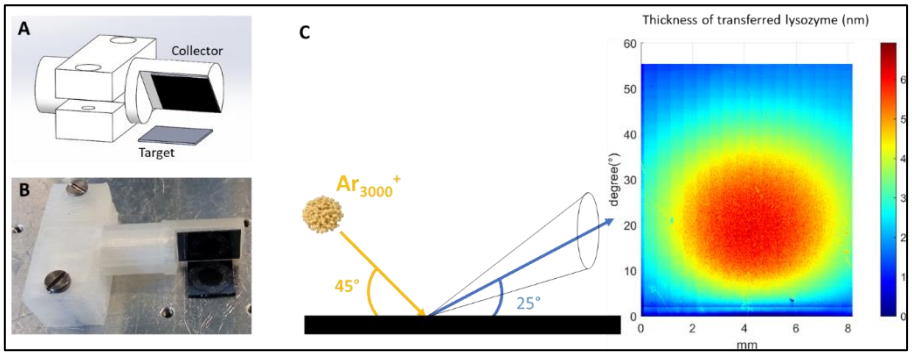


***Figure 4.16**. **a)** Design of the PLA sample holder, with the horizontal target for an optimal desorption (Argon clusters impact at 45°) and the collector on a rotating part that allows a wide range of collecting angles. **b)** Picture of the actual printed sample holder with here the collector set at 90°. **c)** Representation of the transfer geometry with an Ar beam impact angle of 45° (dark yellow) and the collector, illustrated by the thickness map of the deposition, placed at 90° from the horizontal target (black). The maximum of the distribution was observed at 25° (blue). In this case lysozyme was transferred with 10 keV Ar_{3000}^{+}.*

Figure 4.17 compares two 10 keV Ar_{3000}^{+} transfers of lysozyme conducted with the same ion dose (1 x 10^{14} ions, equivalent to approximately 15 min of sputtering). For an incident angle of 15°, the amount of transferred material is extremely small. Moreover, a small crater is observed at the edge of the collector, attributed to energetic backscattered argon particles (as discussed earlier). For an incident angle of 45°, much more material is transferred and the silicon substrate is almost entirely covered. To better characterize the deposition rate enhancement, the new sample holder was employed to perform a series of transfers of lysozyme with 10 keV Ar_{3000}^{+}, in the same fashion as in **Figure 4.13**, blue data points. Using this 45° transfer geometry,

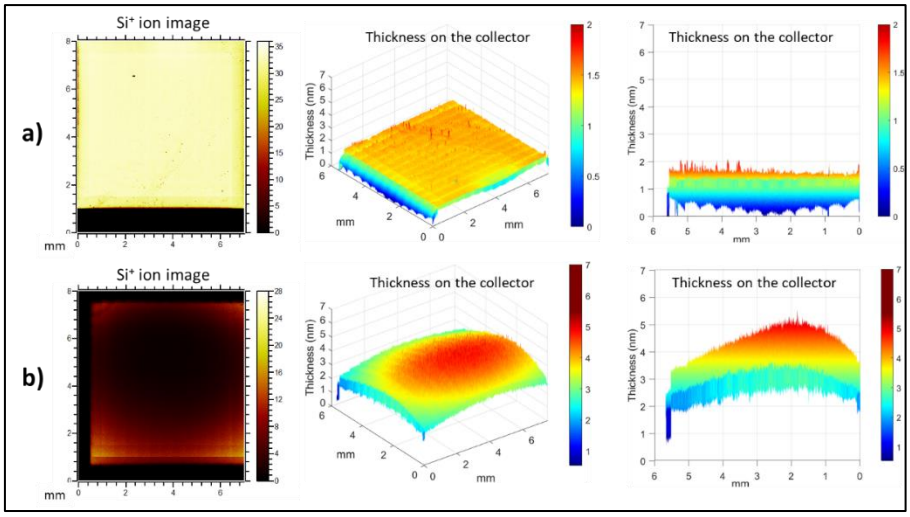


***Figure 4.18**. Comparison between Ar_{3000}^{+} transfer of lysozyme with an incident angle of **a)** 15° and **b)** 45° for a dose of 1 x 10^{14} ions (15min). ToF-SIMS chemical images of the Si^{+} substrate intensity were acquired with 30 keV Bi_1^{+}. The thickness maps were obtained using the MATLAB app (AppTBB1). Both transfers were reproduced twice without any change in the results.*

an 8-fold increase of the deposition rate was observed, as displayed in **Figure 4.18**. In addition, there is no more cratering on the collector. Indeed, at 45°, the argon clusters penetrate more deeply in the target, and therefore release

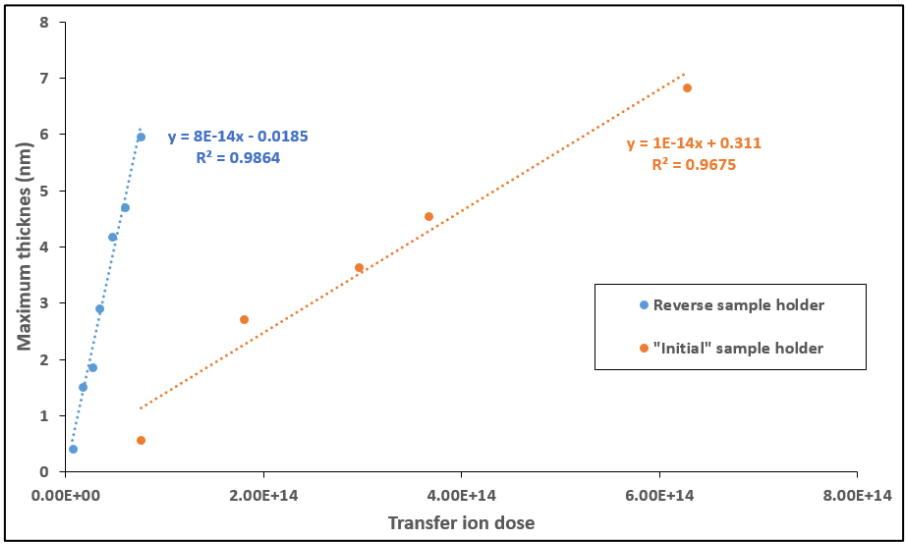


***Figure 4.17.** Maximum thickness deposited on the collector as function of the transfer ion dose. Comparison between the initial transfer geometry (Ar beam impact angle of 15°, in orange) and the optimized transfer geometry (Ar beam impact angle of 45°, in blue). In both cases, lysozyme was transferred using a 10 keV Ar3000+ beam. An 8-fold increase in the transfer efficiency is observed when the Ar beam impact angle is increased from 15° to 45°.*

more of their energy during the impact.[16] The backscattered particles thus have little remaining energy, and do not induce sputtering if reaching the collector. Homogeneity of the deposited films is still not perfect, but is also largely improved using this geometry. It could be further improved simply by moving the X and Y position of the Ar beam on the target during the transfer.

4.4. Conclusion

In this first chapter, the possibility to use large argon gas cluster ion beams for the construction in solvent-free conditions of protein thin films was demonstrated. This approach consists of bombarding a pool of solid-state molecules with argon clusters, and collecting the ejected particles on a desired substrate. Using small peptides (angiotensin and bradykinin) as model protein-like compounds, it was shown that at least a fraction of the transferred molecules were not fragmented in the course of the process. This was confirmed as the molecular ion of the peptides could be detected on the collectors by SIMS routine analyses. This was extended to small proteins, such as insulin, but failed for larger ones, which cannot be detected by SIMS. For these, alternative analytical protocols will have to be devised, as will be discussed in **Chapter 6**. The transferred conditions were then optimized, to control both the fragmentation of the proteins as they are transferred, and the construction of the thin films, in terms of protein amount and thickness uniformity. First, it was established that the fragmentation could be drastically reduced as the E/n in the clusters is decreased. When using a 5 keV Ar_{5000}^{+} beam (E/n of 1eV/atom) to transfer bradykinin, it was found that more than 60% of the collected material was intact protein molecules. Secondly, it was demonstrated that as long as the target is not depleted, the transferred quantity was linearly proportional to the transfer ion dose, and so can be precisely tuned. To highlight this point, a protocol to measure the thickness of the protein layer using the ToF-SIMS instrument was established. This technique also allows the generation of thickness maps of entire collectors. Finally, the transfer geometry was investigated to improve both the deposition rate and the thickness uniformity on the collectors. It was determined that an impinging angle of the clusters of 45° with respect to the target could improve the deposition rate up to 8 times. By collecting the ejecta also at 45°, the resulting films display a better thickness uniformity.

The next two chapters will focus on the use of this cluster-assisted deposition method to on the one hand, achieve transfers on a series of different

substrates to target specific applications (**Chapter 5**). On the other hand, deposition of larger proteins will be attempted, especially enzymes, to further investigate whether these are transferred with retention of their 3D structure/enzymatic activity (**Chapter 6**).

4.5. Bibliography

(1) Lorenz, M.; Shard, A. G.; Counsell, J. D. P.; Hutton, S.; Gilmore, I. S. Angular Distribution of Molecules Sputtered by Gas Cluster Ion Beams and Implications for Secondary Neutral Mass Spectrometry. *J. Phys. Chem. C* **2016**, *120* (44), 25317–25327.

(2) Mansilla, C.; Wirtz, T. Storing Matter: A New Analytical Technique Developed to Improve the Sensitivity and the Quantification during SIMS Analyses. *Surf. Interface Anal.* **2010**, *42* (6–7), 1135–1139.

(3) Mansilla, C.; Wirtz, T. Application of the Storing Matter Technique to the Analysis of Semiconductor Materials. *J. Vac. Sci. Technol. B, Nanotechnol. Microelectron. Mater. Process. Meas. Phenom.* **2010**, *28* (1), C1C71.

(4) Wirtz, T.; Mansilla, C.; Verdeil, C.; Migeon, H. N. Storing Matter: A New Quantitative and Sensitive Analytical Technique Based on Sputtering and Collection of Sample Material. *Nucl. Instruments Methods Phys. Res. Sect. B Beam Interact. with Mater. Atoms* **2009**, *267* (16), 2586–2588.

(5) Wirtz, T.; Migeon, H. N. Storing Matter: A New Quantitative and Sensitive Analytical Technique. *Appl. Surf. Sci.* **2008**, *255* (4), 1498–1500.

(6) Lorenz, M.; Zhang, J.; Shard, A. G.; Vorng, J. L.; Rakowska, P. D.; Gilmore, I. S. Method for Molecular Layer Deposition Using Gas Cluster Ion Beam Sputtering with Example Application in Situ Matrix-Enhanced Secondary Ion Mass Spectrometry. *Anal. Chem.* **2021**, *93* (7), 3436–3444.

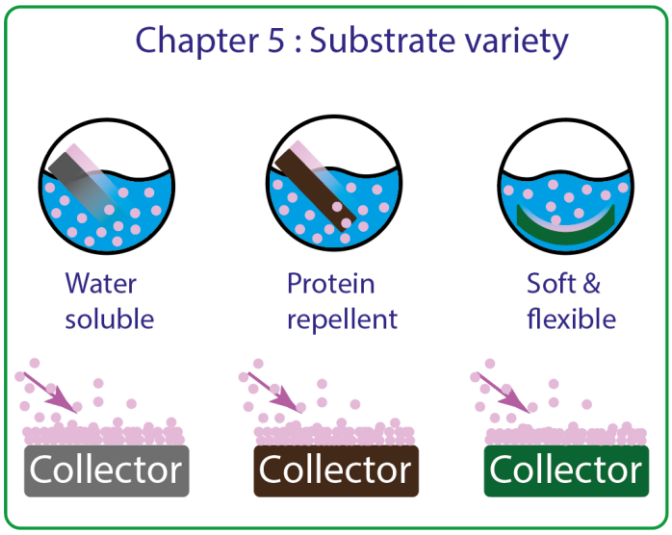
(7) Moshkunov, K.; Tomasetti, B.; Daphnis, T.; Delmez, V.; Vanvarenberg, K.; Préat, V.; Lorenz, M.; Quanico, J.; Baggerman, G.; Lemiere, F.; Dupont, C.; Delcorte, A. Improvement of Biomolecular Analysis in Thin Films Using in Situ Matrix Enhanced Secondary Ion Mass Spectrometry. *Analyst* **2021**, *146* (21), 6506–6519.

(8) Szakal, C.; Kozole, J.; Michael F. Russo, J.; Garrison, B. J.; Winograd, N. Surface Sensitivity in Cluster-Ion-Induced Sputtering. *Phys. Rev. Lett.* **2006**, *96* (21), 216104.

(9) Delcorte, A.; Bertrand, P.; Arys, X.; Jonas, A.; Wischerhoff, E.; Mayer, B.; Laschewsky, A. ToF-SIMS Study of Alternate Polyelectrolyte Thin Films: Chemical Surface Characterization and Molecular Secondary

Ions Sampling Depth. *Surf. Sci.* **1996**, *366* (1), 149–165.
(10) Delcorte, A.; Delmez, V.; Dupont-Gillain, C.; Lauzin, C.; Jefford, H.; Chundak, M.; Poleunis, C.; Moshkunov, K. Large Cluster Ions: Soft Local Probes and Tools for Organic and Bio Surfaces. *Phys. Chem. Chem. Phys.* **2020**, *22* (31), 17427–17447.
(11) Weibel, D. E.; Lockyer, N.; Vickerman, J. C. C60 Cluster Ion Bombardment of Organic Surfaces. *Appl. Surf. Sci.* **2004**, *231–232*, 146–152.
(12) Rabbani, S.; Barber, A. M.; Fletcher, J. S.; Lockyer, N. P.; Vickerman, J. C. TOF-SIMS with Argon Gas Cluster Ion Beams: A Comparison with C 60. *Anal. Chem* **2011**, *83*, 3793–3800.
(13) Delcorte, A.; Cristaudo, V.; Lebec, V.; Czerwinski, B. Sputtering of Polymers by KeV Clusters: Microscopic Views of the Molecular Dynamics. *Int. J. Mass Spectrom.* **2014**.
(14) Seah, M. P.; Spencer, S. J.; Shard, A. G. Angle Dependence of Argon Gas Cluster Sputtering Yields for Organic Materials. *J. Phys. Chem. B* **2015**, *119* (7), 3297–3303.
(15) Cristaudo, V.; Poleunis, C.; Laha, P.; Eloy, P.; Hauffman, T.; Terryn, H.; Delcorte, A. Ion Yield Enhancement at the Organic / Inorganic Interface in SIMS Analysis Using Ar-GCIB. *Appl. Surf. Sci.* **2021**, *536* ,**2020**, 147716.
(16) Delcorte, A. A Microscopic View of Macromolecule Transfer in the Vacuum Using Gas and Bismuth Clusters. *J. Phys. Chem. C* **2022**, *126* (16), 7307–7318.
(17) Yamada, I.; Matsuo, J.; Insepov, Z.; Aoki, T.; Seki, T.; Toyoda, N. Nano-Processing with Gas Cluster Ion Beams. *Nucl. Instruments Methods Phys. Res. Sect. B Beam Interact. with Mater. Atoms* **2000**, *164–165*, 944–959.

Chapter 5 : Transfer on functionalized substrates, water-soluble materials and soft polymers



In this chapter, the versatility of the cluster-assisted deposition approach with respect to the collector's nature (physico-chemical properties) is investigated and demonstrated. It is first shown how the analytical issues encountered with Si collectors for a series of analyses could be circumvented by opting for soft and flexible polymer collectors. Notably, these allowed measuring the total transferred protein mass via BCA assay, offering a very complementary method to that relying on film thickness measurements (**Chapter 4**). Secondly, strategies were devised to prepare functionalized collectors, that should favor the complete release of all transferred proteins once in contact with aqueous solution. While this could also be helpful from the analytical perspective, it could certainly be a good starting point for envisioned release applications. The collectors were coated with either a sacrificial layer, designed to dissolve upon contact with water, or with a protein-repellent layer, promoting protein desorption once immersed in solution. Finally, the ability of building protein thin films on substrates that are out of reach of most widespread adsorption-based methods is demonstrated as proteins were successfully deposited on paper, a common material whose properties are altered when placed in contact with water.

5.1. Introduction

There are multiple reasons and motivations worth investigating the deposition of peptides and proteins on various substrates. One is that the variety of the substrate's nature is among the main limitations inherent to the existing solution-based adsorption methods. Indeed, these can only be performed on substrates that withstand contact with water. Therefore, a series of materials are out of reach of the most widespread strategies. From a fundamental point of view, it seems very relevant to demonstrate that the approach developed in this work expands the scope of compatible substrates for the construction of protein thin films. In theory, this cluster-assisted deposition method could be performed on any solid substrate that is vacuum-compatible. To demonstrate this point, the transfer of proteins on paper, a substrate that clearly does not stand water, will be attempted.

In addition, the chemical and physical substrate properties can prove to determine the success of specific targeted applications. Without seeking particularly complex ones, silicon wafers proved to be an issue for a series of analyses that had to be performed on the collectors. An example was as simple as the quantification of the transferred proteins via bioassays. The issues resulted either from the chemical properties of the Si wafers (interaction with the proteins, interference with bioassays), or from its physical properties (solid/rigid state), making it difficult to handle. To overcome these inconveniences, a few strategies were investigated, with varying degrees of success. These include the transfer on soft polymers, very easy to handle, and the transfer on Si wafers that were functionalized prior to deposition, to favor subsequent desorption of the transferred proteins. Functionalized wafers were coated either with a layer of poly(ethylene glycol) methyl ether, or with a layer of trehalose. The first one is expected to act as a protein repulsive surface once the collector is immersed into solution, while the second one is supposed to act as a sacrificial layer, completely dissolving upon contact with water.

5.2. Materials and methods

5.2.1. Eppendorf tubes

The Eppendorf tubes were purchased from Eppendorf AG (Hamburg, Germany). These are 0.5 mL Protein LoBind tubes (reference 022431064). The Eppendorf tubes were not cleaned or treated before use, and were used only once.

5.2.2. BCA assay on PE sheets in Eppendorfs tubes

The protocol of the BCA assay had to be adapted from the given standard procedure, in order to be performed directly on the collectors. Here, it is described for the case of proteins deposited on a soft sheet of polyethylene (PE) of 1 x 1 cm^2. The small PE sheets were rolled and introduced in a 0.5 mL Eppendorf tube. The working reagent was prepared as follows: reagent A and B were mixed in a 50:1 ratio. Reagent A is an alkaline buffer (basic pH is necessary to allow Cu^{2+} reduction), while reagent B contains the BCA. 200 µL of working reagent are added in the Eppendorf tubes. 20 µL of a 1% SDS solution are further added to each sample to ensure desorption of the proteins from the PE films. The Eppendorf tubes were then closed and incubated in a 60°C water bath for 1 h. After that, the samples were left at room temperature for a few minutes to allow cooling. Then, 180 µL of each tube were transferred into a clear 96-wells plate. Finally, absorbance was measured at 562 nm. A calibration line was always prepared and measured alongside the samples to be quantified. To best mimic the real transferred samples, the calibration samples were prepared by drying known quantities of proteins on the same PE sheets as those used as collectors. These samples were usually dried overnight. The data points of the calibration lines are always given as a mean of three replicates.

5.2.3. Sugars and polymers

Trehalose and fructose were both purchased from Sigma-Aldrich (Steinheim, Germany). Poly(ethylene glycol) methyl ether, ω-thiol-terminated was purchased from Polymer Source Inc. (Dorval, Canada).

5.2.4. Preparation of the PEG-coated collectors

Clean Si wafers were covered by a 100 nm thick gold layer. This metallization was achieved by the Winfab platform (UCLouvain, Begium). Before use, wafers were cleaned. First, they were rinsed in acetone to remove the polymer protection coating deposited on top. Second, they were cleaned in a piranha mixture for no longer than 2 min. Finally, they were cleaned in the UV-ozone equipment. In the meantime, a 1g/L solution of poly(ethylene glycol) methyl ether, ω-thiol-terminated (PEG-SH) was prepared in water. After the UV-ozone treatment, the wafers were dipped in the PEG-SH solution for duration ranging from 30 min to 15 h, to allow the grafting of the

polymer to the gold substrate. Finally, the samples were rinsed under water, and then dried under gentle N_2 flux.

5.2.5. Preparation of the trehalose-coated collectors.

Before being inserted in the sublimation instrument, the trehalose was dried for 24h in an oven heated at 80°C. Getting rid of the water allows the sublimation to take place in a more reproducible way, to obtain smoother layers and to reduce the pumping time of the instrument to reach sufficiently low pressure. Si wafers were cleaned as detailed previously, and then attached to the cupper sample holder using conductive double-sided adhesive tape. Once the experimental set-up was ready to use, the first step was the pumping to reach 10^{-4} mbar. From that pressure, the metallic crucible containing the sugar was heated by an electric resistance, while the cupper rod used as sample holder was cooled by iced water. In order to find the optimal sublimation conditions, the temperature was varied from 120°C to 180°C, and the duration ranged from 30 min to 2 h.

5.2.6. SIMS depth profiles

SIMS depth profiles were carried out using a 10 keV Ar_{3000}^+ beam to erode the sample while the Bi_5^+ LMIG was operated as analysis beam. Depending on the thickness of the layer to be depth-profiled, the current intensity of the sputter beam was adjusted by increasing or decreasing the beam lead off. Typical sputter beam intensities ranged from a few tens of pA to a maximum of 1 nA for the thicker samples.

5.3. Results and discussion

5.3.1. A note about the protein quantification challenge

During this project, the quantification of the transferred protein quantities has proven to be one of the most challenging parts. In fact, the quantification remained inconclusive for more than three years, in spite of the countless efforts that have been made toward that objective. In this first section, the main efforts that have been carried out towards the quantification of the transferred protein quantities will be briefly reviewed.

One of the most popular and straightforward bioassay for the quantification of proteins is the bicinchoninic acid assay (BCA or BCA assay), described in the general materials and methods section. At the beginning, the transfers were achieved using Si wafers as collectors. To quantify the transferred

quantities, the first devised protocol was simply to place the Si wafers in multiwell plates, and to perform the BCA assay directly in the wells containing the wafers. However, it turned out that the silicon was interacting with the assay, as Si reduces the Cu^{2+} ions involved in the BCA assay. Therefore, the response of the test was maximum whatever the protein quantity present at the surface of the Si wafer. The second used protocol was to recover the deposited proteins after the transfer, and to perform the BCA assay on the solution. It must be noted that proteins that were adsorbed in solution are usually irreversibly immobilized on the surfaces.[1,2] However, in this case, protein are immobilized via a forced deposition process. It is therefore uncertain that the same protein-surface interactions will be observed. In addition, multilayers are built, wherein protein-protein interactions may differ with respect to the protein-surface ones. In practice, a drop of water (first pure water, and then second 1% SDS was also tried) was deposited on the collector, and then recovered. Yet this strategy did not prove successful either. Most of the time, the protein quantities seemed to be under the detection limit. Two hypotheses were envisaged to explain this observation. First, it was possible that the amount of transferred proteins was indeed too little to be detected. Note that these experiments were carried out only using the seminal transfer geometry (15°), which was shown later to be far from optimal in terms of transfer efficiency. Nevertheless, the thickness measurements presented in **Chapter 4** tended to indicate that as long as the transfer ion dose was sufficiently high, the transferred quantity should have been in the detection range. Second, and more plausible, the problem could originate from desorption issues. Either the deposited proteins were sticking too strongly to the collector, and were not desorbed. Alternatively, the amount of water necessary to desorb the proteins was too large, hence diluting the recovered protein to a point where it was not detected anymore (the BCA assay is performed on maximum 20 µL of protein solution, and a minimum of 100 µL of water was required to cover the entire wafer). Furthermore, when a drop was deposited on the collector, it was very difficult, not to say impossible to recover it in full, undeniably leaving a fraction of the proteins at the surface.

Afterwards, a series of alternative strategies were considered. These included commercially available protein quantification assay alternatives to BCA, such as the NanoOrange assay and the Qubit assay, both from ThermoFisher Scientific. These two tests, not only were compatible with Si wafers, but also were supposed to be much more sensitive. Yet, none yielded

satisfying results. Other alternatives included much more original ideas, relying for example on homemade multiwell plates, specifically designed to fit to the Si collectors, to ensure using minimal solvent volumes. Nevertheless, all these efforts were in vain.

Therefore, it was decided to explore the use of other materials as collector substrates. The first few sections of this chapter will describe the envisaged strategies and chosen systems. The various strategies were investigated simultaneously, so that as one turned out to be quite successful, the others were somewhat left aside and so were not investigated in depth. It is also important to note that as these strategies were devised, the optimization of the transfer geometry had been performed, and the reverse sample holder (45° impinging angle) was used. It is very likely that this parameter played an important role in the success encountered in the following section, as much more protein molecules were transferred, hence easing their detection.

5.3.2. Transfer on polymers

One of the considered strategies was to find a material that was compatible with the BCA assay, which tended to give the most consistent results with respect to protein quantification. In addition, the material would preferably be easy to handle, readily available, and inexpensive. The choice fell on polymers. The first polymer to be tested as collector material was polyethylene terephthalate (PET). Relatively thick (0.96 mm) and rigid plates were used. These were cut in smaller square pieces (1 x 1 cm^2), and used as collectors. If the transfer of proteins proved to work as efficiently as on Si wafers (to that point, the effect of transferring the proteins on an insulating collector remained unknown), the results of the bioassays did not prove to be more conclusive. Once again, practical issues were encountered as the bioassays were performed. On the one hand, the small PET pieces turned out to float in water, making their use very complicated in multiwell plates for example. On the other hand, the rigid nature of the PET samples prevented it to be folded to be used in very small closed volumes, such as sealed vials.

The idea of performing the bioassays in sealed vials emerged as evaporation issues were experienced. Indeed, in order to avoid dilution of the transferred proteins and so loss of signal intensity, minimal solution volumes had to be used. The multiwell plates typically used for bioassays are not so easy to seal tightly. The BCA assay requiring incubation for 1 h at 60°C, sealing issues ultimately led to rapid evaporation of the content of the wells. The search

for the optimal sealed vial was conducted as thin aluminum sheets were being investigated as a potential collector substrate. The chosen aluminum samples had the very interesting characteristic of being relatively "soft"/flexible. This allowed it to be folded or rolled into a vial to perform the bioassays. A few sealed vials were investigated, and Eppendorf tubes were selected as the most suitable solution. It rapidly turned out that, just as silicon, aluminum also reduced the Cu^{2+}, and so was not compatible with the BCA assay. Nevertheless, the Eppendorf tubes proved to be very convenient to perform bioassays on collectors that could be rolled into them.

The idea was then to find a polymer available as thin and soft sheets, so that it could be rolled just as the aluminum sheets into the Eppendorf tubes. Polyethylene (PE) was selected, in the form of a large roll of very thin PE (0.05 mm). Small 1 x 1 cm^2 pieces were cut and used as collectors. In the first place, a BCA assay calibration line was performed on the PE sheets to assess their compatibility with the assay. To best mimic the samples obtained by transfer, protein solution was drop-casted on the PE sheets. Once dry, the sheets were placed into small Eppendorf tubes, and the BCA assay was performed. The results of such a calibration line are depicted in **Figure 5.1**. Very satisfying results were obtained, showing that PE sheets combined with the use of Eppendorf tubes gave a good experimental set-up to perform bioassays directly on solid surfaces, in small solution volumes. The crucial step was then to use these small PE sheets as collectors, and study the evolution of the transferred mass with that of the primary ion dose. For this set of experiments, the reverse transfer sample holder was used (see **Chapter 4**, impinging angle of 45°). Using a 10 keV Ar_{3000}^+ beam, a series of transfers of bradykinin were performed with increasing ion doses. In this case, the smooth running of transfers was not controlled by large 2D SIMS images. Indeed, the very soft nature of the PE makes it difficult to hold the 1

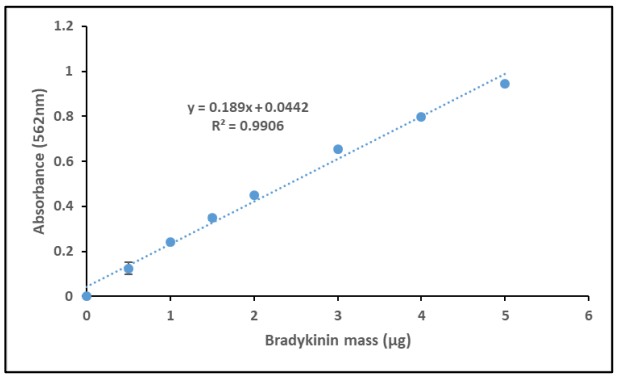


***Figure 5.1**. BCA assay calibration line performed on model samples, prepared by drop-casting a fresh lysozyme solution on small PE sheets. The assay was carried out in Eppendorf tubes.*

x 1 cm² pieces completely flat in the analysis sample holder (crucial for height focusing across large images). After transfer, the collectors were directly inserted in small Eppendorf tubes, and a BCA assay was performed. Each time a BCA assay was performed on transferred samples, a fresh calibration line was prepared alongside, to ensure that both the reference samples and the transferred samples were measured in the same conditions (mostly temperature and duration of the incubation in the water bath). The results are displayed in **Figure 5.2**. As was expected from the thickness data presented in **Chapter 4** (**Fig. 4.13**), it is demonstrated that the deposited protein quantity increases linearly with the transfer ion dose, and so could be further precisely controlled by tuning the ion dose.

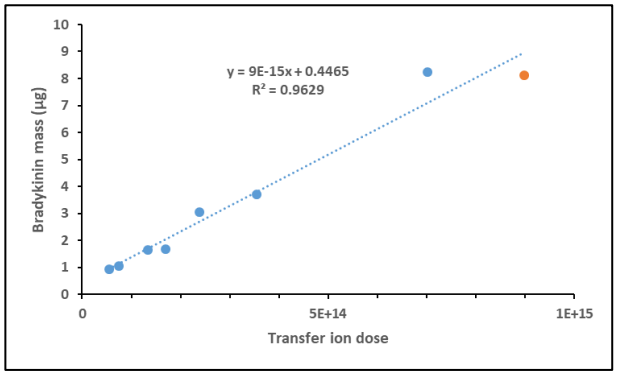


***Figure 5.2**. Results of a BCA assay performed on transferred samples. Bradykinin was transferred on PE collectors using a 10 keV Ar_{3000}^+ beam in the reverse sample holder. The dashed line is a linear fit that was applied to all data points. The data point colored in orange was taken into account to draw the trend line, even though it is clearly lower than expected, probably due to a fully consumed target.*

Even though the correlation coefficient is quite high, i.e. R^2 = 0.96, it was calculated on all the data points presented on the graph. Yet, one can observe that the last point on the right (colored in orange), corresponding to the transfer achieved with the highest ion dose, in slightly off the trend line. It appears to be at a lower mass than expected. Without taking that point in consideration, the R^2 = 0.99. The most logical explanation for this is that when such high transfer ion doses are reached, the target might be depleted in proteins before the end of the sputtering process. As the targets are not completely homogeneous, and their thickness not precisely controlled, it is difficult to predict the exact ion dose at which the Si wafer is reached. In other cases, this effect was observed at ion doses slightly higher or lower. This issue could further be prevented by preparing thicker targets, especially when long transfers were planned.

PE sheets proved to be very effective as collector substrate when targeting the subsequent quantification of the transferred protein quantity by BCA assay. They are indeed very easy to manipulate and to clean, as well as

convenient to combine with Eppendorf tubes for bioassays. Therefore, they were used as collectors for further quantification experiments, using other proteins, such as lysozyme and trypsin. In particular, all three proteins were transferred with various ion doses of a 10 kev Ar_{5000}^{+} beam, to study how the deposition rate evolved with increasing protein mass. In **Chapter 4**, insights regarding that trend were gained through the thickness measurements of transferred bradykinin and lysozyme samples. Clearly, it appeared that the larger protein was transferred less efficiently than the smaller one (**Chapter 4, Fig. 4.13**). However, the comparison was done using the seminal transfer geometry, i.e. with an impinging angle of 15°. It was found later that at such grazing angles, the backscattered argon atoms and small clusters could have an influence on the deposition rate. The importance of this effect could slightly differ from one protein to another. Obviously, the trend is not expected to be different, but results that are more accurate could be obtained by using the reverse geometry. In fact, it was shown that this experimental set-up prevents the effect of the backscattered argon atoms. In addition, comparing the total amount of protein deposited on the collector is also more relevant than comparing the thickness measured in one single point on the collector. Indeed, if the angular distribution of the ejecta varies

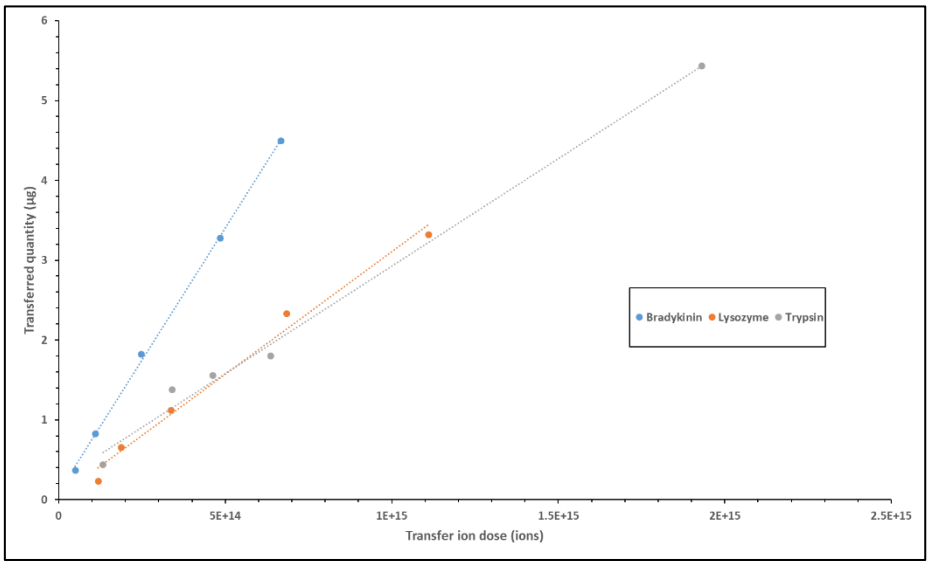


Figure 5.3. *Graphs showing the deposited protein mass as a function of the transfer ion dose for three different proteins: bradykinin (1 kDa) in blue, lysozyme (14.3 kDa) in orange and trypsin (23.8 kDa) in grey. Transfers were achieved using a 10 keV* Ar_{5000}^{+} *beam in the reverse sample holder, and the transferred quantity were measured via BCA assay. Linear fits were applied for each proteins.*

from one protein to another, or if the measurement is not achieved exactly in the area where the maximum material is deposited, comparing samples just by thicknesses measured in one point could induce bias. **Figure 5.3** contains the graphs of the deposited quantity (measured by BCA assay) as a function of the transfer ion dose for the three proteins, using 10 keV Ar_{5000}^{+}, in the reverse sample holder. First, it can be observed that the linearity between the total transferred protein mass and the transfer ion dose is respected for all three proteins. Second, from these data, it is possible to compare the deposition rate as function of protein mass, by looking at the slope of each trend line. The slope/rate was plotted as a function of the protein mass, yielding the graph presented in **Figure 5.4** These results confirm those obtained in **Chapter 4**, as the deposition rate decreases with increasing protein mass. A logarithmic fit was applied, to serve as a guide for the eyes. However, as only three data points are available for the moment, this trend line should be interpreted with caution. If the general trend illustrating that larger proteins are transferred less efficiently was expected, gathering more data points would be recommended to confirm the precise value of the equation linking the deposition rate to the protein mass/size. In addition, as can be observed in **Figure 5.3**, a few additional data points could be worthwhile to refine the results regarding the deposition rate of lysozyme and trypsin, as their fit are not as good as that obtained for bradykinin. With the present data, it is however possible to estimate that to reach the same transferred mass as that of bradykinin, a transfer ion dose roughly 2.15 and 2.45 times higher is necessary in the case of lysozyme and trypsin, respectively. It is important to keep in mind that the BCA assay accounts for all protein materials at the surface of the collector, i.e. intact molecules as well as fragments. Therefore, the deposition rates illustrate not only the efficiency of the intact molecules to be desorbed, but also the efficiency to fragment the molecules and sputter these fragments.

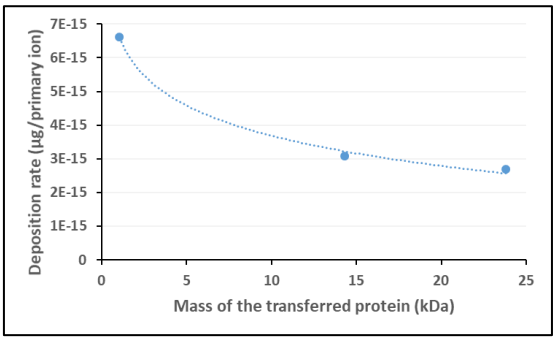


***Figure 5.4**. Graph comparing the transfer rate as a function of protein mass. The deposition rate decreases as the mass of the protein increases.*

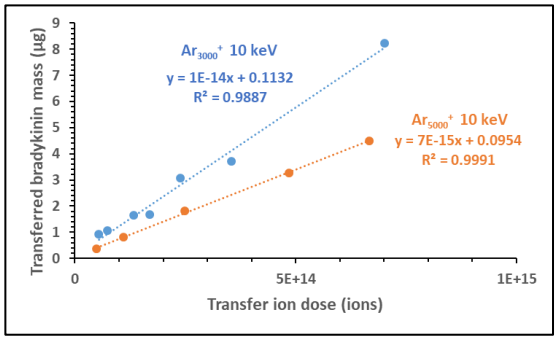


***Figure 5.5**. Comparison of the evolution of the bradykinin deposited mass as a function of the transfer ion dose, when the protein is transferred with a 10 keV Ar_{3000}^+ beam (blue) or a 10 keV Ar_{5000}^+ beam (orange).*

Finally, bradykinin was used to compare the transfer efficiency of a 10 keV Ar_{3000}^+ beam versus that of a 10 keV Ar_{5000}+ beam. Transfers were achieved with both beams, and all the samples were then loaded in Eppendorf tubes to perform a BCA assay. The results are presented in **Figure 5.5**, showing the evolution of the transferred quantity as a function of the transfer ion dose for each cluster size. Using the slope of the two trend lines, it can be measured that bradykinin (or fragments thereof) is transferred nearly two times (1.7 precisely) more efficiently by 10 keV Ar_{3000}^+ than by 10 keV Ar_{5000}^+. This value can be compared to that measured from the data presented in **Chapter 4** (**Fig 4.13**), where the thickness protocol was used to compare the deposition rate. In that case, the ratio Ar_{3000}/Ar_{5000} yielded a value of 2.0, very close to that obtained by measuring the total quantity. The fact that the two methods give similar results is reassuring, and it demonstrates that both techniques can indifferently be used. They are also very complementary, as that relying on thickness measurement is applicable to very small transferred amount, while that relying on total quantification is suitable to larger protein amounts. The small difference observed in the deposition rate ratio measured by the two strategies may arise from experimental errors/approximations, mainly related to the thickness approach, such as those mentioned above (difference in angular distribution leading to different thickness distribution on the collector, measurement performed not exactly where thickness is maximum).

The use of PE sheets as collectors proved to be very successful for the determination of the transferred protein quantities. However, for other types of analysis, such as surface characterization, they are far from ideal (too soft, difficult to keep flat and insulating). For these reasons, several other strategies were investigated at the same time. Yet, as the use of PE *in fine* led to a huge amount of experimental work to collect all the data, the other alternatives could not be studied as in depth as was originally planned, especially as they proved to be more challenging as well. For future

development, it is however relevant to present them, as well as the associated preliminary results, together with a first glance at their potential pros and cons. The next two sections will be dedicated to the two envisaged alternatives to trigger protein release upon contact with water, which are the development of first, a collector coated with a protein-repellent layer, and second, a collector coated with a sacrificial layer.

5.3.3. PEG self-assembled monolayers on gold-coated Si wafers

One of the two alternatives to allow a more efficient desorption of the proteins from the collector and further target delivery applications was to prepare collectors bearing a protein-repellent coating. The idea was that the cluster-assisted transfer method is a forced deposition, so that the proteins are deposited on the collector, regardless of their interactions with it. However, if the proteins are deposited on a protein-repellent surface, they may be more likely to go back into solution once the surface is immersed in water, as illustrated in **Figure 5.6**. To build such collectors, the work of Delcroix on the preparation of stimuli-responsive surfaces was taken as a basis.[3–6] Of particular interest, brush coatings of polyethylene glycol (PEG), also known as polyethylene oxide (PEO), a protein-repellent polymer, were prepared in order to prevent protein adsorption.

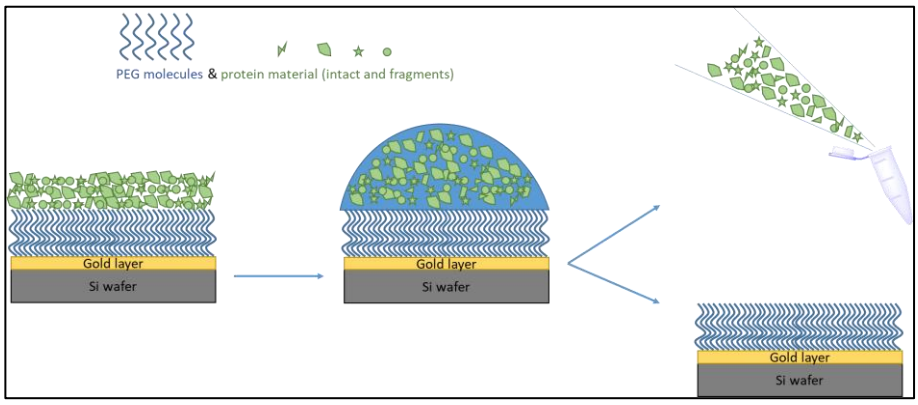


***Figure 5.6**. Schematic illustration of the targeted desorption process associated to the PEG-coated collectors. In an ideal scenario, the polymer brush forms a densely packed coating on which the transferred proteins accumulate. As the PEG is a protein-repellent polymer, it is hoped that it will force all transferred proteins to desorb and go back into solution as the collector is covered with water. In this case, the transferred material can be recovered for further analyses, while the collector can be recycled.*

***Table 5.1**. XPS results confirming the presence of PEG self-assembled monolayer at the surface of the gold substrate. Samples 1 to 3 were prepared by incubating the substrates overnight in the PEG solution, while samples 4 to 5 were prepared by incubating the substrates only 30 min in PEG solution. "Sulfates" signal intensity accounts for non-covalently bonded thiols or contaminations, in both cases most likely physisorbed at the surface, while "S-Au" signal intensity accounts for the covalently bound thiols.*

	Sulfur				**Gold**
	S 2p3/2				**Au 4f**
Sample	**S**ulfates	C-**S**H, **S**-**S**	**S**-Au	**S tot.**	**Au tot**
1	0.8	2.1	2.3	**5.2**	**26.5**
2	0.8	3.1	2.6	**6.5**	**25.5**
3	0.7	3.4	2.3	**6.4**	**22.9**
4	0.7	1.6	2.5	**4.7**	**29.6**
5	0.8	1.8	2.5	**5.1**	**31.2**
6	0.9	2.3	3.0	**6.2**	**28.7**

In a first step, the polymer coatings had to be prepared. Following Delcroix's strategy, thiol-terminated PEG was used, to be spontaneously grafted onto a gold surface.[7–10] The latter was created by deposition of a 100 nm-thick gold layer on a Si wafer. The gold-coated Si wafers were then incubated in PEG solutions, to allow construction of the protein-repellent layer. The construction of the polymer layer was controlled by XPS**. Table 5.1** contains the most important results related to the fixation of the thiol-terminated PEG to the gold surface. The obtained results are in line with those obtained by Delcroix,[6] i.e. similar total amount of Sulfur detected, hence demonstrating the successful construction of the PEG layer. However, a few comments can still be made. First, there is no significant differences in the total PEG quantity detected at the surface whether the samples were incubated in the PEG solution for 30 min (samples 4 – 6) or overnight (samples 1 – 3). In the following, all samples were prepared within 30 min of grafting time. Second, in the present results, the total quantities of sulfur at the surface are slightly higher than those reported by Delcroix. However, the ratio **S**ulfates/**S**-Au is also higher, indicating that the difference probably arises from the presence of more unbound thiols at the surface. This could arise from different rinsing procedures, which look to be less efficient in this case. However, as the presence of physisorbed molecules should not be an issue for the targeted application, the samples were used as they were for the exploratory experimental work. Bradykinin was transferred onto them. Here, in opposition to the PE sheets, the collectors could easily be characterized by

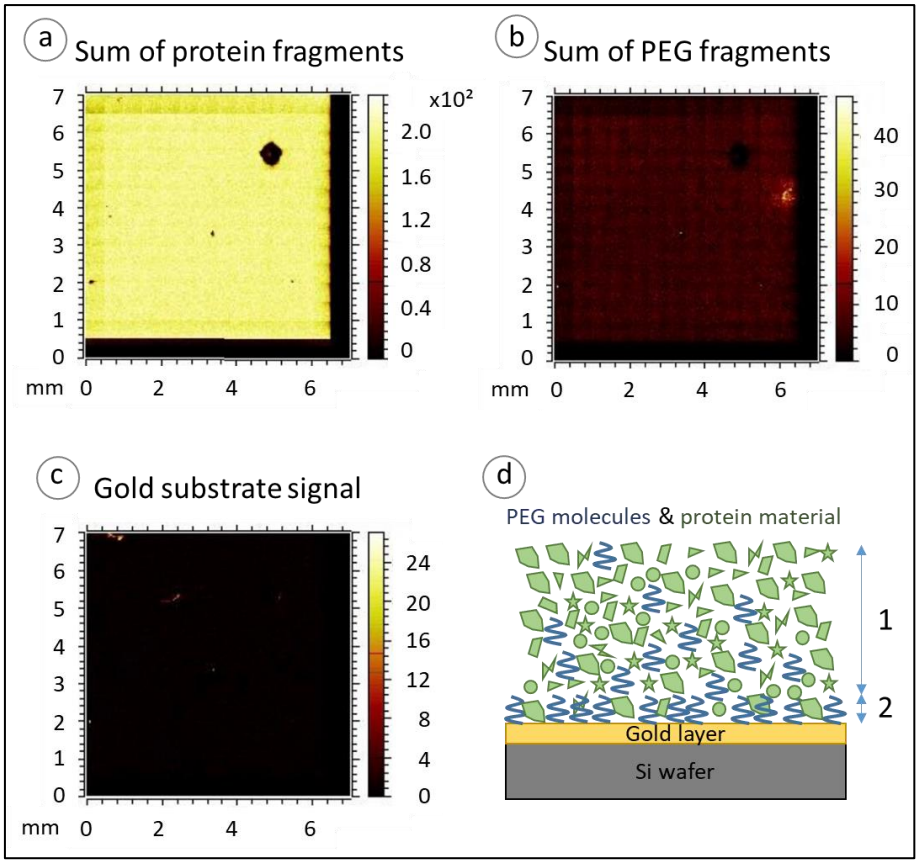


Figure 5.7. *Mosaic 2D images of the collector after transfer of bradykinin with a 10 keV Ar_{3000}^+ beam.* ***(a)*** *Summed intensities of three characteristic fragments of proteins (CH_4N^+, $C_4H_8N^+$ and $C_8H_{10}N^+$, respectively at m/z = 30, 70 and 120).* ***(b)*** *Summed intensities of two characteristic fragment of PEG (CH_3O^+ and $C_2H_5O^+$, respectively at m/z = 31 and 45).* ***(c)*** *Summed intensities of Au^+ and Au_3^+, respectively at m/z = 197 and 591.* ***(d)*** *Schematic illustration of what the layer assembly may look like, from the results obtained by surface imaging and depth profiling. Zone 1 is composed of protein material and unbound PEG molecules, while zone 2 corresponds to the PEG self-assembled monolayer.*

ToF-SIMS. Large 2D maps were acquired to control the transfer. **Figure 5.7** displays the maps of the ion intensity of characteristic peaks of the peptide, the PEG, and the gold, respectively. The map of the characteristic fragments accounting for peptide material displays a relatively high intensity, while the maps representing the PEG and gold layers barely show any signal intensity. These results confirms that peptides were efficiently transferred and cover the entire collector. To gain insights into the depth distribution of all these species, SIMS depth profiles were performed. A typical profile representative of all those obtained on similar samples is presented in **Figure 5.8**. This profile displays very interesting piece of information regarding the thin film

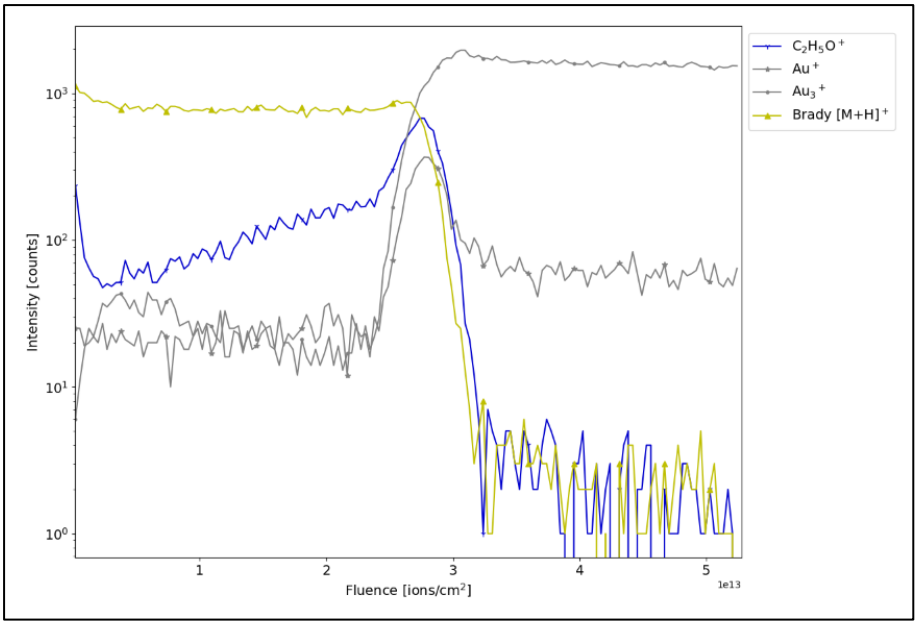


***Figure 5.8**. SIMS depth profile through a sample constructed by the transfer of bradykinin on a PEG coated collector. The peptide signal is colored in yellow, the PEG signal is colored in blue, and the gold substrate signal is colored in grey.*

organization. As expected from the 2D images, the signal accounting for the peptide (yellow signal) is initially more intense than that accounting for the PEG (blue signal). Yet, the latter is observed at a higher intensity than expected. If the bradykinin layer was made of peptidic material only, the signal accounting for the PEG should have been close to noise, until reaching a sharp interface when the entire peptide layer was sputtered and the PEG layer was reached. Surprisingly, the PEG intensity steadily rises until a steep increase is observed very close to the gold interface. A hypothesis to explain this organization would be that a mixing is observed between the peptides and the unbound PEG molecules that were physisorbed at the surface. The diffusion of the PEG into the bradykinin deposited on top would explain the gradient observed in the PEG intensity. The sudden increase of the PEG intensity would then correspond to the place of the profile where the PEG monolayer was reached. The fact that the PEG layer is very thin compared to that of peptide is in line with their estimated layer thickness. Using the thickness calibration presented in **Chapter 4 (Figure 4.13)**, and given the present transfer parameters, the peptide layer should be about 18 nm thick. The PEG layer, on its side, was approximated to 2.5-3.0 nm by Delcroix. Even though this presumed sample organization fits quite well the different expected layer thicknesses, and the diffusion of the unbounded PEG is

plausible, several comments can be made, mostly regarding the PEG layer. First, the sudden rise of the PEG signal intensity near the gold interface could in part be due to a matrix effect (increase of the ionization yield due to the presence of the metallic substrate). Second, the homogeneity of the PEG layer was not controlled or measured. This could be performed by SIMS imaging for example. Third, it must be noted that the initial decrease of the PEG intensity could not be explained, it could arise from surface contamination. Based on this analysis, a schematic illustration of what the layer may look like is proposed in **Figure 5.7d**.

To study whether the presence of the PEG layer could efficiently promote the desorption of the peptides upon contact with aqueous solution, the same sample was exposed to water. Two drops of 100 µL of water were

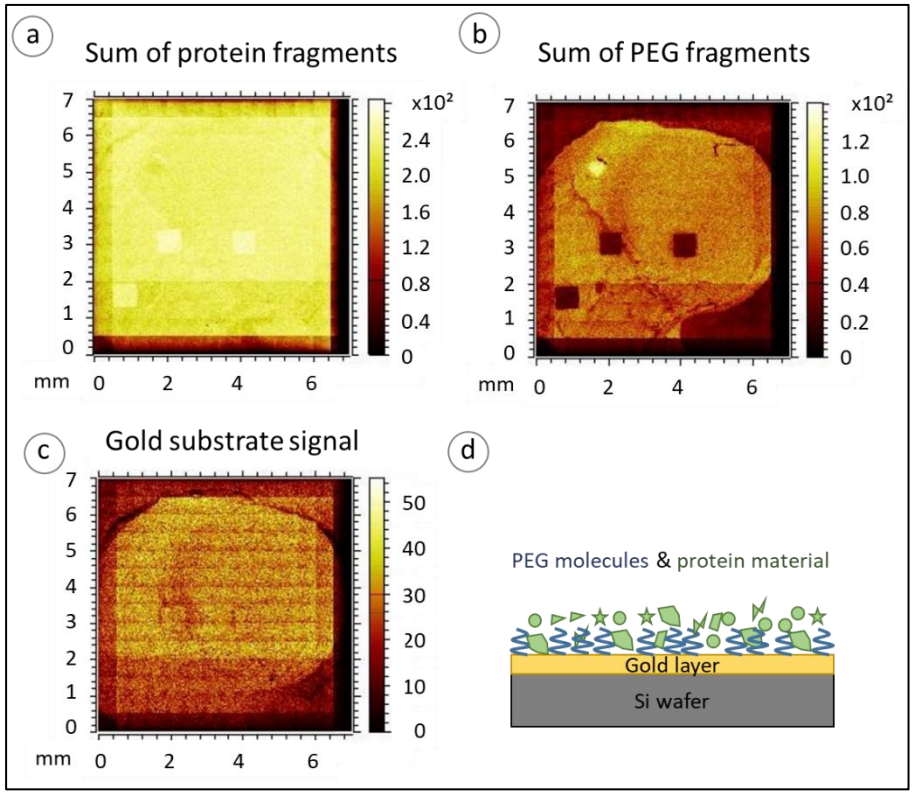


***Figure 5.9**. Mosaic 2D images of the collector after that the sample was covered with water to recover the transferred material. **(a)** Summed intensities of three characteristic fragments of proteins (CH_4N^+, $C_4H_8N^+$ and $C_8H_{10}N^+$, respectively at m/z = 30, 70 and 120). **(b)** Summed intensities of two characteristic fragment of PEG (CH_3O^+ and $C_2H_5O^+$, respectively at m/z = 31 and 45). **(c)** Summed intensities of Au^+ and Au_3^+, respectively at m/z = 197 and 591. **(c)** Schematic illustration of what the remaining layer may look like, from the results obtained by surface imaging and depth profiling.*

successively deposited on the surface, and then recovered using a micropipette. The sample was then dried under N_2 flux, and analyzed by SIMS again. It was expected that a vast majority of the peptides would have been released, leaving at the surface a layer of PEG on top of gold. 2D images of the collector were acquired in the same way as before, and presented in **Figure 5.9**. At first sight, the image displaying the ion intensities of the protein fragments may look as bright as before desorption in water. However, the image of the characteristic peaks of the polymer shows a significant intensity increase, which is only possible if the remaining peptide layer is very thin. This tends to demonstrate that a large fraction of the peptide layer was removed upon contact with water. The rise of the intensity of the gold signal is showing that the remaining organic layer is very thin. To gain better insights about the thickness of each remaining layer, depth profiles were carried out. However, the thicknesses of both the remaining peptide layer and the PEG layer were too thin to be efficiently depth-profiled by SIMS. From these results, it can be concluded that after being immersed in water, a very thin residual peptide layer is left at the surface of the PEG self-assembled monolayer (illustrated in **Figure 5.9d**), indicating the desorption of a vast majority of the peptides. More experimental work including quantification of the protein quantity recovered in solution is still required to draw quantitative results and conclusions.

5.3.4. Trehalose sacrificial layer on Si wafer

Always with the idea of reaching an easier desorption, or to further develop delivery application, where a sudden release of the protein molecules could be useful, another strategy was devised. This one relies on the construction of a protein layer on top of a sacrificial layer, i.e. a layer that would completely dissolve once the sample is immersed in water, hence simultaneously releasing all proteins, as illustrated in **Figure 5.10**. The cluster-assisted deposition method being solvent-free, it is not a concern to work with water-soluble substrates for the time of the protein film construction. The proposed strategy is to build a sugar layer on top of a Si wafer, and then to transfer the protein on top of it.

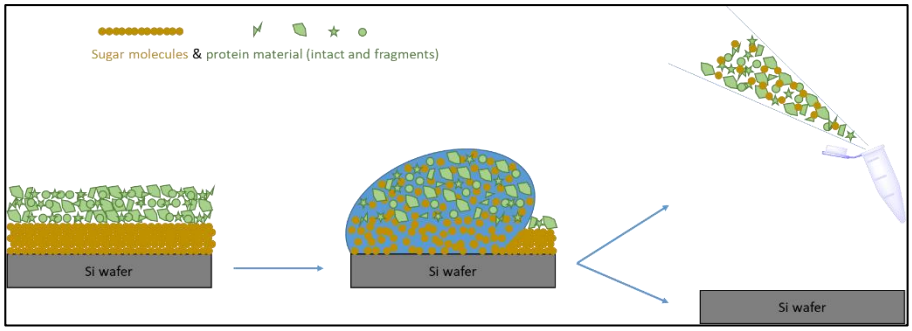


Figure 5.10. *Schematic illustration of the targeted desorption process associated to the collectors coated with a sugar sacrificial layer. In an ideal scenario, the transferred proteins accumulate on top of the sugar layer. As water is added on the collector, the sugar layer is dissolved, taking with it the transferred material into solution. In this case, the transferred material can be recovered for further analyses, while the collector can be recycled.*

Two sugars, fructose and trehalose, were initially investigated. These two sugars were chosen, as they were previously used for ToF-SIMS analysis of proteins (trehalose),[11,12] or to prepare liquid surfaces to improve the efficiency of soft-landing (fructose, combined with glycerol in that case).[13] Here again, the main short term objective was to demonstrate that the proteins were efficiently desorbed from the surface when performing BCA assays on the solutions that were recovered from the samples. In the analyzed solution, the sugar that was used to create the sacrificial layer would thus inevitably be mixed with the protein. Therefore, the first step was to make sure that the sugar does not interfere with the BCA assay. To verify this crucial point, two control calibration lines were performed on lysozyme, with addition of either one of the two sugars in the protein solutions, and compared to that obtained on pure lysozyme solutions. The results, presented in **Figure 5.11**, are striking. If the calibration line performed with trehalose looks perfectly normal, displaying no interaction of the sugar with the BCA assay, the one performed with

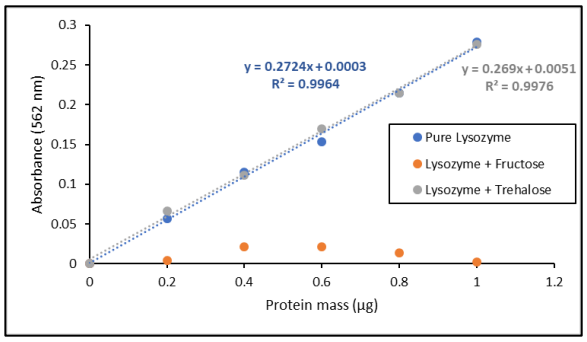


Figure 5.11 Results of a BCA assay performed on lysozyme in a 96-wells plate (in solution). Three calibration lines with identical protein quantities were prepared. The first one (blue) served as a reference. In the second one (orange), fructose was added to each sample. In the third one (grey), trehalose was added to each sample.

fructose is completely saturated, reminiscent of those obtained when performing the BCA assay on Si wafers or aluminum. In **Figure 5.11**, the saturated signal appears as no signal, as for each sample, the absorbance of the blanc (also saturated) was subtracted. In fact, the fructose was further found to be categorized as a reducing sugar.[13] Just as Si or Al, it interferes with the first reaction of the BCA assay, by reducing the Cu^{2+} ions into Cu^{+}. Therefore, fructose could not be used for the preparation of the sacrificial layer, and trehalose was chosen instead. The next step was to find the most appropriate way to prepare the sugar layer. In the first place, the spin-coating technique was envisaged. Yet, it only yielded sugar layers that were relatively thin (few tens of nm). At this point, it was already known that when proteins were transferred on a soft substrate, it could induce mixing, due to diffusion. To avoid too much interaction of the proteins with the Si wafer, thicker layers were preferred. Drop casting was not an optimal alternative either as it resulted in very inhomogeneous layers, making the thickness difficult to control, and so preventing the preparation of reproducible samples.

In the lab, a homemade instrument to perform vapor deposition (sublimation) was designed and built by colleagues. It was initially used for the vapor-deposition of MALDI-matrices onto samples, to perform matrix-enhanced SIMS, but could very well be used for the vapor deposition of other compounds, such as sugars. The instrument, schematically depicted in **Figure 5.12**,[14] works under vacuum conditions, and is composed, roughly, of a crucible linked to a heating device, a sample holder with a cooling system, pumping units, and a vacuum gauge. It works as follows: the compound to

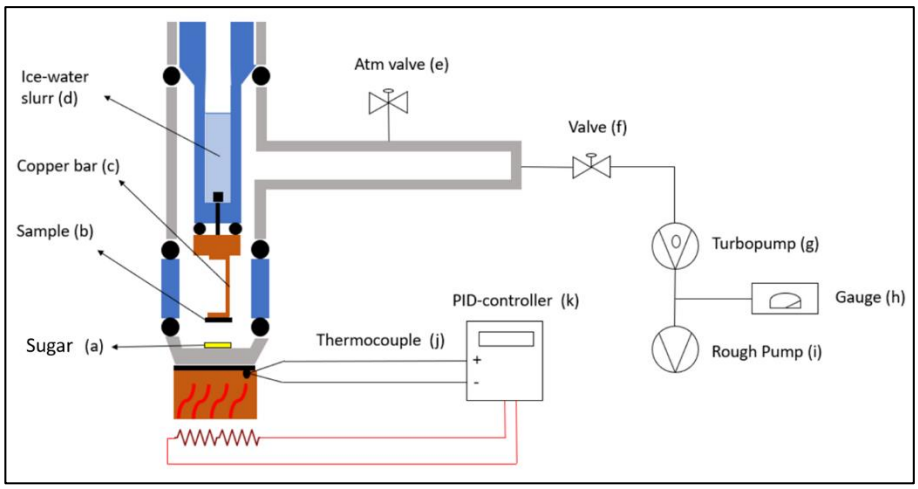


Figure 5.12. *Schematic representation of the homemade sublimation instrument.*

be vapor-deposited is placed in the crucible, and the latter is heated. A few centimeters higher, the metallic sample is fixed to a conductive cupper rod. The rod, and so the sample, are cooled using iced water. As the compound sublimates from the crucible, it reaches the cool sample where it condenses. Provided that a calibration line is prepared (deposited thickness vs time of vapor deposition, at a given temperature), this technique delivers samples of relatively good homogeneity and of controlled thickness.

The sublimation temperature varies from one compound to another. In the case of trehalose, a few trials were performed at various temperature to find out the most suitable one. Vapor deposition attempts were started at 120°C, then with 20°C step increases until thick (> few hundreds nm) film thickness could be formed on the Si wafers. In the end, a sublimation of 2 h at 180°C proved to yield thick sugar layers, with good homogeneity (checked by sight). The thickness and the roughness of the sugar films could however not be measured precisely (at least using straightforward protocols and easily available instruments). For example, the sugar layer turned out to be so soft that the tip of the profilometer went through it, directly reaching the underlying hard Si substrate. The roughness was only defined as acceptable by sight, while the thickness could be estimated to several µm, relying on the sputtering ion dose required to reach the Si interface when performing SIMS profiles. As these were seminal experiments, the samples were used as they were. The next step involved the transfer of a peptide, bradykinin in this case, on top of the sugar layer. Using 10 keV Ar_{3000}^{+}, bradykinin was transferred for 6 h, so that a relatively thick layer of peptide should have been deposited. After transfer, samples were analyzed by SIMS. First, large 2D images were acquired, to make sure that the transfer was successful. **Figure 5.13** displays chemical images of the collector after transfer of the peptides. As can be observed, the peptide layer completely covers the trehalose layer, whose intensity is nearly zero throughout the whole collector. Depth profiles were then carried out on the sample to gain insights into the depth organization of the layers.

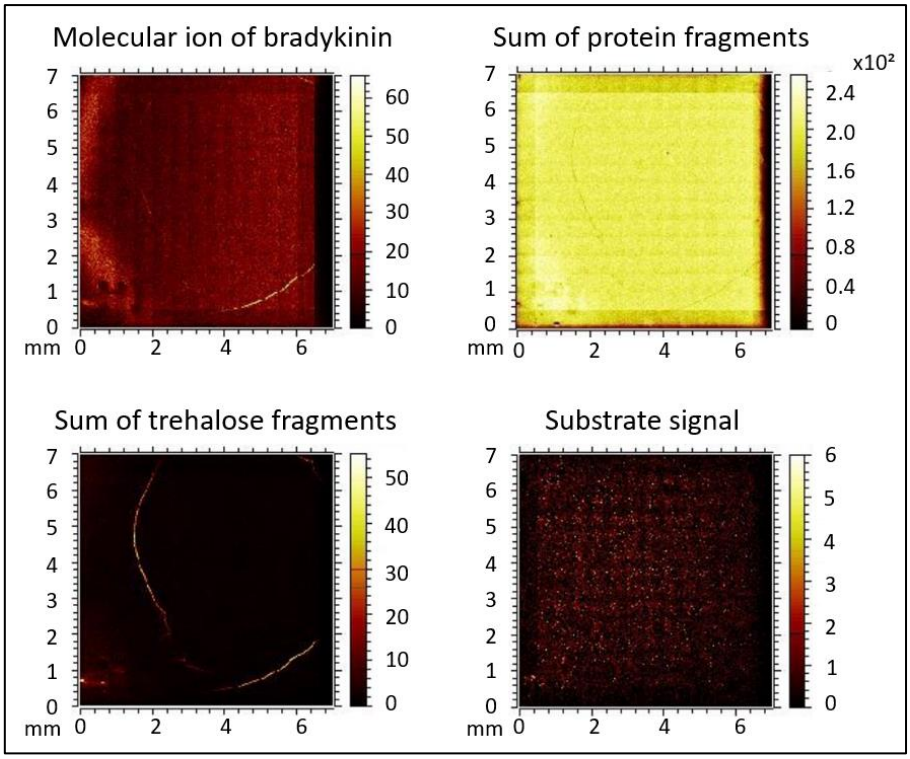


Figure 5.13. *Mosaic 2D images of the collector after transfer of bradykinin with a 10 keV Ar_{3000}^{+} beam.* ***Top left****: intensity of the molecular ion of bradykinin.* ***Top right****: summed intensities of three characteristic fragments of proteins (CH_4N^+, $C_4H_8N^+$ and $C_8H_{10}N^+$, respectively at m/z = 30, 70 and 120).* ***Bottom left****: summed intensities of two characteristic fragments of trehalose ($C_6H_{11}O_5^+$ and $C_{12}H_{21}O_{10}^+$, respectively at m/z = 163 and 325).* ***Bottom right****: intensity of Si+, respectively at m/z = 28.*

The depth profiles revealed a very interesting piece of information regarding the stability of the layers. Two examples of such profiles are given in **Figures 5.14 & 5.15**. The first profile (**Fig. 5.14**) was achieved with a high sputter beam intensity, in order to reach the interface of the Si wafer. The important ion dose (>1x10^{16} ions/cm²) required to erode the whole sugar layer illustrates the large thickness of the sugar layer that was deposited by sublimation within only two hours. Due to this large thickness, charging of the sample was observed during the analysis, inducing large variations in the total secondary ion yield. To allow a smoother reading of the profiles, all the peak intensities were normalized to the total ion yield. In a second profile (**Fig. 5.15**), the intensity of the sputter beam was lowered, in order to obtain a more precise depth profile of the first tens of nm, where the interface between the peptide and the sugar layers seemed to be observed. The second profile was not carried out until the Si wafer was reached, as that

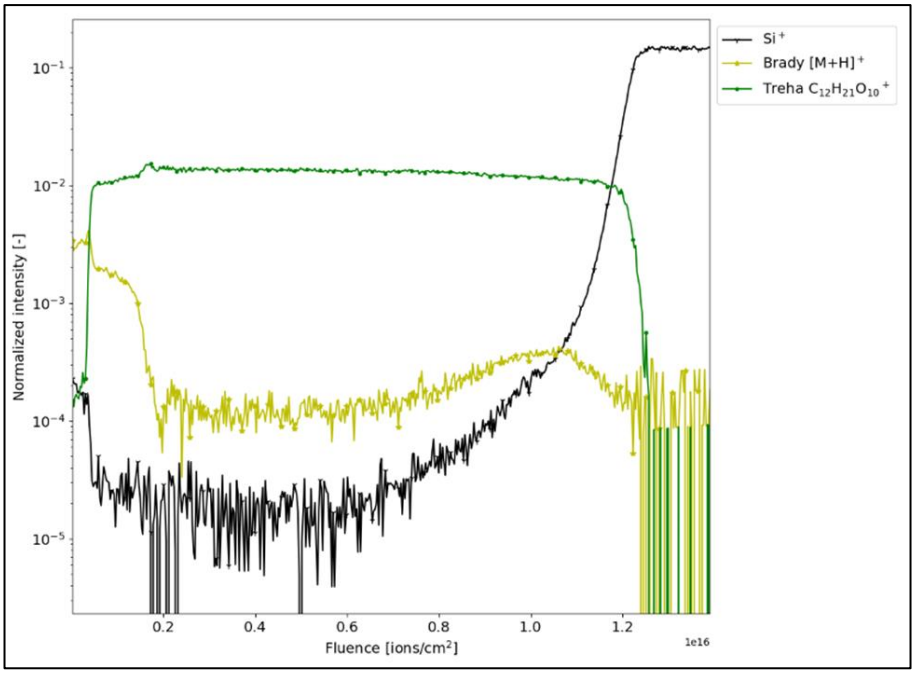


***Figure 5.14**. SIMS depth profile through a sample prepared by transferring bradykinin on top of a sugar layer. The profile was carried out until the Si substrate was reached. The peptide signal is colored in yellow, the trehalose signal is colored in green, and the Si substrate signal is colored is black.*

would have been too time-consuming, for no additional information. The peptide/sugar interface, more visible in the second profile, had a quite surprising behavior. In the beginning, and as expected, the peptide signal (yellow signal) is much higher than that of the sugar (green signal). Then, a sudden fall of the peptide intensity is observed, while the sugar intensity rises. This is believed to be the point where all the peptide layer has been sputtered and the sugar layer was reached. However, as the profiling continued, the peptide signal intensity did not immediately fall into noise, but rather followed a steady decrease, until a steep fall was observed. The steady decrease may arise from mixing between the peptide and the sugar molecules, induced by diffusion. Furthermore, as the peptide molecules land on the surface, the energy deposited in the topmost layers induces transient increases of the temperature and the pressure in that precise area, favoring the mixing with the sugar layer. The steep fall however is yet to be explained. If the diffusion was the only cause to the steady decrease of the peptide signal through the sugar layer, the same trend should have been observed until the signal fell into noise. The sudden change in the slope of the peptide signal probably arose from another effect.

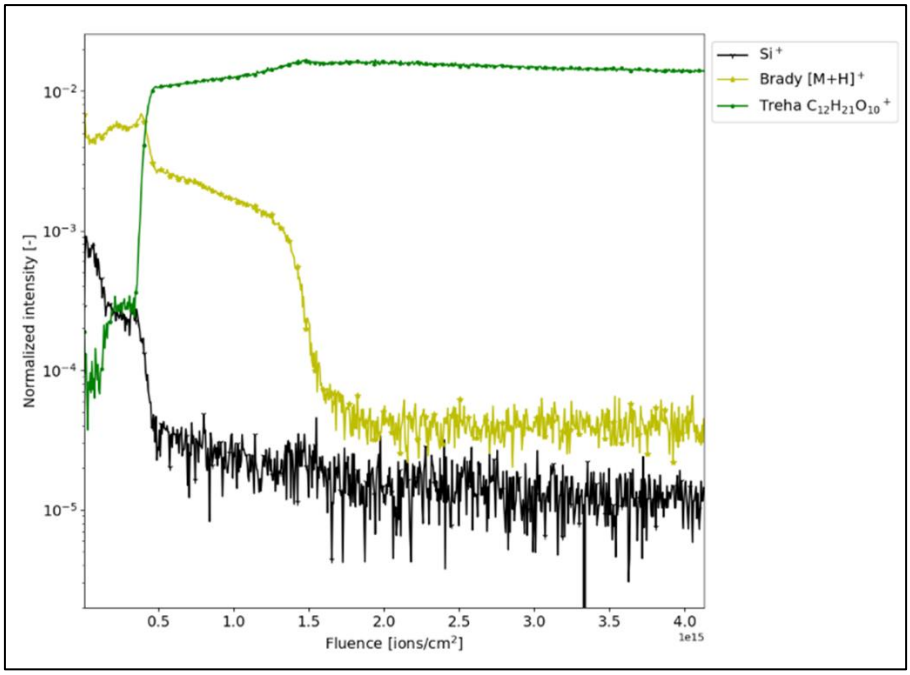


***Figure 5.15**. SIMS depth profile through a sample prepared by transferring bradykinin on top of a sugar layer. The profile was only conducted on a relatively small depth scale in order to have a better resolution around the first interface (peptide/sugar). The peptide signal is colored in yellow, the trehalose signal is colored in green, and the Si substrate signal is colored is black.*

This observation remained without explanation for some time. A hypothesis to explain this behavior of the sample resulted from a random observation. A similar sample to that presented in the profiles was prepared, and then left in ambient conditions for a few days. Interestingly, after only a few hours, the sample turned out to be completely altered. In fact, it had adsorbed water from the environment, and under the capillary forces, the homogeneous layer had started to form patches at the surface of the wafer. As the samples were exposed to air for a few hours between the vapor deposition of the sugar layer and the transfer of the peptides, then again exposed to air before the SIMS analysis, it is believed that the sample already started to increase significantly its water content, therefore largely favoring the mixing of the peptides with the trehalose. This could be part of the explanation why sudden changes in the peptide decrease through the sugar layer was observed. This issue is not necessarily a barrier to the use of sugar as sacrificial layer, but should be kept in mind further targeting specific applications.

Before going further with the desorption of the layer, a general remark can be made with respect to the profiles presented above. The Si signal intensity seems to begin at a level clearly above noise, and then rapidly drops into noise until it rises again once the Si wafer is reached. Surprising at first glance, this can be easily explained by the fact the transfer ion dose used for the transfer of bradykinin was very high. It is very likely that towards the end of the transfer, the target was depleted in peptides and the Si substrate was reached. Even though the sputtering yield of metals by large argon clusters is known to be low, a small amount of Si can still be transferred from the target onto the collector. It should be noted that no PDMS was observed in the mass spectra.

This being said, the fact that mixing is observed should not prevent the pursuit of the main objective, which is to study whether the presence of the sacrificial layer allows complete and rapid desorption of all transferred peptides. For this purpose, the same sample as that investigated above was used. A 100 µL drop of water was deposited at the surface of the collector, left for a few tens of seconds, and then recovered using a micropipette. The same operation was repeated once more to maximize the amount of material recovered from the sample. The sample was then dried under gentle N_2 flux, before it was analyzed by SIMS again. The same large 2D chemical images as previously were recorded (**Figure 5.16**). On the image displaying the molecular ion of bradykinin, it can be observed that in comparison with the image achieved just after transfer, the intensity dropped to almost zero across the entire collector. The same result is obtained for the signal intensity of the characteristic peaks of trehalose, with the exception of the bottom-right corner. This is probably resulting from the drying step, upon which the sugar remaining at the surface concentrated in the small volume of water that could not be recovered, and which evaporated as is was pushed away from the collector by the N_2 flux. Regarding the image of the characteristic fragments of proteins, if a small decrease of the intensity is observed, the entire surface is still covered with them. However, if analyzed in combination with the image of the underlying Si substrate, it can be concluded that the fragments layer does not exceed a few nm, as the Si^+ is detected. To make sure that the quantity left at the surface did not exceed that of roughly one monolayer, a few profiles were recorded across the collector. A

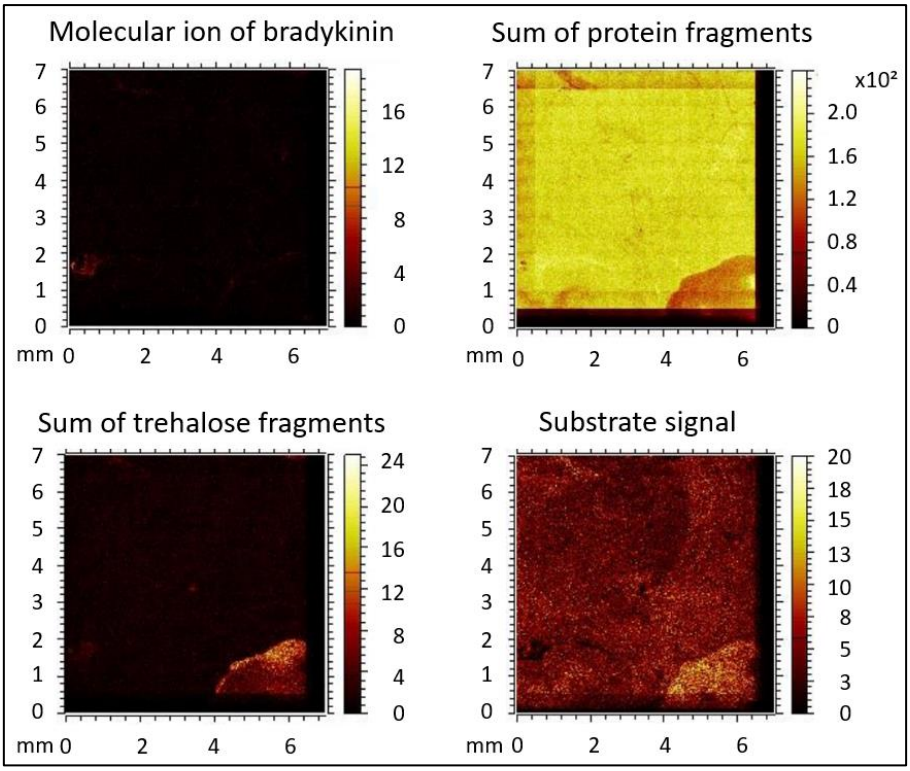


***Figure 5.16**. Mosaic 2D images of the collector after it was exposed to water to recover the transferred material. **Top left**: intensity of the molecular ion of bradykinin. **Top right**: summed intensities of three characteristic fragments of proteins (CH_4N^+, $C_4H_8N^+$ and $C_8H_{10}N^+$, respectively at m/z = 30, 70 and 120). **Bottom left**: summed intensities of two characteristic fragments of trehalose ($C_6H_{11}O_5^+$ and $C_{12}H_{21}O_{10}^+$, respectively at m/z = 163 and 325). **Bottom right**: intensity of Si+, respectively at m/z = 28.*

representative example of these profiles is shown in **Figure 5.17**. It can be observed that from the beginning of the profile, the Si^+ signal accounting for the wafer (ion intensity profile in black in **Fig.5.17**) is increasing, while the intensity of all other species decreases to rapidly fall into noise. This highlights the fact that the remaining layer is ultra thin (<5 nm). In addition, these profiles, where the interface between the organic layer and the substrate is not clearly visible, are typical of layers too thin to be properly resolved by SIMS profiling. These results, though relatively exploratory, tend to show that most of what was at the surface of the collector was desorbed by only 200 µL of water, which is quite promising. Upon mixing in solution, it is likely that protein material is forming a monolayer at the surface of the collector, by spontaneous adsorption. The layer is probably made of intact bradykinin as well as fragments. However, the intact molecular ion is hardly

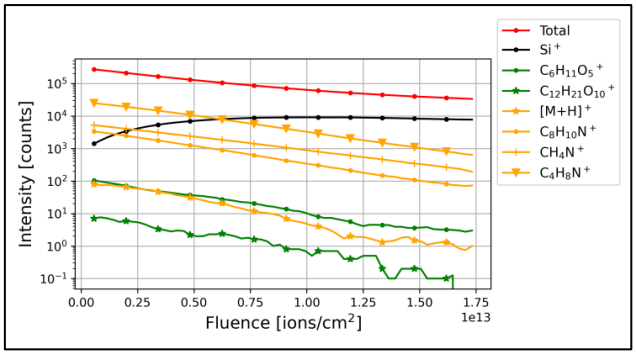


***Figure 5.17**. SIMS depth profile through the sample after it had been covered with water to recover the transferred material. The protein signal (molecular ion and fragments) is colored in yellow, the trehalose signal is colored in green, and the Si substrate signal is colored is black.*

detected at the surface on the large 2D image, most likely due to the presence of a very small quantity. Typical SIMS effects such as a favored fragmentation when analyzing ultra-thin organic films on a hard substrate may also explain why fragments are more detected than the molecular ion.

Due to time constraints, and because of the concerns regarding a few technical issues (for example the rehydration of the sugar layer after the sublimation step for the sacrificial layer strategy, or the construction of the PEG layer for the protein-repellent layer strategy), these two approaches were temporarily left aside in favor of alternatives that were more promising on a short-term basis. They should however not be completely forgotten, as a few optimization steps could lead to very interesting results.

In line with the transfer on a sacrificial layer, the last section of this chapter will focus on the demonstration that the proposed transfer method allows the construction of protein thin films on substrates that are not compatible with solution-based techniques.

5.3.5. Transfer on paper

The most widespread method for biomolecules immobilization, i.e. spontaneous adsorption in solution, faces difficulties or completely fails if the targeted substrate is altered by the solution or is soluble in it.

To illustrate the versatility of the method in terms of substrate nature, a peptide (bradykinin) layer was constructed on top of a sheet of paper, which is hardly compatible with solution-based methods (swelling, etc.). The resulting sample is then compared with that obtained by drop casting a peptide aqueous solution directly on the paper substrate, to mimic aqueous adsorption (not an option, as paper would suffer structural deformation, making further ToF-SIMS analysis impossible). The transferred sample was prepared with a 10 keV Ar_{3000}^+ beam, while the drop-casted sample was prepared by evaporating a 10 µL drop of a 20 mg/mL solution. Both samples were analyzed by ToF-SIMS, using the 3D depth-profiling mode. **Figure 5.18** shows the comparison of the depth profiles obtained for each sample. The paper is identified in the spectra by the presence of the hexosan peak $[C_6H_9O_4]^+$, a characteristic fragment of cellulose, while bradykinin is identified by its molecular ion peak. When the peptide is transferred (**Fig. 5.18a**), the paper substrate (orange signal) is covered by a layer of bradykinin (green).

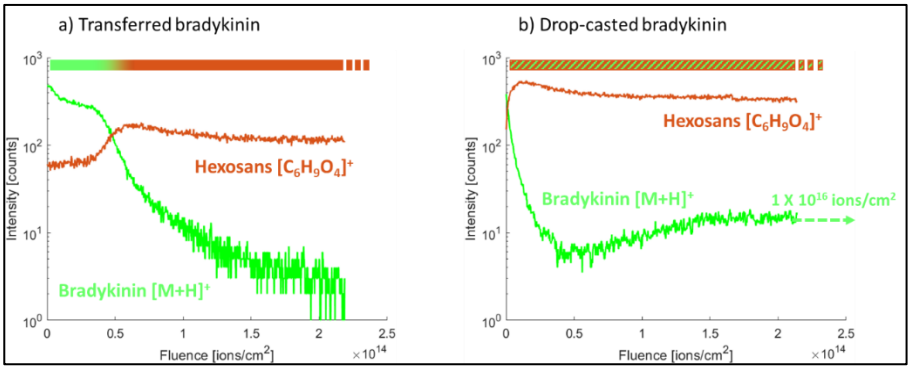


*Figure 5.18. ToF-SIMS depth profiles recorded on the collectors after deposition of bradykinin on paper by **a)** transfer or by **b)** drop-cast.*

After a certain fluence, the bradykinin signal drops drastically until reaching the noise level. At the same time, the paper signal increases and becomes constant at a high intensity. This shows that the transfer method allowed the construction of a peptide layer strictly on top of the paper, without diffusion into the cellulose fibers network. In contrast, when the peptide is drop-casted from water (**Fig. 5.18b**), the signal of bradykinin (green) instantly decreases, and then levels off at a substantial intensity. It remains constant up to a sputtering dose of 1 x 10^{16} ions/cm^2. The paper signal (orange) remains roughly constant throughout the entire profile. If the initial drop of the bradykinin signal may suggest a partial accumulation of the peptide at the surface, the continuous detection of bradykinin across the paper

indicates that the peptide molecules diffused between the cellulose fiber of the network or directly in swollen fibers. Chemical images acquired at the surface and inside the paper for both samples can be found in **Figure 5.19**. In addition, the deposition of a drop on the paper causes mechanical deformation of the paper and generates huge roughness. The transfer method allows the deposition of peptides/protein thin films on substrates that could not be considered when working in aqueous solution. This demonstration using paper paves the way for many other original systems that could previously not be envisioned, such as soluble substrates, or more complex designs for further release applications.

5.4. Conclusion

In this chapter, the transfer of peptides and proteins on a series of different substrates was investigated. In the first place, various strategies were proposed and studied in order to find suitable conditions to perform quantification of the transferred protein quantities. From that perspective, the transfer on soft polyethylene, and its combination with BCA assay carried out in Eppendorf tubes proved to be very successful. It allowed to

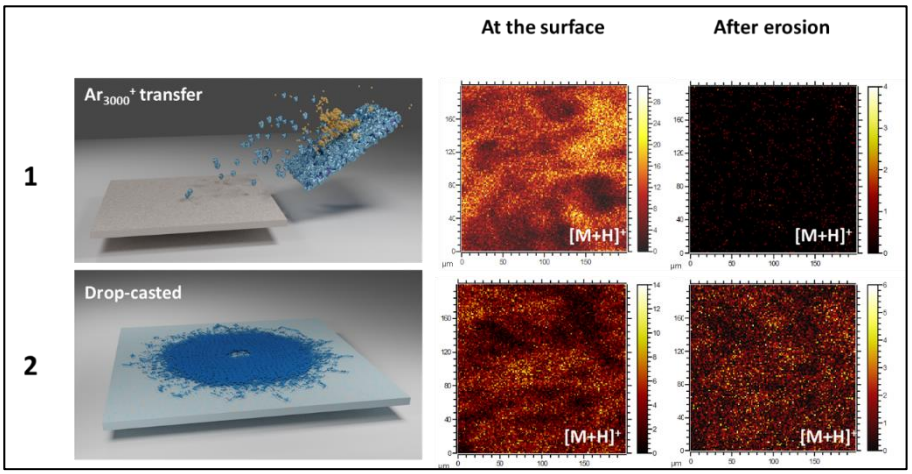


***Figure 5.19**. Comparison between bradykinin thin films deposited on paper via 1) Argon cluster transfer and 2) drop-casting method. On the left, illustration of the deposition method. On the right, ToF-SIMS chemical images of the samples, showing the bradykinin molecular ion intensity at the surface and deeper in the paper bulk after an erosion performed with a 10 keV Ar_{3000}^+ beam (ion dose density of 1 x 10^{16} ion/cm^2). On the transferred sample, bradykinin is exclusively observed at the surface of the sample, showing that the protein did not diffuse into the paper. On the contrary, on the drop-casted sample, bradykinin is observed throughout the bulk of the sheet of paper, indicating that the presence of solvent (water) favored the diffusion of the protein deep into the cellulose fiber network.*

demonstrate that the total protein mass deposited at the surface of the collectors was strictly proportional to the transfer ion dose, regardless of the protein nature or of the cluster size. It also allowed the comparison between the deposition rate of several proteins, showing a decrease in the transfer efficiency as the size of the protein increases. Finally, this strategy was used to compare the transfer efficiency of 10 keV Ar_{3000}^+ and 10 kev Ar_{5000}^+ beams. As expected, the transfer was shown to be lower as the E/n in the cluster was decreased. All these results confirmed those obtained in **Chapter 4** using the thickness measurement approach, further demonstrating that the two methods can be used, and are very complementary one to another. The thickness method allows the characterization of very small protein quantities, while the one relying on the BCA assay enables the determination of large amount of proteins. Apart from the deposition on soft PE, two other strategies devised to ease complete desorption of the transferred proteins were explored. Both relied on the preparation of functionalized collectors, specifically designed to promote release of the proteins once in contact with water. The first one implied the construction of a protein-repulsive coating, made of a protein-repellent polymer, namely poly(ethylene oxide). The second one implied the construction of a sacrificial layer, made of a water-soluble sugar, trehalose in this case. If the two strategies could not be studied as in depth as originally planned, they delivered promising preliminary results. In both cases, the analysis of the collectors by SIMS after recovering material from the surface with a small amount of water indicated that most of the transferred material was desorbed, with the exception of a monolayer. However, the work achieved in that direction mostly highlighted the many difficulties that may be encountered when aiming to transfer proteins on more complex collectors. Additional work is necessary towards the preparation of optimal systems. Finally, the flexibility of the transfer method toward substrate nature was demonstrated by deposition of a protein thin film on the surface of paper, a material hardly compatible with solution-based adsorption methods.

5.5. Bibliography

(1) Norde, W.; Haynes, C. A. Reversibility and the Mechanism of Protein Adsorption. **1995**, 26–40.

(2) Norde, W.; MacRitchie, F.; Nowicka, G.; Lyklema, J. Protein Adsorption at Solid-Liquid Interfaces: Reversibility and Conformation Aspects. *J. Colloid Interface Sci.* **1986**, *112* (2), 447–456.

(3) Delcroix, M. " Ionic Strength and PH-Dependent Conformation of

Mixed Polymer Brushes for Cycles of Protein Adsorption and Desorption, UCL-Université Catholique de Louvain, 2013.

(4) Delcroix, M. F.; Laurent, S.; Huet, G. L.; Dupont-Gillain, C. C. Protein Adsorption Can Be Reversibly Switched on and off on Mixed PEO/PAA Brushes. *Acta Biomater.* **2015**, *11* (1), 68–79.

(5) Delcroix, M. F.; Demoustier-Champagne, S.; Dupont-Gillain, C. C. Quartz Crystal Microbalance Study of Ionic Strength and PH-Dependent Polymer Conformation and Protein Adsorption/Desorption on PAA, PEO, and Mixed PEO/PAA Brushes. *Langmuir* **2014**, *30* (1), 268–277.

(6) Delcroix, M. F.; Huet, G. L.; Conard, T.; Demoustier-Champagne, S.; Du Prez, F. E.; Landoulsi, J.; Dupont-Gillain, C. C. Design of Mixed PEO/PAA Brushes with Switchable Properties toward Protein Adsorption. *Biomacromolecules* **2013**, *14* (1), 215–225.

(7) Kumar, A.; Biebuyck, H. A.; Whitesides, G. M. Patterning Self-Assembled Monolayers: Applications in Materials Science. *Langmuir* **1994**, *10* (5), 1498–1511.

(8) Love, J. C.; Estroff, L. A.; Kriebel, J. K.; Nuzzo, R. G.; Whitesides, G. M. Self-Assembled Monolayers of Thiolates on Metals as a Form of Nanotechnology. *Chem. Rev.* **2005**, *105* (4), 1103–1169.

(9) Boisselier, E.; Astruc, D. Gold Nanoparticles in Nanomedicine: Preparations, Imaging, Diagnostics, Therapies and Toxicity. *Chem. Soc. Rev.* **2009**, *38* (6), 1759–1782.

(10) Häkkinen, H. The Gold–Sulfur Interface at the Nanoscale. *Nat. Chem. 2012 46* **2012**, *4* (6), 443–455.

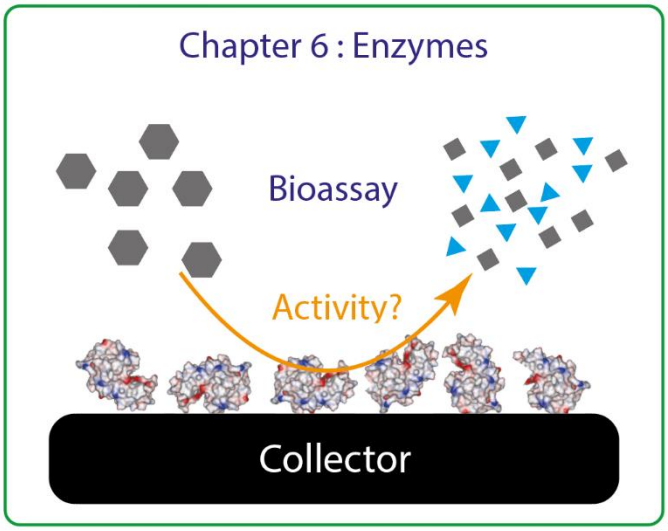
(11) Xia, N.; Castner, D. G. Preserving the Structure of Adsorbed Protein Films for Time-of-Flight Secondary Ion Mass Spectrometry Analysis. *J. Biomed. Mater. Res. Part A* **2003**, *67A* (1), 179–190.

(12) Xia, N.; May, C. J.; McArthur, S. L.; Castner, D. G. Time-of-Flight Secondary Ion Mass Spectrometry Analysis of Conformational Changes in Adsorbed Protein Films. *Langmuir* **2002**, *18* (10), 4090–4097.

(13) Gologan, B.; Takáts, Z.; Alvarez, J.; Wiseman, J. M.; Talaty, N.; Ouyang, Z.; Cooks, R. G. Ion Soft-Landing into Liquids: Protein Identification, Separation, and Purification with Retention of Biological Activity. *J. Am. Soc. Mass Spectrom. 2004 1512* **2004**, *15* (12), 1874–1884.

(14) Tomasetti, B. MALDI matrix sublimation for sensitivity enhancement in molecular SIMS | Mémoire UCL

Chapter 6 : Transfer of enzymes



In this chapter, the transfer of enzymes will be investigated. Of main interest is the question whether the transferred proteins retain their 3D structure upon transfer. In the first instance, strategies to detect the molecular ion of proteins over 10 kDa by ToF-SIMS were explored. The first devised strategy was to promote ionization via salt addition to the samples, in order to favor the formation of salt adducts. The second way envisioned to improve detection was by tuning post-acceleration at the detector. In addition to ToF-SIMS, other mass spectrometry techniques were used to analyze the material deposited on the collectors, namely MALDI-MS and ESI-MS. Along these mass spectrometry techniques, SDS-PAGE electrophoresis turned out to be a very successful alternative toward detection of large proteins at the surface of the collectors. It indicated that both lysozyme and trypsin could be transferred intact. In addition, enzymatic activity assays demonstrated the preservation of the biological function of transferred lysozyme, which is related to the conservation of its three-dimensional structure.

A paper closely related to this chapter is published: **V. Delmez, H. Degand, C. Poleunis, K. Moshkunov, M. Chundak, C. Dupont-Gillain*, and A. Delcorte*. The Journal of Physical Chemistry Letters 2021 12 (2), 952-957**

6.1. Introduction

In the two previous chapters, peptides and small proteins were used as model biomolecules to demonstrate the ability of large argon cluster ion beams to be used as a tool for the controlled construction of protein thin films. If larger proteins were transferred to compare the deposition rate, no information could yet be obtained regarding their integrity at the surface of the collectors. However, to expand the scope of applications of this approach, it must be demonstrated that larger proteins can be transferred intact as well. For this purpose, enzymes represent a category of interest. On the one hand, enzymes perform an enormous variety of functions that could prove useful for a series of targeted applications. On the other hand, they will allow investigating the impact of the transfer on the 3D structure of the proteins, by assessing their bioactivity at the surface of the collectors. Enzymes, even the smallest ones, are seen as large molecules at the ToF-SIMS scale, and their molecular ions are usually out of the mass range of detectable ions. Lysozyme (around 14 kDa), the first model enzyme used in this study, stands at the limit of the molecular weights reported to be detectable by SIMS using large argon cluster ion beams. Indeed, if lysozyme itself was never reported in the SIMS literature, cytochrome C (around 12 kDa), was detected by SIMS, as reported by Mochiji et al. in 2009.[1] Here, efforts were first made to detect the molecular ion of lysozyme by SIMS. These were tested on insulin, a protein whose molecular ion is detectable by SIMS. In the meantime, alternative strategies were investigated to analyze the integrity of the deposited protein molecules, both in terms of the amino acid chain (primary structure) and in terms of 3D structure (secondary and tertiary structures). These included other mass spectrometry techniques such as MALDI-MS or ESI-MS, and different approaches such as electrophoresis. The protocols devised to probe the integrity of lysozyme at the surface of the collectors will further be used to investigate the transfer of trypsin, an even larger enzyme.

6.2. Materials and Methods

6.2.1. SDS-PAGE gel electrophoresis

Collectors cut in small pieces were incubated for 15 min in an Emmi-H40 (EMAG, Germany) ultrasonic bath at room temperature with 50 µL of reducing Laemmli buffer.[2] Electrophoresis analysis was carried out in 4-20 % iD polyacrylamide gel (Eurogentec, USA). Prestained (815-968-0747) Protein

Ladder (Thermoscientific, USA) was loaded as molecular weight markers. Protein detection was performed using a colloidal Coomassie Blue staining method.[3]

6.2.2. In-gel trypsin digestion

Coomassie Blue-stained protein bands were manually excised. Gel plugs were transferred with 200 µL of HPLC water to 0.5 mL polypropylene Protein LoBind Eppendorf tubes. Water was removed and gel plugs were incubated under shaking at 20°C for 5 min with 200 µL of a solution containing 50 mM ammonium carbonate (pH 8.0) in 50 % (v/v) acetonitrile. This solution was removed and gel plugs were incubated under shaking at 20°C for 5 min with 200 µl of 10 % (v/v) acetonitrile. Acetonitrile was removed and gel plugs were dried under vacuum with a Savant Speed Vac Concentrator. 20 µl of a digestion buffer containing 100 mM TEAB (triethylammonium bicarbonate) (pH 8.0) and 0.5 µg of trypsin (Promega, USA) were added to each tube to rehydrate gel plugs. Proteolysis was allowed to continue overnight at 37°C and stopped by adding 10 µL of 1 % (v/v) trifluoroacetic acid (TFA). Supernatants of each tube were recovered and transferred in new 0.5 mL polypropylene Protein LoBind Eppendorf tubes. 50 µL of peptide extraction solution containing 50 % (v/v) acetonitrile and 0.1 % (v/v) TFA were added to the gel plugs. After incubation for 5 min, extracts were combined with the first. A second extraction with 50 µL of 100 % (v/v) acetonitrile was done for 5 min. Extracts were combined with the first and dried under vacuum with Savant Speed Vac Concentrator.

6.2.3. Trypsin digestion on the collector

100 µl of 100 mM TEAB, pH 8.5 were added to collector pieces in 1.5 mL Eppendorf tube. Proteins were reduced by 5mM DTT (dithiothreitol) and alkylated by 15 mM iodoacetamide. Proteolysis was performed with 0.5 µg of sequencing grade trypsin (Promega, USA) and allowed to continue overnight at 37°C. Sample was dried under vacuum with Savant Speed Vac Concentrator.

6.2.4. Peptide separation using nanoUPLC

Before peptide separation, the sample was dissolved in 20 µL of 0.1 % (v/v) formic acid and 2% (v/v) acetonitrile (ACN). Peptide mixture was separated by reverse phase chromatography on a NanoACQUITY UPLC MClass system

(Waters) working with MassLynx V4.1 (Waters) software. 200 ng of digested proteins were injected on a trap C18, 100Å 5 μm, 180 μm x 20 mm column (Waters) and desalted using isocratic conditions at a flow rate of 15 μL/min using a 99% formic acid and 1% (v/v) ACN buffer for 3 min. Peptide mixture was subjected to reverse phase chromatography on a C18, 100Å 1.8 μm, 75 μm x 150 mm column (Waters) PepMap for 35 min at 35°C at flow rate of 300 nL/min using a two part linear gradient from 1% (v/v) ACN, 0.1 % formic acid to 35 % (v/v)) ACN, 0.1 % formic acid and from 35% (v/v) ACN, 0.1 % formic acid to 85 % (v/v)) ACN, 0.1 % formic acid. The column was re-equilibrated at initial conditions after washing 10 min at 85% (v/v)) ACN, 0.1 % formic acid at a flow rate of 300 nL/min. For online LC-MS analysis, the nanoUPLC was coupled to the mass spectrometer through a nano-electrospray ionization (nanoESI) source emitter.

6.2.5. LC-IMS (Ion Mobility Separation)-ESI-QTOF-MS Analysis (HDMS^E)

IMS-HDMS^E (Ion Mobility Separation-High Definition Enhanced Mass Spectrometry) analysis were performed on an SYNAPT G2-Si high definition mass spectrometer (Waters) equipped with a NanoLockSpray dual electrospray ion source (Waters). Precut fused silica PicoTip^R Emitters for nanoelectrospray, outer diameter: 360 μm; inner diameter: 20 μm; 10 μm tip; 2.5" length (Waters) were used for samples and Precut fused silica TicoTip^R Emitters for nanoelectrospray, outer diameters : 360 μm; inner diameter: 20 μm; 2.5" length (Waters) were used for the lock mass solution. The eluent was sprayed at a spray voltage of 2.4 kV with a sampling cone voltage of 25 V and a source offset of 30 V. The source temperature was set to 80°C. HDMS^E method in resolution mode was used to collect data from 15 min after injection to 106 min. With this method, MS^E spectra were acquired in positive and resolution mode over the m/z range from 50 to 2000 with a scan time of 1 s with a collision energy ramp starting from ion mobility bin 20 (20 eV) to 110 (45 eV). The collision energy in the transfer cell for low-energy MS mode was set to 4 eV. For the post-acquisition lock mass correction of the data in the MS method, the doubly charged monoisotopic ion of [Glu^1]-fibrinopeptide B was used at 100 fmol/μl using the reference sprayer of the nanoESI source with a frequency of 30 s at 0.5 μl/min into the mass spectrometer.

6.2.6. ESI-QTOF data processing

$HDMS^E$ data were processed with Progenesis QI (Nonlinear DYNAMICS, Waters) software using a local database containing the lysozyme sequence. Carbamidomethylation as the fixed cysteine modification, oxidation as the variable methionine modification, trypsin as the digestion enzyme were selected and one miss cleavage allowed.

6.2.7. Activity assay protocol adapted to be performed on Si wafers

In this case, the samples/collectors consist in 1.4 x 1.4 cm^2 Si wafer, bearing dried proteins. Lysozyme was deposited either by transfer (probed samples) or by evaporation of drops of fresh lysozyme solution of known concentration (calibration line samples). The activity of the deposited lysozyme was assessed directly on the surface using a fluorescent assay. A silicone o-ring was placed on the collector to create a well on the Si wafer, and was filled with 180 µL of acetate buffer (10mM) at pH 5 and ionic strength adjusted to 10 mM with NaCl. Then, 20 µL of 4-methylumbelliferyl β-D-N,N',N''-triacetylchitotrioside (0.1 gL^{-1}) in dimethyl sulfoxide /water 2:1 (v:v) solution were added as lysozyme substrate in each sample. The wells were finally sealed with a PET cap to avoid evaporation. The samples were then kept at 40°C for 24h. 180µL of reactional media were then transferred to a black 96-well plate and mixed with 50 µL of 50 mM glycine buffer at pH 10.6 (adjusted with NaOH) to stop the reaction. Finally, fluorescence was measured with excitation and emission wavelengths respectively set at 360 nm and 450 nm. Data points of the calibration lines were always acquired in triplicate.

6.3. Results and discussion

6.3.1. Lysozyme

Lysozyme is a readily available enzyme, which was used as a model for many studies reported in the literature. According to Norde's concepts (see **Chapter 1, section 1.3.1**), lysozyme is a hard protein, meaning that is has a low propensity to unfold and denature upon adsorption.[4] It is a globular protein (a small sphere) with strong intramolecular interactions. These attributes should favor the desorption of intact molecules versus fragmented ones, as well as a retention of the native 3D structure of the protein molecules.

6.3.1.1. Efforts to detect lysozyme by SIMS

As was discussed in the **introduction section** (**Chapter 1**), large molecules (> 10 kDa), including proteins, are difficult, if not impossible to detect by ToF-SIMS analysis. This is most probably due to a combination of effects. First, the desorption efficiency is much reduced for larger molecules. If this was already mentioned in the literature,[5] it was further demonstrated in **Chapter 4 & 5**, when comparing the deposition rate as function of the protein mass. This seems logical, since the larger the molecule, the more interactions it has with the surface, or with the other surrounding molecules. It then requires more energy to leave the surface. Secondly, the fragmentation probability will be larger for larger proteins; therefore, less intact molecules are desorbed and available for analysis. Third, the sensitivity of the detector significantly decreases with decreasing velocity of the secondary ions. In fact, the detection also depends on the mass, but main the impact comes from the velocity of the ions.[5] All ions being accelerated at the same energy, the lighter ones travel to the detector with a much higher velocity. To further increase the detection efficiency, the secondary ions are post-accelerated just before reaching the detector, usually at 10 keV. Despite this post acceleration, the detection of large molecules over 10 kDa was rarely reported in the literature. However, as mentioned in the introduction, Mochiji et al. detected the molecular ion of cytochrome C (about 12kDa) by ToF-SIMS, using large argon gas clusters as primary ion beam (5 keV Ar_{1400}^{+}, 3.57 ev/atom).[1] To our knowledge, this is the largest protein molecular ion detected by ToF-SIMS with typical primary ion sources, Bi-LMIG or Ar-GCIB. This striking result has drawn our attention, and it was decided to investigate a few leads that could influence positively the detection of a larger protein, lysozyme in the present case.

Two strategies were devised. On the one hand, it was attempted to improve ionization. To this end, addition of salt to the protein samples was investigated. On the other hand, it was attempted to improve the efficiency of the detector towards the detection of high masses by increasing the post acceleration in the instrument settings.

As was reported in the literature, and notably in the article by Mochiji et al.,[1] proteins, and biomolecules in general, sometimes tend to form salt adducts. In SIMS spectra, it is common to observe molecular ions of biomolecules as $[M+X]^{+}$, where X is a metal, often Na, or K. In fact, the charge of the adduct comes from the metal, which is preferably in the form of Na^{+} or K^{+}. Adding

salt may be a solution to promote the formation of such adducts, leading *in fine* to an increase of the ionization yield of the proteins. To improve the detection of lysozyme, it was mixed in NaCl solutions of various concentrations (10 to 100 mM), then spin-coated on Si wafers. The samples were then analyzed by SIMS, using 10 kev Ar_{3000}^+ and Ar_{5000}^+ as analysis beams. Despite the presence of salt, the molecular ion of lysozyme could never be detected. In addition, it even seemed that as the salt concentration was increased, the intensities of the peaks related to the protein were decreasing in the low mass range (1 - 100 Da). As the molecular ion of lysozyme was never detected whatever the experimental conditions, it was probably not the best candidate to perform the preliminary experiments. To characterize more precisely the effect of salt addition on ionization and so on the detection of large molecular ions, it was decided to study such effect on insulin, whose molecular ion is detected by 10 keV Ar_{3000}^+. Solutions of

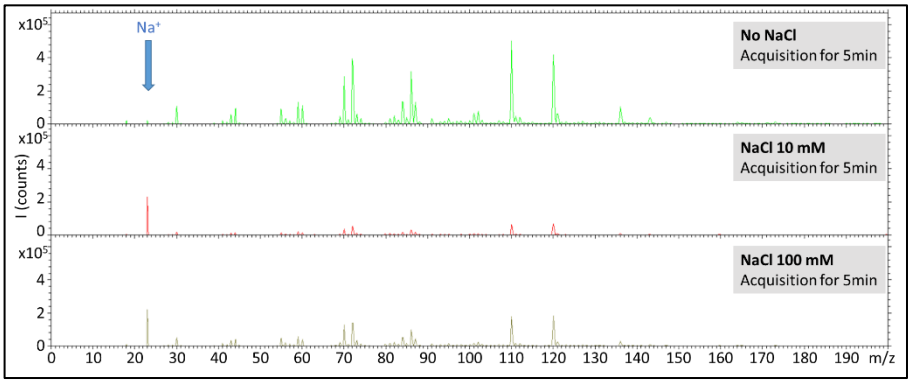


***Figure 6.1**. Low mass range of ToF-SIMS spectra recorded on insulin spin-coated samples with top: no NaCl; middle: 10 mM of NaCl and bottom: 100 mM of NaCl.*

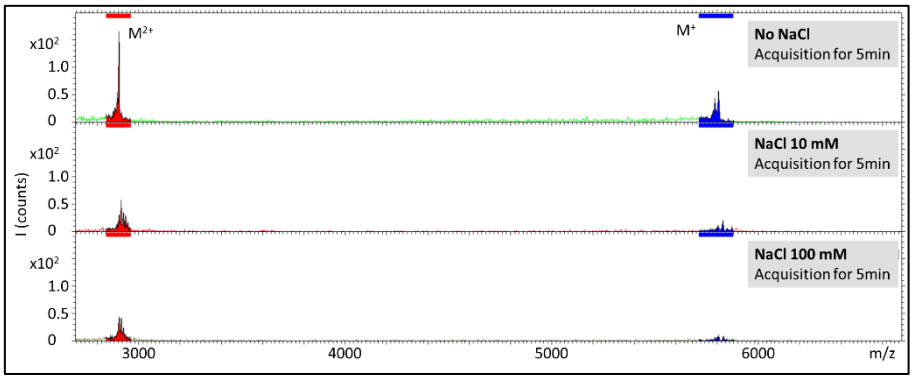


***Figure 6.2.** High mass range of ToF-SIMS spectra recorded on insulin spin-coated samples with top: no NaCl; middle: 10 mM of NaCl and bottom: 100 mM of NaCl.*

insulin were prepared with either 10 or 100 mM of NaCl. Samples were spin-coated and analyzed by ToF-SIMS, using the 10 keV Ar_{3000}^+ analysis beam. As can be seen in **Figure 6.1**, the effect of salt addition is far from that intended. Even at the lowest salt concentration, the intensity of all protein-related peaks is significantly decreased. The effect is observed in the low and high mass ranges. Indeed, the same trend is observed for the singly and doubly charged molecular ions (**Figure 6.2**). It seemed that the spectra are saturated with Na^+. It is possible that the salt crystalizes at the surface of the sample, yielding a sort of coating on top of the protein layer. As the addition of salt did not seem to yield any conclusive results with respect to an improved ionization yield, this approach was not further investigated.

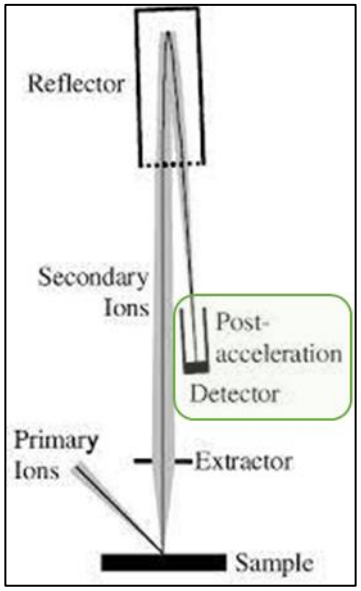


***Figure 6.3**. Schematic illustration of a ToF-SIMS experimental set-up to highlight where the post-acceleration takes places.*

The other strategy investigated to improve the detection of high mass ions was to increase the post acceleration. It takes place at the end of the field-free path, just before the ions reach the detector, as depicted in **Figure 6.3**. In the ToF-SIMS.5 instrument, the default value of the post acceleration is set at 10 kV. It is however possible to increase it up to 20 kV. This time, insulin was used in the first place, to assess the effect of increasing the post acceleration. Pure insulin solutions were spin-coated on Si wafers, and analyzed using 10 keV Ar_{3000}^+, with the post acceleration selectively set at 10 and 20 kV. The high mass regions of the spectra (displaying the singly- and doubly-charged molecular ions) are shown in **Figure 6.4**. As can be observed, this time the effect was as intended, that is an increase of the intensity for the high m/z secondary ions. To compare the two post acceleration conditions, the M^+/M^{2+} ratio was calculated for both spectra. The ratio is equal to 0.58 and 3.23 at 10 and 20 kV, respectively, meaning that the relative intensity of the ion with the higher m/z value is increased about 5.5 times for a post acceleration of 20 kV

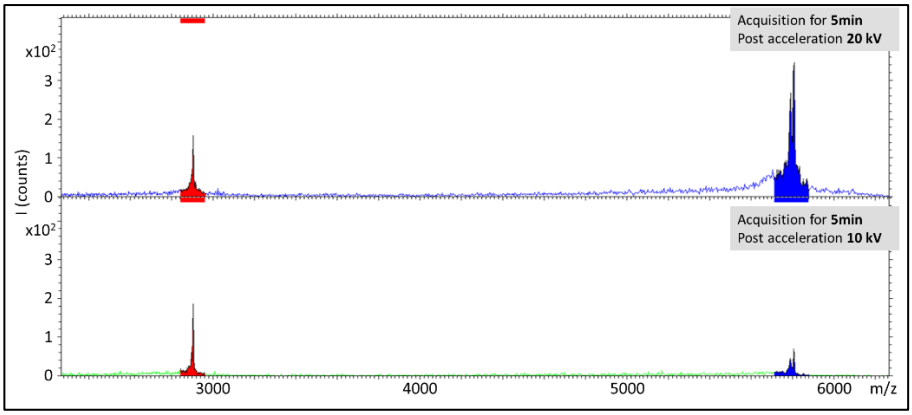


***Figure 6.4**. High mass range of ToF-SIMS spectra recorded on insulin spin-coated samples with top: 20 kV post-acceleration and bottom: 10 kV post-acceleration.*

compared to 10 kV. This result demonstrates that the efficiency of detection of high m/z ions can be improved by increasing the post acceleration. Knowing this, mass spectra were recorded on fresh lysozyme spin-coated samples, using 10 keV Ar_{3000}^+ and Ar_{5000}^+, with the post acceleration set at 20 kV. Despite many efforts and variation in sample thickness or substrates hardness (softer PET samples were tried), the molecular ion of lysozyme could never be detected, nor any large secondary ion whose mass is close to that of lysozyme.

After investigating these two strategies, it was agreed that the molecular ion of lysozyme would be very difficult to detect with our instrument. It was thus decided to explore other techniques that would allow to probe the presence of intact lysozyme at the surface of the collectors after transfer. The first techniques to be applied were other mass spectrometry alternatives, namely matrix-assisted laser desorption ionization mass spectrometry (MALDI-MS) and electrospray ionization mass spectrometry (ESI-MS). Their investigation is described in the next section of this chapter.

6.3.1.2. Efforts to detect lysozyme by other mass spectrometry techniques

If so many efforts have been made towards the detection of the molecular ion of lysozyme by SIMS, it is because the prospect of having a technique to analyze the surface of the collector as it is after the transfer was quite appealing. From this perspective, the choice of first alternative technique to analyze the collectors naturally fell on MALDI-MS. It is a mass spectrometry technique, especially popular for mass spectrometry imaging, and is known

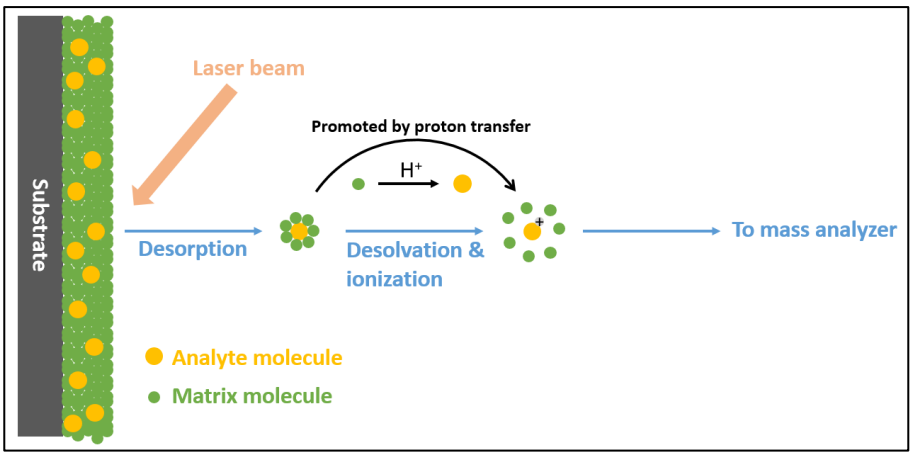


***Figure 6.5**. Schematic illustration of the basic principle of MALDI-MS.*

as one of the two "soft" ionization techniques, alongside ESI. This soft ionization feature allows for the sensitive detection of large, nonvolatile and labile molecules by mass spectrometry. MALDI-MS is far from being a central technique to this work. Therefore, it will only be briefly described, and more detailed information can be found elsewhere.[6] MALDI-MS relies on the discovery that laser radiations could be used to generate ions for mass spectrometry analysis. The seminal experiments of laser ablation mass spectrometry date back to only a few years after the invention of the laser, in the sixties.[7,8] The actual principle of MALDI-MS, depicted in **Figure 6.5**, and its acronym were first described in 1985.[9,10] The basic principle of MALDI-MS is to use a chemical matrix to absorb the laser energy, and trigger desorption of large amounts of material, as well as ionization of a fraction of the desorbed molecules. The matrix is usually in the form of small organic molecules, and is mixed in large excess with respect to the analyte. MALDI-MS rapidly proved to be suitable for the analysis of proteins. The first spectra of proteins with masses exceeding 10 and even 100 kDa were already reported in 1988.[11,12]

In the simplest way to perform a MALDI-MS experiment, the solution containing the analyte is mixed with that containing the matrix, and the resulting mixture is drop-casted. As the solvent evaporates, the matrix co-crystallizes with the analyte, yielding an optimal sample to be analyzed. This strategy was applied to a reference lysozyme solution. The resulting mass spectrum is presented in **Figure 6.6**. As can be observed, MALDI-MS, in opposition to ToF-SIMS, allows a straigthforward detection of the molecular ion of lysozyme. In addition to the singly charged molecular ion, present in

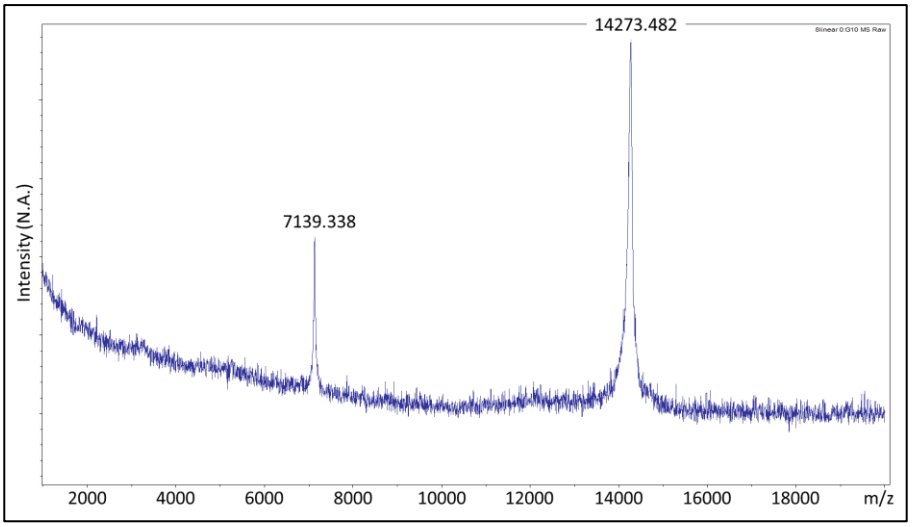


***Figure 6.6**. High mass range of a MALDI-MS spectrum recorded on a reference spin-coated lysozyme sample. Both the singly and doubly-charged molecular ions were detected with high intensity.*

the spectrum at an m/z of 14273, one can also see that the doubly charged molecular ion is present in the spectrum, at an m/z of 7139. The next challenge was to find a procedure to perform these experiments directly on the collectors. Indeed, in the present case, mixing the matrix solution with that of the protein is not an option, as the material to be analyzed is already deposited at the surface by transfer from the target. However, MALDI-MS can also be performed by matrix deposition on top of a solid sample. In this case, a relatively thick matrix layer is sprayed on the sample, and the analyte molecules diffuse into the matrix layer. This approach was attempted on the collectors. In spite of several trials, the molecular ion of lysozyme could never be detected. This does not necessarily mean that there is no intact lysozyme at the surface of the collector. It is very likely that compared to the matrix layer deposited on top of it, the lysozyme quantity/layer thickness is too small. In that scenario, the lysozyme could either migrate through the matrix layer but be too diluted to be detected, or either simply not migrate far enough into the matrix layer. One solution could have been to perform longer transfers to make sure that sufficient protein material was available for the analysis. However, at that time, the 15° transfer geometry was used, meaning that transfers were not so efficient. Deposition of large amounts of protein would have required days of transfer. Therefore, it was decided to explore the next analytical technique on the list, namely ESI-MS.

The basic principles of ESI-MS were given in the **introduction section** (**Chapter 1**), as this ion source was used to develop soft-landing techniques. ESI-MS requires to have the analyte in solution. For reference analysis, this was not an issue: a lysozyme solution was prepared and analyzed. The resulting mass spectrum is displayed in **Figure 6.7**. The molecular ion is detected as a series of ions bearing multiple charges. One of the characteristic of ESI is indeed that it produces multiply charged ions, thereby lowering the m/z of the initial ion and favoring its detection. Regarding the transferred samples, the fact that the measurements can only be performed in solution was more of a concern, as the deposited material had to be desorbed after transfer. As was mentioned in **Chapter 5** (**section 5.3.1**), simply depositing a drop of water on the Si wafer to recover the proteins did not prove to be very successful. In this case, it was attempted to desorb the proteins directly with the mixture that is used for the ESI-MS experiments, that is a diluted aqueous solution of either methanol or formic acid. To this end, the collectors (1 x 1 cm^2) were cut into four small pieces, and placed inside an Eppendorf tube. The ESI-MS solvent was added, and then measurements were performed on the solution hopefully containing the transferred and desorbed protein molecules. However, the results never showed the presence of the molecular ion of lysozyme. Despite efforts to increase the quantity of the transferred protein (longer transfer time) or to concentrate the solution by gathering up to three collectors in the same Eppendorf, intact lysozyme could never be detected.

Just as for MALDI-MS previously, the fact that lysozyme could not be detected within this set of ESI-MS experiment was not by any mean the demonstration that lysozyme could not be transferred intact. If the quantity was probably the limiting factor in the case of MALDI-MS, and could still be in this case, ESI-MS added the concern of the solubilization. Indeed, it is well known that proteins tend to accumulate at interfaces, for a series of reasons detailed in the introduction section. Therefore, the transferred protein molecules might not favorably and spontaneously leave the surface to go back into solution, or at least not all of them. For many applications, if one wants to solubilize adsorbed protein, it is common to add a detergent to the solution. Sodium dodecyl sulfate (SDS) is the most popular one. Yet ESI-MS analyses are not compatible with samples containing SDS. In the presence of such ionic detergent, the resulting mass spectrum is saturated with its ions, making the detection of the protein molecules impossible, especially the ions of weak intensity, such as the molecular ions of lysozyme.

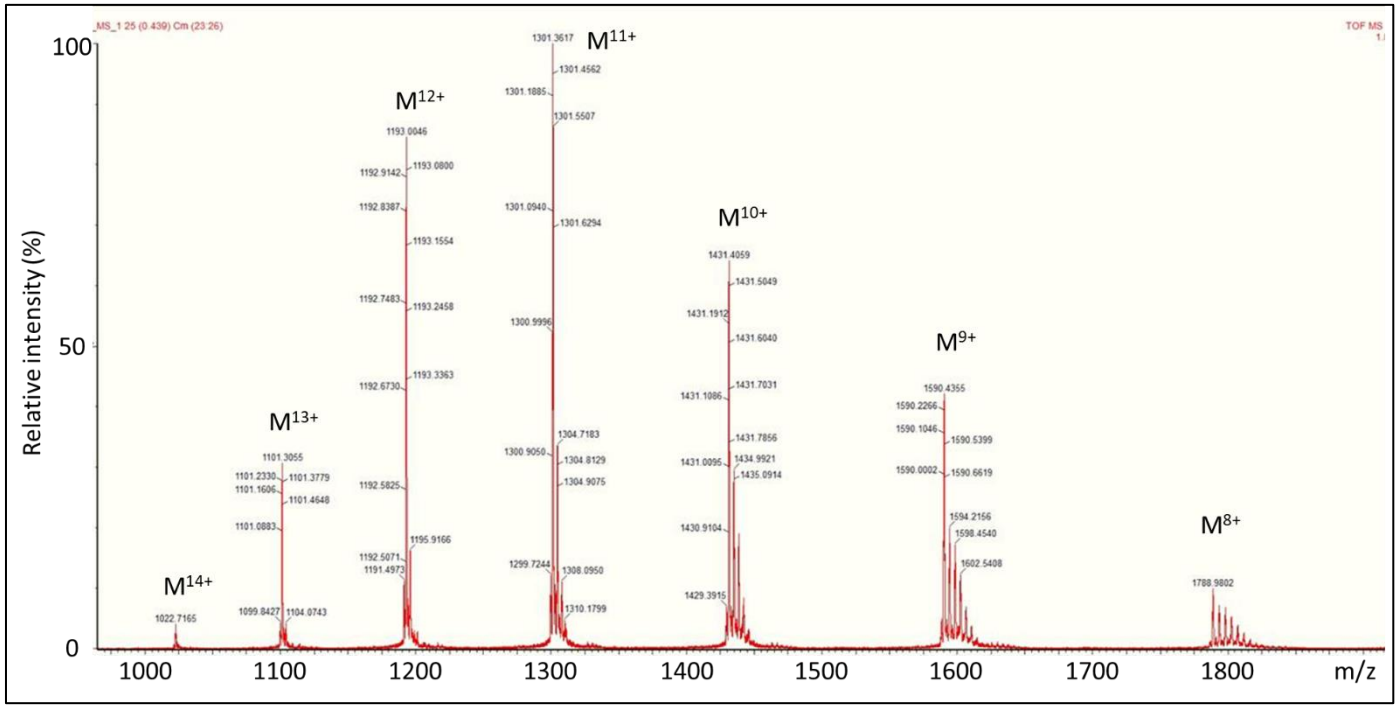


Figure 6.7. *High mass range of an ESI-MS spectrum recorded on a reference lysozyme sample. Multiply charged molecular ions were detected with high intensity.*

In this section, it was shown that for the tested experimental conditions, mass spectrometry techniques such as MALDI-MS and ESI-MS did not prove successful for the detection of the intact molecular ion of lysozyme at the surface of the collectors. However, unlike ToF-SIMS, these techniques could detect lysozyme in reference samples, suggesting that either the problem was originating from the transferred samples themselves, or from the protocols that have been implemented for the preparation of the samples. As was discussed, two main issues are likely to come into play. For both techniques, the transferred quantity might be too small to allow detection. In the case of MALDI-MS, the fact that the transferred protein layers are covered and have to diffuse through a thick layer of matrix represents a major drawback, whereas in ESI-MS, the solubilization step is of main concern, especially since the use of effective ionic detergents is prohibited.

Nevertheless, still driven by the established fact that peptides and small proteins were transferred intact (**see Chapter 4**), and by molecular dynamic simulations that indicated that this should also be the case for larger ones, it was decided to pursue the efforts toward the detection of lysozyme at the surface of the collectors. In the next section, the use of a well-known method for the separation and identification of proteins is investigated, namely sodium dodecyl sulfate–polyacrylamide gel electrophoresis (SDS-PAGE).

6.3.1.3. Detection of intact lysozyme by sodium dodecyl sulfate–polyacrylamide gel electrophoresis (SDS-PAGE)

Electrophoresis is a widespread method to separate and identify proteins contained in complex mixtures, such as blood.[13–17] It also delivers information about the integrity of the polypeptide chain length. Electrophoresis of proteins is usually performed on a highly cross-linked gel matrix that acts as a sieve through which the protein molecules move in response to an electric field. The electrophoresis separation relies on the fact that smaller proteins migrate faster than larger ones. Yet, if proteins are loaded on a gel in their native form, the migration on the gel is influenced primarily by their size, but also, to a lower extent, by their structure and their overall charge. To get rid of these second order contributions, Laemmli, in 1970, proposed to add sodium dodecyl sulfate (SDS) to the buffer that was used to load the proteins on the gel.[2] SDS is a detergent displaying a strong protein-denaturing behavior, and it further binds to the protein backbone with a constant molar ratio. Consequently, proteins unfold into linear chains with an overall negative charge proportional to their size/amino-acids chain length. The

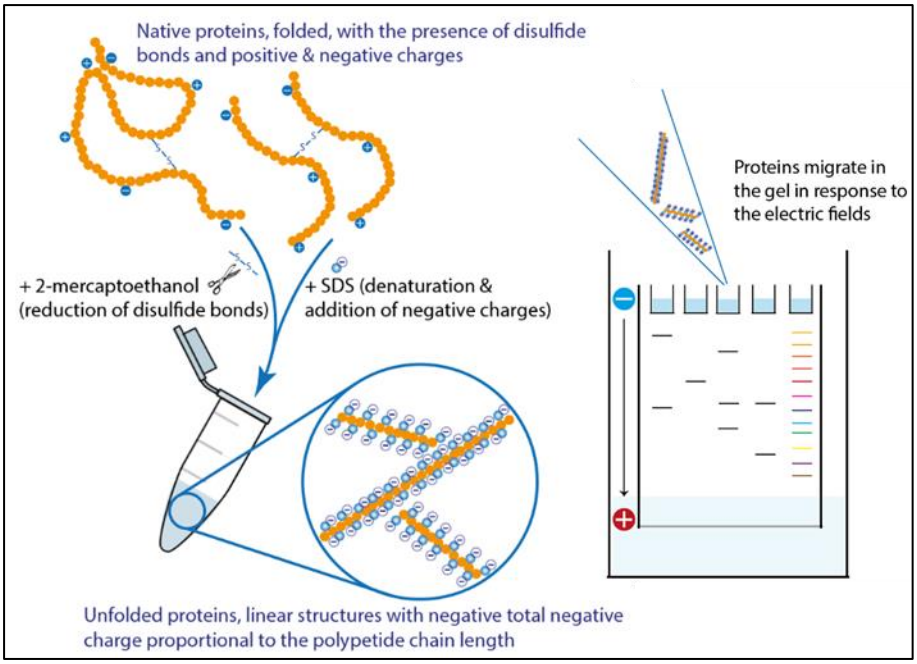


***Figure 6.8**. Schematic illustration of a SDS-PAGE electrophoresis experiment.*

proteins then migrate at a speed only proportional to their size, which allows comparing proteins that initially have completely different structures and charges. A schematic of a SDS-PAGE experiment is depicted in **Figure 6.8**.

To perform such experiments on the proteins transferred on the collectors, desorption was once again necessary. However, in contrast with ESI-MS, SDS-PAGE not only tolerates the presence of detergent, but also requires it, in relatively high concentration, i.e. 2% of SDS in the final mixture. This should largely favor the desorption of the protein molecules from the collector. The Si wafer collectors were once again cut into smaller pieces, and placed into Eppendorf tubes. They were then incubated directly with the Laemmli mixture, containing SDS. The solution was then loaded on the gel to perform the electrophoresis experiment. **Figure 6.9** shows the result of the SDS-PAGE separation carried out with transferred protein material desorbed from the collector. A reference lysozyme sample gives a wide band just below 15 kDa, corresponding to the lysozyme molecular mass. The transferred material reveals a thin band at the same position, indicating the presence of intact lysozyme molecules on the collector. Note that the upper band around 70 kDa and the diffuse area below 10 kDa could not be identified. While the

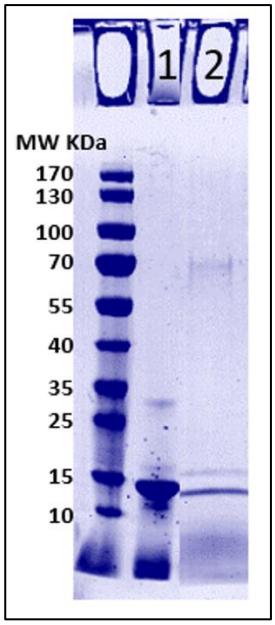


***Figure 6.9**. Result of a SDS-PAGE carried out on (1) reference lysozyme sample, and (2) transferred lysozyme sample.*

upper band probably arises from a contamination, the diffuse area below 10 kDa most likely results from random fragmentation occurring during transfer. To ensure that the observed band corresponding to intact lysozyme is not an artefact nor a contamination, it was decided to analyse the content of the band by means of mass spectrometry, ESI-MS in this case. As previous experiments tend to show that the transferred quantities were too small to allow detection of the molecular ion, sequencing experiments were conducted instead, aiming at finding the amino-acid sequence specific to lysozyme. For this purpose, the band corresponding to intact lysozyme was cut from the gel and mixed with trypsin (a protease), yielding smaller protein fragments that were then analysed by mass spectrometry. Four peptides related to lysozyme could be identified, accounting for 40% of the total sequence (**Table 6.1**), confirming that the observed band contains lysozyme. A sketch of the workflow used to obtain these data is represented in **Figure 6.10 (left)**. However, trypsin digestion is not optimal on proteins trapped in a gel. To go further, trypsin digestion was also performed directly

***Table 6.1.** Results of the ESI-MS experiments performed on the band corresponding to intact transferred lysozyme. The band was trypsin-digested before the fragments were analysed. At the bottom of the table, the amino acid sequence of lysozyme is given, with in green the four peptides that were identified.*

Component name	Protein name	Fragment label	Peptide	Sequence start	Sequence end
1:T8+H⁺	Lysozyme	1:T8	NTDGSTDYGILQILQINSR	46	61
1:T16+H⁺	Lysozyme	1:T16	GTDVQAWIR	117	125
1:T7+H⁺	Lysozyme	1:T7	FESNFNTQATNR	34	45
1:T13+H⁺	Lysozyme	1:T13	IVSDGNGMNAWVAWR	98	112
Observed mass (Da)	Mass Error (ppm)	Observed RT (min)	Response	Observed m/z	Charge
1753.8378	1.5	16.92	241613	877.4225	2
1045.5429	0.4	16.73	134416	523.2751	2
1428.6526	1.7	14.04	123334	714.8300	2
1675.8079	4.1	14.44	26335	559.2741	3
Sequence coverage : 40%					

KVFGRCELAA AMKRHGLDNY RGYSLGNWVC AAK**FESNFNT QATNRNTDGS TDYGILQILQINS**
RWWCNDGRTP GSRNLCNIPC SALLSSDITA SVNCAKK**IVS DGNGMNAWVA WR**NRCK**GTDV QAWIR**GCRL

on a collector after lysozyme transfer, by mixing the trypsin with the collector pieces in an Eppendorf tube. In this case, 60% of the sequence could be identified, as shown in **Figure 6.10 (right)**. These results clearly demonstrate the presence of intact lysozyme molecules at the surface of the collector. This strategy can further be employed when other large proteins have to be identified.

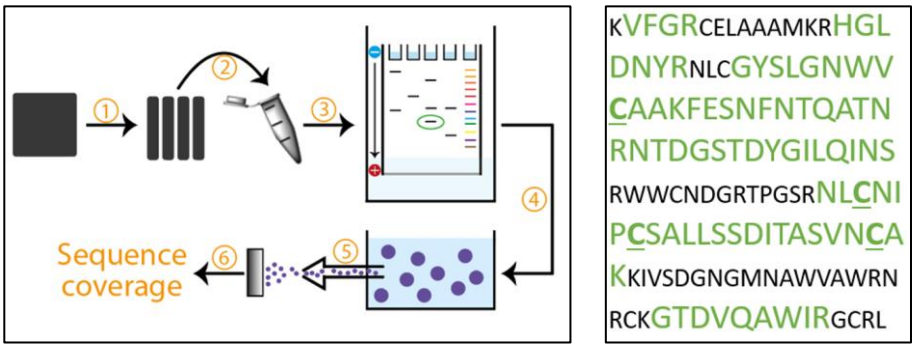


Figure 6.10. *Left: experimental workflow towards the detection of intact lysozyme on the collectors. Right: amino-acid sequence of lysozyme, with in green the peptides that were observed in the ESI-MS spectrum. Prior to the mass analysis, lysozyme was trypsin digested directly at the surface of the collectors.*

The favourable outcome of these experiments was finally the proof that relatively large proteins could be desorbed and transferred intact by gas cluster ion beams. This result is not only important for the development of the cluster-assisted deposition method, but also has an impact on the SIMS community, as to our knowledge, such large molecules were never reported in ToF-SIMS spectra (with typical primary ion sources, Bi-LMIG or Ar-GCIB). It tends to confirm that with respect to large biomolecules, ionization and detection are more limiting than the desorption itself. Regarding the development of the cluster-assisted protein deposition method, however, this result provides an answer to only half of the research question. Indeed, the ultimate goal is to build thin films of intact but also active proteins. The SDS-PAGE experiments show that there are intact lysozyme molecules in terms of amino-acid chain, but deliver no information regarding the 3D conformation of the proteins at the surface of the collector, and therefore no clue whether the proteins were still active or not. The next section is focused at performing enzymatic assays at the surface of the collectors to assess whether lysozyme is still active or not.

6.3.1.4. *Lysozyme activity assessment*

Confirming the activity of an enzyme provides insights regarding its three dimensional structure, due to the structure-activity relationship. A fluorescence-based enzymatic activity assay was performed at the surface of the collectors. Just as the quantification assays, those to assess the bioactivity proved to be very challenging to be performed directly at the surface of the collectors. Following tens of trials, not detailed in this chapter, a protocol relying on a quite complex experimental set-up was developed. The latter is detailed in the materials and methods section of this chapter. The results of this enzymatic assay suggest that the activity detected on the collectors is roughly equivalent to that of 0.9 µg of fresh lysozyme (**Figure 6.11)**. This result indicates that at least a fraction of the transferred protein molecules can be found on the collector in their native functional conformation. However, some protein molecules may unfold to a certain extent upon desorption, and refold once relaxing on the collector surface. Moreover, the enzymatic assay being performed in solution, slightly unfolded proteins might fold back to their native conformation. Both unmodified and refolded proteins contribute to the measured activity. In comparison with the obtained value of 0.9 µg, a monolayer of lysozyme can be approximated to 0.115 - 0.230 µg/cm^2 based on its molecular footprint. The collector surface being roughly 2 cm^2, if the proteins were deposited homogeneously, enough material would be transferred to build two to four molecular layers with the ion dose of 4x10^{14} ions that was used. It is worth emphasizing that the total quantity of transferred material is undoubtedly superior to that obtained with the activity assays, yet it could not be precisely quantified. Two explanations support this claim. The first one is that, with these beam conditions (E/n = 2 eV), some fragmentation is still likely to occur (cf. SDS-PAGE result below 10 kDa, and **Chapter 4**, section on fragmentation). In addition, while the Ar beam distribution is centred on 5000 atoms, it is quite

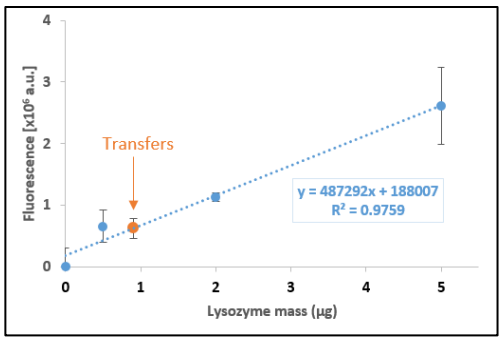


***Figure 6.11**. Activity assay of lysozyme. In blue, the calibration line, performed on fresh lysozyme. In orange, the activity measured on the transferred lysozyme samples. Activity on the collectors is equivalent to that of 0.9 µg of fresh lysozyme.*

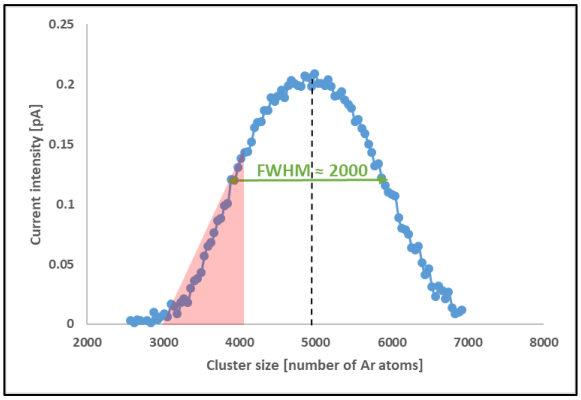


Figure 6.12. *10 keV Ar5000+ cluster size distribution, with highlighted in red the energetic tail of the distribution.*

wide, with a full width at half maximum of about 2000 (**Figure 6.12**). Therefore, the contribution of higher E/n clusters, inducing more bond scissions upon impact, is not negligible. As a result, a significant fraction of proteins should be transferred as non-active fragments. The second explanation lies in the possibility that the specific activity could differ from reference to transferred lysozyme samples. Indeed, the protein structure might in part be affected by the transfer (see *supra*), and substrate diffusion might be limited when multilayers are deposited.

6.3.2. Trypsin

As soon as it was demonstrated that at least a fraction of the transferred lysozyme molecules was deposited intact and showed retention of its enzymatic activity, it was exciting to investigate the transfer of larger proteins. The next chosen enzyme was a larger protein, namely trypsin. With a mass of about 23.8 kDa, trypsin seemed to be a good intermediate candidate before investigating the transfer of even larger proteins. Trypsin also presents the advantage that relatively simple activity assays are commercially available. Just as lysozyme, trypsin can be easily detected by MALDI-MS or ESI-MS, so these techniques could have also been investigated for the analysis of the collectors. However, in light of the work previously achieved on lysozyme, and all the encountered detection issues, it was decided to skip these two techniques and directly focus on those that proved efficient for the detection of lysozyme, that is SDS-PAGE electrophoresis, and specific activity assay. The results obtained with these two approaches are presented and discussed in the following sections.

6.3.2.1. Detection of intact trypsin by electrophoresis

Trypsin was transferred using a 10 keV Ar_{5000}^{+} beam (in the reverse sample holder, to maximize the transferred quantity). As the preparation of the solution samples to be loaded on the SDS-PAGE gel is straightforward in Eppendorf tubes, PE collectors were chosen for this set of experiments (see **Chapter 4**). The SDS-PAGE experiment was carried out following the exact same protocol as the one developed for lysozyme. The result of such an electrophoresis performed on trypsin transferred samples is depicted in **Figure 6.13**. In the first well, the protein mass ladder was loaded. In the second one, a reference of lysozyme was loaded just for comparison. The third well was intentionally left empty. The fourth one was loaded with the reference solution of trypsin. Finally, three transferred samples were loaded in the wells 5, 6, and 7. The rest of the wells were left empty. As can be observed, one of the wells containing a transferred sample (well 5) displays a protein band at the exact same height/mass in the gel as that observed in the reference well (n°4). From this transferred sample, it can be concluded without any doubt that intact trypsin molecules could be transferred from the target onto the collector. In the meantime, this successful outcome was somewhat balanced by the results of the two other transferred samples, which did not indicate the presence of intact trypsin. However, it would be very surprising that transfers conducted in the exact same conditions (mainly the same cluster size and energy) would deliver different results regarding the fragmentation of the transferred trypsin. A first hypothesis to explain the absence of intact trypsin in samples loaded in wells 6 and 7 is that the transfer ion dose used to prepare them was too small. In that case, too little quantity was deposited on the collector, and the resulting protein mass loaded on the gel is under the detection limit. A second hypothesis is that the

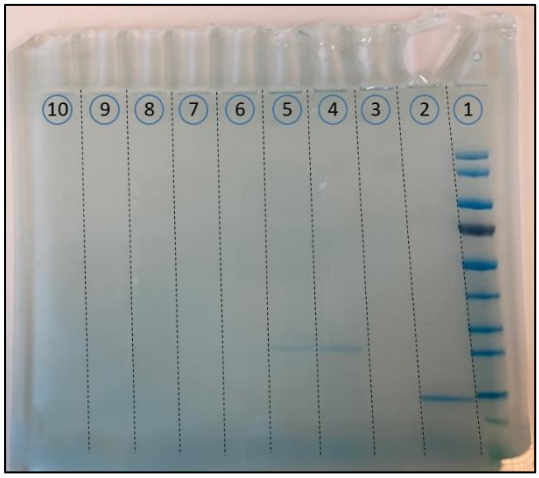


***Figure 6.13**. Result of a SDS-PAGE. (1) Protein ladder. (2) Lysozyme reference. (3) Empty. (4) Trypsin reference. (5 to 7) Trypsin transferred samples. (8 to 10) Empty.*

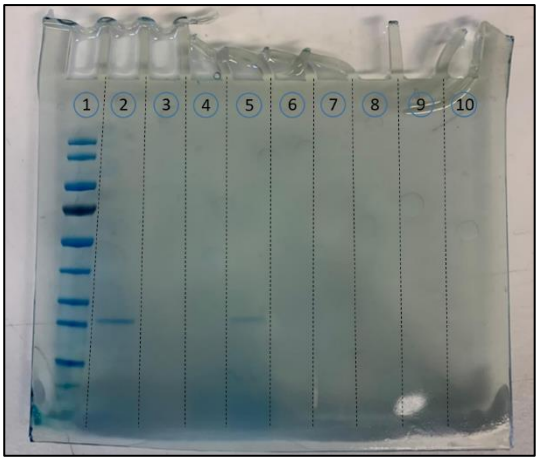


Figure 6.14. *Result of a SDS-PAGE. (1) Protein ladder. (2) Trypsin reference. (3 to 5) Trypsin transferred samples. (6 to 10) Empty.*

transferred material was not properly desorbed from the PE collector when the SDS-PAGE solution sample was prepared. Indeed, some practical issues were encountered during the desorption step, as agitation of the Eppendorf tubes made the PE collectors moving towards the top of the tube, so that they were not immersed in the solution anymore. A third hypothesis is that something went wrong during the transfer. This hypothesis highlights one of the main drawback of working with PE collectors. As their analysis by SIMS is somewhat complicated, the protein deposition is not controlled, making the experimentalist completely blind with respect to the sample preparation. It is only once the final result of the electrophoresis is revealed that one gains information about the sample quality. For instance, a wrong positioning of the argon beam with respect to the target could lead to no protein transfer, or at least no deposition on the collector. To make sure that the trypsin observed in the sample loaded in the fifth well was not the result of a contamination during sample preparation, it was decided to carry out the same experiment once more. Three new transferred samples were prepared, and then loaded on a gel, which is shown in **Figure 6.14**. On this gel, the protein mass ladder was loaded in the first well. The reference trypsin solution was loaded in the second well, while the transferred samples were loaded in the wells 3, 4 and 5. The rest of the wells were left empty. Here again, different results were obtained, as intact trypsin was observed in only one of the three samples. Given the circumstances, given the comments made here above (blind transfer, long procedure with many steps until final result), this experience confirms that when the whole procedure goes along the plan, trypsin can be transferred intact. As was specified for lysozyme in the previous section, the electrophoresis results only provide information regarding the primary structure of the protein. In this case, when the protein is said to be intact on the collector, it only means that the amino acid chain was not broken in the course of the transfer. To

assess whether the protein has retained its secondary and tertiary structure, that is its 3D folding, further analyses are required. It can for example be investigated in an indirect manner by conducting activity assay, as was done for lysozyme. At this time, this could not yet be performed.

6.4. Conclusion

In this chapter, the transfer of larger proteins was investigated. Enzymes were transferred, as probing their activity on the collectors would deliver information regarding the retention of their 3D structure upon transfer. Lysozyme (14.3 kDa), a protein known to be relatively hard, was used as model enzyme. Before investigating its activity, the first step was to demonstrate that intact lysozyme was present on the collector. As its mass is very close to that of the largest protein detected by ToF-SIMS with typical primary ion sources, Bi-LMIG or Ar-GCIB, i.e. cytochrome C, efforts were made to improve ionization yield and detection efficiency of lysozyme, in order to detect it by ToF-SIMS. Strategies included adding salt to promote ionization via adducts formation, or improve the detection efficiency by increasing the post acceleration. However, none of these strategies allowed the detection of the molecular ion of lysozyme. Therefore, other mass spectrometry techniques were investigated, namely MALDI-MS and ESI-MS. Yet neither of these methods yielded more successful results than ToF-SIMS with respect to collector analysis. For MALDI-MS, the transferred quantities were probably too small compared to the large matrix layer deposited on top, diluting the protein to such an extent that it cannot be detected. For ESI-MS, solubilization of the deposited material to allow analysis from solution was likely to be the main issue. In this respect, the preparation of collectors that favor the release of the protein once in solution may help significantly (see **Chapter 5**). For this purpose, the sacrificial layer approach is probably not the best alternative, as the sugar molecules will enter in competition with the proteins with respect to the ionization. However, the approach based on the construction of a protein repulsive layer might be promising. This could be investigated in the near future. As a final note regarding these attempts, now that it has been established that the 45° transfer allows the deposition of much higher proteins quantities is similar transfer times (see **Chapter 1**), it might be worth giving another try at MALDI-MS and ESI-MS on the transferred samples. Meanwhile, SDS-PAGE electrophoresis turned out to be a very efficient alternative, allowing the detection of intact lysozyme at the surface of the collectors. After that, enzymatic activity assays performed at

the surface of the collector demonstrated that lysozyme was not completely denatured upon transfer as it retained its bioactivity. If these experiments do not allow to confirm with 100% confidence that the 3D structure is unmodified, it indicates that it is at least partly preserved, with the reactive site at least kept intact. The protocols developed for lysozyme could further be applied to the analysis of larger transferred proteins. The work was started for trypsin (23.8 kDa). SDS-PAGE experiments revealed the presence of entire protein molecules on the collectors. These results, alongside those obtained for lysozyme, are stricking, as they reveal desorbing capabilities of large argon cluster ions beams that were never reported before.

N.B. At the time of writing this chapter, the protocol of the trypsin enzymatic assay is still under optimization towards its use directly on collectors, and no trials were yet performed on transferred samples.

6.5. Bibliography

(1) Mochiji, K.; Hashinokuchiy, M.; Moritani, K.; Toyoda, N. Matrix-Free Detection of Intact Ions from Proteins in Argon-Cluster Secondary Ion Mass Spectrometry. *Rapid Commun. Mass Spectrom.* **2009**, *23* (5), 648–652.

(2) Laemmli, U. K. Cleavage of Structural Proteins during the Assembly of the Head of Bacteriophage T4. *Nat. 1970 2275259* **1970**, *227* (5259), 680–685.

(3) Neuhoff, V.; Arold, N.; Taube, D.; Ehrhardt, W. Improved Staining of Proteins in Polyacrylamide Gels Including Isoelectric Focusing Gels with Clear Background at Nanogram Sensitivity Using Coomassie Brilliant Blue G-250 and R-250. *Electrophoresis* **1988**, *9* (6), 255–262.

(4) Norde, W. My Voyage of Discovery to Proteins in Flatland …and Beyond. *Colloids Surfaces B Biointerfaces* **2008**, *61* (1), 1–9.

(5) Wu, K. J.; Odom, R. W. Matrix-Enhanced Secondary Ion Mass Spectrometry: A Method for Molecular Analysis of Solid Surfaces. *Anal. Chem.* **1996**, *68* (5), 873–882.

(6) Hillenkamp, F.; Jaskolla, T. W.; Karas, M. The MALDI Process and Method. *MALDI MS. A Pract. Guid. to Instrumentation, Methods, Appl. 2nd Ed.(Ed. F. Hillenkamp, J. Peter-Katalinic), Wiley Blackwell, Weinheim, Ger.* **2014**.

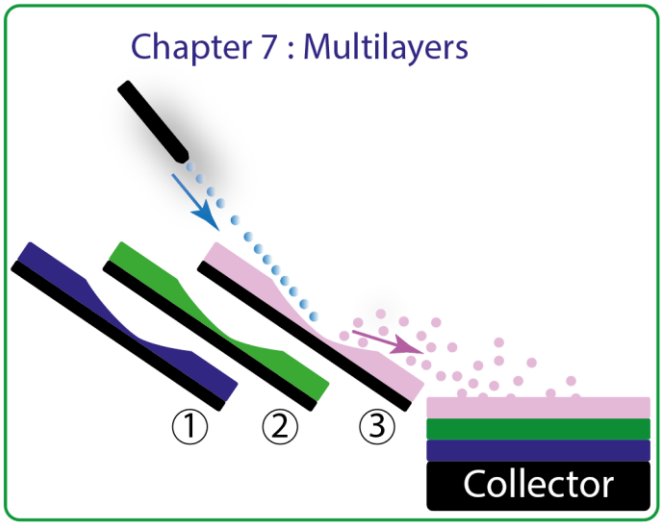
(7) Fenner, N. C.; Daly, N. R. Laser Used for Mass Analysis. *Rev. Sci. Instrum.* **1966**, *37* (8), 1068.

(8) Vastola, F. J.; Mumma, R. O.; Pirone, A. J. Analysis of Organic Salts by Laser Ionization. *Org. Mass Spectrom.* **1970**, *3* (1), 101–104.

(9) Karas, M.; Bachmann, D.; Bahr, U.; Hillenkamp, F. Matrix-Assisted

Ultraviolet Laser Desorption of Non-Volatile Compounds. *Int. J. Mass Spectrom. Ion Process.* **1987**, *78* (C), 53–68.
(10) Karas, M.; Bachmann, D.; Hillenkamp, F. Influence of the Wavelength in High-Irradiance Ultraviolet Laser Desorption Mass Spectrometry of Organic Molecules. *Anal. Chem.* **1985**, *57* (14), 2935–2939.
(11) Tanaka, K.; Waki, H.; Ido, Y.; Akita, S.; Yoshida, Y.; Yoshida, T.; Matsuo, T. Protein and Polymer Analyses up to m/z 100 000 by Laser Ionization Time-of-Flight Mass Spectrometry. *Rapid Commun. Mass Spectrom.* **1988**, *2* (8), 151–153.
(12) Karas, M.; Hillenkamp, F. Laser Desorption Ionization of Proteins with Molecular Masses Exceeding 10 000 Daltons. *Anal. Chem.* **1988**, *60* (20), 2299–2301.
(13) Su, Y.; Gao, L.; Ma, Q.; Zhou, L.; Qin, L.; Han, L.; Qin, W. Interactions of Hemoglobin in Live Red Blood Cells Measured by the Electrophoresis Release Test. *Electrophoresis* **2010**, *31* (17), 2913–2920.
(14) Schägger, H.; Bentlage, H.; Ruitenbeek, W.; Pfeiffer, K.; Rotter, S.; Rother, C.; Böttcher-Purkl, A.; Lodemann, E. Electrophoretic Separation of Multiprotein Complexes from Blood Platelets and Cell Lines: Technique for the Analysis of Diseases with Defects in Oxidative Phosphorylation. *Electrophoresis* **1996**, *17* (4), 709–714.
(15) Gallagher, S. R. SDS-Polyacrylamide Gel Electrophoresis (SDS-PAGE). *Curr. Protoc. Essent. Lab. Tech.* **2012**, *6* (1), 7.3.1-7.3.28.
(16) Manns, J. M. SDS-Polyacrylamide Gel Electrophoresis (SDS-PAGE) of Proteins. *Curr. Protoc. Microbiol.* **2011**, *22* (1), A.3M.1-A.3M.13.
(17) Schägger, H. Tricine–SDS-PAGE. *Nat. Protoc. 2006 11* **2006**, *1* (1), 16–22.

Chapter 7 : Construction of multilayers



In this chapter, the developed deposition method will be used to investigate the construction of more complex architectures that are out of the scope of current approaches. Notably, the construction of multilayers was demonstrated. Successive transfers were achieved on the same collectors, which were then characterized by ToF-SIMS depth profiling. Here, multilayers were constructed with two peptides, bradykinin and neurotensin, as well as with Irganox, an antioxidant molecule. Bilayers composed of two proteins as well as composed of one protein and Irganox were successfully prepared. No mixing was detected between the layers, and the multilayers were found to be stable after being exposed to ambient conditions for up to 7 days. Finally, a trilayer was build, with all three compounds. In practice, unlimited number of layers could be envisaged. These results open the way to the fabrication of more sophisticated thin films.

This chapter is the result of a fruitful scientific collaboration with Benjamin Tomasetti, with whom I shared the experimental work as well as the data treatment and the results interpretation. Benjamin is greatly acknowledged for his contribution.

7.1. Introduction

It has now been established that the cluster-assisted approach allows the controlled construction of protein thin films. It has also been demonstrated that the proteins are transferred with retention of their 3D structure, and therefore preserve their bioactivity at the surface of the collectors. In **Chapter 5**, it was shown that this method already surpasses existing protein deposition methods in terms of the variety of the substrate nature that can be employed, especially when compared to the widespread solution-based techniques. In this chapter, the goal is to take advantage of the developed technique to overcome another issue encountered by spontaneous adsorption and its derivative approaches, that is the construction of multilayers. The concern associated to the construction of multilayers in solution is that each time the sample is immersed in order to add a layer, the previous one(s) may be altered. For instance, if both molecules are soluble and deposited using the same solvent, the previously deposited molecule might be solubilized. The resulting film would then simply be a mixture of both compounds, resulting from the competition between the two molecules with respect to their affinity for the substrate. Here, the possibility to achieve successive transfers on a single collector is investigated. The strategy is schematically depicted in **Figure 7.1**. This approach should in

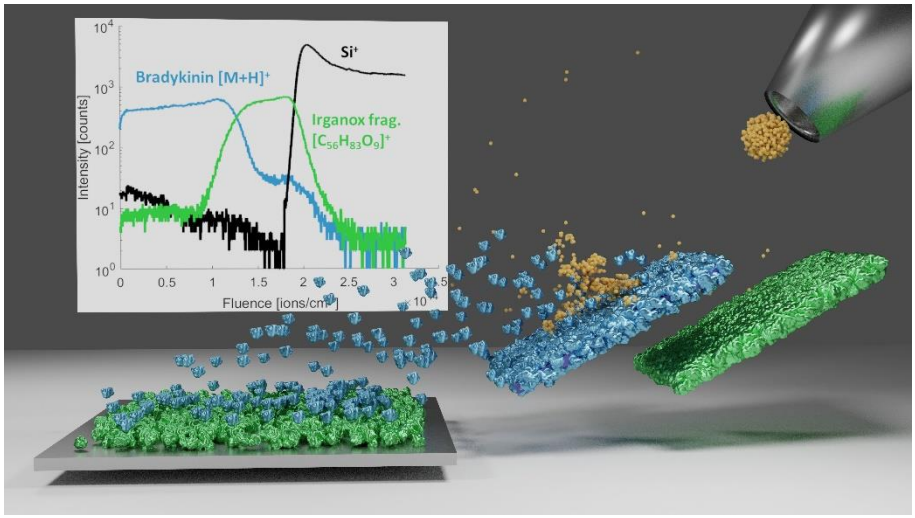


***Figure 7.1**. Schematic illustration of the construction of multilayers. Successive transfers are achieved on the same collector, to allow deposition of multiple layers. In principle, the number of repetitions is unlimited.*

theory allow the deposition of multiple layers (in principle unlimited number) of different materials on top of each other, leading to complex architectures out of reach of current deposition methods.

7.2. Materials and methods

7.2.1. Protein and Irganox targets

Protein targets were prepared following the same protocol as that described in the **General materials and methods section** (**Chapter 3**). Irganox targets were prepared in a similar fashion. Irganox was dissolved in toluene, in order to reach a solution concentration around 20 g/L. The target substrates were also thick Si wafers (0.3 x 1.0 cm²). Successive drops were evaporated on the Si wafer.

7.2.2. Successive transfers for the multilayers construction

All samples presented in this chapter were prepared using the reverse sample holder, i.e. with a cluster impinging angle of 45°. (Note that **Figure 7.1** illustrates the multilayer construction using the seminal sample holder (15° geometry), as the first trials were made with that geometry.) Due to the technical and geometrical constraints, only one target can be mounted at the time on the reverse sample holder. Therefore, a first transfer was achieved, and then the sample holder was taken out of the instrument to remove the first target and replace it by the next one (made of the next compound to be transferred), and so forth. Transfers were achieved with 10 keV Ar_{3000}^+ or 10 keV Ar_{5000}^+.

7.2.3. ToF-SIMS depth profile analysis of the multilayers

The multilayers were mainly analyzed by depth profiling. As only small compounds were transferred, their molecular ions could be followed through the layers. The instrument was operated in the dual-beam mode, with 10 keV Ar_{3000}^+ as sputter beam, and 30 keV Bi_5^+ as analysis beam. Their rasters were set at 600 x 600 µm² and 200 x 200 µm², respectively. The current intensity of the sputter beam was adjusted from one sample to another, depending on the overall thickness of the film. It ranged from a few tens of pA to a few hundreds pA. In some cases, charge compensation was required. For those charging samples, the electron gun was turned on, with its energy set at 5 eV to avoid fragile molecule degradation.

7.3. Results and discussion

Using the transfer method developed in this work, it is quite straightforward to envision the construction of multilayers. In principle, it only requires to perform successive transfers on the same collector, using targets made of different molecules, as illustrated in **Figure 7.1**. To start with an ideal model case, from the analytical viewpoint, the first multilayer was constructed with a peptide, bradykinin, and Irganox1010, an antioxidant molecule. The reason for that is that these two compounds are easily detected by SIMS, and their mass spectrometric signature is very different, easing the interpretation of the SIMS depth-profiles performed on the collectors.

7.3.1. A simple model: bradykinin/Irganox1010 multilayers

In the present case, bradykinin (Mw = 1060 g/mol) and Irganox 1010 ($C_{73}H_{108}O_{12}$, Mw = 1176.7 g/mol) were chosen, as both molecular ions are detectable in ToF-SIMS without interfering with one another. A 10 keV Ar_{3000}^+ beam was used to transfer both compounds, each time reaching an ion dose of 5 x 10^{14} ions. In the first place, bradykinin was deposited on top of Irganox. Given the ion dose used for transfer, the bradykinin layer thickness should be around 40 nm (calculated via the calibration given in **Chapter 4**). The sample was then depth-profiled by ToF-SIMS, in both positive and negative polarities. The profiles are shown in **Figure 7.2 a & b**. As the bradykinin molecular ion peak is not very intense in the spectra in negative polarity, a characteristic fragment is also shown. The same was applied for Irganox in positive polarity. The profiles show that the multilayer was nicely constructed, as the two layers are discernable. Yet, one may notice that the bradykinin signal does not immediately drop to minimal intensity when Irganox starts to be detected. A plateau of low intensity is maintained through the Irganox layer. Further data analysis performed on other multilayers samples (see later in this section) allowed determining that this plateau is in fact mirroring differences in background noise levels from one layer to another. These results have allowed to rule out the hypothesis of mixing between the layers. The same depth profiles were performed after exposure of the sample to atmospheric conditions for 7 days (**Figure 7.2 c &**

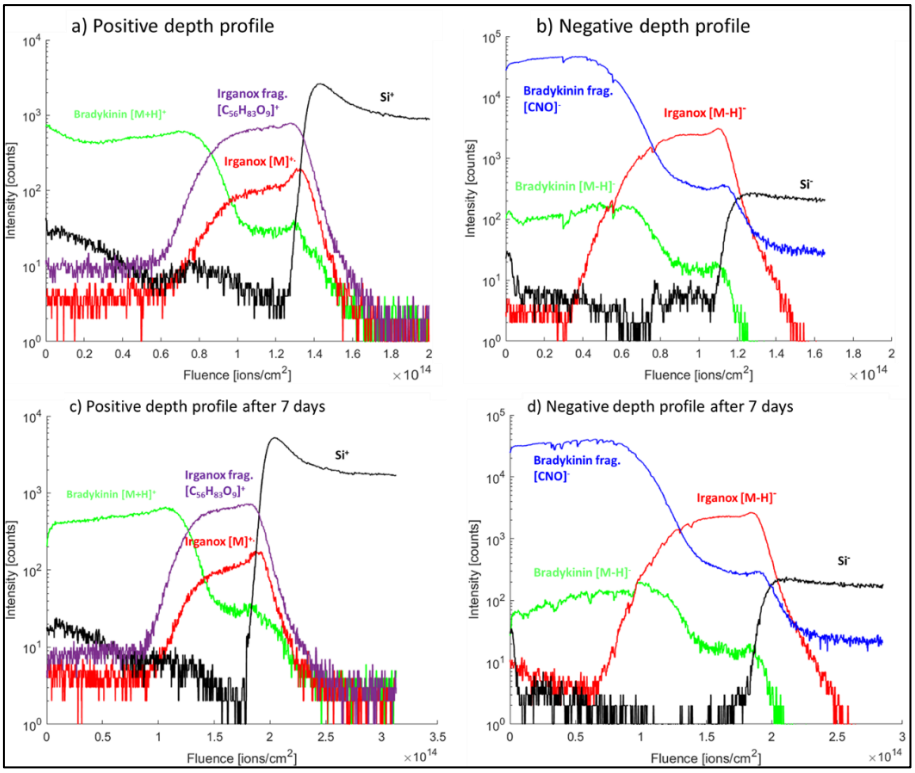


***Figure 7.2**. **a)** Positive and **b)** negative depth profiles of a mixed multilayer constructed by successive transfer of Irganox and bradykinin on a silicon substrate, using 10 keV Ar_{3000}^+. **c)** and **d)** are the profiles performed in the same fashion after the sample was exposed to air for 7 days.*

d). Those profiles look the same as the ones performed on the fresh sample, confirming the stability of the multilayer construction. The reverse multilayer, with Irganox on top of bradykinin, was also constructed. Once again, the profiles, shown in **Figure 7.3**, confirmed that the two distinct layers could be obtained. At some point, it was believed that the plateau of bradykinin observed through the Irganox layer could arise from molecular mixing occurring as the second layer was deposited onto the first one. If this was the case, then the mixing should be influenced by the kinetic energy of the transferred molecules, and so by the primary ion beam. Indeed, it was reported in the literature that the kinetic energy of the desorbed molecules vary with the E/n of the primary particles, as long as E/n is lower than 10 eV/atom.[1] Therefore, to investigate whether the transfer ion beam had an influence on the construction of the multilayers, the same bilayer was constructed with 10 kev Ar_{5000}^+ instead of 10 kev Ar_{3000}^+. In this case, the desorbed molecules should reach the collector with a significantly lower

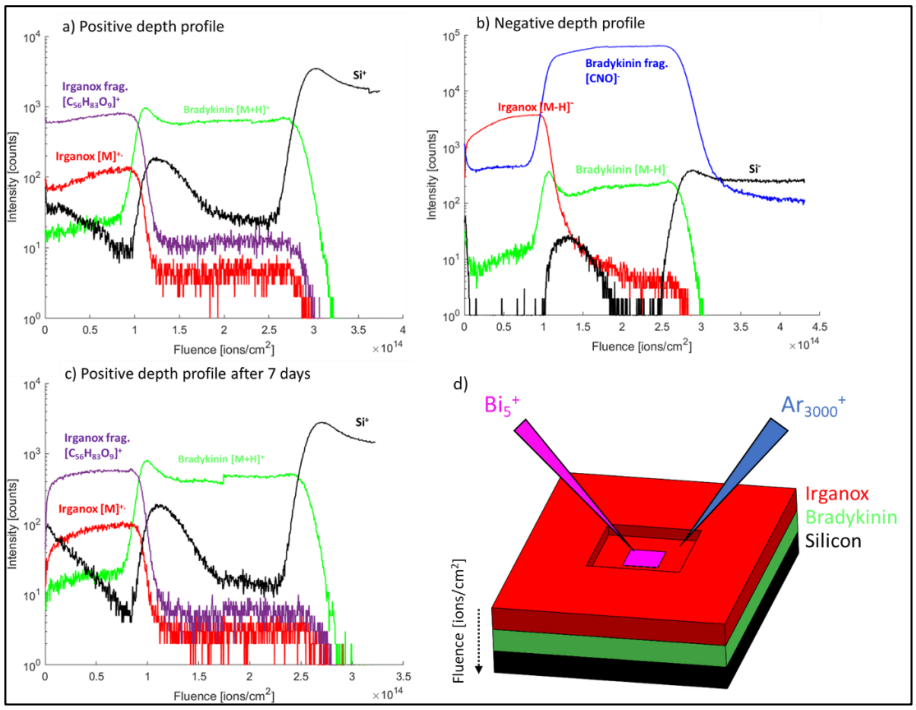


Figure 7.3. a) *Positive and* ***b)*** *negative depth profiles of a mixed multilayer constructed by successive transfer of bradykinin and Irganox on a silicon substrate, using 10 keV* Ar_{3000}^{+}. ***c)*** *Positive profile performed in the same fashion after the sample was exposed to air for 7 days.* ***d)*** *Schematic illustration of the depth profiling experiment.*

kinetic energy, hence reducing the mixing. A new bilayer was constructed, using 10 kev Ar_{5000}^{+}, with bradykinin transferred on top of Irganox. The depth profiles, displayed in **Figure 7.4**, show that the bilayer was successfully built. However, the same plateau of the bradykinin intensity through the Irganox

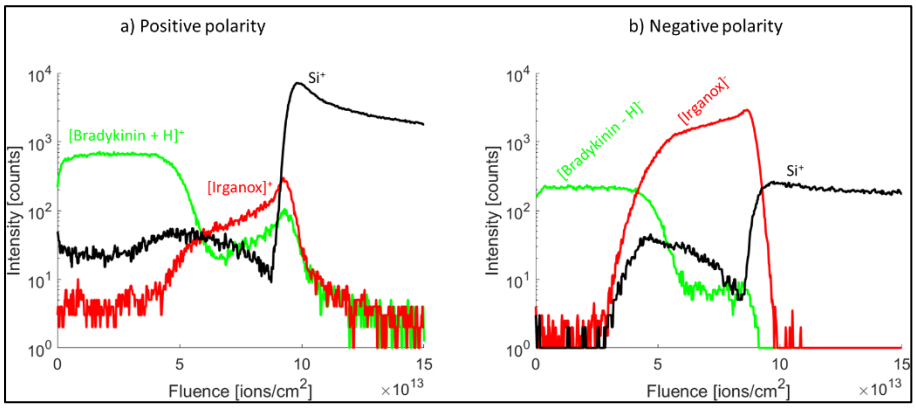


Figure 7.4*.* ***a)*** *Positive and* ***b)*** *negative depth profiles of a mixed multilayer constructed by successive transfer of Irganox and bradykinin on a silicon substrate, using 10 keV* Ar_{5000}^{+}.

layer was observed, with very similar intensities to that observed on the multilayer constructed using 10 kev Ar_{3000}^{+}. At this point mixing favored by the kinetic energy of the landing species could be eliminated.

7.3.2. A dual protein system: bradykinin/neurotensin multilayers

To explore the variety of systems that can be built using the cluster-assisted deposition approach, a dual protein multilayer was also investigated. For the first attempt, to keep the analysis simple, two proteins whose molecular ions are detectable by ToF-SIMS were chosen, namely bradykinin and neurotensin (1673 Da). These were successively transferred using 10 keV Ar_{3000}^{+}. Neurotensin was deposited on top of bradykinin. The depth profiles recorded on the collector are presented in **Figure 7.5**. Once again, the multilayer was efficiently constructed. However, this time, the interface between the two protein layers appeared very sharp on the spectra, in both polarities. No plateau was observed for any of the two proteins through the layer of the other one. On the one hand, this confirmed the previous thoughts on the absence of mixing and diffusion between the layers. If none of these is observed between the two proteins, it would be very surprising that it suddenly takes place between bradykinin and Irganox, as all these compounds have relatively equivalent masses. On the other hand, it raised the question of why a plateau of the bradykinin intensity was observed through the Irganox layer. As data regarding the behavior of neurotensin with respect to Irganox was missing, it was decided to carry out another

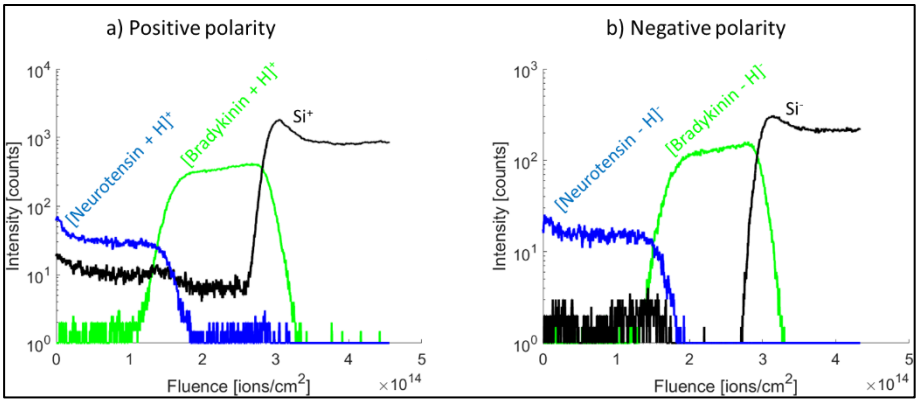


***Figure 7.5**. **a)** Positive and **b)** negative depth profiles of a mixed multilayer constructed by successive transfer of bradykinin and neurotensin on a silicon substrate, using 10 keV Ar_{3000}^{+}.*

multilayer construction. This time, three layers were deposited in the following order: bradykinin, Irganox and neurotensin. In this way, it could be possible to study simultaneously the behavior of each protein with respect to the Irganox layer. In addition, it is a step towards the demonstration that an unlimited number of layers can be deposited.

7.3.3. Towards more complex multilayers

The trilayer was built using 10 kev Ar_{3000}^+. The positive and negative depth profiles are presented in **Figure 7.6**. In negative polarity, a characteristic amino acid fragment was added, CNO^- (purple line). It makes very clear where the protein layers are. In addition, it highlights the importance of detecting the molecular ion of the proteins in order to differentiate them in the SIMS spectra. A first important remark regarding the positive polarity spectrum must be made. The Si substrate signal intensity appears with a relatively high intensity in both protein layers, while it lies in the noise for the Irganox layer. By analyzing the mass spectra specific to these three zones, it could be concluded that this observation comes from the contribution of the CO^+ ions (at m/z = 28, just like Si^+), whose intensity is particularly high in the mass spectra of proteins. In fact, without the contribution of the CO^+, the level of the Si^+ would be as low as that observed through the Irganox layer. This is confirmed by analyzing the negative polarity spectrum, where the Si^- intensity is nearly zero across all three layers, until it suddenly increases at the interface with the substrate. Next, regarding the potential mixing of the

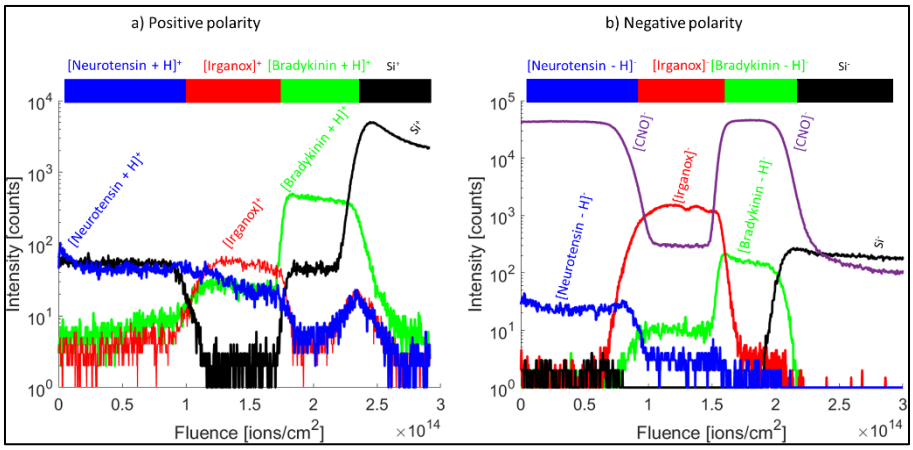


Figure 7.6. a) *Positive and* ***b)*** *negative depth profiles of a mixed multilayer constructed by successive transfer of bradykinin, Irganox and neurotensin on a silicon substrate, using 10 keV* Ar_{3000}^+.

deposited layers, this sample brought a very interesting piece of information. As can be observed, the intensity levels of both proteins are relatively high through the Irganox layer, but fall into noise as one protein reaches the other protein layer. As was previously mentioned, this observation is very unlikely to arise from mixing between the layers. To find the cause of this observation, the positive profile of the trilayer was divided into four zones, as depicted in **Figure 7.7**. For each zone, the mass spectrum was reconstructed. This data treatment allows precise comparison of the mass spectra composition of the sample at a specific depth, instead of looking at the total mass spectrum. If one compares the molecular fragment of neurotensin through these four layers, the results are particularly revealing. As one can see in **Figure 7.8**, the molecular ion peak of angiotensin is detected with a good intensity in the first zone of the spectrum (**Figure 7.8a**). However, in the second zone (Irganox layer), where the intensity of neurotensin appears relatively high in the spectrum, the molecular ion peak is not detected at all. All the ion counts correspond to noise (**Figure 7.8b**). In fact, the noise intensity level is much higher in the Irganox layer than it is the neurotensin layer. This probably originates from different sputtering dynamics as the profile goes from the protein material layer to the Irganox layer (differences in sputtering yield, ionization yield, potential charging effect, unimolecular dissociation, etc.). It is likely that the analysis mode also plays a certain role in the observation of such high noise level. The depth profiles were conducted in "interlaced mode", with a cycle time of 200 µs, meaning that within that time interval, the instruments operates the sputter beam, the flood gun, and the analysis beam. Such a short amount of time may not be sufficient to completely avoid charging issues, especially if its extent varies from one layer to another. Moving to another analysis mode, i.e. non-interlaced mode, where longer relaxation time intervals are guaranteed, may significantly reduce the noise

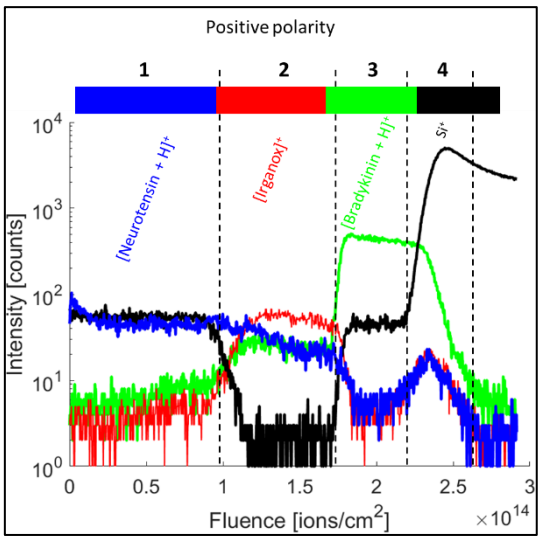


***Figure 7.7**. Subdivision of the depth profile into four zones, each corresponding to a deposited layer.*

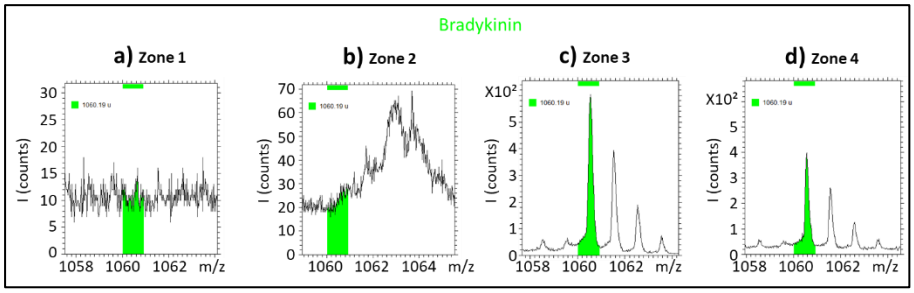


***Figure 7.8**. Molecular ion peak of bradykinin in each zone of the profile. Bradykinin is only detected in the third and fourth zone. In the other ones, its intensity is only accounted for by noise and contributions of Irganox-related peaks.*

in the spectra, and therefore should lower the protein signal intensities in the Irganox layer. As can be observed in **Figure 7.8 c & d**, neurotensin is also absent from zones 3 and 4. The exact same discussion can be made for the bradykinin (**Fig. 7.9**), with one additional point. As can be seen in **Figure 7.9b**, in the second zone (Irganox layer), a peak is observed very close to where the bradykinin is expected. However, this peak could be attributed to a fragment of Irganox. The contribution of this peak in the total ion counts accounting for bradykinin explains why bradykinin appears at a relatively high intensity (higher than the neurotensin) through the Irganox layer.

From these analyses, it can be concluded that the relatively high intensity of both protein signals through the Irganox layer are due to experimental artefacts. There is in fact no or very little mixing between the deposited layers, as the mass spectra reconstructed for each zone clearly demonstrate the absence the proteins in the Irganox layer.

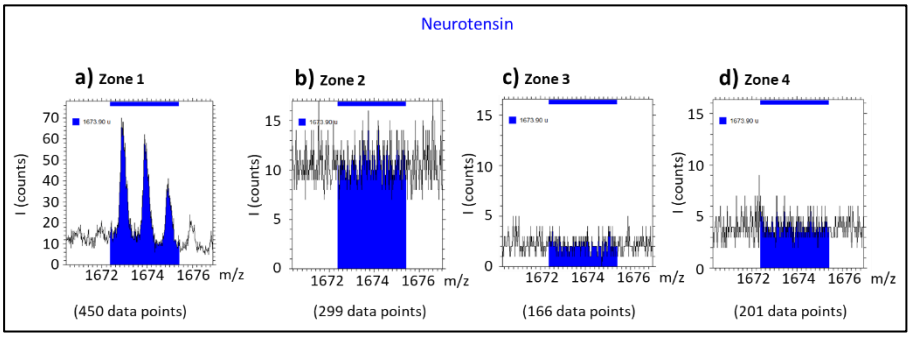


***Figure 7.9**. Molecular ion peak of neurotensin in each zone of the profile. Neurotensin is only detected in the first zone. In the other ones, its intensity is only accounted for by noise.*

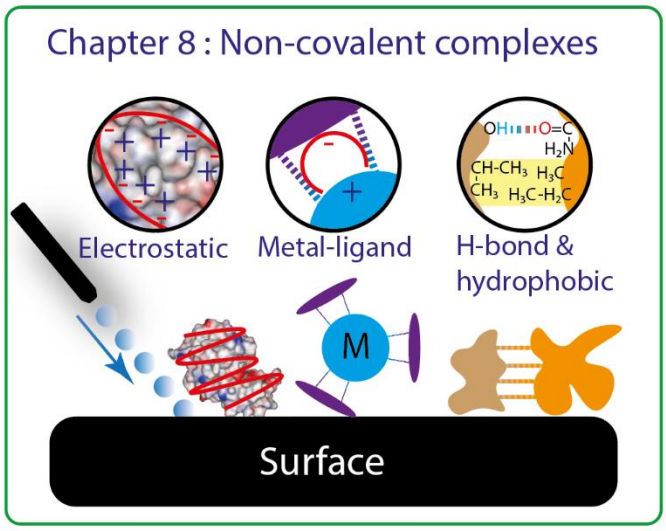
7.4. Conclusion

In this chapter, the ability of the cluster-assisted deposition approach to build alternated layers was demonstrated. Multilayers composed proteins (bradykinin and neurotensin) and Irganox were successfully constructed by successive depositions on the same collector. Bradykinin-Irganox, bradykinin-neurotensin and bradykinin-Irganox-neurotensin multilayers were achieved. SIMS depth profiles demonstrated that the multilayers were nicely constructed, as for every sample, a distinct layer for each compound was discernable. At first sight, mixing seemed to be observed, especially between the proteins and the Irganox layers. However, decomposition of the profile demonstrated that the relatively high intensity level of the proteins through the Irganox layers were arising from experimental artefacts, as no characteristic peaks of the proteins were detected in the mass spectra corresponding to the Irganox layer. Instead, for both proteins, their intensity was coming from higher noise levels in the Irganox layers. This highlights how careful one must be when interpreting SIMS data. To summarize, the deposition method developed in this worked allowed the construction of multilayers that could not be envisioned by solution-based alternatives. The layers were shown to be stable over time, even after storage for several days at ambient conditions. These results pave the way towards the construction of more complex architectures.

7.5. Bibliography

(1) Delcorte, A.; Poleunis, C. Mechanistic Insight into Gas Cluster-Induced Sputtering of Kilodalton Molecules Using Kinetic Energy Distribution Measurements. *J. Phys. Chem. C* **2019**, *123* (32), 19704–19714.

Chapter 8 : Transfer of non-covalent complexes



In this chapter, the desorption, detection and transfer of non-covalently bound complexes was investigated. First, it was envisaged to prepare and transfer protein-polyelectrolyte complexes. It was believed that trapping the proteins in polymers would provide them with a more stable environment, protecting them from the cluster impacts and favoring the transfer of intact proteins versus fragmented ones. Complexes were successfully prepared with lysozyme and trypsin, complexed to polystyrene sulfonate and poly(acrylic acid), respectively. However, their transfer failed, as no material seemed to be desorbed from the targets. In contrast, the desorption and detection of smaller organo-metallic complexes turned out to be relatively straightforward. Phthalocyanine green could further be transferred intact, while $Cr(tfac)_3$ fragments indicating loss of one ligands were identified on the collectors. It is not yet certain whether the absence of the intact $Cr(tfac)_3$ on the collector was due to loss of a ligand during transfer, or arose from favored fragmentation during analysis on the collector, due to thinner layer. Finally, a very weakly bound complex composed of vancomycin and a small peptidic ligand could be detected by ToF-SIMS. The two moieties are interacting only through H-bonds, hydrophobic and van der Waals interactions. Even though their transfer failed, the detection of such weakly bound complexes is promising, especially for the analysis of biological tissues, an expanding area of ToF-SIMS.

8.1. Introduction

Throughout the first four chapters of this manuscript, it was demonstrated how large cluster ion beams could be employed as a tool to perform the transfer of proteins and other organic molecules from one surface onto another. This approach was optimized to enable the controlled construction of biofilms. The fact that the proteins were found intact on the collectors, at least a fraction of them, indicated that covalent bonds could resist to the bombardment by low E/n cluster ions. This is of course not a breakthrough, as for more than twenty years now, large cluster ion beams have demonstrated the ability of desorbing intact biomolecules.[1] What was completely novel however is that the proteins retained their three-dimensional structure, at least partially, upon the transfer process. Even though a proposed hypothesis was that, the proteins were refolding once back into solution, it seemed unlikely that the proteins were completely denatured upon transfer. Interestingly, the 3D structure of the proteins is dictated by non-covalent interactions, such as hydrogen bonding, coulomb or polar interactions.[2] Of course, a certain degree of fragmentation is observed, but most of the bonds were not affected by the collision, desorption, or landing of the molecules on the collector. Could it be then that non-covalent interactions survive impact by large argon cluster ions? From a fundamental perspective, this observation/question is quite puzzling, and ultimately triggers the question whether this can be somehow quantified. In this chapter, the desorption of non-covalent complexes will be investigated. First, this was approached from an application point of view. Indeed, a strategy was devised to transfer proteins that were complexed to polyelectrolytes. This was envisaged as a way to protect the proteins during the transfer, and improve the fraction of intact molecules vs fragmented ones that was found at the surface of the collector. Second, the desorption of non-covalent complexes was studied in a more fundamental way. To this end, smaller non-covalent complexes, with various types of bonds, were used to study their ability to be desorbed and detected by SIMS, and further transferred.

8.2. Materials and methods

8.2.1. Turbidimetry measurement

Proteins and PE solutions were mixed in different ratios in a 96 multi-well plate, and then the absorbance of those suspensions was measured in the

420-450nm wavelength range using a spectrophotometer SpectraMax iD3 instrument. Measurements were performed in triplicate and basic statistical analyses were achieved (standard deviation and confidence interval).

8.2.2. BCA assay to quantify the complexation

A 96-well plate was loaded with 20 µL of either pure protein solutions of known and increasing concentrations for the calibration curve or of the supernatant solution recovered after centrifugation of the PPCs suspensions. Afterwards, 200 µL of BCA working reagent were added in each well. The plate was then incubated for 1 hour at 60°C before absorbance was measured at 562nm using a spectrophotometer SpectraMax iD3 instrument. Measurements were performed in triplicate and basic statistical analyses were performed (standard deviation and confidence interval).

8.2.3. Enzymatic activity assay of Lys-PSS complexes

A 96 well plate was loaded with 20 µL of either pure lysozyme solutions of known and increasing concentration for the calibration curve or with Lys-PSS complexes. 180 µL of an acetate buffer (10mM) at pH 5 and ionic strength adjusted to 10 mM with NaCl were added to each well. After that, 20 µL of a 4-methylumbelliferyl β-D-N,N,Ntriacetylchitotrioside (0.1 g/L, Steinheim, Germany) in dimethyl sulfoxide /water 2:1 (v:v) solution was added to each well. The multi well plate was then incubated 24 h at 40°C. Afterwards, 180µL were taken from each well and transferred into a black 96-wells plate and mixed with 50 µL of glycine buffer (50 mM) at pH 10,6 (adjusted with NaOH) in order to quench the reaction. Ultimately, fluorescence measurements were performed on the SpectraMax iD3 instrument, with excitation and emission wavelengths set at 360 and 450 nm, respectively. Measurements were performed in triplicate and basic statistical analyses were achieved (standard deviation and confidence interval).

8.2.4. ESI-MS analyses on “vancomycin-ligand” system

The ESI-MS measurements performed to validate the presence of the non-covalent complexes in solution were carried out on a Q-Exactive spectrometer (ThermoFisherScientific). Experiments were performed by R. Rozenberg (UCLouvain). The instrument was used with a scan type in full MS and a scan range between 300 and 1700 m/z in positive mode. The resolution

was of 140000. The spray voltage was of 3.5 kV and the capillary temperature of 300°C

8.3. Results and discussion

8.3.1. Protein-polyelectrolytes complexes to protect the proteins during transfer

Protein-polyelectrolyte complexes (PPCs), illustrated in **Figure 8.1**, have systematically been reported in the literature as efficient building blocks for the construction of protein thin films, notably via the layer-by-layer (LBL) assembly method.[3] In fact, proteins are polyampholytes, as they are composed of amino acids that can be either positively or negatively charged (or neutral). This characteristic of proteins makes them particularly tricky polymers to work with when willing to integrate them in LBL constructions. The complexation of the proteins with a polymer is an efficient way of standardizing the protein overall charge. In this way, it can be integrated into LBL more easily. As this method was developed, PPCs have been shown to provide the proteins with a highly hydrated environment, favoring the retention of their native three-dimensional structure as well as their specific activity in LBL constructions.[4] As the protein deposition approach developed in this work takes place under vacuum conditions, the possibility to maintain the proteins in relatively stable environment seemed an interesting strategy to investigate. In addition, since a polymer would surround the proteins, another benefit that could arise from these complexes is that the polymer could absorb a significant fraction of the energy transferred to the sample by the impinging argon clusters. This could result as a decrease in the fragmentation of the transferred proteins. Here, three different systems were studied to evaluate this approach. Since

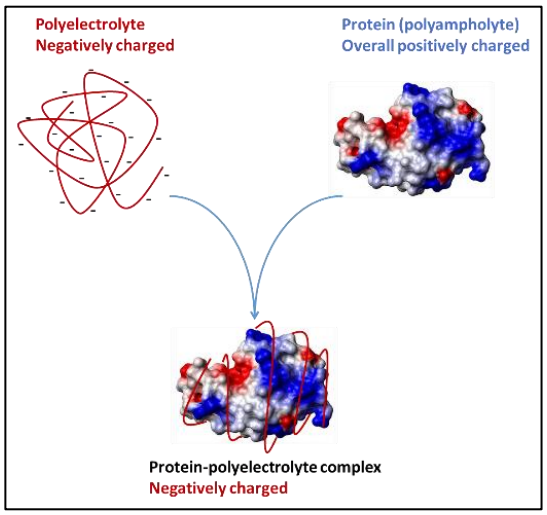


Figure 8.1. *Schematic illustration of the formation of a protein-polyelectrolyte complex by mixing a negatively charge polymer with a protein displaying an overall positive charge.*

lysozyme was previously selected as a model enzyme, and was transferred alone, it was decided to take lysozyme as protein counterpart for the first and model system. In addition, a lot of work had been previously achieved in the lab by vander Straeten with respect to the complexation of lysozyme, thus providing optimized conditions and protocols for the preparation of the complexes.[5] In parallel, two other systems were investigated, with two other proteins that were previously transferred alone as well, namely insulin and trypsin.

8.3.1.1. PPCs synthesis

As the main objective of this section was simply to use PPCs as target molecules for transfer, a thorough literature review or a detailed theory underlying PPCs would be out of the scope.[6] Only key points regarding the synthesis of the PPCs will be provided. The results regarding the preparation of the complexes will be briefly detailed for lysozyme, and provided in the form of a table for the other proteins, as the same procedures were applied. Three crucial parameters need to be finely optimized to perform an efficient protein-polymer complexation. First, the polymer must be wisely chosen, so that its charge state is suitable for the complexation in the medium conditions (mainly pH and ionic strength). Second, the buffer conditions, i.e. ionic strength and pH, in which the complexation will take place must be finely tuned. Third, the protein-polyelectrolyte ratio must be optimized. As it was reported in the literature as an efficient combination, polystyrene sulfonate (PSS), a negatively charged polymer (complexation depicted in **Fig. 8.1**) was selected as counterpart for the complexation of lysozyme.[4] In a first step, the optimal pH for the complexation was found to be 5.5. At such a pH value, the lysozyme carries a net positive charge of 10 (calculated via PROPKA software). The charge of the PSS was calculated by multiplying the charge of a monomer by the number of monomers in the chain (calculated as a ratio between the mass of the PSS chain and the mass of a single monomer, in this case 7540/206 = 36.6). Hence, PSS carries a net negative charge of

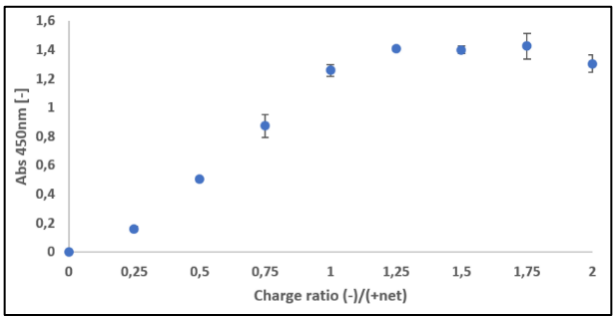


***Figure 8.2**. Turbidimetry measurement: absorbance of Lys-PSS complexes as a function of the charge ratio.*

36.6 per molecule. For the complexation, the ratio between the polymer and the protein is expressed as a net charge ratio (-)/(+). To find out the optimal ratio, the complexation was performed with various ratios and followed by turbidimetry (decrease of the transmitted light through a solution as it gets scattered by suspended particles). The results are displayed in **Figure 8.2**. As can be observed on the graph, the absorbance, and so the complexation increase with increasing (-)/(+) ratio until it reaches a plateau at a ratio value between 1.0 and 1.25. A charge ratio of 1.0 was selected to continue with the experiments.

Turbidimetry experiments give good insights regarding the optimal charge ratio for the complexation, but it only provides relative values, comparing the efficiency of the complexation of one ratio to another. To really quantify how much of the initially free lysozyme is actually complexed, another experiment is required. To answer this question, the quantification BCA assay was used. The protocol is as follows: the PPCs were prepared in small Eppendorf tubes, at pH 5.5, and at a charge ratio of 1.0. A known quantity of lysozyme was used, and that of PSS was calculated to fit the charge ratio. After complexation, the samples were centrifuged, in order to precipitate the complexes. Finally, the supernatant solution was recovered, and used to perform a BCA assay. To calculate the amount of protein complexed, one simply has to subtract that measured in the supernatant solution from the initial mass introduced in the Eppendorf tube. An example is given in **Figure 8.3**, for the complexation of 10 µg of lysozyme with PSS. A calibration line was performed on a free lysozyme solution, in blue on the graph. If no complexation had occurred, the quantity of free lysozyme detected in the supernatant solution should have been equivalent to 10 µg (red dashed line). Yet, the mass of free lysozyme was measured to be around 1.14 µg, represented by the orange data point on the graph. From this result, it could be calculated that 88.6%

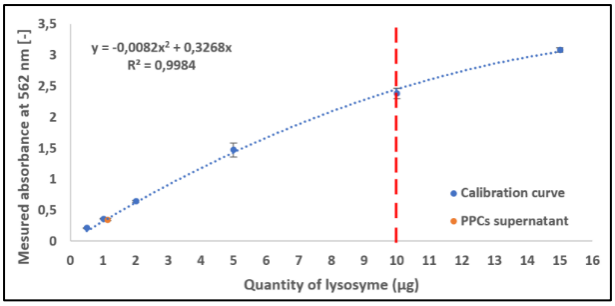


***Figure 8.3**. BCA on the supernatant solution recovered from Lys-PSS complexes. The blue data points are part of the calibration line. The red line represents the initial lysozyme mass that was present in solution. The orange data point represents the lysozyme mass detected in the supernatant solution, i.e. the mas that did not form complexes.*

of the lysozyme was complexed, demonstrating the efficiency of the complexation with PSS.

The results regarding the preparation of complexes with the two other proteins are summarized in **Table 8.1**. The same experimental protocols were followed for the determination of the charge/mass ratio and of the complexation efficiency. The polymeric counterparts were chitosan and poly(acrylic acid) (PAA) for insulin and trypsin, respectively. For the trypsin, the optimal mass ratio "protein/polyelectrolyte" was found to be 0.5, and the percentage of complexed proteins was around 82%. For the insulin, complexation with chitosan turned out to be more complicated than for the two other proteins. The turbidimetry experiments did not indicate any complexation (at any test pH conditions), while the BCA assay was biased by interaction of the chitosan with the reagent. Due to these inconveniences, insulin was discarded from the rest of the study.

***Table 8.1**. Summary of the complexation results for lysozyme, trypsin and insulin.*

Protein	Polymer	pH	Charge/Mass ratio	% of complexed proteins
Lysozyme	Polystyrene sulfonate	5.5	1 (in charge)	88.6 ± 2.2
Trypsin	Poly(acrylic acid)	4	0.5 (in mass)	82.2 ± 1.2
Insulin	Chitosan	3-7	N.A.	N.A.

8.3.1.2. Impact of the complexation on the protein activity

Before attempting to transfer the PPCs, the influence of the complexation on the activity of the enzymes had to be controlled. This was achieved for lysozyme. The same activity assay as that presented in **Chapter 6** was used. Complexes were prepared with 5 µg of lysozyme, and then compared to a calibration line performed on free lysozyme solutions. The results are presented in **Figure 8.4** (calibration line in blue, complex sample in red). The impact of the complexation was quite strong, as the PPCs demonstrated an activity equivalent to that of 2.4 µg of free lysozyme. Meaning that the specific activity of the complexed lysozyme is approximatively divided by two (this value is consistent with those reported by vander Straeten).[7] This result really challenged the use of PPCs to improve the transfer of lysozyme. Indeed, even in the ideal scenario where the presence of the polymer around

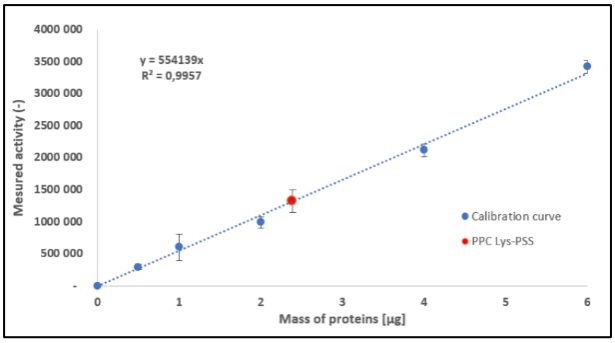


Figure 8.4. *Lysozyme activity assay. The calibration line (free lysozyme) is in blue. The red data point corresponds to lysozyme complexed with PSS. The solution was prepared with 5 µg of lysozyme, yet its activity corresponds to that of 2.5 µg of free lysozyme.*

the proteins helps by reducing the fragmentation of the proteins, if the latter are inherently less active, it does not solve the problem at all.

The above-mentioned negative effect of the complexation on the activity of the lysozyme prevents the use of complexes for the construction of stable layers. However, it was reported that the lysozymes could be released from such complexes by mixing the PPCs with the appropriate positively charged polymer.[7] This strategy could be combined with the cluster-assisted deposition method for development of drug-delivery devices and biomaterials. For the lys-PSS complexes, the positively charged poly (allylamine hydrochloride) (PAH), acts as very efficient counterpart to release the lysozymes, as it has a strong affinity to PSS. The release of the lysozymes from the complexes was investigated, and their activity was measured after their release. Complexes were prepared with 5 µg of lysozyme, and then PAH was added to the PPCs solutions. An activity assay was performed on these solutions and the results were compared to those of a calibration line performed on free lysozyme solutions. The results are shown in **Figure 8.5**. In this case, the activity measured for the "complexed" lysozyme was equivalent to that of 4.86 µg of fresh lysozyme (green data point on the graph), meaning that almost no activity loss was

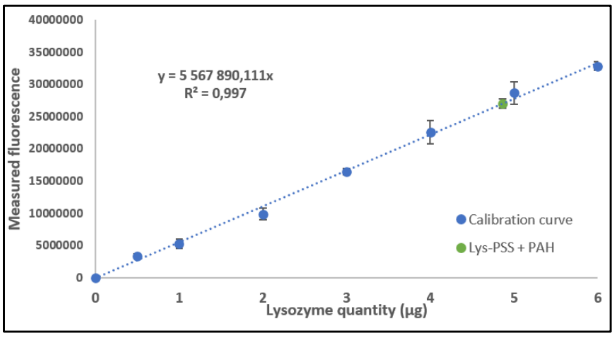


Figure 8.5. *Lysozyme activity assay. The calibration line (free lysozyme) is in blue. The green data point corresponds to lysozyme complexed with PSS, then released from the complexes by addition of PAH. The solution was prepared with 5 µg of lysozyme and its activity corresponds to that of 4.86 µg of free lysozyme.*

observed. The impact of complexation on the activity of trypsin was not investigated. Next, the transfer of PPCs using large cluster ion beams was attempted, in order to study the influence of the complexation on the fragmentation of the proteins and on the retention of their specific activity.

8.3.1.3. Transfer of protein-polyelectrolyte complexes

Targets of lys-PSS and tryp-PAH were prepared just as those made of pure proteins, by drop casting. The first transfers were achieved using a 10 keV Ar_{5000}^+ beam, in order to keep the fragmentation relatively low. At that time, the transfers were achieved using the initial transfer sample holder, with a cluster-impinging angle of 15°, and the collectors were Si wafers. As the first analysis were carried out with SIMS, it rapidly seemed that very small amounts of materials were transferred, regardless of the composition of the complexes. Therefore, transfers were also achieved with a 10 keV Ar_{3000}^+ beam, to increase the deposited quantities. 2D images of the collectors were acquired after these transfers, as illustrate in **Figure 8.6**. As can be seen, material was transferred, but on a relatively small area given the high transfer ion dose that was used. The image accounting for the substrate

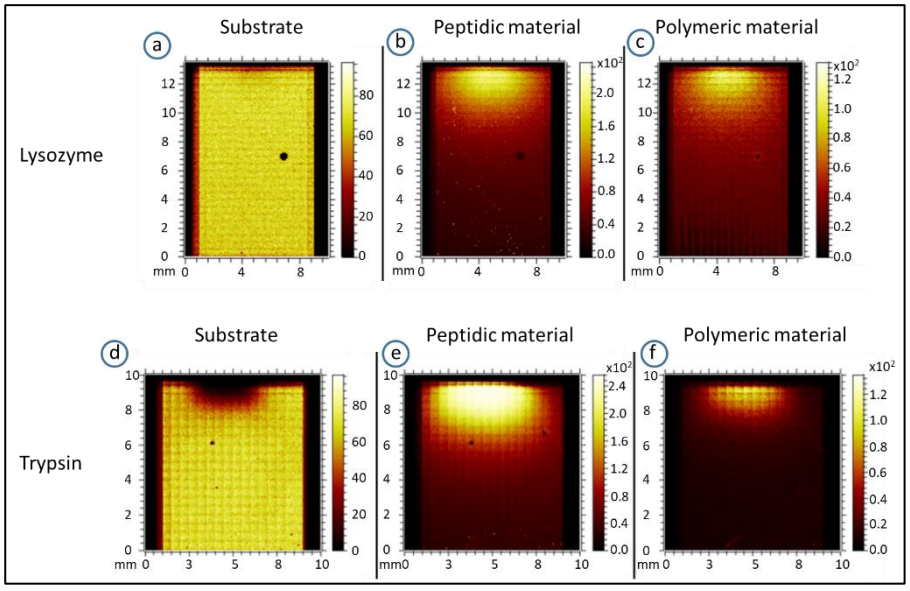


***Figure 8.6**. ToF-SIMS chemical signal intensity images, in negative polarity, after transfer of PPCs on Si wafers. Top: Lys-PSS complexes. (a) Substrate signal intensity, as the sum of Si^- and SiO_3H^- signal intensities. (b) Protein material, as the sum of CN^- and CNO^- signal intensities. (c) PSS material, as the sum of SO_3^- and $C_8H_7SO_3^-$. Bottom: Tryp-PAA. (d) Substrate signal intensity, as the sum of Si^- and SiO_3H^- signal intensities. (e) Protein material, as the sum of CN^- and CNO^- signal intensities. (f) PAA material, as the sum of CHO^-, $C2HO^-$ and $C_3H_3O_2^-$.*

intensity was only shadowed in the very top area for trypsin (**Fig. 8.6d**), while in the case of lysozyme, almost no attenuation was observed (**Fig. 8.6a**). In good correlation, the images accounting for the protein fragments (**Fig. 8.6 b & e**) and the polymer fragments (**Fig. 8.6 c & f**) display high intensities in the same top area. These images highlight the little quantities that are transferred. Few further analyses were carried out with the aim of releasing the lysozyme from the complexes and so from the collectors, for quantification and activity measurements, but did not deliver any conclusive results at all. By the time that the method to measure the deposited thickness had been developed, it was decided to investigate the deposition rate of the complexes. The Lys-PSS complexes were used. They were transferred with increasing ion doses of a 10 keV Ar_{3000}^{+} beam, and then the Bi_1^{+} analysis beam was used to investigate the thickness of the deposited layers. A graph similar to that presented in **Chapter 4** is given for the transfer of the complexes in **Figure 8.7**. As can be observed, slightly negative thickness values were obtained, most likely indicating that the deposited thicknesses were below 2 nm, where the trend line is no longer statistically relevant and cannot be used, due to substrate and ionization effects. Furthermore, no evolution was observed, indicating that the transferred quantity does not significantly increases, even when reaching high ions doses. A hypothesis that could explain these results is that the complexes do not form simple assemblies with one protein and one molecule of PSS, but rather a large polymeric network made of numerous PSS molecules with the proteins entangled in it. This is schematically illustrated in **Figure 8.8**. Therefore, the targets resulting of drying such complexes solutions would become too difficult to erode by large cluster argon beams, especially at the extremely grazing bombardment angle that was used. The PSS molecules, forming a densely packed and interlaced network, would require more energy to break the additional bonds and trigger sputtering. The proteins being trapped in the network, they should not be transferred either. A possibility to increase the desorption rate would be

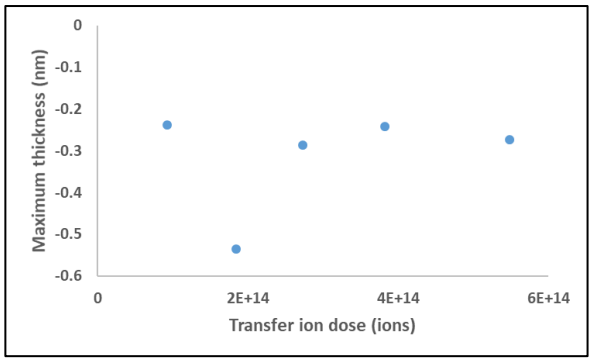


***Figure 8.7**. PSS-Lys film thickness as a function of the transfer ion dose. No increasing trend is observed.*

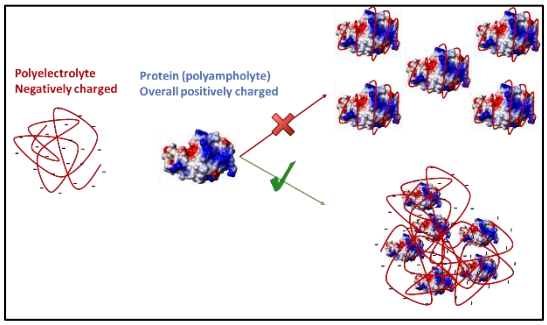


***Figure 8.8**. Illustration of the more realistic dense and entangled polymer network with the proteins trapped in it, resulting from the mixing of PSS with lysozyme.*

to increase the energy of the beam, but this would then lead to more fragmentation of the proteins, which is counterproductive. However, sputtering of polymers by large argon cluster ion beams was reported in the literature, with clusters having E/n in the same range than those used in this study.[8] Therefore, it is believed that the grazing impact angle of the clusters on the target played an important role in the absence of emission observed in this case. These experiments were not repeated using the reverse sample holder, allowing transfer with an impact angle of 45°, equivalent to that of regular analysis conditions. The outcome of such experiments might be more successful.

8.3.2. Investigating the transfer of various types of non-covalent complexes

In this final section, a more fundamental study is reported, whose goal was to gain insights into the most weakly bound complexes that could be detected by ToF-SIMS, and eventually further transferred as complexes from one surface onto another, using large argon cluster ion beams. It was triggered by an intriguing observation made during a reference analysis of an insulin spin-coated sample by ToF-SIMS. As a very long (roughly 210 min) mass spectrum was recorded with a 10 keV Ar_{3000}^+ beam, insulin dimers could be detected, at a peak emerged at an m/z around 11616 Da (which corresponds to the theoretical mass of an insulin dimer) (**Fig. 8.9**). The resolution is not sufficent to assess whether the dimer is in the form of $[M_2]^+$, $[M_2 + H]^+$, or even $[M_2 + Na]^+$. However, the observation of insulin dimers itself raises fundamental questions. It is unlikely that two independent insulin molecules that would have been desorbed apart one from another, would have then formed a dimer in the course of leaving the surface or as they were

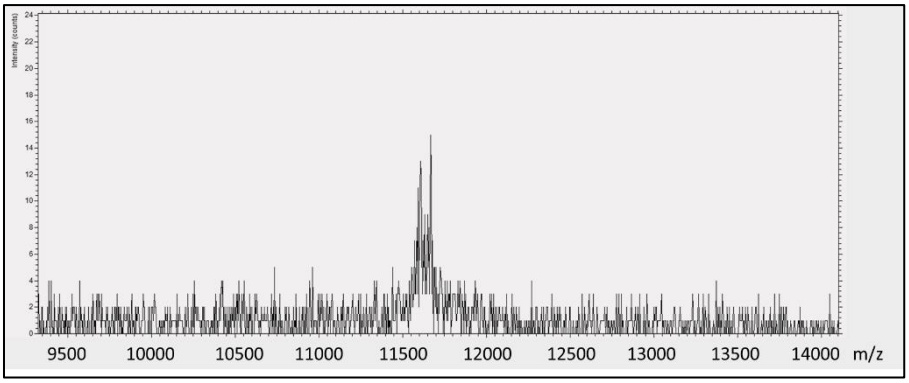


Figure 8.9. *High-mass range of a ToF-SIMS spectrum acquired on a reference spin-coated sample of insulin. The analysis beam was 10 keV Ar_{3000}^{+}. A peak at a m/z corresponding to an insulin dimer singly charged is observed.*

traveling in the field free region. The most likely explanation is that the observed dimers were formed by molecules that were neighbors at the surface, and probably already non-covalently bound.

Insulin is a small globular protein, composed of two amino-acid chains (a 21-residue A-chain, and a 30-residue B-chain), linked together by two interchain disulfide bridges, as depicted in **Figure 8.10**. One possibility to form dimers is that two proteins, in the close vicinity of one another, simultaneously see one of their disulfide bridge being disrupted, and further react with each other to create a disulfide bridge between the two insulin molecules. If this is in theory not impossible, the chance that it actually happens is extremely low. Therefore, the most logical explanation to the formation of dimers is that the two intact insulin molecules bond to each other via non-covalent interactions. These interactions include hydrogen bonding, ionic interactions, metal-ligand coordination, π-interactions, van der Waals interaction and

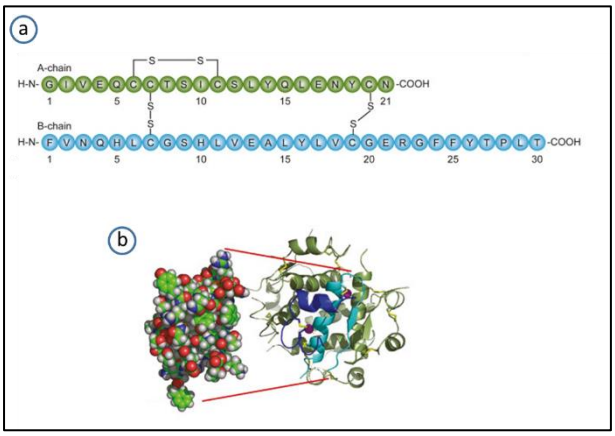


Figure 8.10*. Schematic representation of insulin. (a) Primary structure, highlighting the presence of two chains, and three intramolecular disulfide bridges. (b) 3D representation of insulin.*

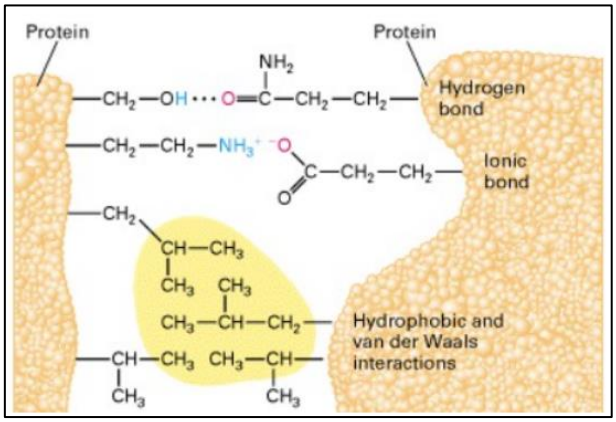


***Figure 8.11**. Schematic representation of the various weak interactions usually observed between two proteins. These are hydrogen bonds, ionic bonds, hydrophobic and van der Waals interactions.*

hydrophobic interactions. They are weak in comparison to covalent bonds, which involve intimate electron sharing. The strength of the non-covalent bonds usually arises from their multiplicity and diversity. In fact, the formation of a non-covalent complex very likely results from a multitude of non-covalent interactions, and in most cases originates from the combination of different ones. All the cited non-covalent interactions can be observed when studying protein dimers, depending on the protein nature and chemical composition. However, the most common ones are hydrogen bonding, ionic bonding, van der Waals interactions and hydrophobic effect, as illustrated in **Figure 8.11**. In the case of insulin, it is mostly these interactions that come into play. The fact that two distinct molecules bound by such low energy interactions could be desorbed as intact complexes by large argon cluster ion beams attracted our attention, and it was decided to test other systems, bonded by other types of interactions. The systems that were investigated were metal-ligands complexes, bonded by relatively strong interactions, and an antibiotic-ligand system, known to be only weakly bonded by few hydrogen bonds.

8.3.2.1. Organo-metallic complexes

There exists numerous different systems composed of metals complexed to organic ligands. The ones chosen for this study were first the phthalocyanine green, a copper complex of formula $Cu(C_{32}N_8Cl_{16})$ (**Fig. 8.12**), and second a series of metal trifluoroacetylacetonate complexes, later referred to as $[M(tfac)_n]$ (**Fig. 8.14**). These complexes represent a good starting point as the ligands are linked to the metal center via two bonds, making them relatively robust in comparison to other complexes not displaying any chelate effect.

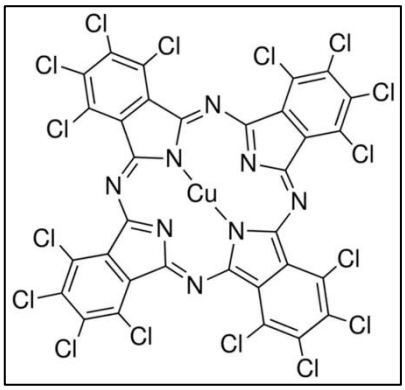


***Figure 8.12**. Structure of the phthalocyanine green.*

The phthalocyanine green was the first complex to be investigated. It is a synthetic green pigment from the group of phthalocyanine dyes, a complex of copper (II) with chlorinated phthalocyanine used in oil and acrylic based paints. SIMS reference spectra were recorded on fresh spin-coated samples, using 30 keV Bi_5^+ analysis beam. **Figure 8.13a** shows the mass spectrum in the mass range of the molecular ion. The intact complex is detected with high intensity, as well as the complex having lost up to four chlorine atoms. The phthalocyanine green was then

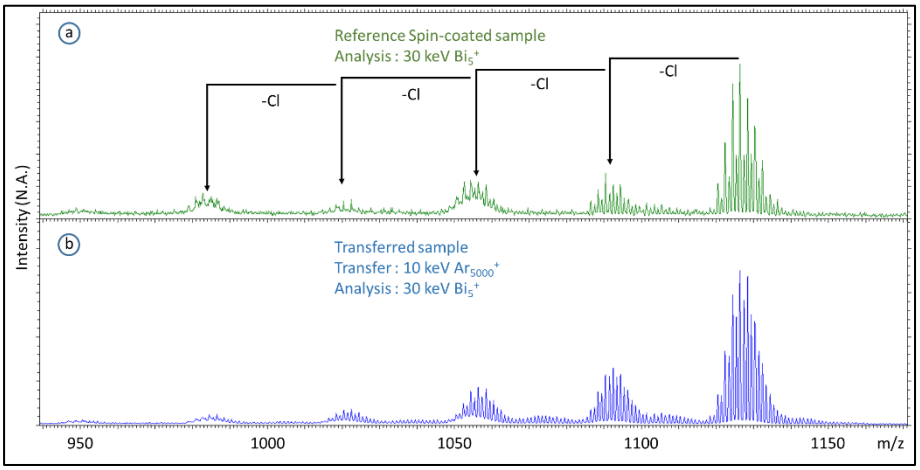


***Figure 8.13**. ToF-SIMS mass spectra of phthalocyanine green, in positive polarity. **(a)** Reference spin-coated sample. **(b)** Transferred sample. In both cases, the intact molecular ion of the complex is detected with high intensity, as well as loss of a few Cl atoms.*

transferred, using 10 kev Ar_{5000}^{+}, onto a Si collector. SIMS analysis were finally carried out on the collector, using the same analysis beam as for the reference spectrum. Satisfyingly, as illustrated in the spectrum of **Figure 8.13b**, the intact complex was detected just as on the reference sample, indicating that the compound was mostly transferred without loss of the metal center or of the ligand, even fragments of it.

To investigate other types of complexes, a selection of four $[M(tfac)_n]$ complexes (**Fig. 8.14**) were initially screened for this study, these are chrome-, nickel-, cobalt- and copper-based complexes. The complexes were kindly provided by Pr. S. Hermans (IMCN, UCLouvain), and were synthesized by chemistry students during practical classes. In the first place, all the complexes were analyzed by SIMS, as spin-coated samples, in order to investigate their ease of detection, and chose one or two candidates for transfer experiments, which were conducted in the second place.

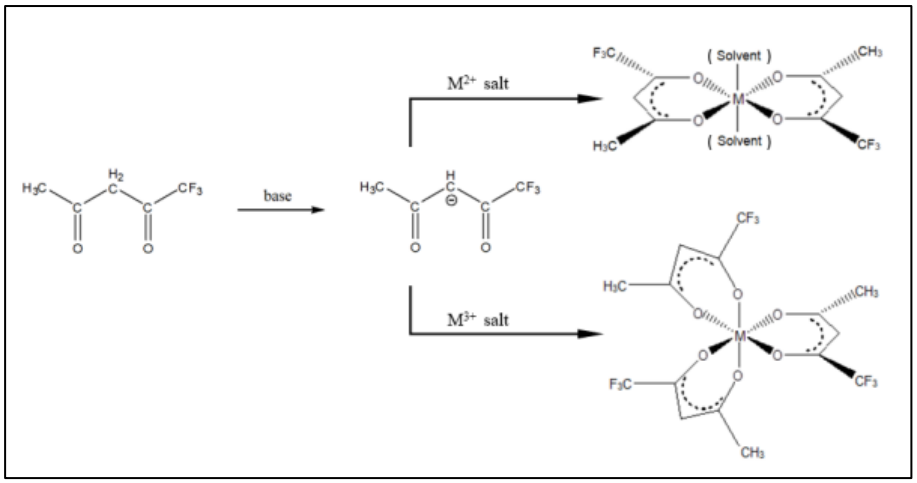


***Figure 8.14**. Synthesis pathway of $[M(tfac)_n]$ complexes (with n = 2 or 3), along with their general structure.*

Solutions of all four complexes were prepared, and spin-coated onto Si wafer. These samples were analyzed by ToF-SIMS. Given that their mass do not exceed a few hundred Da, the analysis was initially carried out using the 30 keV Bi_5^{+}. The complexes were studied both in positive and negative polarities. If the metals are usually detected in positive polarity, as they easily form cations, the tfac ligand is negatively charged, and should therefore be detected in negative polarity. **Table 8.2** gives the expected molecular mass (calculated based on the most abundant isotope of each element) of each of the complexes, with the metal atom bearing one, two or three ligands. In

general, the spectra obtained for these compounds were quite complex, with tens of high intensity peaks to m/z up to 700-800. Precisely attributing each peak to a fragment would have been time-consuming, and complicated, as the received complex powders were certainly not 100 % pure, so that contaminations could also participate in the complexity of the spectra. Therefore, it was decided to focus on the fragments given in **Table 8.2**, and their ions, including protonated and deprotonated species.

***Table 8.2**. Expected molecular mass for the different complexes. Calculated based on the most abundant isotope of each element.*

	Cr	Ni	Co	Cu
1 tfac	204.96	210.95	211.94	215.95
2 tfac	357.97	363.97	364.96	368.96
3 tfac	510.99	516.98	517.98	521.98

Among the four investigated complexes, three turned out to yield spectra that were very complicated to interpret. $Ni(tfac)_2$, $Co(tfac)_2$ and $Cu(tfac)_2$ could at first sight be detected intact, with their two ligands, but taking a closer look at the spectra, they were detected with small mass shifts. To this point, the origin of these mass shifts could not be explained. It might arise from degradation or rearrangements of the molecules. On the other hand, $Cr(tfac)_3$ yielded much nicer spectra, including a deprotonated $Cr(tfac)_3$ peak, as shown in **Figure 8.15c**, in the negative spectrum. The peaks at masses corresponding to the complex having lost one and two ligands were also detected with a high intensity as positive ions (**Fig. 8.15, a & b**). The two complexes have lost at least one negatively charged ligand, and so are inherently positively charged. They do not require any proton transfer or salt adduct to gain a positive charge. In contrast, $Cr(tfac)_3$ must lose a proton to result with a negative charge. Ionization mechanism is probably the reason why $Cr(tfac)_3$ could not be detected in positive polarity. Peaks with relatively high intensity were found in the spectrum well above the mass of $Cr(tfac)_3$. Some of these groups of peaks displayed an isotopic distribution similar to that of a compound containing two chromium atoms, supporting the hypothesis that just as proteins, non-covalent multimers of these complexes could be desorbed. These peaks could also result from reactions that are taking place between the complex molecules, either before the analysis, or promoted by the bombardment with the energetic clusters, or from contaminations.

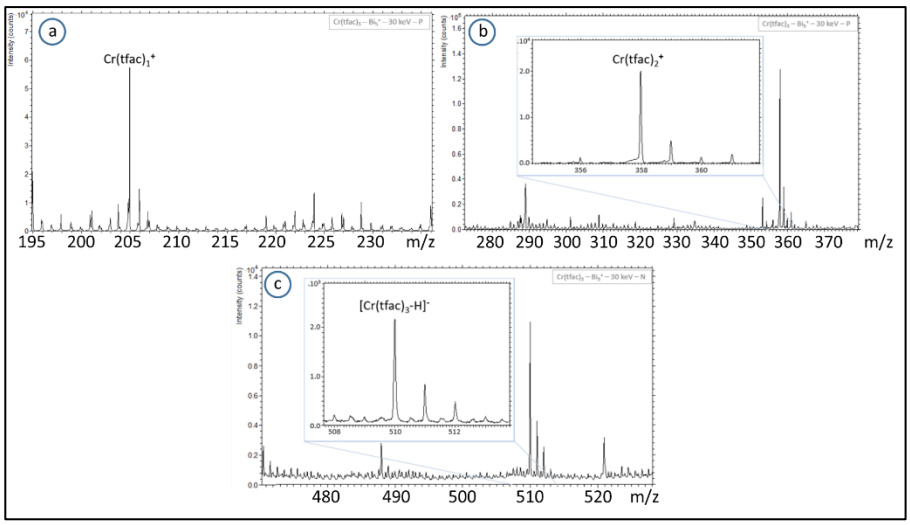


Figure 8.15. *ToF-SIMS mass spectra recorded on a reference spin-coated sample of $Cr(tfac)_3$. Spectra were obtained with 30 keV Bi_5^+ analysis beam. In positive polarity, the complex having lost one (a) and two (b) ligands are well detected. In negative polarity, the intact original complex bearing its three ligands (c) was detected with good intensity.*

Next, the transfer of these complexes was investigated. To this end, targets were prepared by evaporating $Cr(tfac)_3$ solution on Si wafers, following the same procedure as that detailed previously. In the first place, a 10 keV Ar_{5000}^+ was used for the transfer, in order to begin with soft bombarding conditions. Si wafers were used as collectors. After the transfer, they were first imaged using the mosaic mode of the instrument, and then regular spectra were recorded for the sake of qualitative analysis. As the large 2D images very much resemble many of those previously reported, they are not shown and discussed in this section. Briefly, they allowed determining that material was efficiently transferred to the collector, as the Si^+ substrate signal intensity was shadowed on a large area. More relevant information was found in the spectra recorded in the same fashion as those obtained on the reference samples (30 keV Bi_5^+ analysis). In the positive mode, Cr(tfac) and $Cr(tfac)_2$ could be detected with high intensity (**Fig. 8.16**), just as they were in the reference spectrum. As $Cr(tfac)_3$ was not detected in the positive reference spectrum, it was not expected to be further detected on the collector. However, in negative mode, the intact complex, i.e. the metal atom bearing its three ligands, could not be detected. Two hypotheses can be given to explain the absence of $Cr(tfac)_3$ in the mass spectrum. First, it could indicate that large cluster ions failed at transferring intact complexes. Yet, this would be quite puzzling, as the complexes were shown to be efficiently desorbed

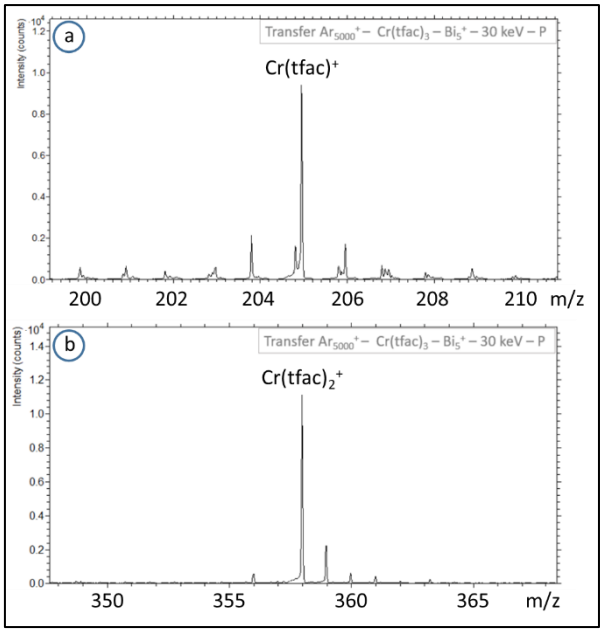


***Figure 8.16**. ToF-SIMS mass spectra recorded on a collector after transfer of $Cr(tfac)_3$ with 10 keV Ar_{5000}^+. Spectra were obtained with 30 keV Bi_5^+ analysis beam. In positive polarity, the complex having lost one **(a)** and two **(b)** ligands are well detected. The intact original complex bearing its three ligands could not be detected, whatever the polarity.*

intact by much more energetic Bi_5^+ cluster ions, known to be more destructive. Second, it could be that intact complexes were transferred to the collector, but that they could not be detected. Reasons for that could include too small transferred quantities (low deposition of the 15° transfer geometry). As a direct consequence of a low deposition rate, the resulting film would be very thin at the surface of the collectors, possibly impacting the sputtering yield, the ionization yield/mechanism and favoring the emission of fragments versus intact molecules. In order to make sure that the absence of intact $Cr(tfac)_3$ in the mass spectrum recorded on the collector does not arise from changes in the analysis conditions, characterization of the collectors, notably in terms of thickness, should be performed. In addition, transfer on soft polymers could be investigated, to avoid dealing with the influence of a hard underlying substrate. Performing the transfers using the 45° transfer geometry would also certainly help, as more material would be deposited and available for analysis.

8.3.2.2. Vancomycin ligands complexes

In parallel, weakly bound non-covalent molecular complexes were investigated. The model system was picked in the literature, as a series of studies attracted our attention. Commencing the year 1999, Jørgensen et al. investigated the molecular recognition between glycopeptide antibiotics and bacterial receptor peptides, by means of electrospray ionization mass spectrometry.[9–14] The interactions between the antiobiotic and the ligands were non-covalent, mostly relying on hydrogen bonding and to a lesser extent on electrostatic and hydrophobic interactions. One of their system involved vancomycin, to be tested against several small peptide cell-wall analogs, such as *N,N'*-diAc-Lys-D-Ala-D-Ala (KAA) and *N*-Ac-D-Ala-D-Ala (AA), as depicted in **Figure 8.17a**. Using ESI-MS, they were able to detect the complexes in the mass spectra (**Figure 8.17b**), and following the complexation of the vancomycin molecules with the different peptides allowed determining binding constants. Even though ESI is reported as a much softer ionization source than SIMS, it was decided to investigate whether suitable conditions could be found in order to detect such weakly bounded complexes using a ToF-SIMS instrument, and potentially further carry out similar quantitative studies or transfer them using GCIBs. The simple fact of detecting such biologically relevant non-covalent complexes could be seen as a major breakthrough for the analysis of biological tissues.

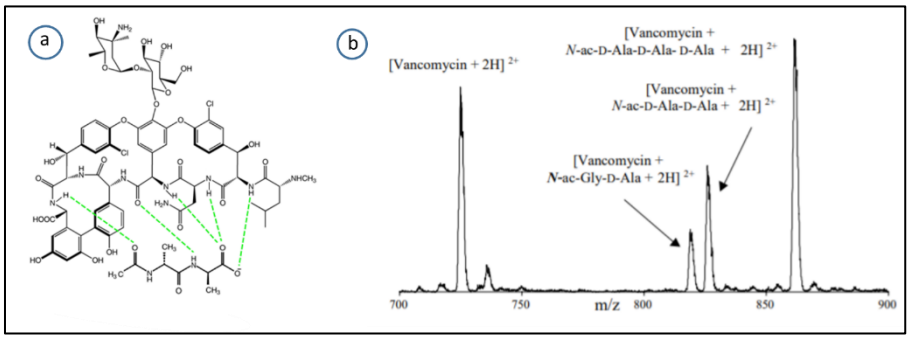


***Figure 8.17**. **(a)** Chemical structures of the vancomycin and the KAA peptide, with highlighted in green the five hydrogen bonds expected as they form a non-covalent complex. **(b)** ESI mass spectrum of the complex, obtained by Jorgensen et al.[10]*

In the first place, SIMS reference spectra were recorded on each compound to be involved in the complexes, to make sure that they were detectable. In fact, SIMS spectra of vancomycin were previously reported in the literature, so it was just a matter of control.[15] Spin-coated samples were prepared, and the mass range of interest of the resulting mass spectra are shown in **Figure 8.18**. The same results were obtained in the negative polarity, but are not shown here. Two observations are worth mentioning regarding the reference spectrum of vancomycin. First, the molecular ion is detected as a mixture between $[V + H]^+$ and $[V + Na]^+$. Second, just as was demonstrated for insulin previously, dimers of vancomycin were detected in the spectrum. Interestingly though, if the vancomycin monomer signal intensity was roughly equally distributed over the proton and the sodium adduct, the dimer was almost only detected as a proton adduct. A small bump is visible in the spectra at a slightly higher m/z value, but its intensity is extremely small. This illustrates once again the complexity of the ionization mechanisms and probabilities encountered in SIMS, which can be different even for very similar molecules. Yet, the observation of dimers in the spectrum again demonstrates the ability of SIMS to desorb intact non-covalent complexes, only held together through hydrogen bonding, electrostatic and hydrophobic interactions.

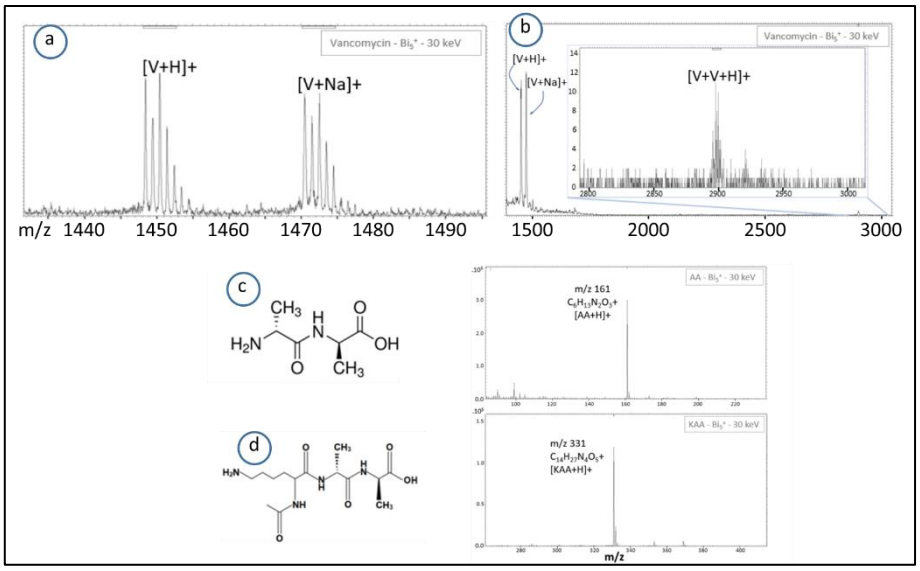


***Figure 8.18**. ToF-SIMS mass spectra of reference spin-coated samples of **(a)** & **(b)** vancomycin, **(c)** D-Ala-D-Ala ligand and **(d)** acetyl-L-Lys-D-Ala-D-Ala.*

To investigate if vancomycin-ligands complexes were detectable by ToF-SIMS, complex solutions were prepared with either AA or KAA as counterpart. For the first few trials, the solutions were prepared following the procedure reported by Jørgensen et al, which leads to equimolar solutions of both compounds, in 66.67 µmol/L concentration. The solution was then spin-coated on Si wafers and mass spectra were recorded with 30 keV Bi_5^+, 10 keV Ar_{1500}^+ and 10 keV Ar_{3000}^+, in both positive and negative polarities. Despite increasing the analysis time up to a few hours, no sign of the complex arose in any mass spectrum, regardless of the primary ion beam. The absence of the complexes could be explained by a multitude of factors other than simply assuming that complexes were present at the surface, but could not be desorbed intact by any primary ion beam. Other hypotheses include: (i) Complexes not forming properly in solution; (ii) Solution concentration too low leading to very small quantities deposited at the surface by spin coating, ultimately leading to ultra-thin layer. Consequently, the complexes could be under the detection limit, or the close vicinity of the underlying hard Si substrate could significantly promote the dissociation of the complex upon bombardment by the primary ions. (iii) Ionization issues could be encountered. (iv) The complexes could be desorbed intact, but dissociate in the course of leaving the surface, or while travelling towards the detector. This hypothesis is supported by the fact that in the complex, there is a significant mass mismatch between the two components, as vancomycin is roughly 10 and 5 times heavier than the ligand, in the case of AA and KAA, respectively. This could favor dissociation of the complex under centrifugal effect. For all these reasons, it was decided to carry on with the analysis of the complexes, and explore a large set of experimental conditions by varying the solution concentration, the layer thickness and the substrate nature.

First, the formation of complexes in solution was validated. The same complex solutions were prepared, and analyzed by ESI-MS. The results, shown if **Figure 8.19**, demonstrate that both complex, [V + AA] and [V + KAA] were present in solution. Knowing this, the first parameter tuned was the layer thickness. The goal was to increase it, in order to both increase the amount of material available for analysis, and reduce the influence of the underlying hard substrate. To do so, solution concentration was increased from 66.67 µmol/L to 1mmol/L, and the solution was spin-casted instead of spin-coated, which should ultimately result in much thicker layers. The samples were once again analyzed using the same three primary ions beams as before. Despite many efforts, the complex [V+AA] could never be detected. However, the hope persisted for the [V+KAA] complex, as a peak seemed to slowly arise around an m/z of 1780 after one hour of analysis under 10 keV Ar_{3000}^{+} bombardment, as depicted in **Figure 8.20**. The fact that [V+KAA] is more likely to be detected than [V+AA] could be explained by two factors: (i) the mass-mismatch is significantly more important between vancomycin and AA; and (ii) the lysine moiety present in the KAA allows the formation of five hydrogen bonds with the vancomycin molecules, whereas AA is only able to make four of them. It was thus decided to continue with studying only the [V+KAA] complex, which seemed more likely to be detected.

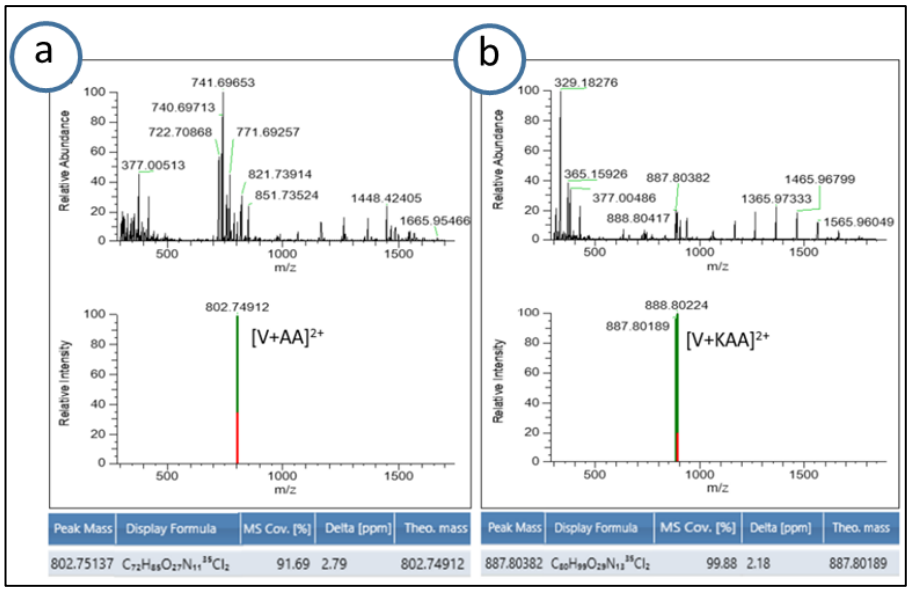


***Figure 8.19**. ESI mass spectra of complexes (a) V + AA and (b) V + KAA. The complexes were both detected at their exact expected mass.*

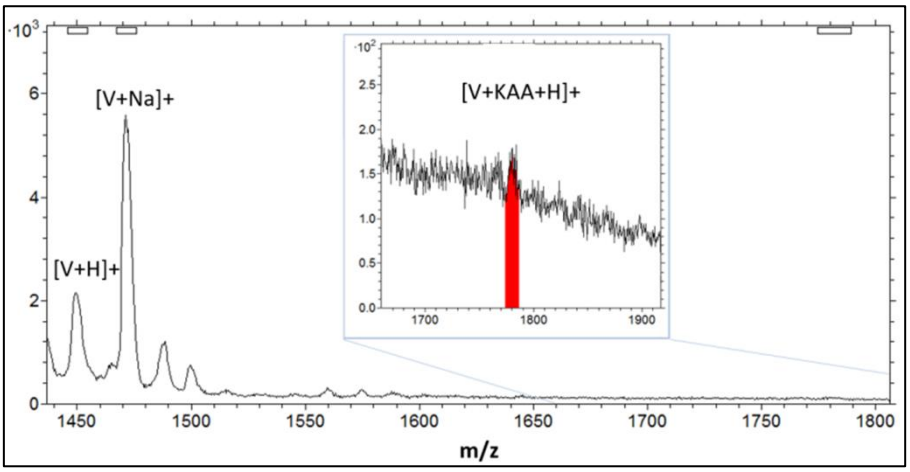


***Figure 8.20**. First ToF-SIMS mass spectrum tending to show that the complex V + KAA could be detected intact. Analysis beam was 10 keV Ar_{3000}^+.*

Increasing the thickness already yielded an improvement in the detection of the complexes, but was still far from optimal. As could be observed in the mass spectra, the peaks accounting for the molecular ion of vancomycin always displayed a much higher intensity, probably mirroring the solution composition. In order to promote the complexation, and so the ratio complex to vancomycin, complex solution were prepared with increasing ligand concentration, in order to reach vancomycin/ligand ratios of 1:2, 1:5, and 1:8. All these solutions were analyzed by ESI-MS in the same conditions, and the resulting spectra were compared to that of the 1:1 solution (**Figure 8.21**). As can be observed, the ratio complex/vancomycin increases as the ligand concentration increases. However, a multitude of non-attributed peaks, possibly originating from contamination present in the ligand solution followed the same trend, with an even more impressive increase, rapidly dominating the mass spectrum. Therefore, it was decided to carry on using a 1:2 ratio.

1:2 ratio solutions were drop-cast and analyzed by SIMS. This time, results were much better, and the complex $[V+KAA]^+$ could be detected by both 10 kev Ar_{3000}^+ and 10 keV Ar_{1500}^+, as showed in **Figure 8.22, a & b**. The two spectra were recorded on the exact same sample, yet they display few discrepancies between them. First, in the spectrum obtained with Ar_{1500}^+ (**Fig. 8.22a**), the molecular ion peak appeared as a doublet, just as if an adduct was also detected (denoted $[V + X]^+$). This peak duplication was also observed for the $[V + Na]^+$ and for the $[V+KAA]^+$ peaks. These peaks were not observed

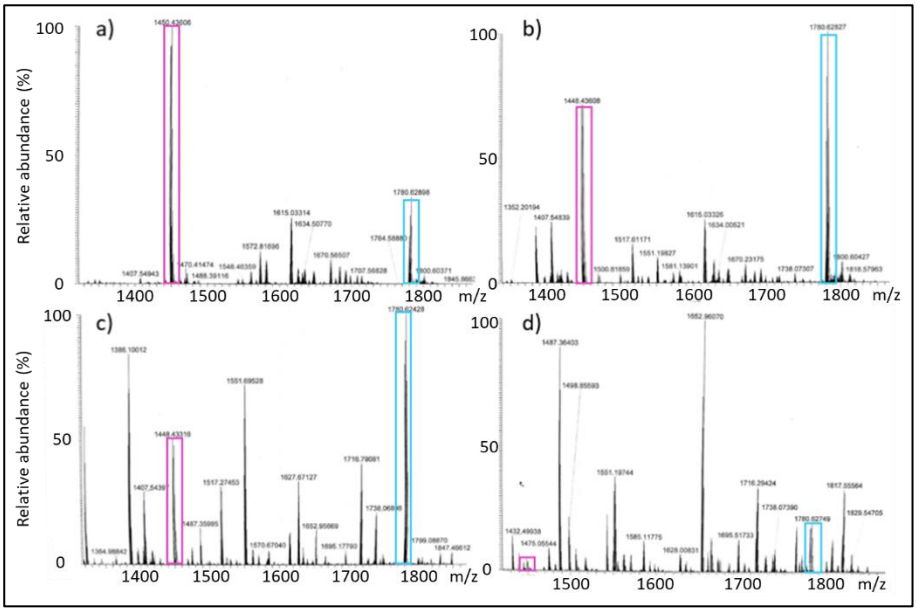


***Figure 8.21**. ESI mass spectra of V + KAA complexes with increasing KAA ratios. The V : KAA ratios are (a) 1 : 1, (b) 1 : 2, (c) 1 : 5 and (d) 1 : 8. Boxed in magenta is the molecular ion peak of vancomycin. Boxed in blue is the peak accounting for the complex [V+KAA].*

in the spectra obtained with Ar_{3000}^+. It is hardly possible to consider that chemical reactions and rearrangements that take place under 10 keV Ar_{1500}^+ bombardment would not be observed under 10 keV Ar_{3000}^+ bombardment. A plausible explanation to this observation would be that these peaks result from a local contamination on the surface. The mass difference, + 6 amu compared to the $[V + H]^+$ complex, could possibly correspond to the hydrogen atom being replaced by a lithium atom, which is an adduct often seen in ToF-SIMS. However, the lithium peak intensity is rather low in the spectrum, therefore this hypothesis should not be taken for granted and additional experimental work should be undertaken to confirm these initial results. In addition to this peaks duplication observed in the Ar_{1500}^+ spectrum, another unattributed peak was detected with relatively high intensity, but this time under both Ar_{1500}^+ and Ar_{3000}^+ analysis beams. Indeed, a peak (duplicated in the case of Ar_{1500}^+) was detected at an m/z around 1820. This molecular species could not be identified, and could arise from adduct formation with a degradation product of either the vancomycin or the ligand moiety present in solution.

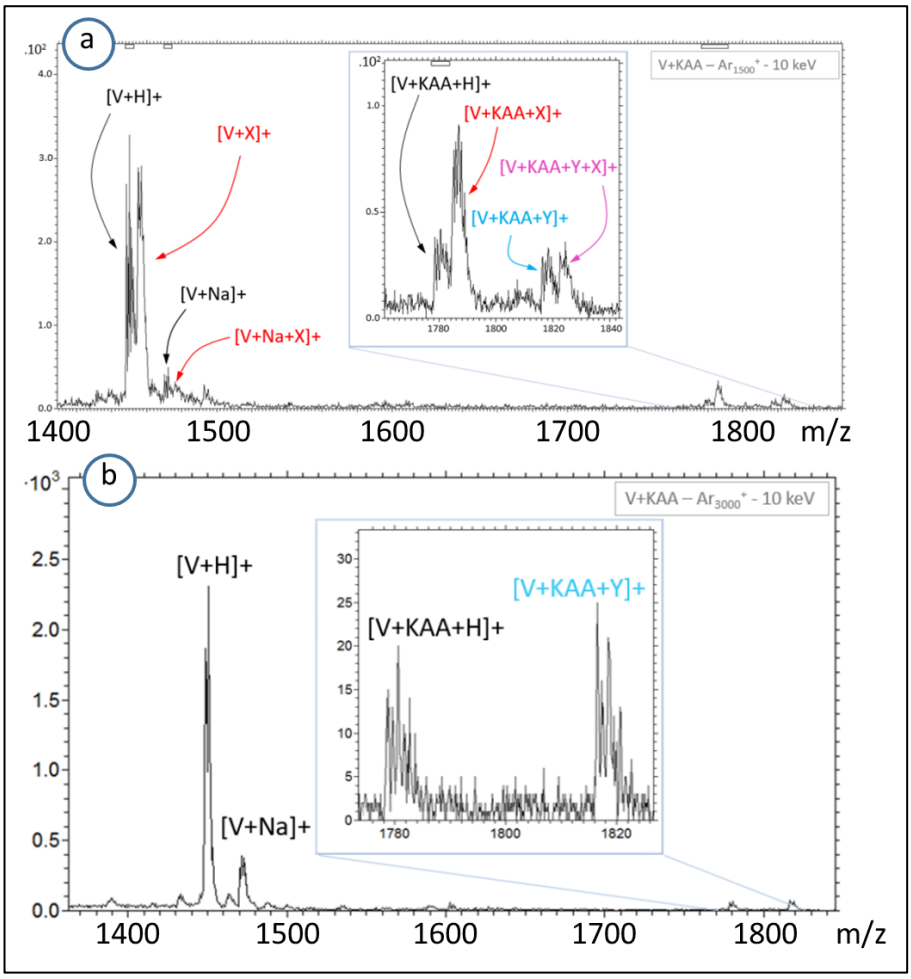


Figure 8.22. ToF-SIMS mass spectra of V + KAA complexes. (a) Using 10 Ar_{1500}^+ as analysis beam. (b) Using 10 Ar_{3000}^+ as analysis beam.

Finally, as the complexes could now be detected, it was attempted to transfer them from one surface onto another, and investigate whether they could further be detected intact on the collector surface. Si wafers were used as collectors. Unfortunately, complexes could never be detected after transfer with 10 keV Ar_{3000}^+ and 10 keV Ar_{5000}^+. In all cases, the molecular ion of both the ligand and the vancomycin were detected separately in the mass spectrum, indicating that both compounds could be transferred intact. If there is a possibility that the transfer of these complexes simply does not work, the fact that they are not detected could also results from the same problems as those encountered before, especially that of the thickness. The complexes were transferred using the 15° geometry, so that the deposited

layers were probably very thin. In these conditions, the underlying Si substrate could have a significant impact on the measurements. It could be worth attempting these experiments either using the 45° geometry, in order to transfer more material and so build thicker layers, or to transfer the complexes on soft polymer collectors, to avoid the influence of an underlying hard substrate.

8.4. Conclusion

In this chapter, non-covalent complexes were investigated. On the one hand, protein-polyelectrolyte complexes were prepared, with the objective of improving the transfer of intact and bioactive proteins using large argon cluster ion beams. Two complexes were successfully assembled, i.e. Lys-PSS and Tryp-PAA. However, the targets prepared with such complexes proved to be very difficult to erode with the low energy per atom cluster ions. Indeed, thickness measurements revealed no increase in the deposited quantities even as high transfer ion doses were reached. It is likely that the grazing impact angle of the primary ion beam on the target had a pronounced effect on the desorption efficiency. Using the 45° geometry could probably deliver significantly different results. However, even in the case were it does slightly improve the desorption, the later would always be lower than that observed for proteins alone. In the ideal case were the fragmentation and denaturation would be decreased by the presence of the polymer, this advantage would be balanced by the lower deposition rate. To increase the transfer rate, one would need to increase the energy per atom, which would in turn increase the fragmentation. Therefore, it is not believed that preparing PPCs for the transfer of proteins is a valuable approach worth devoting much more efforts. On the other hand, a study was led to investigate whether small non-covalent complexes could be desorbed intact from a surface and detected by ToF-SIMS. From a fundamental perspective, the detection of non-covalent complexes could be very powerful for biological tissues analysis, especially in combination with 2D imaging. With respect to the developed transfer method, this would provide insights into the most weakly bound complexes that could be transferred in vacuum from one surface onto another. It was demonstrated that organo-metallic complexes of general formula $[M(tfac)_n]$ could be desorbed intact. After being transferred, Cr atoms bearing one and two tfac ligands could be detected on the collectors, but never the intact original complex with its three ligands. However, absence of detection could arise from thickness or

ionization issues, and do not necessarily indicate that complexes were not transferred intact. In addition, another type of organo-metallic complex, the phthalocyanine green, a copper-based complex, could be transferred intact using 10 keV Ar_{5000}^{+}. Finally, it was demonstrated that a biologically relevant non-covalent complex, i.e. vancomycin-ligand, could be detected by ToF-SIMS even though the two moieties are only bound through H-bonding, electrostatic and hydrophobic interactions. The conditions needed to be optimized in order to allow detection, clearly indicating that using the present instrumentation would probably not allow the detection of such non-covalent complexes in complicated biological tissues, were their concentration is extremely low. However, these results could pave the way to the investigation of other systems and to a better understanding of the influence of each experimental parameter on the detection of non-covalent complexes.

8.5. Bibliography

(1) Mahoney, C. M. *Cluster Secondary Ion Mass Spectrometry: Principles and Applications*; John Wiley \& Sons, 2013.

(2) Chothia, C. Principles That Determine the Structure of Proteins. *Annu. Rev. Biochem.* **1984**, *53*, 537–572.

(3) vander Straeten, A.; Lefèvre, D.; Demoustier-Champagne, S.; Dupont-Gillain, C. Protein-Based Polyelectrolyte Multilayers. *Adv. Colloid Interface Sci.* **2020**, *280*, 102161.

(4) vander Straeten, A.; Bratek-Skicki, A.; Germain, L.; D'Haese, C.; Eloy, P.; Fustin, C.-A.; Dupont-Gillain, C. Protein-Polyelectrolyte Complexes to Improve the Biological Activity of Proteins in Layer-by-Layer Assemblies. *Nanoscale* **2017**, *9* (44), 17186–17192.

(5) vander Straeten, A. Protein-Polyelectrolyte Complexes for the Surface Immobilization of Bioactive Proteins. UCLouvain 2019.

(6) Xia, J.; Dubin, P. L. Protein-Polyelectrolyte Complexes. *Macromol. Complexes Chem. Biol.* **1994**, 247–271.

(7) Vander Straeten, A.; Dupont-Gillain, C. Self-Reorganizing Multilayer to Release Free Proteins from Self-Assemblies. *Langmuir* **2020**, *36* (4), 972–978.

(8) Cristaudo, V.; Poleunis, C.; Czerwinski, B.; Delcorte, A. Ar Cluster Sputtering of Polymers: Effects of Cluster Size and Molecular Weights. *Surf. Interface Anal.* **2014**, *46* (S1), 79–82.

(9) Jørgensen, T. J. D.; Delforge, D.; Remacle, J.; Bojesen, G.; Roepstorff, P. Collision-Induced Dissociation of Noncovalent Complexes between Vancomycin Antibiotics and Peptide Ligand Stereoisomers:

Evidence for Molecular Recognition in the Gas Phase. *Int. J. Mass Spectrom.* **1999**, *188* (1–2), 63–85.
(10) Jørgensen, T. J. D.; Staroske, T.; Roepstorff, P.; Williams, D. H.; Heck, A. J. R. Subtle Differences in Molecular Recognition between Modified Glycopeptide Antibiotics and Bacterial Receptor Peptides Identified by Electrospray Ionization Mass Spectrometry. *J. Chem. Soc. Perkin Trans. 2* **1999**, *0* (9), 1859–1863.
(11) Heck, A. J. R.; Jørgensen, T. J. D. Vancomycin in Vacuo. *Int. J. Mass Spectrom.* **2004**, *236* (1–3), 11–23.
(12) Heck, A. J. R.; Jørgensen, T. J. D.; O'Sullivan, M.; von Raumer, M.; Derrick, P. J. Gas-Phase Noncovalent Interactions between Vancomycin-Group Antibiotics and Bacterial Cell-Wall Precursor Peptides Probed by Hydrogen/Deuterium Exchange. *J. Am. Soc. Mass Spectrom. 1998 912* **1998**, *9* (12), 1255–1266.
(13) Jorgensen, T. J. D.; Hvelplund, P.; Andersen, J. U.; Roepstorff, P. Tandem Mass Spectrometry of Specific vs. Nonspecific Noncovalent Complexes of Vancomycin Antibiotics and Peptide Ligands. *Int. J. Mass Spectrom.* **2002**, *219* (3), 659–670.
(14) Jørgensen, T. J. D.; Roepstorff, P.; Heck, A. J. R. Direct Determination of Solution Binding Constants for Noncovalent Complexes between Bacterial Cell Wall Peptide Analogues and Vancomycin Group Antibiotics by Electrospray Ionization Mass Spectrometry. *Anal. Chem.* **1998**, *70* (20), 4427–4432.
(15) Du, L.; Yang, X.; Li, W.; Li, H.; Feng, S.; Zeng, R.; Yu, B.; Xiao, L.; Liu, Y.; Tu, M.; Nie, H.-Y. Time-of-Flight Secondary Ion Mass Spectrometry Analyses of Vancomycin. *Biointerphases* **2018**, *13* (3), 03B401.

Chapter 9 : General conclusions and future prospects

9.1. Conclusions

This original project aimed at using large gas cluster ion beams to desorb biological molecules (mostly peptides and proteins) from a solid sample, and further collect the ejecta on a desired substrate to build thin films of intact and active biomolecules. The ultimate goal was to develop an optimized and tunable method which would offer fine control over the deposited quantities/thicknesses, the homogeneity of the constructed films, both in terms of surface roughness and deposition pattern, and of course retention of the 3D structure of the transferred proteins, to make sure their bioactivity was preserved.

It was successfully demonstrated that large argon cluster ion beams could be used as a tool for the controlled construction of biofilms containing intact and active proteins. In the first place, small peptides and proteins were used as model molecules to set up the experimental conditions. Angiotensin and bradykinin, both displaying a mass of roughly 1 kDa, were found to be transferred intact, as their molecular ions were clearly detected in the ToF-SIMS spectra recorded on the collectors. These peptides were further used to elucidate the influence of a series of parameters on the efficiency of the transfer, and on the damage suffered by the molecules upon transfer. It was shown that the fragmentation of the transferred species was mainly function of the energy per atom of the primary cluster ions. Among the six primary ion beam conditions that were used, the fragmentation followed the trend of the E/n ratio, being minimal for the mildest conditions, i.e. 5 keV Ar_{5000}^{+} (1 eV/atom). For the transfer of bradykinin under these bombardment conditions, more than 60% of the collected material was in the form of intact molecules. It was also demonstrated that the deposited quantity was linearly correlated to the transfer ion dose, and so could be precisely controlled, which is one of the main features of this novel deposition approach. This is valid for all tested cluster beam sizes and energies, as well as for various proteins. Furthermore, the deposition rates could be compared as a function of the beam E/n, and of the transferred molecule sizes. Quite unfortunately, the desorption rate decreased as the E/n was lowered, as expected, forcing to work with a compromise between the deposition rate and the level of fragmentation induced to the transferred molecules. However, in principle, as long as the target is not depleted in proteins, the transfer can be carried out for as long as desired, leading to transferred quantities that are not

limited whatever the ion beam efficiency. This is another main feature of this innovative cluster-assisted deposition method, as it allows deposition of protein quantities hardly reachable via other existing alternatives. These results were drawn from thickness measurements at the surface of the collectors. In order to ease and accelerate the deposited biofilm thickness measurement, a protocol was devised to link the thickness of the organic layer to the SIMS signal intensity of the underlying Si substrate. This protocol also allowed the generation of thickness maps of the entire collector, by combining this approach with the 2D mosaic-imaging mode of the ToF-SIMS instrument. The thickness maps provided accurate data regarding the deposition pattern, especially bringing to light the variation of thickness across the collector when transfers were achieved using the seminal transfer sample holder. The developed thickness measurement method turned out to be very efficient, and could probably be adapted for a series of other organic compounds. As a straightforward way to quantitatively compare the deposition rate and thickness uniformity was available, it was further taken advantage of it to optimize the transfer geometry. The initial transfer sample holder was designed in such a way that the primary cluster ions were impinging the target with an angle of 15°. Such a grazing angle was far from optimized to promote an efficient desorption, and so kept the deposition rate relatively low. In addition, it favored the backscattering of argon clusters towards the collectors, which was found to be problematic as it probably induced sputtering from the collectors. To overcome these drawbacks, other geometries were tested, and an optimal incident angle was found to be 45°, which displayed up to an 8-fold increase in the deposition rate in comparison to 15°, as well as yielding thin films that were homogeneous on a much larger area.

All the above-mentioned results were obtained with “typical” silicon wafers as collectors. If these present a series of advantages for surface characterization, they also turned out to be limiting for other types of analysis. With the objective of performing quantification bioassays that were not compatible with the use of Si wafers as collectors, other materials were tested as collector substrates. From this perspective, polyethylene delivered the most successful results, as it allowed the quantification of the total amount of material deposited at the surface, via development of a procedure to perform BCA assay directly at the surface of the collectors. The results obtained via BCA confirmed the conclusion drawn from thickness measurements, which is that the transferred quantity increases linearly with

the transfer ion dose. The two methods are complementary, as the one relying on thickness measurements is reliable for ultra-small amounts, while the BCA requires a minimal amount to allow detection, but then is reliable up to 10 µg (probably even more, but it was not tested). In this work, quantities up to 8 µg of proteins were deposited in only a few hours, using 10 keV Ar_{3000}^+ as primary ion beam, which is quite impressive. Varying the substrate nature also led to the confirmation of a key feature expected from this solvent-free deposition approach, which is its compatibility with a priori, any solid material that withstands vacuum. This is particularly relevant for substrates that cannot be used in combination with the most widespread solution-based methods (spontaneous adsorption and variants thereof). To demonstrate this point, the transfer of bradykinin was successfully achieved with paper as collector substrate. This versatility towards substrate nature paves the way to preparation of biomaterials and biosensor devices that could not be envisioned before.

Transferring small peptides intact was a major step for the development of the novel deposition strategy, and they represented ideal candidates for all the seminal experiments and optimization steps. However, they were lacking straightforward ways of investigating their 3D structure. The fact that their molecular ion could be detected in by ToF-SIMS only indicated that their primary structure was intact, but delivered no relevant information regarding their 3D structure at the surface of the collectors. Retention of the native conformation is crucial, as it governs the bioactivity of the proteins. To gain insights into the structure of the deposited proteins, the transfer of enzymes was studied. Enzymes are good candidates to investigate the preservation of the 3D structure upon transfer, via specific bioactivity assays, in reason of the structure-activity relationship. To this end, the transfer of lysozyme and trypsin was investigated. The first challenge associated to their transfer was to determine whether they could be transferred intact, in terms of primary structure. Due to their relatively high mass (14.3 and 23.8 kDa, respectively), they are out of the ToF-SIMS mass range. Alternative methods were investigated, and SDS-PAGE electrophoresis proved to be successful, as both proteins could be identified intact on the collectors after being sputtered by 10 keV Ar_{5000}^+. Activity assay measurements on transferred lysozyme samples further demonstrated the presence of almost 1 µg of active proteins at the surface of the collectors. At the time of writing this conclusion, activity assay measurements could not yet be performed on trypsin transferred samples, as the optimization of the experimental protocol

faces more difficulties than expected. It must be emphasized though that these results not only were contributing to the success of the cluster-assisted deposition method being developed, but also were quite a breakthrough for the SIMS community. To our knowledge, it is the first experimental proof that large cluster ion beams are capable of desorbing such large (bio)molecules intact, further demonstrating that their non-detection by ToF-SIMS is more a matter of low ionization probabilities and poor detection efficiencies. It gives clues as to the direction to take for future research aiming at the detection of large molecules by ToF-SIMS.

The ability of the developed method to successfully achieve the construction of more complex architectures, out of reach of current alternatives, was further demonstrated by the construction of multilayers. In a model system, successive depositions of two organic molecules, bradykinin and Irganox1010, were achieved on the same collectors. ToF-SIMS depth-profiles confirmed that two distinct layers were built, one on top of the other, with very low mixing between the layers. These multilayers were found to be stable after several days of exposure to ambient conditions. Next, bilayers of two different proteins were successfully deposited, with bradykinin and neurotensin. Finally, a trilayer was build, with bradykinin, Irganox and neurotensin. Very little mixing is observed between the layers, which are all clearly discernable in the depth profiles. In principle, as many layers as desired can be successively deposited. These results open up new perspectives regarding the preparation of sophisticated thin films composed of distinct layers.

Finally, large cluster ion beams were used for the analysis, and further transfer, of non-covalent complexes. Protein-polyelectrolytes were envisaged as a way to protect the proteins during the transfer, and increase the percentage of intact and active proteins at the surface. Complexes were prepared with both lysozyme and trypsin, with PSS and PAA as polymeric counterpart, respectively. Their transfer however, failed, as their sputtering yield turned out to be extremely low. It is likely that a very dense and entangled polymeric network was formed, with the proteins trapped in it. In addition, these transfer trials were carried out using the 15° geometry, which was shown to be far from optimal. Therefore, to investigate the desorption and transfer of non-covalent complexes, smaller systems, with masses in the accessible mass range of ToF-SIMS were studied as models. Organometallic complexes were chosen as first candidates. Phthalocyanine green, a copper-based complex of formula $Cu(C_{32}N_8Cl_{16})$ could be transferred intact. In

addition, a series of [M(tfac)$_n$] (M = Cu, Ni, Co and Cr) complexes were investigated. However, these complexes lacked purity, which led to very complex mass spectra. Therefore, the study was only conducted on [Cr(tfac)$_3$], which could be detected intact on reference samples. It was further transferred with 10 keV Ar_{5000}^+. Fragments corresponding to the initial complex having lost one or two ligands could be detected on the collectors, but not the intact complex with the three ligands. During the study, it was found that parameters such as the film thickness, the underlying substrate or the primary ion beam nature play significant roles on the desorption efficiency, the ionization probability, and the fragmentation of the species. To draw conclusions whether these complexes can or cannot be transferred intact, more experimental work would be necessary to first control and characterize the deposited films at the surface of the collectors. The last system that was investigated was a weakly bound (mostly H-bonds) non-covalent complex, made of vancomycin linked to either one of two small peptide ligands, AA or KAA, respectively. It was successfully demonstrated that, in optimal conditions, the [vancomycin-KAA] complex could be detected by ToF-SIMS. As this complex is only held together through H-bonds, electrostatic and hydrophobic interactions, this result is promising and paves the way towards the detection of biologically relevant non-covalent complexes, for example with respect to tissues analysis.

9.1.1. A wrap up

Large cluster ion beams were found to be an efficient tool to build protein thin films in a controlled fashion. In many ways, the developed approach surpasses the most widespread protein adsorption methods, and allows overcoming some of the drawbacks still encountered today with respect to protein immobilization. Peptides and small proteins (up to M_w = 23.8 kDa) could be transferred intact, with a precise control over the deposited quantity/the resulting film thickness. Reducing the E/n of the impinging clusters led to a decrease in the fragmentation of the transferred molecule. At 1 eV/atom, more than 60% of the deposited bradykinin were found as intact molecules. Lysozyme was shown to be transferred with retention of its bioactivity, indicating that the 3D structure of the transferred proteins was at least partially preserved. Construction of protein thin films on paper demonstrated the versatility of the method towards the substrate nature, and building multilayers further illustrated the ability of this approach to build complex architectures that are out of reach of solution-based alternatives.

9.2. Future prospects

Throughout this work, it was demonstrated that cluster ion beams could be successfully used to sputter intact proteins from a solid target and transfer them onto a collector in order to build protein thin films at the surface of a priori any solid material. However, this work represented the early development stage of this novel approach. Accordingly, many directions were explored, to provide solutions to the issues that were encountered. As reported in the five results chapters, these were solved with more or less success, but along the way, insights into the potential and limitations of the method were gained, allowing us to refine the future work regarding the development of this method. From the experience gained through trials and errors, a few prospects to pursue this work will be provided. These include some ideas regarding the instrumentation, the applications, and other leads that were briefly investigated and that would be worth exploring in more details.

9.2.1. Instrumentation

The ToF-SIMS instrument proved to be a providential commercial tool to be used for the seminal experiments, especially the argon gas cluster ion source mounted on the equipment, as it enabled demonstrating the proof of concept of this original project. However, it was clear that the apparatus was not designed to perform such *in-situ* transfer/deposition experiments. The ToF-SIMS is a very complex instrument compared to what is required to achieve the deposition of molecules, as was aimed. Many of the analytical parts, including the extractor, the ToF-analyzer, the detector, etc. are of no use for the transfer application. Using such a cutting edge instrument implies high cost and a lot of maintenance. In addition, it imposes some restrictions regarding the size and geometry of the sample holders that can be introduced in the main analytical chamber. Moreover, with the current sample holder, the alignment of the ion beam with respect to the target, as well as that of the target with the collector, is done by sight, leading to lack of precision and sometimes reproducibility issues. Last but not least, the argon cluster source of the ToF-SIMS was not particularly designed to generate very high current intensity beams, as this is not required for analysis. For all these reasons, if the cluster assisted deposition method is to be further developed as an emerging tool for the fabrication of thin films; its development should ideally be supported by the development of an

instrument specifically designed for this use. In particular, progress towards cluster ions sources that are able to produce very large Ar_n clusters, with n > 5000, displaying high current intensities while keeping the E/n relatively low would be an enormous step forward for the transfer. Higher current intensities would enable higher deposition rate, thus significantly reducing sample preparation times. Higher cluster nuclearity (and thus lower E/n at identical total cluster energy) would reduce the fragmentation of the transferred species, and could possibly lead to the desorption of larger molecules/proteins. In addition, designing a specific chamber for transfer would allow considering the use of other sample holders that could display advantages over those used until today.

Other sample geometries could offer considerable benefit when aiming at covering larger surface areas, or at producing homogenous thin films (in terms of thickness). Strategies could imply spinning or at least moving collectors in order to cover a large area with a homogeneous coating. It could also be envisaged to move the target with respect to the ion beam, or vice versa. By scanning the target instead of aiming at the same area during the entire transfer, depletion of the target could be avoided. Therefore, targets could be prepared with less material, lowering the waste of proteins and other compounds that may sometimes be expensive. Finally, as an instrument is to be built, it is crucial to make sure that whatever the sample holder, positioning and focusing of the ion beam on the target, as well as alignment of the target with respect to the collector can be done in a safe and reproducible way. It could be done by having a fixed position for both the target and the collector. In this way, one would avoid many concerns.

9.2.2. Towards larger proteins

Even without the development of a more “powerful” gas cluster ion source (in terms of cluster size and current intensity), the transfer of larger proteins and other biomolecules should be investigated. As the largest protein investigated in this work, trypsin, could be transferred intact, at least in terms of its primary structure, it is plausible that the size limit of what can be desorbed intact by large cluster argon beams, and further deposited on a collector, has not yet been reached. Larger proteins should thus be on the list of next transfer candidates. These could include horseradish peroxidase (44 kDa) and glucose oxidase (160 kDa, divided into two subunits of 80 kDa). Furthermore, these two enzymes are part of a catalytic reaction cascade, thus their activity and their interaction at the surface could be probed

simultaneously. Before that, their integrity could be assessed by means of SDS-PAGE electrophoresis, as was demonstrated for lysozyme and trypsin. Molecular dynamics simulations performed by A. Delcorte indicated that large Ar clusters could desorb an intact polystyrene molecule of 60 kDa,[1] so there is good hope that proteins in the same mass range could be desorbed intact as well. However, within the present experimental conditions, and given what has been discovered so far, i.e. a transfer rate decreasing with increasing protein size, the transfer efficacy could turn out to be a major obstacle, as low amount of transferred material will be available for analysis. At the moment, to overcome this issue, the only possibility is to increase the transfer time, making the preparation of samples evermore time-consuming.

9.2.3. ToF-SIMS as an analytical tool to investigate the enzymatic activity

As was reported in this work, especially in **Chapter 6**, assessing whether the transferred enzymes were still active or not turned out to be one of the major challenges. Adaptation of the standard procedures of the commercial activity assays so that they could be performed at the surface of collectors was sometimes very tricky. It is possible that the transfer on soft PE sheets, which allowed bioassays to be performed in Eppendorf tubes, brings new possibilities for testing, and may enable the use of straightforward protocols. However, the volumes required to recover the entire collectors in the Eppendorf tubes are sometimes large, and it dilutes the proteins considerably. This solution might therefore not be applicable in all cases. To circumvent these obstacles, a very original strategy was envisaged in the course of developing activity assay protocols for the transferred lysozyme. This approach, illustrated in **Figure 9.1**, relies on the use of ToF-SIMS to detect the activity of the lysozyme directly at the surface of the Si collector. The ultimate strategy would be as follows: (a) the lysozyme substrate, the tri-sugar 4-Methylumbelliferyl β-D-N,N',N''-triacetylchitotrioside, is deposited at the surface of the collector, by spin-coating or drop-casting; (b) lysozyme is transferred onto the collector; (c) a drop of water is added on the collector, so that the lysozyme is mixed in solution with its substrate, allowing the enzymatic digestion of the sugar to take place, until all the water has evaporated; (d) the collector is analyzed by ToF-SIMS, and if the digestion of the sugar by the lysozyme has taken place, a significant increase in the intensity of the sugar fragments resulting from the digestion should be detected in the mass spectrum, in comparison with that of a reference of the

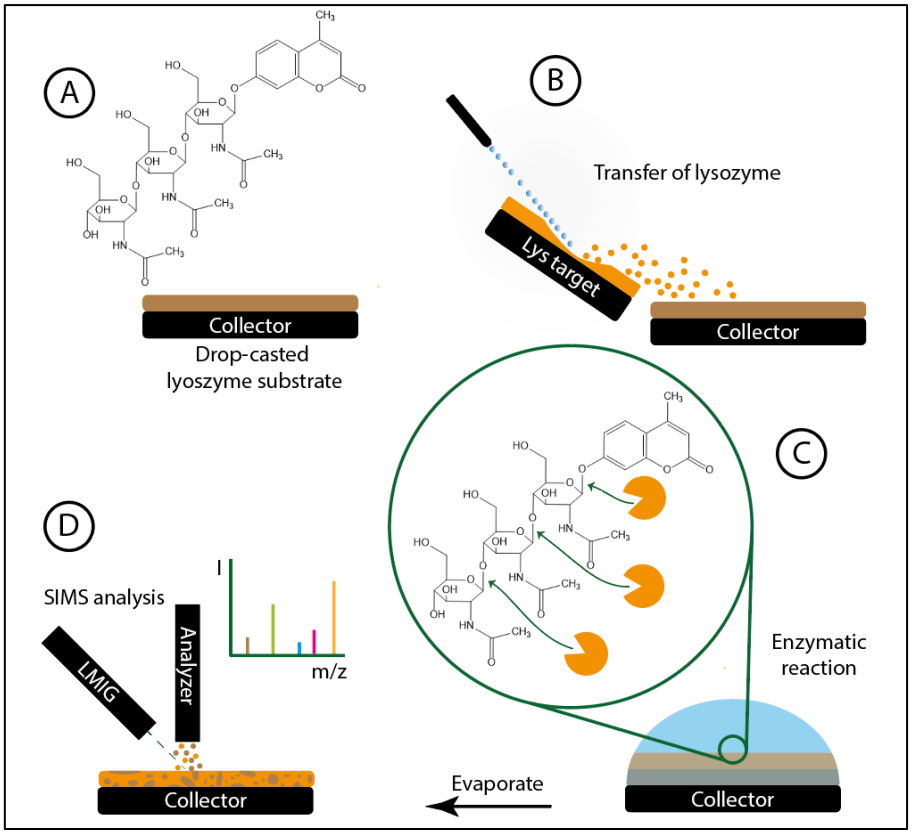


Figure 9.1. *Envisioned strategy to probe the activity of the transferred lysozyme using ToF-SIMS.*

tri-sugar substrate (as well as a decreased intensity of the parent molecular ion of the enzymatic substrate). Preliminary experimental work has been carried out in that direction, leading to very interesting results, though it did not reach the transfer stage. Hence, these results will briefly be presented in this section but should be seen as an incentive for future work, rather than as the outcome of a complete set of experiments. What has been done is a model experiment (depicted in **Figure 9.2**), in which a known quantity of lysozyme was drop-casted at the surface of a Si wafer. Then, a drop of the reaction buffer (AcONa, pH = 5, FI = 10) containing the enzymatic substrate was added, and the wafer was left at 40°C until total evaporation of the solution. The sample was then analyzed by ToF-SIMS and the results were compared to the mass spectra recorded on a pure spin-coated sample of the enzymatic substrate. Unfortunately, the mass spectra recorded on the digested sample could simply not be of any use. These spectra were completely saturated with sodium, which undoubtedly came from the reaction buffer. To overcome this issue, a simple question arose: even

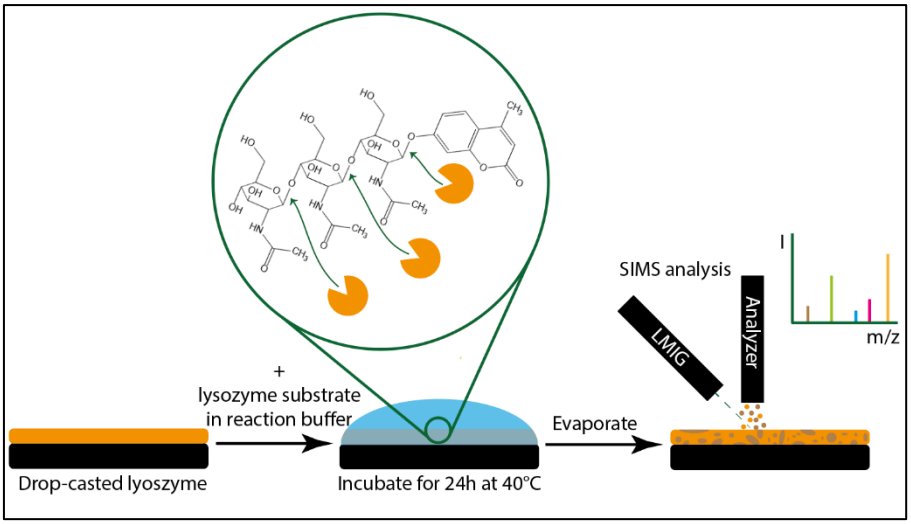


Figure 9.2. *Schematic illustration of the preliminary experiments that were performed to probe the activity of lysozyme on surfaces, using ToF-SIMS.*

though the activity assay of lysozyme was supposedly optimized with these buffer conditions, could it be that the test works as well when performed in pure water? To answer this question, a calibration line of the activity assay was performed, with the buffer replaced by pure water. The results were surprisingly good, as it yielded a perfect calibration line, meaning that the lysozyme was perfectly active in pure water (**Figure 9.3**). Knowing this, a second trial of the model experiment was attempted. This time, after that lysozyme was deposited at the surface of the Si wafer, the enzymatic substrate was added in a pure water solution. The sample was left at 40°C until evaporation, and then analyzed by ToF-SIMS. In this way, the spectra were not saturated with sodium, and could be compared to those of the reference enzymatic substrate. The comparison is shown in **Figure 9.4 and 9.5**. Several peaks display a huge intensity increase in the spectrum of the sample in which the

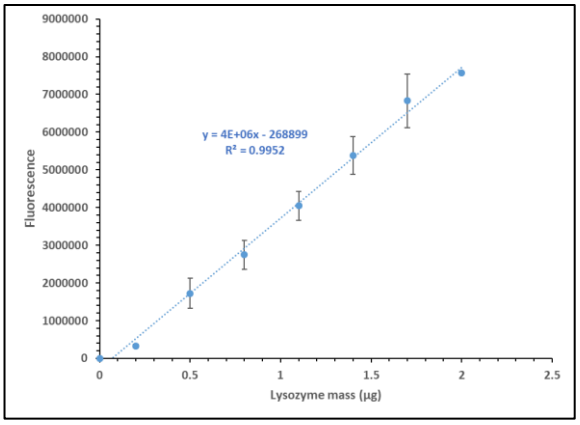


Figure 9.3*. Lysozyme activity assay calibration line, performed in pure water.*

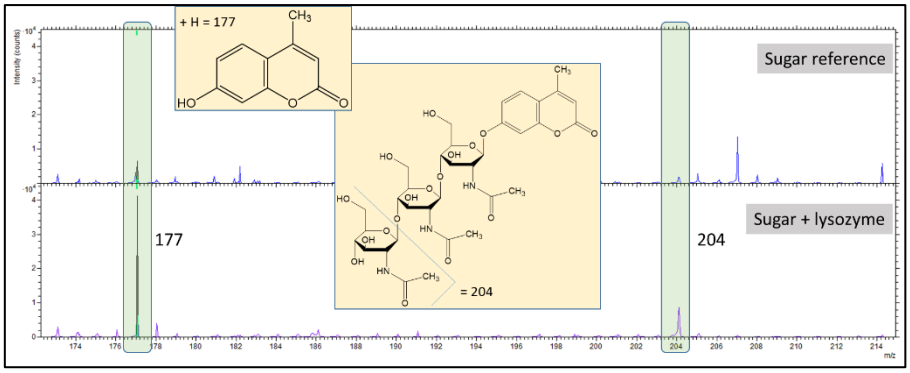


***Figure 9.5**. ToF-SIMS spectra comparison between a reference lysozyme substrate sample **(top)** and a sample were the substrate was digested by lysozyme **(bottom)**.*

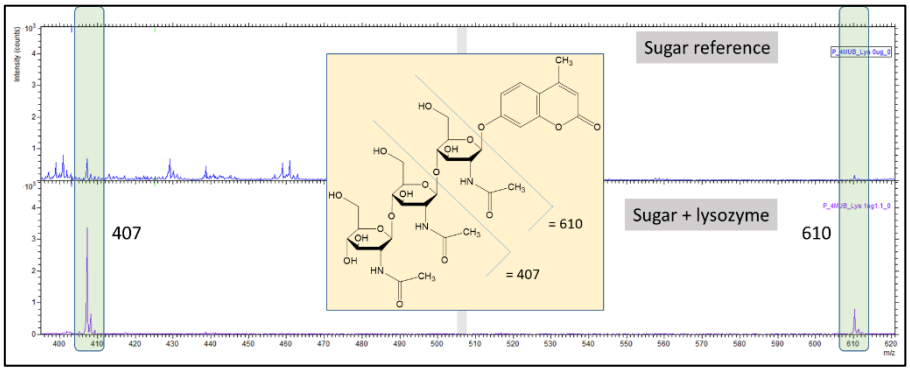


***Figure 9.4.** ToF-SIMS spectra comparison between a reference lysozyme substrate sample **(top)** and a sample were the substrate was digested by lysozyme **(bottom)**.*

sugar substrate was mixed with lysozyme, at m/z = 177, 204, 407 and 610, respectively. These peaks could be attributed to sugar fragments resulting from digestion by the lysozyme. The peak at m/z = 177 accounts for the metylumbelliferone moiety, once it has been cleaved from the rest of the compound. It appears at the expected mass if a proton adduct was to be formed. The three other peaks displaying a significant intensity increase are accounting for the tri-sugar moiety of the substrate molecule, depending whether the digestion took place after the first, second or third sugar residue. To quantitatively compare the intensity increase and make sure it is not due to matrix effect, the ratio of each fragment peak intensity to that of the molecular ion was plotted (**Figure 9.6**). The results on the graph illustrate the intensity increase for each fragment after digestion by lysozyme, in comparison to the pure substrate reference.

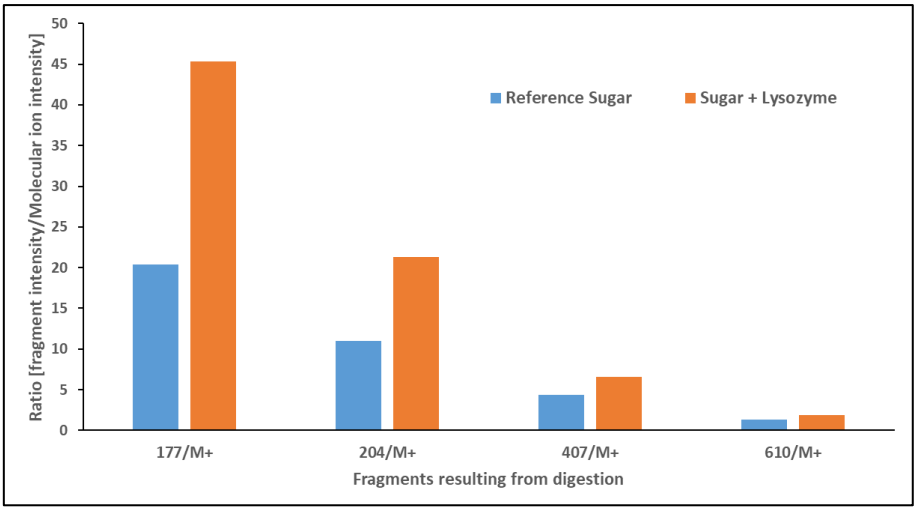


***Figure 9.6**. Comparison of the sugar substrate fragment intensities in SIMS spectra of substrate reference (blue) and substrate digested at the surface by lysozyme (orange). The intensity of each fragment is increased after digestion.*

In the same manner, a similar strategy could be envisaged for trypsin. The latter is a protease, hence digesting other proteins. A way to investigate its activity using SIMS would be to transfer trypsin on a collector coated with another protein, which presents trypsin-cleaving sites. Neurotensin represents an ideal candidate for a model experiment as it presents a single trypsin cleavage site, yielding only two fragments that are easily detectable by SIMS. After transfer, a drop of water could be added on the collector, and then evaporated before the sample is analyzed by ToF-SIMS. If effective digestion took place, significant changes could be observed in the mass spectrum of the bradykinin, such as decreased intensity of its molecular ion peak, and increased intensities of several other characteristic fragments. Model protocols could be devised before aiming at real transferred samples. Ultimately, the two proteins could be transferred successively to form a multilayer, allowing investigating the presence of enzymatic activity in a non-aqueous environment.

9.2.4. Detection of large proteins by ToF-SIMS

To our knowledge, the results presented in this work are the first experimental proofs that proteins with masses over 14 kDa can be desorbed intact by large argon cluster ion beams. These observations lead back to the question of understanding why these molecules cannot be detected by SIMS. Having demonstrated that desorption is not the issue, the absence of

detection can probably be attributed to either ionization or detection efficiency. In this work, two approaches were explored to promote the detection of lysozyme, i.e. salt addition to favor ionization and post acceleration tuning to increase sensitivity to higher m/z ions. However, none of these strategies proved to be conclusive. In the future, other strategies including varying the cluster nature or using matrices could be tested to improve ionization. In addition, instrumental development regarding the detector could lead to improved detection efficiencies. Detection of large compounds should definitely be a major objective of the SIMS community, as it will contribute to the success of SIMS, especially as it is more and more used for investigation of biological tissues.

9.2.5. Non-covalent complexes: fundamental thoughts

Investigating the desorption (and the transfer) of non-covalent complexes by Bi_5^+ and large gas cluster ion beams yielded relatively satisfying results. However, it also raised fundamental questions. Indeed, it not so clear how the concepts of non-covalent interactions that are valid in solution can be transferred to the vacuum environment of SIMS. In solution, solubilized molecules are initially separated, and surrounded by solvent molecules. Therefore, specific interactions between two or more partners in order to reach a more stable state (energetically favored) are strongly influenced by the presence and the nature of the solvent. For instance, the main driving force leading to the formation of protein dimers is believed to be hydrophobic interactions, in order to minimize the contact between hydrophobic regions of the proteins with the surrounding water molecules. However, under vacuum, the absence of solvent could modify the behavior of the proteins with respect to their surrounding neighbors. The influence of the absence of solvent on these non-covalent interactions is relatively unknown. In this work, it was presumed that the interactions that were observed in solution would be preserved as the solvent was evaporated. This hypothesis suited well the observation made in the ToF-SIMS mass spectra, but could as well turn out to be pure speculation. The formation of ions (desorption, ionization) in SIMS strongly differs from other mass spectrometry techniques that are performed on solution samples. In SIMS, the sample is in the solid form. Therefore, whether driven by (non-covalent) interactions or not, all the molecules are stacked together, in the absence of solvent. Whether this promotes or not the observation of interactions between the molecules is an interesting question. These thoughts should be

kept in mind when comparing the observation made in SIMS with those made in solution. The SIMS results may not always reflect the well-established situation in solution. This is especially important if one investigates the presence of non-covalent complexes in biological tissues.

9.2.6. Towards applications

In essence, the iBeam project was very fundamental, aiming at answering some theoretical questions rather than targeting short-term applications. However, after a few years of development, it appears that the results have exceeded expectations in some way. The transferred protein quantities that can be reached within only a few hours, along with the low fragmentation under optimal sputtering conditions, and the fact that enzymes tend to keep their bioactivity after transfer are many reasons why in the future, the research associated with this project should be in part dedicated to applications. At this point it is not straightforward to give precise examples. Yet directions can be envisaged. Biosensors could be a field where the deposition method developed in this work may provide a significant additional value. The biosensors could be prepared in a dry protocol, and so provide samples that can be shelf-stored for a certain time before use. Other testing/biosensing applications could arise from the feature of being able to transfer biomolecules of interest on water-soluble substrate. This strategy could be investigated for release applications. Finally, the preparation of multilayers could be prove beneficial when two or more proteins that are part of an enzymatic cascade need to be “stored” at the surface without reacting until they are placed in solution. Preparation of such samples is not feasible with solution-based strategies, where the proteins would react as the sample is prepared.

9.3. Bibliography

(1) Delcorte, A. A Microscopic View of Macromolecule Transfer in the Vacuum Using Gas and Bismuth Clusters. *J. Phys. Chem. C* **2022**, *126* (16), 7307–7318.